

Accelerated Ageing

An experimental study on the weathering behaviour
of a 3D printed polymer façade element

Dat Bui

 **TU Delft**

DUS

Aectual

 **TEN
TECH**

Accelerated Ageing

An experimental study on the weathering behaviour
of a 3D printed polymer façade element

By

Dat Bui

in partial fulfilment of the requirements for the degree of

Master of Science
in Building Engineering

at the Delft University of Technology
Friday the 30th of November 2018

Chairman:	Prof. dr. ir. R. Nijse	TU Delft
Thesis committee:	Dr. ir. F.A. Veer	TU Delft
	Dr. ir. H.R. Schipper	TU Delft
	Ir. R. Houtman	Tentech BV



LUẬN ÁN NÀY DÀNH RIÊNG CHO CHA MẸ TÔI.
THIS THESIS IS DEDICATED TO MY PARENTS.

Acknowledgements

This graduation project was carried out for the MSc Building Engineering at the Delft University of Technology in collaboration with Tentech BV, DUS Architects and Aectual. Personally, it felt like I was thrown in at the deep end when I started with the subject: '3D printing'. However, in the end, my learning curve went steeper, and I developed myself on many levels. At the beginning of this report, I would like to thank all the persons involved in this progress for sharing their knowledge and experience.

First, I would like to thank the director of Tentech BV, Rogier Houtman offering me the opportunity to get involved in this exciting project and providing me with generous help and encouragement. I also would like to thank, Martine de Wit, Chief Print Officer of Aectual and co-founder of DUS Architects, who has introduced me to the world of 3D printing and product development.

My deepest gratitude to the members of my graduation committee: The Chairman Professor Rob Nijssse, who always advised me to be critical, while staying curious and open for new ideas. My daily-supervisor, Roel Schipper, who advised me on the academic level, helped me to organise my report and guided me through the research process. Many thanks for my laboratory-supervisor, Fred Veer, for his practical tips and tricks around the mechanical testing and for showing me the fun of breaking stuff. Even though it was not my field of study, I appreciated for giving me the opportunity of working with the various laboratory techniques. Again, my appreciations for my work-supervisor, Rogier Houtman, for offering a listening ear in times of need, while giving me the freedom to develop myself.

Many thanks to all my colleagues at DUS Architect, Aectual and Tentech BV for sharing their precious knowledge and experience contributing to this project. Also, thanks to the employees of the TU Delft from the faculty of Civil Engineering and Geosciences, Aerospace Engineering and Applied science, for their guidance and advice during the experiments.

Finally, I would like to thank my supportive girlfriend, annoying housemates, neighbours, friends and family. Especially my lovely mother and father, who have given me their great trust and support during my entire study career. Even though, I know that they do not want to hear a word about 3D printing anymore, I am grateful for their endless love and appreciation.

Dat Bui
November 2018

Abstract

Additive manufacturing, popularly known as 3D printing, could positively change the fabrication of façade panels. Benefits include manufacturing each façade element uniquely without the use of a mould while having the potential of integrating functions as water drainage and solar shading within the object. Recycling polymers, obtained from industrial waste, could also reduce the panel's CO₂-footprint. Despite these benefits of the self-developed pellet-extrusion XL 3D print technology, less research has been done on the feasibility of the façade panel under outdoor weather conditions. Since thermoplastic polymers are highly vulnerable to weathering factors (solar radiation, temperature and humidity), preserving their mechanical integrity under outside circumstances could be an issue.

This research aims to have a better understanding of the potential environmental risks of a 3D printed product: the Aectual façade element. First, a broadening study has been conducted, in which several potential risks were investigated. Potential risks include the effects of wind and thermal load on the façade element and the material's resistance against fire, thermal shock and frost. The broadening study led to an in-depth study, where the effect of ultraviolet (UV) radiation and the use of UV stabilisers on the tensile strength of a 3D printed polypropylene-based (PP) composite has been researched.

During the experimental study, 3D printed materials, in the form of tensile test samples, were accelerated aged by an indoor UV test chamber. After several exposure time intervals, exposed and unexposed samples were tested on their tensile strength. We found highly scattered data of the tensile properties of the 3D printed material and no significant influence of the UV radiation on the tensile strength between the exposed and unexposed samples. However, it is observed that the extruded material itself became brittle over time. Even at an ageing of 2088 hours (87 days), an increase in tensile modulus and a decrease in yield strain were measured. Adding UV stabilisers to the same print compound tend to accelerate the brittleness of the material over time. As mentioned, the test suffers from highly scattered results due to the various print qualities and sample slippage during testing. These factors led to a reduction of the characteristic tensile strength properties of the 3D printed composite as material for building applications. Conventional flat-die-extruded PP-based materials, obtained from a PP-sheets manufacturer, were tested in the same manner and confirm this conclusion.

Further material experiments were conducted to gain a better understanding of the effect 3D printing on the physical structure of the polymer-based composite. Techniques involve differential scanning calorimetry, digital and scanning electron microscopy and Fourier-transform infrared spectroscopy. The result shows that the 3D printed material exhibits different polymer characteristics such as the degree of crystallinity, surface structure and chemical composition compared to the raw, injection-moulded and flat-die-extruded materials.

In the discussion, the limited effect of UV degradation on the polymer's mechanical strength is explained by several reasons, including the impact of the 3D printing itself. The conclusion includes a summary of all the findings throughout the whole research, with emphasising on the low characteristic tensile values of the 3D printed samples compared to the conventional flat-die-extruded samples. Sample slippage and inconsistent print qualities are factors contributing to this result. In the end, a list of potential improvements is given, including several techniques to further investigate the effect of 3D printing on the material properties of polymers and the development of 3D print technology for building applications.

Keywords: 3D printing, façade element, recycled polypropylene, ultraviolet degradation

Table of Content

Acknowledgements	6
Abstract	8
Table of Content	10
Chapter 1	16
Introduction	16
1.1 Relevance of research	17
1.2 Research questions and objectives	17
1.3 Research scope	18
1.4 Research methodology	19
PART I Broadening Research	22
Chapter 2	23
Additive Manufacturing in the Building Industry	23
2.1 Introduction	23
2.2 Additive manufactured façade panels	24
2.3 Manufacturing methods	26
2.4 Investigated material	28
Chapter 3	30
Environmental Risks	30
3.1 Wind load study	30
3.2 Temperature development	35
3.4 Thermal shock resistance	39
3.5 Fire resistance	40
3.6 Thermal expansion and bowing	42
3.7 Frost resistance	47
3.8 Summary	47
PART II In-Depth Research	52
Chapter 4	53
Ultraviolet Degradation	53
4.1 Introduction	53
4.2 Ultraviolet degradation	53
4.3 The influence of additives	54
4.4 Weathering test methods	55
4.5 Natural weathering of the Aectual façade	55
4.6 Summary	57
PART III Experimental	60
Chapter 5	61
Test Protocol	61
5.1 Introduction	61
5.2 Test description	64

5.3	Laboratory weathering testing	66
5.4	Mechanical testing	67
5.5	Summary	69
Chapter 6		70
Test Results		70
6.1	Tensile strength	70
6.2	Charpy impact strength	87
6.3	Influencing factors	88
6.4	Characteristic value of the tensile properties	90
6.5	Summary	93
PART IV Further Analysis		96
Chapter 7		97
Thermal Analysis		97
7.1	Thermal history of polymers	97
7.2	Test procedure	98
7.3	Test results	100
7.4	Observations and discussion	103
Chapter 8		106
Microscopy		106
8.1	Microscopy	106
8.2	Test procedure	106
8.3	Test results	107
8.4	Observations and discussion	114
Chapter 9		116
Fourier-Transform Infrared Spectroscopy		116
9.1	Infrared spectrum	116
9.2	Test procedure	116
9.3	Test results	117
9.4	Observations and discussion	117
PART V Evaluation		120
Chapter 10		121
Discussion		121
10.1	The influence of ultraviolet radiation	121
10.2	The effect of 3D printing	122
Chapter 11		125
Conclusions		125
11.1	Mechanical testing	125
11.2	Thermal analysis	126
11.3	Microscopy	126
11.4	FTIR Spectroscopy	127
11.5	General conclusion	127
Chapter 12		128
Recommendations		128
12.1	Product development	128

12.2	Mechanical testing	128
12.3	The effect of 3D printing on the material	129
12.4	Further development of the 3D printing technology	129
Appendices		134
Appendix A		135
Material Information		135
Appendix B		140
Effective Length		140
Appendix C		142
Coefficient of Variation		142
Appendix D		143
UV Test Chamber		143
Appendix E		144
Wind Load Assumptions		144
Appendix F		147
Raw Test Results		147
Appendix G		161
Heat Transient Analysis		161
Bibliography		164
Reference		165
List of Figures		170
List of Tables		174

“FAILURE IS SIMPLY THE OPPORTUNITY TO BEGIN AGAIN,
THIS TIME MORE INTELLIGENTLY.”

HENRY FORD

Chapter 1

Introduction

Additive manufacturing, popularly known as 3D printing, is starting to emerge in the building industry. The general idea of this innovative technology can be explained briefly: a three-dimensional model, designed on a computer, is converted into a predesigned print path. This path is sent to a printer that creates the object, in this case, layer by layer (Bogue 2013). In 2014 the Dutch designing company DUS Architects decided to print a house with a large-scale version of the fused deposition modelling (FDM) 3D print technique (**Figure 1**). Within this process, a thermoplastic material, which is heated until it reaches an appropriate liquid state, is extruded by a printer's nozzle. When deposited, the thermoplastic material hardens itself during the cooling process in open air. After creating one layer on the printer bed, another layer is built on the previous one until the object is finished (Hager, Golonka, and Putanowicz 2016). The self-developed pellet-extrusion 3D XL print technique of DUS Architects uses pelletized material instead of a thermoplastic filament and is larger of scale compared to the traditional Ultimaker 3D printers (Petch 2017).



Figure 1: 3D printed house by DUS (left), the 'KamerMaker' (right) (Petch 2017).

Additive manufacturing can bring significant advantages to the construction industry compared to traditional fabrication techniques. Benefits include increased customisation, reduced construction time, reduced workforce and reduced construction costs (P. Wu, Wang, and Wang 2016). In addition to that, DUS Architects aims at the use of recycled and biodegradable plastics with the idea of lowering the CO₂-footprint of the printed object. During this research project, DUS Architects and the 3D print company, Aectual are developing a 3D printed product: the Aectual façade. 3D printing of façade panels could have benefits in comparison with the conventional manufacturing methods. Advantages include customisation, whereby each façade element could be made unique. Also, integration of building functions within the print could be beneficial regarding rain drainage and solar shading. Although developments exist in the design and the fabrication of the façade elements, little research has been done on the material behaviour when exposed to the outdoor weather (**Figure 2**).

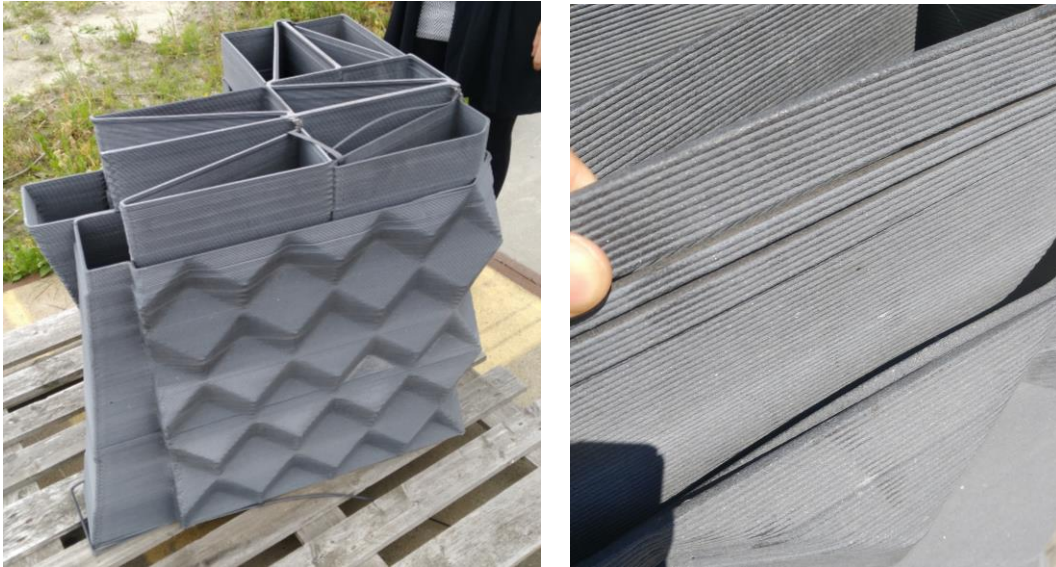


Figure 2: Exposed 3D printed object by DUS Architects (left), close-up (right).

1.1 Relevance of research

Weathering is the adverse response of a material to climate, often causing premature product failure (Azuma et al. 2009). Weathering factors such as sunlight (ultraviolet radiation (UV)), temperature and moisture could affect the visual and physical aspects of the façade's material (Brookes and Meijs 2008), leading to discolouration, cracks or even fracture of the material. The weathering behaviour of the 3D printed material must be understood, to prevent material degradation when in use. In the past researchers developed various indoor and outdoor weathering tests to study the material behaviour under outdoor conditions (Chew 1998). The Aectual façade element purely consists out of one polymer-based composite which is in comparison to brick or concrete, more sensitive for weathering conditions. It is thereby vital to understand how to design and conduct these weathering tests properly.

The in-depth study attempts to have a better understanding of the effect of UV radiation on the strength of a 3D printed façade panel made of recycled thermoplastic polymer. Since testing material properties under actual weathering conditions would be a time-consuming process, it is chosen to conduct an accelerated laboratory test. During the experiment, 3D printed samples were accelerated aged by an ultraviolet exposure device and tested on their mechanical strength. Comparison of the results of degraded and unexposed samples will indicate the material behaviour of the 3D printed thermoplastic polymer under solar radiation in the Dutch climate.

1.2 Research questions and objectives

Several former TU Delft students finished their thesis based on the 3D printing of large-scale building elements with recycled thermoplastic polymers. Van der Veen laid the foundation of the 3D print research at the TU Delft, in cooperation with DUS Architects, Aectual and Tentech BV (Van der Veen 2014). Van der Veen studied the structural feasibility of the printable polymers for houses with the use of mechanical tests. Subsequently, the students, Pawel and Wang, mainly focused on the possibility of printing moulds for concrete objects using laboratory experiments and numerical analysis (Baran 2017) (Wang 2018).

During this graduation project, DUS Architects and Aectual are focussing their production on non-loadbearing printable objects. This research took, the product development of the 3D printed exterior façade panel: the Aectual façade, as a starting point. The façade element consists entirely

out of a recycled polypropylene-based composite, obtained from industrial waste. The main objectives of the research contain the following questions:

- 1) What are the potential risks of a 3D printed façade element made of recycled thermoplastic composite?
- 2) What are the effects of long-term ageing and ultraviolet exposure on the tensile strength properties of 3D printed thermoplastic composite?
- 3) What is the effect of the addition of ultraviolet stabilisers to the composite on the UV resistance of the 3D printed thermoplastic composite?
- 4) What are the differences in strength and UV resistance between 3D printed and flat-die-extruded polypropylene-based composites?

These questions were investigated and answered in this research based on the literature study and several laboratory experiments including mechanical testing, accelerated weathering exposures, digital microscopy representations and differential scanning calorimetry measurements.

1.3 Research scope

Studies on the feasibility of large-scale 3D printing technology with thermoplastics are still in their infancy. To avoid a never-ending study, this research applied the following framework:

- Although different thermoplastic print materials are in development at Aectual, one print compound is chosen for this research study based on the first material of the Aectual façade: a glass fibre reinforced recycled polypropylene-based composite.
- The material investigation has been limited to relevant mechanical properties related to cross-sectional strength and stiffness: a tensile strength in transverse and longitudinal direction. A Charpy impact strength test has been added to the mechanical testing as an exploration test.
- Only long-term ultraviolet exposure effects which influence the material strength were tested, other environmental loads (wind, thermal) will be discussed briefly but are not the core of the research. Other long-term effects (creep and fatigue) are out of the scope of this project.
- Subjects based on the general structural mechanics and connections of the Aectual façade are out of the scope. Answers could be found in the thesis parallel during this research.

Although the scope of the research is based on several conditions, the outcome and conclusion of the study should be sufficient for answering the proposed questions including a general overview for the further analysis of this subject. Further testing is expected to extend the understanding of the 3D print material behaviour against ultraviolet exposure.

1.4 Research methodology

The thesis has been divided into five parts, which are summed up below and illustrated in **Figure 3**, to guide the reader through the graduation project:

- | | | |
|-----------------|---------------------|------------------|
| ▪ Part 1 | Broadening Research | Chapter 2 to 3 |
| ▪ Part 2 | In-Depth Research | Chapter 4 |
| ▪ Part 3 | Experimental | Chapter 5 to 6 |
| ▪ Part 4 | Further Analysis | Chapter 7 to 9 |
| ▪ Part 5 | Evaluation | Chapter 10 to 12 |

In Part 1 of this thesis, the use of 3D printing in the building industry is introduced. Here, the Aectual façade element and its manufacturing technique are introduced. After this chapter, the findings of broadening research have been described based on several potential environmental risks of the 3D printed product. In this research, several literature studies and small experiments have been performed to formulate a list of clear recommendations for the product development of the Aectual façade.

The broadening research led to an in-depth study in Part 2. whereby one potential risk of the thermoplastic façade will be further elaborated: ultraviolet (UV) degradation. This chapter contains several subjects relating to the effect of UV radiation on the material and testing of it.

Part 3 will cover the experimental research based on the literature study of the previous stage. Every experiment will be explained briefly, based on the chosen material's strength properties. An indoor weathering device accelerated aged the samples of the 3D printed material. A comparison is made with the data obtained from the tensile test with the degraded and unexposed samples. As a reference, differently manufactured polymer-based samples were tested in the same manner since tensile tests results show scattered and low tensile properties for the 3D printed thermoplastic material.

The results of the mechanical testing led to further questions about the characteristic of the 3D printed material. Therefore, a further research analysis is described in Part 4 where different techniques have been used with the goal to have a better understanding of the effect of 3D printing on the polymer. Test methods include differential scanning calorimetry (DSC), microscopy and Fourier-transform infrared (FTIR) spectroscopy.

In Part 5 a comprehensive evaluation of the graduation project is made. It firstly consists of a discussion of the effect of UV and 3D printing on the strength of the polymers. Subsequently, an overview of the conclusions made based on the analysis of the test results and measurements produced in the experimental research. Finally, this stage provides a list of recommendations including the further product development of the Aectual façade and the study about the effect of ultraviolet and 3D printing on the strength of the extruded polymers.

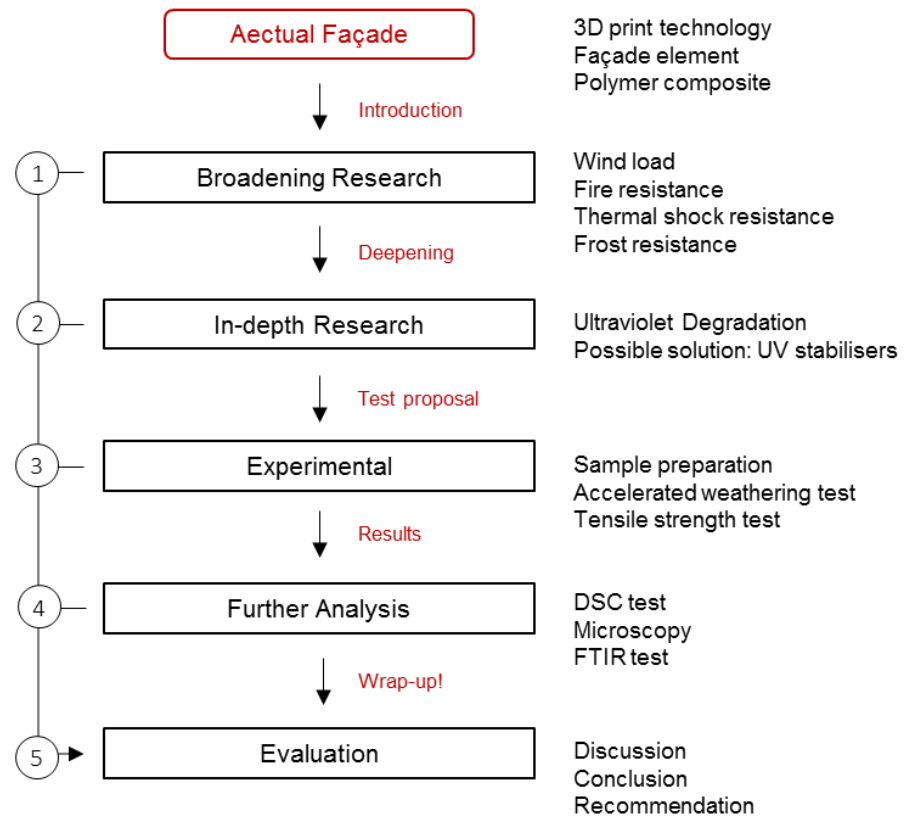


Figure 3: Research method.

PART I
Broadening Research

Chapter 2

Additive Manufacturing in the Building Industry

2.1 Introduction

Prefabrication is deeply integrated into the building industry. Complete sandwich panels, precast structural parts or even building units are produced in factories nowadays. These building elements are transported, depending on their size, to the building site resulting in a quicker and more economical construction process compared to the traditional way of building in situ. Casting, moulding, extrusion, injection and other techniques are used to make prefabrication possible for all conceivable uses. To make prefabrication financially beneficial, the fabricated elements must be as repetitive as possible. Using moulds, for example, only makes sense when a product is highly repetitive. In this way, choosing this method could reduce the price impact on each piece. However, the building industry is different from other industries by nature. Standardization in this industry cannot be compared with the standardization process of, for example, the automotive industry (Kasperzyk, Kim, and Brilakis 2017).

The disadvantage of prefabrication in the building industry is the lack of flexibility and form freedom. When focussing on building façades, this repetitive method creates affordable panels, however, each panel's design is look-alike which make the total façade appearance rather monotonous. A new manufacturing method to deal with the problem of monotony, but still benefiting of automatically production, is additive manufacturing. This innovative way of producing, also known as 3D printing, has made its way in the building industry. Products are built on a layer-by-layer basis, through a series of cross-sectional slices (Wu, Wang, & Wang, 2016). Compared to traditional building processes, implementing additive manufacturing in the fabrication stage could have numerous benefits (Hager, Golonka, & Putanowicz, 2016):

- The cost of fabrication construction elements of buildings is much lower than traditional construction methods due to the limited material transportation and storage if printed on site.
- Environmental friendly construction processes due to the focus on material savings and the use of recycled or biodegradable materials.
- Reduced number of injuries and fatalities on site as the printers will be able to do most hazardous and dangerous works reducing the human factor.
- The construction time required to complete a unique building can be considerably reduced.

Despite the above-mentioned benefits, still much research and development must be done to integrate this technology into the building industry. Nowadays this innovative technique is highly dependent on the available work, availability of the correct print materials and the development of the printing itself (Wu et al., 2016). In 2014 the Dutch, DUS Architects initiated to build a house by manufacturing its parts by a giant 3D printer named the 'KamerMaker' (Bogue 2013) as can be seen in **Figure 1**. This was the first construction project that was realized entirely by 3D printing technology in Europe. The project called '3D print Canal House'. Nowadays the architects are assisted by the printing company Aectual, the factory and technical department of DUS. The goal of this cooperation was to show that by printing components of the house directly on site is possible.

Including the benefits of eliminating the human factor while minimizing building waste and transport costs (Bogue 2013).

2.2 Additive manufactured façade panels

Aectual is working on the product development of a 3D printed façade panel: the Aectual façade (**Figure 4**). The façade is a non-load-bearing product since the current print material is still not well developed enough to be structurally safe for load bearing applications (Van der Veen 2014). The 3D printing of façade panels has been made possible by the implementation of easy-to-use parametric design software for architecture and construction. Compared to the traditional building industry, implementing additive manufacturing in the production of façade panels could have numerous benefits (Nadal et al. 2017). Quick production of long series of variable parts, such as slightly differentiated façade panels is made possible using the 3D printing technique. Each façade panel could be designed uniquely without extra manufacturing costs. Whereby possibilities are created to integrate various building functions like rain drainage and solar shading within the panel.

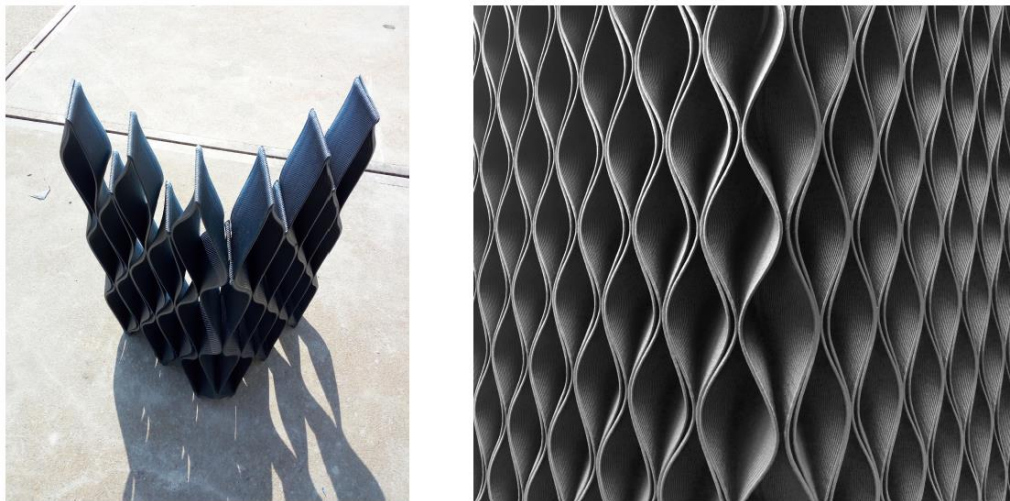


Figure 4: Aectual façade: mock-up (left), close-up (right).

The parametric design is an important characteristic of the 3D printed façade panel. The wave-structure consists of a consistent and operational pattern as illustrated in **Figure 5**. The consistent pattern ensures the stiffness and stability of the whole façade as a mesh. The operational pattern situates within the consistent mesh and is adjustable. The angle in which these 'eyes' twist from open to close is between 0-45° and it is based on the possible printing angle with the used printing technique. With the operational pattern in each façade panel, it is possible to create different figurations in the whole façade. In the future, these parametric designs could be used for integrating customized solar shading or to lower the wind pressure on the façade by increasing the number of openings.

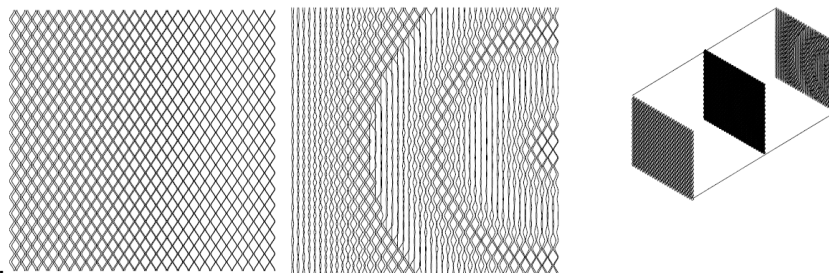


Figure 5: Aectual façade: the consistent and operational pattern.

DUS Architects and Aectual are not the only companies who see the potential in the 3D printing of façade panels. Several other projects are developing cladding or complete façade walls of thermoplastic polymers with the use of additive manufacturing. Each project is discussed below based on their own unique purpose and characteristics:

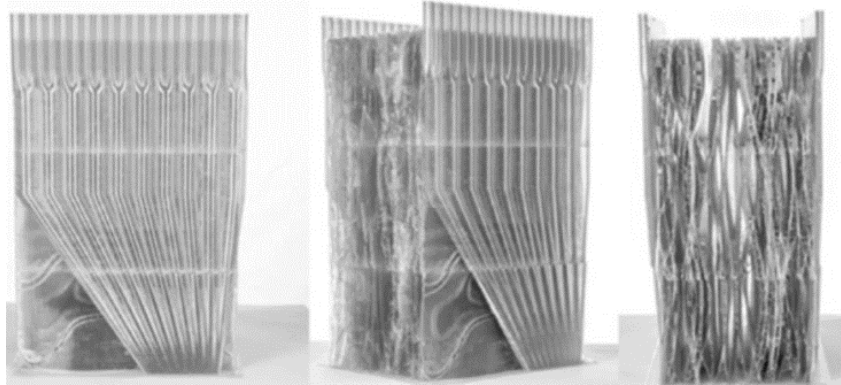


Figure 6: Spon3D-project: mock-up (Sarakinoti et al., 2017).

The Spon3D-project, which is started due to collaboration between Delft University of Technology and Eindhoven University of Technology, showed how a façade system could be 3D printed with a complex and organic structure. This façade panel, as can be seen in **Figure 6**, would be able to optimize a building's thermal performance. With the use of a 3D printer, a complex structure of cavities could be produced that combines different functions as thermal insulation and heat storage. In these air cavities, liquid flows through a series of channels around the outer edges, storing and transferring heat when needed. In this way, the façade could react to different climate conditions to improve the thermal performance of offices and houses (Sarakinoti et al. 2017).

Fluid Morphology is a German project led by Moritz Mungenast in collaboration with the Technical University of Munich (**Figure 7**). As in the Spon3D project, a 3D printer is used to create a multi-functional building façade made of translucent material. Cells inside the façade panels are made thick enough to be stable while creating the possibility to insulates the building by its air-filled cavities. The geometry of the façade panel is printed in layers of waves to create shadows. Thin embedded tubes allow air to circulate within the panel to provide a natural air flow. The uneven printed surface could create ideal acoustic insulation and the whole façade can be customized to meet individual needs without additional cost (Scott 2017).



Figure 7: Fluid Morphology project (Scott, 2017).

The last example of an additive manufactured façade panel is from LAB3d. The Dutch 3D printing company is developing a lightweight, yet energy efficient façade for the Delta Sync project with the

use of additive manufacturing. Their focus is the integration of insulation, window frames and even piping by 3D printing in high resolutions. A special connection system for smaller 3D printed objects, including plug-like connectors and spring systems are made with the thermoplastic PLA as can be seen in **Figure 8**. The printed wall has an outer and inner shell of 4 mm with a honeycomb structure in between. This honeycomb structure provides strength and stiffness for the façade element, but also provides sufficient insulating properties (Krassenstein 2015).

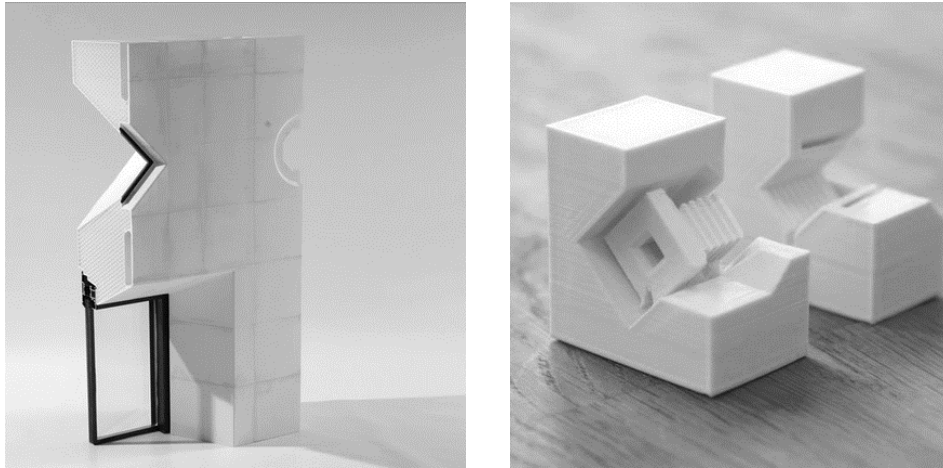


Figure 8: Lab3D: façade part (left), detail (right) (Krassenstein, 2015).

2.3 Manufacturing methods

As mentioned, 3D printing is an automated, additive fabricating process for producing three dimensional solid objects based from a digital model. In other words, a CAD-model is transformed into a route of printing lines which will be sent to the printer to construct the model (Bogue 2013). Currently, there are five main types of 3D printing technology: stereolithography, inkjet powder printing, selective laser sintering, contour crafting and to be investigated fused deposition modelling (FDM) technique (P. Wu, Wang, and Wang 2016). DUS Architects and Aectual have developed their own FDM-based print technique: the pellet-extrusion XL 3D print technology (Petch 2017). To understand the advantages and disadvantages of this innovative 3D print-extrusion technology, conventional polymer manufacturing methods, such as inject-moulding and flat-die-extrusion, are also described in this section.

2.3.1 3D print-extrusion

The self-developed print technique of Aectual is based on the fused deposition modelling (FDM) technology. The FDM-technique was invented in 1988 by Steven Scott Crump and utilizes continuous extrusion of a fibre-reinforced thermoplastic compound. This material is heated up to an appropriate melting temperature of the material before to being extruded. The molten thermoplastic is placed in layers in the XY-plane, based on the path defined by a drawing file. While finishing each layer, the movable frame equipped with a nozzle and processing machinery moves up along the Z-axis compensating the growth in component's height (Hager ea., 2016). There are many processing parameters that can be controlled and affect the properties of the printed object. Parameters include the print temperature, the print bed temperature, the ambient air temperature, the print speed, the print orientation, the layer-to-layer orientation, the layer thickness, the filament diameter and the nozzle diameter. Additionally, the filament material composition plays a large role in the end material properties of the printed object (Anthony A. D'Amico ea., 2017).

The self-developed pellet-extrusion XL 3D technology of Aectual differs from the conventional FDM-technique. The printer itself, the 'KamerMaker' (see **Figure 1**), is a large-scale version of the conventional small 3D printers. Instead of a filament, a hopper feeds pelletized material to the

nozzle, where it can be extruded into the desired shape (Petch 2017). The maximum print dimensions of the KameMaker equal to $2.2 \times 2.2 \times 3.5 \text{ m}^3$.

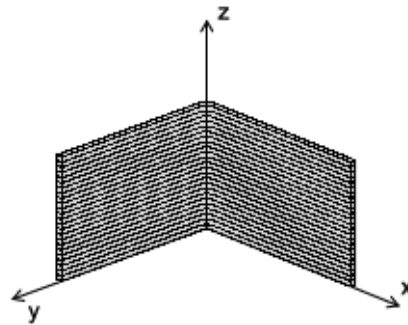


Figure 9: Printing coordinates of the KameMaker II (Baran 2017).

Since the to be printed object is built up layer by layer, a difference in mechanical properties can be expected between planes in the longitudinal and transverse direction of the printing lines as illustrated in **Figure 9**. In previous studies, it is shown that prints in the longitudinal directions show much higher (tensile) strength and reproducible qualities than prints loaded in the transverse direction (Baran 2017; Van der Veen 2014; Wang 2018).

Although being relatively simple and clear, it has numerous limitations and issues, among which the most serious are:

- The inability to print higher than from the previous print layer.
- The anisotropic behaviour of the extruded material.
- Still uncontrollable mechanical qualities in between layers.
- The high thermal sensitivity of the extruded thermoplastic material.
- Strength is dependent on the cross-sectional print quality of the extruded material.

Taking these drawbacks into account (with emphasis on print quality issues) and focussing on the goal to print a whole canal house, printing load-bearing elements is a good start. However, to apply a material with an unpredictable behaviour would be not safe. Applying the 3D printing technology to non-structural building elements, such as façade panels, will be a better purpose.

2.3.2 Injection-moulding

Injection-moulding of polymers is a manufacturing process for producing parts by injecting molten material into a mould. Plastic pellets are fed into the machine through a hopper. The screw moves the pellets down a path towards the mould. As the pellets move they are pressed against the heated inner walls of the screw chamber and are melted into a viscous liquid. At the end of the moulding machine the polymer liquid is injected into a predesigned mould and controlled cooled by a coolant (usually water). The coolant absorbs heat from the mould and keeps the mould at a proper and controllable temperature (Bryce 1996).

2.3.3 Flat-die-extrusion

Flat-die-extrusion, also known as sheet/film extrusion is used to extrude plastic sheets that are too thick to be manufactured by injection-moulding. The process is similar to injection moulding in that melted polymer is moved along by a screw. The polymer, however, is continually thread through an open die to form a continuous part with constant cross-sectional shape. Cooling is typically by pulling through a set of cooling rolls or a water bath (Bryce 1996).

2.3.4 Comparison of the plastic extrusion methods

In the experimental stage of this thesis a test has been conducted to measure the tensile strength of 3D printed and conventional manufactured polymers. A comparison is made of the mentioned

plastic extrusion methods as can be seen in **Table 1**, to have a better understanding the impact of the technique on the extruded material.

Technique	Mould	Object	Extrusion temperature	Cooling condition
3D print-extrusion	No	Layered	Uncontrolled (air)	Air
Injection-moulding	Yes	Freeform	Controlled	Coolant (water)
Flat-die-extrusion	No	Planar	Controlled	Cooling rolls

Table 1: Comparison of the several plastic extrusion methods.

2.4 Investigated material

2.4.1 Thermoplastic polymers

Polymers could be separated into two groups, thermoplastic and thermosetting polymers. Thermoplastic polymers consist of either chained or branched chain molecules which can be reshaped during heating. Thermosetting polymers have a molecular network structure and once solidified they cannot be reshaped due by heating. Thermoplastic polymers are separated into two major categories, amorphous and semi-crystalline. Amorphous thermoplastics has no long-range order in their structure. **Figure 10** illustrates the linear and branched chain molecules together with amorphous and semi-crystalline molecular structure of thermoplastic polymers (Packham 1994).

In the amorphous thermoplastic polymers, the randomly discorded molecule chain is frozen in a liquid state. In semi-crystalline polymers, on the other hand, have a partial order in their molecule structure. Compacted parts in the molecule chain are called crystallites and are created during chain folding. Since the crystallinity of the polymer never will be completed the polymer is called semi-crystalline. This is due to the large length of polymer chaining which prevents complete crystallinity.

When the polymer chains are in a tangled mess, the polymer group is called amorphous. In case polymer chains are arranged in a neat orderly manner, then the group called crystalline. Stacking and folding multiple crystalline groups led to a lamella. The crystallinity degree, X_c (%), is the fraction of crystalline molecules within a polymer. Polypropylene is a semi-crystalline thermoplastic, which has a crystallinity degree of between 30% to 50% (Janevski, Bogoeva-Gaceva, and Mäder 1999).

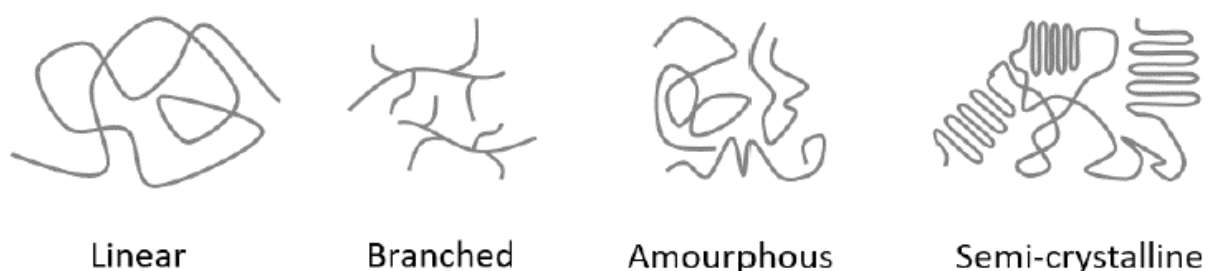


Figure 10: Molecule structures of thermoplastics (Packham 1994).

2.4.2 Recycled plastic

Recycling post-consumer plastics have been the focus of DUS Architects and Aectual for their products. In the world's waste stream, low-density polyethene (LDPE), high-density polyethene (HDPE) and polypropylene (PP), are some of the most common polymers (Agarwal and Gupta 2017). One of the reasons that these plastics are popular is their cheap production for the large packaging industry. However, their environmental impact is disturbing. Due to its low density and the hollow shape of the one-way packaging items, like bottles, containers, bags, etc, which are contributing ending up in waters or landfills. The large volume makes them more conspicuous as

nature pollutants than other waste products of equivalent weight (Wypych 1999). Aectual and DUS are focussing to recycle these materials in their products, reducing the CO₂-footprint for their product.

2.4.3 Polymer composite of the Aectual façade element

For the first Aectual façade panels, the companies are experimenting with the thermoplastic polypropylene. The use of polypropylene for 3D printed façades could have several advantages. The material is widely available in its original and recycled state and compared to other material is relatively inexpensive. Together with its thermal and electrical conductivity, it provides a good protecting layer for the building. However, polypropylene is also known for its relatively high thermal expansion coefficient which limits its use for high-temperature applications. In addition to that, the thermoplastic it is susceptible to ultraviolet and thermal degradation and is highly flammable (Gijsman, Meijers, and Vitarelli 1999). Adding additives to the polymer could tackle these risks. Due to its favourable characteristics of price, density and versatility, PP is chosen for the Aectual façade project and will be investigated material in this research.

As mentioned, the base material of the composite is recycled polypropylene (PP), an industrial waste mainly used for packaging and labelling. Aectual has the intention to reduce the carbon footprint in the construction industry by using recycled PP. It also has a low-cost post-processing method to be able to reuse it and has no cost for acquiring it, which means lower production costs. During this research project, the 3D-print extruded composite consists of the following materials:

- 75 % of polypropylene (PP)
- 20 % of glass fibres (GF)
- 10 % of talc
- 5 % of anti-oxidants

Approximately one-quarter of the composition consists of glass fibres to strengthen the polymer-based material. It is added in small length (smaller than 3 mm) to the mixture. The glass fibres increase the tensile strength of the polypropylene, that has a tensile strength of 31.6 MPa. Adding 30% glass fibres to the PP the tensile strength is increased to 392 MPa in the transverse direction of the printing line and 2109 MPa in the longitudinal direction of the printing line (Alwin Wang, 2018). Polypropylene with short glass fibres was observed to have a higher tensile strength and a lower elastic modulus as compared to talc filled polypropylene. Talc has relatively high stiffness and increases the crystallinity index of the material. However, it has a weak interfacial bond with polypropylene and creates voids, resulting in reduced strength (Eftekhari and Fatemi 2016).

While Wang's material only consists of PP and glass fibres, talc and antioxidants are added to the composition, after receiving the PPGF of the suppliers. The purpose of adding talc is to prevent the difference in creep between the longitudinal and the transverse direction of the extruded material. In other words, talc is added to prevent delamination of the layers. Other options like glass beads and wollastonite could be added for this purpose but are more difficult to add to the mixture than talc. The last material added to the mixture are the antioxidants. The antioxidants are added to secure the colour and to receive a better quality of the extruded outcome. Besides securing colour and printing quality the antioxidants function as UV protectors and are an important part of the chemical construction of the material. It is still unknown if this percentage is sufficient against UV degradation of the PP.

Chapter 3

Environmental Risks

When developing a new building product that will be exposed to weather conditions, it is important to understand the possible defects that can be caused to the material due to its environment. Defects such as cracking, discolouration, buckling, delamination, deflection or simply falling down of the product should be considered (Chew 1998). When the product is fully made out of plastic, which compared to concrete and brick, can react in a different way to moisture, thermal, fire and ultraviolet rays (Azwa et al. 2013), should be tested on its durability before applying it as, in this case, a cladding material. This broadening research discussed the different potential risks for the product development of a 3D printed façade panel made of a recycled polypropylene-based material. The following potential risks are described briefly:

- Wind load
- Thermal development and its effects
- Fire resistance
- Thermal shock resistance
- Frost resistance

The scope of this study are the environmental risks which will have an effect on the extruded material. Other long-term effects, such as creep and fatigue, are important, however, these effects are considered beyond the scope of the broadening research. Each environmental risk is studied based literature and material properties are assumed based on previous graduation studies(Wang 2018). When financially and practically possible, small and quick experimental tests were conducted to the (parts of) the façade panel. After this broadening study one potential risk is chosen to be further studied. The choice of this risk based on the necessity for further research from the client's perspective and whether the (laboratory) research is practically and financially possible.

3.1 Wind load study

Wind load is mostly the first external load determined when designing a building. According to the NEN-EN 1991-1-4 determining the wind load happens in several steps (Nederlands Normalisatie-Instituut 2011b). To simplify, the design wind load, P_d ($N/(mm^2)$), follows from the formula (Geurts 2004):

$$P_d = \gamma Q C_{dyn} C_f$$

Where the factor Q is the design wind velocity and depends on the geographic region, terrain category, shielding and the topographic location of a building site all according to the international standard. Data of weather stations could be used to determine the most occurring wind directions. The safety factor γ ensures an appropriate level of safety during the lifetime of the structure. The factor C_{dyn} is an adjustment for effect on the structure, this coefficient will not be discussed further in this study.

The last factor, C_f (or c_f), represents the wind pressure coefficient, which depend on the geometry of the building. As seen in the previous chapter Aectual panels consist of a complex parametric geometry and different permeabilities. Determining the design wind load is a challenge since these geometrical characteristics will have an influence on the wind pressure coefficients and a lack of

clear guidelines when following the international standards (Giannoulis et al. 2012). The goal of this wind load study is to determine or to give a range of the wind pressure coefficients of the façade including its geometrical characteristics and installation context. The following parameters are studied: its porosity, the gap width between the inner and outer panel, and the panel's thickness. Each parameter will be studied based on several wind studies regarding their influence on the wind load of a permeable façade.

3.1.1 Influence of the porosity

Several types of researchers have studied the influence of the porosity on freestanding walls in the past with the use of permeable nets and clothed scaffolding (Giannoulis et al. 2012). The permeable panel is characterized by its porosity (p) or its solidity ratio (ϕ) and is given by the formula:

$$p = \phi - 1 = \frac{A_c}{A}$$

Where A (mm^2) is the sum of the projected area of the solid members of the panel and A_c (mm^2) is the gross area of the face that is the area enclosed between the boundaries of the panel. Although it seems logical that with an increased porosity, a decreased in wind pressure coefficients could be expected. However, different wind load studies don't seem to have the same wind pressure coefficients (C_f) with respects of the panel's mesh as could be seen in **Figure 11**. The spread data points could be explained in the way the studies differs in material, degrees in porosity and aerodynamic environments (Giannoulis et al. 2012). These factors have highly influence on the presented results.

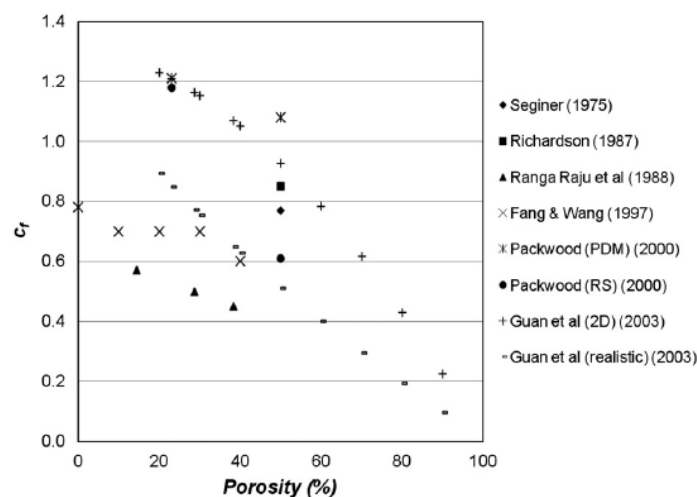


Figure 11: The wind pressure coefficients w.r.t mesh's porosity (Giannoulis et al., 2012).

Despite the scattered data points, the previous study is a sufficient starting point to determine the wind pressure coefficients for the Actual façade, based on its porosity. Since most studies are done with a steel wire mesh the following relation between the wind pressure coefficient and the porosity is for the Actual façade with a thickness of 1-10 mm and is illustrated in **Figure 12**. When dividing the solid area with the gross area of the Actual façades panels the porosity of a panel could be found between $p = 0\%$ and $p = 87.5\%$. The 87.5% solidity-limit is illustrated with a vertical dash line as illustrated in the **Figure 12**.

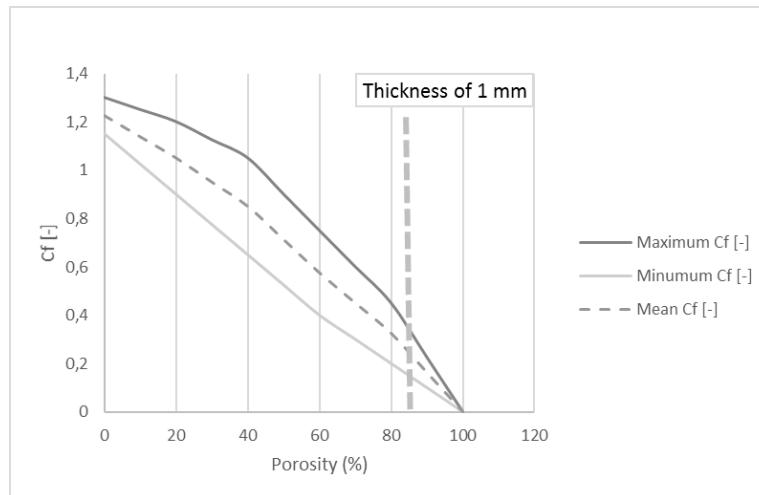


Figure 12: Assumption: The wind pressure w.r.t mesh's porosity, thickness: 1 mm.

3.1.2 Influence of the thickness

The thickness of the permeable panel should be considered when determining the wind load pressure. In this study, it is assumed that the thicker the panel is, the more friction loads the panel will take due to the wind contact area, A_{fr} (mm^2), created by the porosity. The frictional load may be taken into account by adding a friction drag force coefficient (c_{fr}) in the range of 0.01 - 0.04, which depends on the surface roughness. Due to the rough and ribbed 3D printed surface, a c_{fr} of 0.04 will be used, according to the Dutch standard of wind loads (Nederlands Normalisatie-Instituut 2011). When adding this factor to the previous formula, the next formula could be constructed:

$$c_{f_{net}} = c_f + (c_{fr}A_{fr})$$

Where A_{fr} (mm^2) is the inner area within the wall and is panel thickness-dependent. **Figure 13** shows that the wind pressure coefficient range-curve is slightly higher with increasing thickness. The maximum thickness of the Aectual panel is 70 mm and is set as the maximum thickness in this study.

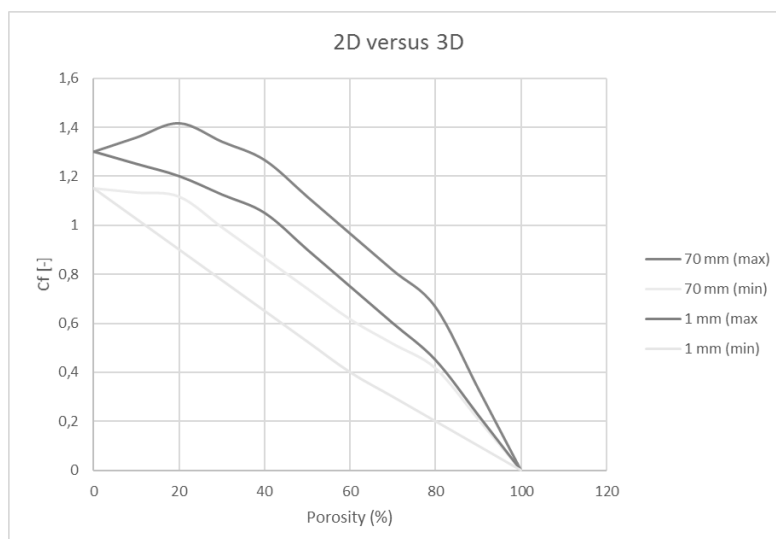


Figure 13: Assumption: The wind pressure w.r.t mesh's porosity, thickness: 1 - 70 mm.

3.1.3 Influence of the installation context

The static wind load assumptions of a freestanding porous wall were widely studied, as shown at the beginning of this wind load study. However, there is less research done relating to the permeable walls in their installation position. The area between the panel could cause an aerodynamic interaction with the inner closed façade and will modify the design wind loading (Kemper and Feldmann 2012). In this paragraph, the influence of the gap width, the distance between the inner and outer wall, on the wind load of the outer wall will be discussed. Since the Aectual façade could be used as a second skin as seen in **Figure 14**, this factor is highly important when determining the wind load of the façade panel.

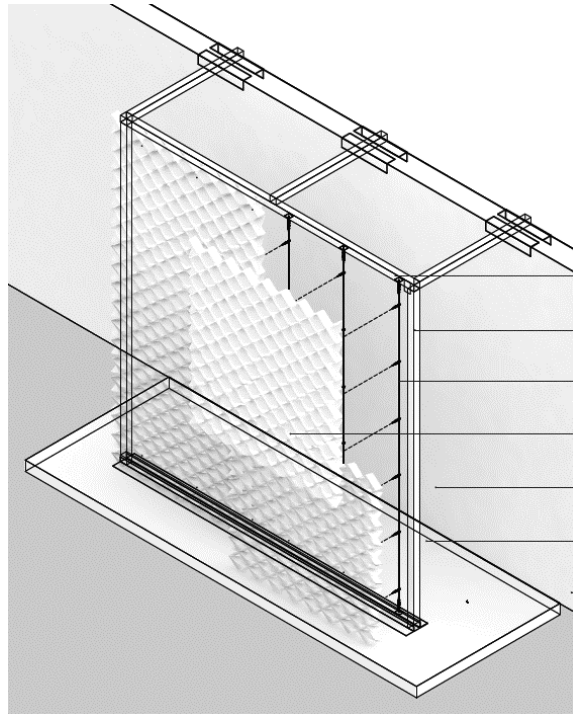


Figure 14: Representation: the Aectual façade with 600 mm gap distance.

Gerhardt and Janser investigated elements with low porosity in a building context (1994). The researchers conducted experiments in the boundary layer wind tunnel to investigate the internal pressure behaviour of ventilated double layer façades. In this case, the outer layer was permeable (**Figure 15**). However, this research is mainly based on façade panels of very low porosities (0.5% -1%) and will not be representative for this actual case.

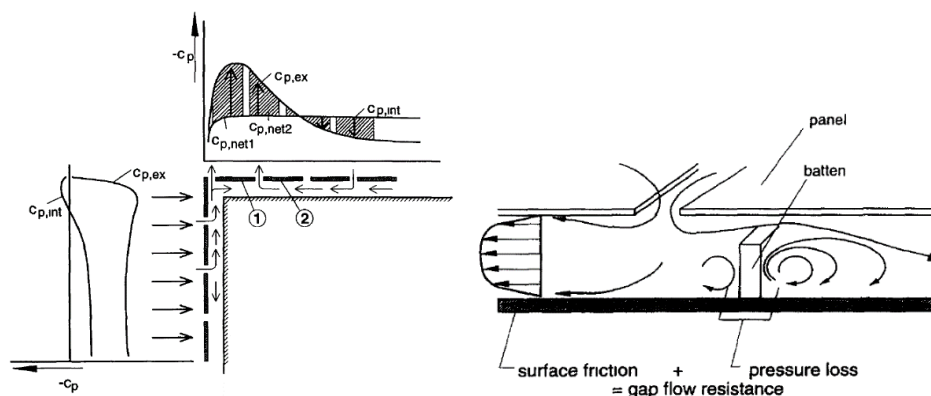


Figure 15: Pressure equalization in the gap width (Gerhardt & Janser, 1994).

There is one research on cladding elements with high porosity, which reconsiders its installation context (Kemper and Feldmann 2012). This research shows that the gap distance, between an inner closed façade and an outer permeable skin, influence the wind load. The researchers found out that with increasing porosity, the wind load on the outer skin decreases while the peak load for the inner skin increases. Also, the wind load of the permeable skin is slightly higher towards the edges. With large-scale and in situ wind tunnel experiments, Kemper and Feldman formulated wind load assumptions on a permeable mesh as a sole cladding layer and a mesh in front of a closed inner wall as can be found in **Figure 113** & **Figure 114**. Kemper & Feldmann stated that the highest negative wind pressure at the closed inner façade of the windward wind parallel edge is noticeably lower due to the existence of the permeable skin. This effect becomes clearer with increasing gap distance. However, the previous study is based on a thin steel wire mesh and can't be directly used for the 3D printed façade panel. This effect becomes clearer with increasing gap distances (Kemper and Feldmann 2012). A relation of the wind pressure coefficients of the façade panel is made and its degree of porosity and installation context is made using the graph in **Figure 13** and the wind load assumptions of Kemper and Feldmann. The self-developed wind load assumptions for the Aectual façade could be found in **Figure 115**.

3.1.4 Other assessment methods

The wind load assumption gives a minimum and maximum range of the relation between the wind load coefficient and the porosity of the façade panel depending on the installation context. These assumptions are based on the combination of wind load studies on wire mesh frames and could differ from the actual wind load. Other assessment methods are available to determine the wind load coefficient of the façade and are described below:

Computational fluid dynamics (CFD)

Due to its parametric design, the geometry of the façade could be different for each project. An idea was to investigate the possibility with the help of computational fluid dynamics (CFD) on the computer. The final element modelling software simulates a virtual wind tunnel where the façade is exposed to a wind flow. The wind pressure could be compared between different designs without having the panels printed and using real wind flows. However, using a virtual wind tunnel with CFD to calculate the wind pressure on building applications is still not common and drastically depends on the computational power of the software and skill of the user. The CFD-model, thereafter, must always be validated by a wind tunnel test or by in situ wind load measurements.

In situ wind measurements

An in-situ wind measurement could be done at on site where the mock-up of the façade panel is installed. Pressure sensors could be placed on the façade to measure the wind pressure. Wind speed and direction data could be obtained from the nearest weather station and based on the information received, a calibrated wind force coefficient could be formulated for the façade panel. The disadvantage of this method is that these coefficients are only applicable for the investigated the design mock-up and could not be representative for different designs of the 3D printed panel. Besides that, the influence of the whole façade is not considered since only one module is installed. More disadvantages are that the in-situ wind measurements are expensive, laboriously, time-consuming and highly dependent on the weather conditions.

Wind tunnel measurements

A more controlled and repeatable method to analyse the wind load on the permeable second skin façade is using a wind tunnel. Within the tunnel, the wind velocity could be controlled, and the correct turbulence could be received. Real and small-scale models could be placed within the tunnel. By using different scale models, the effect of the porosity on the wind pressure could be determined. The disadvantage of this method is that it is an expensive procedure and there is a limited amount of scale models that can be used.

3.2 Temperature development

The change of temperature within the material is directly considered as a risk. However, it is important to understand the mechanical behaviour of the façade under thermal effects, which will be discussed in the following sections. The Aectual façade will be exposed to solar radiation when installing outdoor. The polymer will absorb energy by the solar radiation, leading to a rise in the material's temperature. A rise of this temperature could lead to material dimensional changes of the geometry of the panel such as expansion or bowing as illustrated in **Figure 16**. Thermal stresses could arise when these dimensional changes are restricted (Rabinovitch Elvira B., Quisenberry Joseph G., and Summers James W. 2004).

The amount of heat build-up in the façade panel depends on several material properties such as the specific heat, the panel's thickness, the coefficient of thermal expansion, the density at the colour. Normally, the darker the colour the more solar radiation is absorbed and the higher the energy heat build-up is within the material. The specific heat capacity is the amount of heat that is required to increase the temperature of 1 *gram* of the material with 1°C. In this study a heat transient analysis has been developed, to determine the temperature within several points of the panel's cross-section.

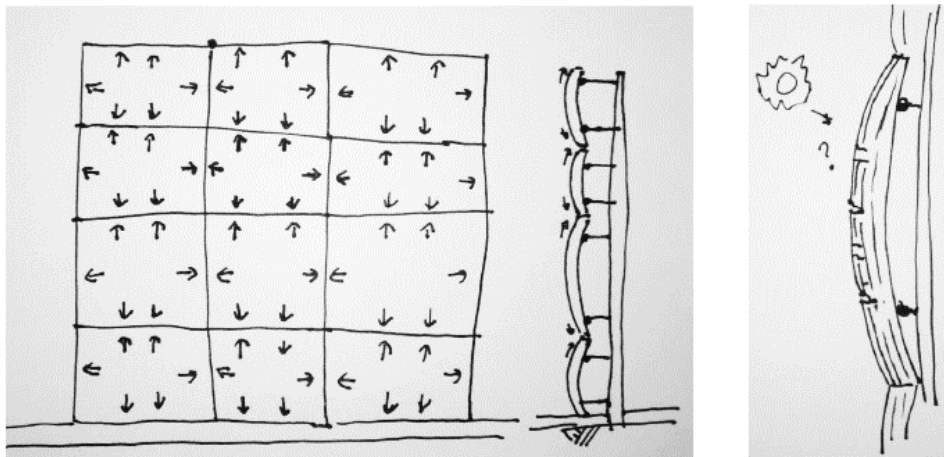


Figure 16: Sketch: Thermal expansion and bowing of the façade panels.

3.2.1 Heat transient analysis

The heat flux through the façade panel is calculated using a heat transient analysis in 2D, to obtain the temperature difference (ΔT) between inner and outer side of the façade element. This model describes the temperature propagation in 2D with taking account the material properties as:

- The absorption coefficient of the outer surface layer, a_z (—)
- Heat conductivity coefficient of the material, λ ($\frac{W}{mK}$)
- The thickness of the panel, d (mm)
- The specific heat of the material, c ($\frac{J}{kgK}$)
- Area of the panel, A (mm²)
- The thermal expansion coefficient of the material, α ($\frac{m}{mK}$)

The heat flows used in the heat transient analysis are the absorption of the income solar radiation, convection, conduction and radiation. The solar radiation (Q_s) is the income direct radiation on the panel. Part of this energy is absorbed by the body as heat (Q_a) and of it is reflected (Q_r). An energy balance based on the sun's energy could be constructed:

$$Q_s = Q_r + Q_a$$

The solar radiation on the façade panel depends on the wall orientation, latitude, time of year, and incident angle. To observe the temperature transition within the material the cross-section is divided into various layers. Each layer has an own temperature with respect to time depending on the heat flows. To simplify the calculations the following assumptions are made for this analysis:

- Only direct solar radiation will be absorbed by the panel, indirect solar radiation will be not taken into account.
- The cross-section of the panel is divided into three parts.
- The complex geometry of the façade panel will be modelled as a simplified solid panel with a constant thickness of 70 mm.
- Only direct and diffuse sunlight will be included in the model, indirect sunlight is not considered.

The obtained energy of solar radiation is formulated with the following function:

$$E_{sol} = q_z a_z \left[\frac{W}{m^2} \right]$$

Where a_z is the absorption coefficient of the material and depends mostly on its colour. When the panel is of a black coloured material, the absorption coefficient is taken as $a_z = 0.9$. Conventional energy transfer occurs between the temperature of the ambient air (T_{extern}) and the material's surface (T_0) and is formulated as:

$$E_{conv} = h(T_0 - T_{extern}) \left[\frac{W}{m^2} \right]$$

Where h is the heat transfer coefficient and depends on environmental factors. TNO states that the heat transfer coefficient of an exterior surface of an outer wall is $24 W/(m^2K)$ and for an interior surface the $h = 4 W/(m^2K)$. The heat transfer through radiation occurs by long energy waves between the material and the atmosphere. (Tumbuan & Cauberg 2005) determined a constant value for the material radiation in the Netherlands of $E_{rad} = 100 W/m^2$. However, in this case, the of energy transfer radiation is based on the next formula with respect to the ambient air temperature:

$$E_{rad} = \sigma T_{extern}^4 (1 - a - b\sqrt{p}) \left[\frac{W}{m^2} \right]$$

Where σ is the Stefan-Boltzmann constant of $\sigma = 5.67 * 10^{-8} W/(m^2 K^4)$. The constants a and b are empirically determined environmental factors and are set for a sea climate: $a = 0.55$ and $b = 0.0056$. The factor p is the partial water damp stress, a value of moisture in the air is taken as $2340 Pa$. With the material properties and heat flows a heat transient analysis has been developed to determine the material's temperature at a certain point. The following formulas had been used to simulate the heat transfer and temperature difference between points:

$$E_1 = \frac{\lambda_1}{d_1} (T_0 - T_1)$$

$$E_2 = \frac{\lambda_2}{d_2} (T_1 - T_2)$$

$$E_{in} = E_{in} + E_{conc} + E_{rad} + E_{cond}$$

$$\Delta T_0 = \frac{E_{in} t}{A d_1 \rho_1 c_1} [^{\circ}C]$$

$$\Delta T_1 = \frac{E_1 t}{A d_2 \rho_2 c_2} [^{\circ}\text{C}]$$

In **Table 2** the input parameters of the 2D heat transient analysis could be seen. The material properties are based on the thermal properties of polypropylene since this is the base material of the 3D printed façade panel (Sahin and Yayla 2005).

Heat transient analysis			
Absorption coefficient	a_z	0.9	-
Heat conductivity coefficient layer 1/3	λ_t	0.22	W/mK
Heat conductivity coefficient layer 2/3	λ_a	0.22	W/mK
Heat conductivity coefficient layer 3/3	λ_s	0.22	W/mK
Convection coefficient external	α_e	24	W/m ² K
Convention coefficient internal	α_i	4 or 24	W/m ² K
Thickness layer 1	d_t	0.0233	m
Thickness layer 2	d_s	0.0233	m
Thickness layer 3	d_a	0.0233	m
Density layer 1	ρ_t	1488	kg/m ³
Density layer 2	ρ_s	1488	kg/m ³
Density layer 3	ρ_a	1488	kg/m ³
Specific heat layer 1	c_t	1542	J/kgK
Specific heat layer 2	c_a	1542	J/kgK
Specific heat layer 3	c_s	1542	J/kgK
Panel surface area	A	1	m ²
Temperature expansion coefficient	α	35	10 ⁻⁶ , m/(mK)

Table 2: Input parameters for the heat transient analysis.

3.3.2 Results of the heat transient analysis

The heat transient analysis is conducted to understand the temperature propagation of the material due to solar radiation. For this analysis, the two scenarios are simulated with the outer surface temperature (T_o) and the inner temperature (T_i) over the hottest day of 2017. Weather data is obtained by the KNMI. The first scenario is when the façade panel is used as a rain screen closely attached to the inner wall. The temperature progradation is projected in **Figure 17**. The second scenario is when the panel is installed as a free standing (second skin). This second scenario is projected in **Figure 18**.

Both outer surfaces are in direct contact with the ambient air and thereby the heat flow by convection on both sides are set equal. The inner conventional heat transfer, however, differs between the two cases due to the different installation context.

The results of the heat transient analysis show that both scenarios have the same maximum temperature of 59°C for the outer layer of the façade panel, which is exposed to solar radiation. When observing the temperature difference, the first scenario where the panel is used as a rain screen has the highest temperature difference between the outer and inner layer with a $\Delta T = 49^{\circ}\text{C}$.

Comparing the results of the heat transient analysis and temperatures of the 'Eurocode 1: Actions on structures - Part 1-5: General actions - Thermal actions' both the calculated T_{max} and ΔT are calculated much lower than the standard (Nederlands Normalisatie-insituut 2011). The maximum temperatures obtained from the heat transient analysis is $T_{max} = 59^{\circ}\text{C}$, while the standard has a maximum surface temperature of $T_{max} = 75^{\circ}\text{C}$. The maximum difference temperature obtained from the self-developed analysis is $\Delta T = 49^{\circ}\text{C}$, while the standard has a maximum temperature difference of $\Delta T = T_{max} - T_{in} = 58^{\circ}\text{C}$.

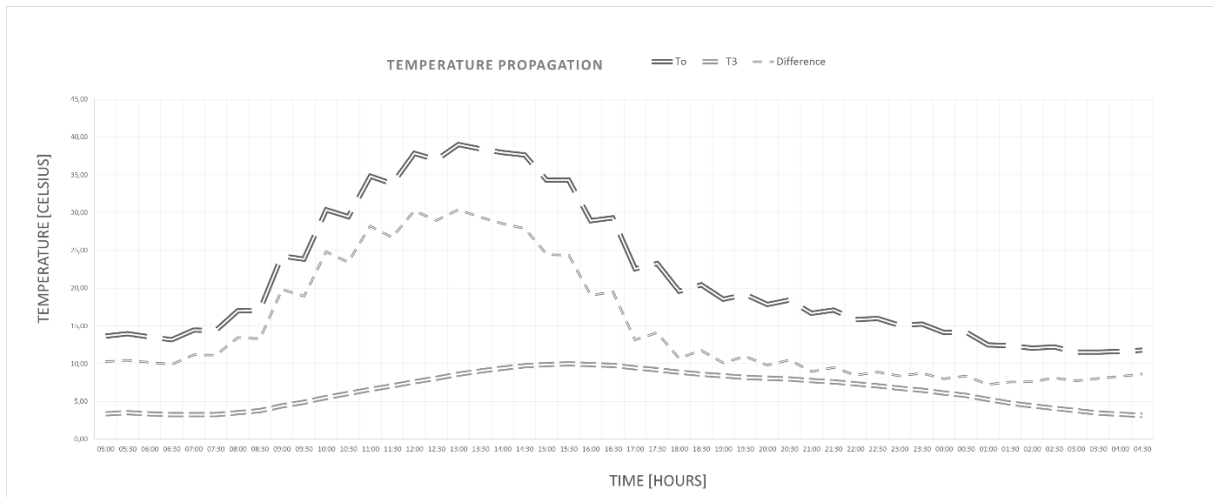


Figure 17: Temperature propagation of the Aectual façade: rain cladding.

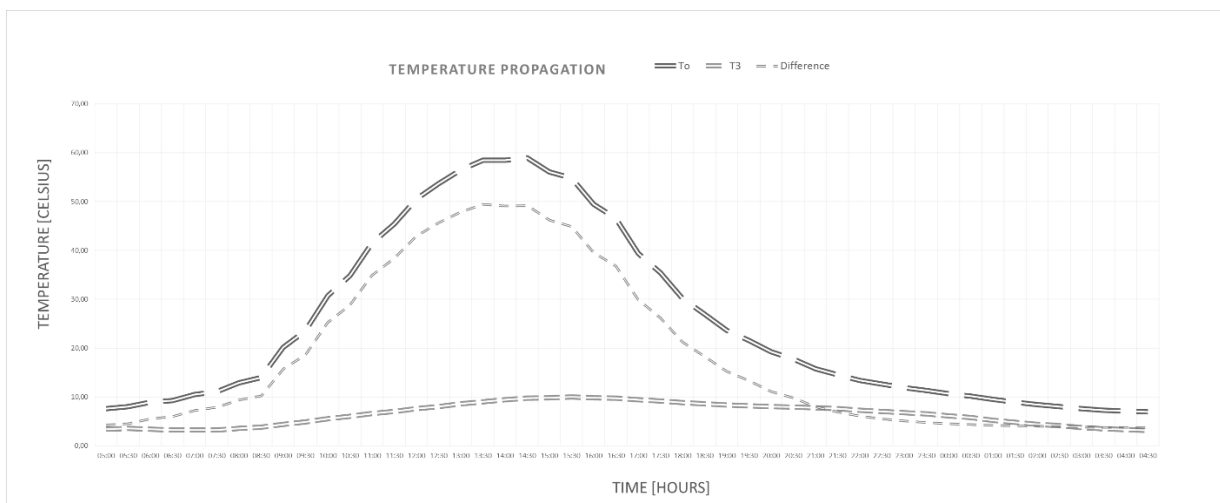


Figure 18: Temperature propagation of the Aectual façade: second skin.

3.3.3 Evaluation of the heat transient analysis

From the data obtained from self-developed 2D heat transient analysis, it can be concluded that:

- The maximum temperature and the temperature difference between the outer and the inner surface layer are calculated lower than according to the international standards.
- The 2D heat transient analysis is based on the solid façade panel, while the Aectual façade consists of complex surfaces leading to more air contact. This suggests that more conventional heat transfer will occur and thereby a decrease in the material's heat build-up leading to a lower T_{max} and ΔT .
- As can be seen in **Table 18: Summary: Point temperatures of the façade element over time, 1-June-2017, the Netherlands.**, the heat flow moves slowly from the exposed side to the other side. The based material, polypropylene, is known to its low conductivity, which explains the low temperatures at the back of the panel.

3.4 Thermal shock resistance

When a façade panel is exposed to solar radiation, the material's surface temperature could rise to 75°C depending on the material and colour, according to NEN-EN 1991-1-5 (Nederlands Normalisatie-instituut 2011). When rapidly cooled down, for example by a sudden rainstorm, thermal changes within the material could produce internally stresses leading to cracks, delamination or even fracture. This phenomenon is called thermal shock and is most common with brittle structures such as glass and ceramics. The thermal shock fracture resistance is the maximum change in surface temperature which a material can sustain without cracking (Lu and Fleck 1998).

In material ageing, the thermal shock resistance is tested by a number of cycles of heating and cooling of a material specimen, while focussing on the change of material properties as colour and strength. In this part, the thermal shock part focusses on the temperature difference, a part of the façade can resist without failure. According to Lu and Fleck, thermal shock fracture depends on multiple material properties like thermal expansion coefficient (α), thermal conductivity (k), thermal diffusivity (κ), elastic modulus (E), fracture toughness (K_{IC}), tensile strength (σ_f) and addition parameters like heat transfer coefficient (h), specimen size (H) and duration of the thermal shock (T). The most commonly used parameter is the formula who captures the ignition of the thermal shock cracking (Lu and Fleck 1998): $\sigma_f / (E\alpha)$.

When comparing the thermal shock resistance of ceramics, metals and polymers, it can be stated that ceramics have the lowest thermal shock resistance. Metals, however, have a better resistance against thermal shock due to their high fracture toughness. The low Young's modulus of polymers, compared to the other materials, makes their thermal shock resistance reasonable and lies between the range the ceramics and metals (Lu & Fleck, 1998). However, 3D printed polymer behaves brittly, when it is aged for a period of time. This brittleness could be due to the high percentage of glass fibres and talc, which were added to increase its strength and the printability. A small experiment is conducted with samples of the 3D printed façade as seen below.



Figure 19: Thermal shock resistance test specimens.

Five corner samples of the façade panel, as can be seen in **Figure 19**, are heated up with a speed of 50°C/hour each with various temperature 80°C-140°C for 60 minutes in a Heraeus controlled oven. After heating up the samples were rapidly cooled down with water and visually inspected for cracks, delamination and fractures. At the temperature of 140°C, the surface of the specimen became glossy, given an indication of melting. After cooling down at this temperature the first print layer starts to delaminate minimally. The experiment stopped at this temperature since a higher temperature was not reasonable and to avoid the material to melt down. In general, no extreme cracks, delamination or fracture was seen on the surface of the material and besides that also no noticeable warping and bending were established.

The adjusted thermal shock test was a broadening experiment of the thermal shock behaviour with samples of different geometries. When conducting a more reproducible and repeatable test the samples should be of the same geometry and the sample count should be higher.

3.5 Fire resistance

Compared to brick and concrete, plastic is more likely to ignite at a lower temperature. When developing a façade panel made of the thermoplastic polymer the fire resistance should be considered. The fire resistance of a product is the duration for which a passive product can withstand a standard fire resistance test. Plastics, such as polypropylene, exposed to open flames could burn fast. When using the material as a building application, it should have a sufficient fire resistance or treated with effective fire retardants, to slow down the rate of fire spread (Shields & Zhang, 1999).

An example where the fire resistance of cladding was not sufficient was the Grenfell Tower case. On 14th June of 2017, a huge fire started in 27-story tower block in West London. Fire safety experts have indicated the cladding on the building as a possible reason why the fire spread so quickly. Footage has shown the fire travelling up one side of the building, before engulfing the entire block. The cladding had a metal outer coating and an expanded foam interior. This polyethene core was less fireproof than other alternatives and quickly spread the fire over the entire building. This fire caused 72 deaths and 70 injured (Van Leeuwen, 2018).

3.5.1 Adjusted fire test

It is important to study the fire resistance of the material when using it for building applications. To observe the fire behaviour a broadening experiment has been done. An Aectual panel is exposed to a small fire outdoor in the open wind as can be seen in **Figure 20**.

When a fire object was placed under the façade panel, the flames spread immediately. Even when the fire object was replaced away from the façade panel, the fire continued to spread over the whole façade. When looking closely small flame droplets appeared from the burned area. The dark smoke arises from the fire indicates several (toxic) gasses. This broadening fire test points out that more research and measurements should be done on the fire resistance of the 3D printed façade panel.

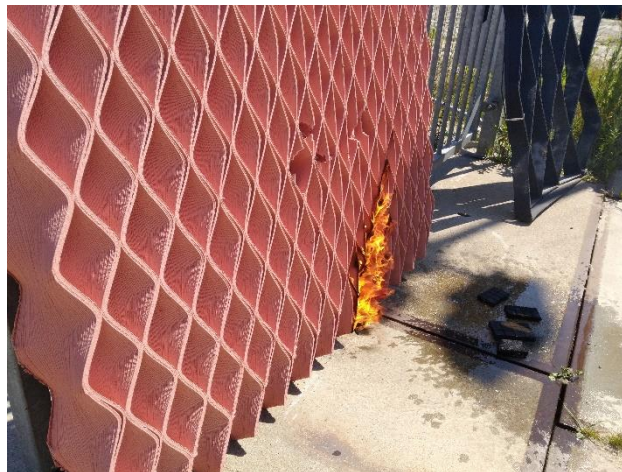


Figure 20: Aectual façade panel during a fire resistance test.

3.5.2 Fire safety test methods

The following fire test methods are specified in relation to the object's reaction to fire classification according to the EN 13501-1. There are several test methods and are summed up in this paragraph:

- Non-combustibility test (NEN-EN-ISO 1182): This test determines in what order the panel will contribute to a fire.
- The heat of combustion test (NEN-EN-ISO1716): This test evaluates the maximum total heat release of the panel when it is completely burned.

- Ignitability test (NEN-EN-ISO 11925-2): This test determines the ignitability of the cladding when exposed under a relatively small fire source.
- Single burning item test (NEN-EN-ISO 13823): This test evaluates the potential contribution of the façade panel when the material has started to burn, within a pre-set fire situation.

As a starting point, a Single burning item test is advised from the standard EN 13823 and is based on the NEN-EN-ISO 13501-1+A1. In this test the material will be heated up by a 30 kW flame for 20 minutes to obtain the following parameters:

- Fire Growth Rate (Figra) [W/s]
- Total Heat Release (THR) [MJ]
- Smoke Growth Rate (Smogra) [m^2/s^2]
- Total Smoke Production (TSP) [m^2]
- Falling burning drops

The goals that Aectual made for the façade panel, based on the fire resistance, are composed in three factors. Regarding the fire development, the requirement is level D. For the smoke development, the minimum level is S2 and for the fire extension of the minimum is 30 min WBDBO (Weerstand tegen Brand- Doorslag en Brand-Overslag).

3.5.3 Increasing the fire resistance

There are several ways to improve the fire resistance of the façade panel. Adding a fire retardant to the print compound could down the increased burning of the material (Zhang and Horrocks 2003). It is a logical step since the 3D print company Aectual mostly mixes the plastic base material with different additives to establish a colour or a better print quality. A risk of this solution is that the fire retardants could affect the mechanical properties of the material. Also, the vulnerability of ultraviolet degradation could be change when adding these additives to the compound. The fire retardants contain chlorine and bromide and could be a health hazard when printing at a temperature of 180°C when toxic gasses could occur. It should be considered when adding fire retardants, the material is safe to print without any health hazards.

Applying a coating to the façade panel could be another solution. The advantage is that comparing adding additives, it will affect the material properties less and is independent of the printing process. A disadvantage is that the surface of the façade panel is quite rough. It is more difficult to spray the coating on the entire 3D print façade than a façade with a smooth and more reachable surface. To be sure that the durability of the adhesion of the coating and façade panel for a particulate service life a weathering test should be done. In this test, the quality and adhesion of the coating will be tested under the influence of different weathering factors like radiation, temperature and moisture. Also, a scratching test should be done to test the coating on vandalism, since the coating will be removed from the vulnerable plastic material.

The fire resistance is a potential risk for the Aectual façade panel since the product is polypropylene-based. Adding fire retardants to the material could be a solution, however, it should be considered that the material properties could change due to the change in the print compound. Besides that, the new extruded material should be tested and checked if it is still safely printable without releasing any toxic gasses leading to health hazards.

During this research, Aectual is experimenting with stone-like materials which could be promising for improving the fire resistance of the material. Applying a fire-resistant coating could be a solution, however, the adhesion and quality of the coating should be tested on its resistance to different weathering conditions and vandalism.

3.6 Thermal expansion and bowing

This paragraph gives a short description of the behaviour of the façade panel when exposed to thermal effects. The façade panel in this paragraph is replaced with a beam, to simplify this study. Increase in temperature could be the consequence of the solar radiation or a nearby fire source. Two mechanical behaviours due to heating will be discussed in this section: thermal expansion, this phenomenon mostly happens due to when an object is heated under uniform heating and thermal bowing when the beam is heated non-uniformly.

3.6.1 Thermal expansion

When a beam is heated uniformly, this induces a thermal expansion strain (ϵ_T) in most building materials. This strain is given in the formula:

$$\epsilon_T = \alpha \Delta T$$

The coefficient of thermal expansion, α (K^{-1}), is the relative expansion divided by the change in temperature and is mostly temperature-dependent. When a rise in uniform temperature exhibits throughout the material cross-section, ΔT , of a simply supported beam without axial restraints, expansion or increase in length occurs as shown in below **Figure 21**.

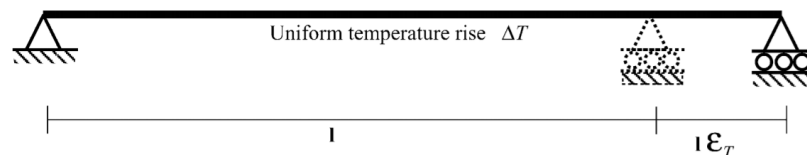


Figure 21: Uniform heating of a simply supported beam (Usmani ea., 2001).

Therefore, the total strain (say ϵ_T) is equal to the thermal strain and there is no mechanical strain (say ϵ_M) which means that no stresses develop in the beam

$$\Delta L = \epsilon_T * L$$

It is interesting to determine at which temperature the façade is expanded so far that the material will yield, plastically deform, and will be non-reversible. It is a complex process since the material properties of the thermoplastic polymer are temperature dependent.

$$\Delta T_y = \frac{\epsilon_y(T)}{\alpha(T)}$$

Thermal expansion against rigid lateral restraints

When the façade panel is installed on the frame and locked between the frames, the panel will be restrained at its edges during thermal expansion. In this case, the total strain ϵ_t is zero since the thermal expansion is cancelled out by equal and opposite contraction caused by the restraining force P . There now exists a uniform axial stress σ in the beam equal to $E\epsilon_m$. The magnitude of the restraining force P and is pointed out in **Figure 22**.

$$P = -EA\epsilon_T = -EA\alpha\Delta T$$

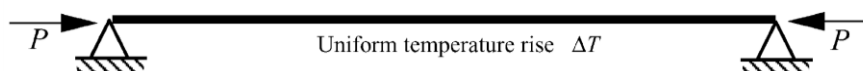


Figure 22: Axially restrained beam subjected to uniform heating (Usmani ea., 2001).

So, if the temperature rises without stopping, then there will be two basic responses, depending upon the slenderness of the beam. The axial stress of the beam will reach the yield stress σ_y of the material. Mostly when the beam is stocky. When the material has an elastic–plastic stress–strain relationship, then the beam will continue to yield without any further increase in stress. The temperature when this phenomenon occur is the yield temperature, ΔT_y (Timoshenko & Goodier, 1960).

$$\Delta T_y = \frac{\sigma_y}{E\alpha} \text{ or } \sigma_x = \alpha\Delta TE$$

The second response, when the beam is rather slender, it will buckle before the material reaches its yield stress. The Euler buckling load P_{cr} for a beam/column.

$$P_{cr} = \frac{\pi^2 EI}{l^2}$$

Equating this to the restraining force P led to the following equation:

$$EA\alpha\Delta T = \frac{\pi^2 EI}{l^2}$$

which led to a critical buckling temperature of,

$$\Delta T_{cr} = \frac{\pi^2}{\alpha} \left(\frac{r}{l}\right)^2 = \left(\frac{\pi^2}{\alpha\lambda^2}\right)$$

Where r is the radius of gyration and l is the slenderness ratio (l/r). This expression is valid when it is assumed that the material is elastic, and no thermal degradation occurs during the heating. A rise in thermal expansion will increase the deflection of the beam, δ , as illustrated in **Figure 23**.

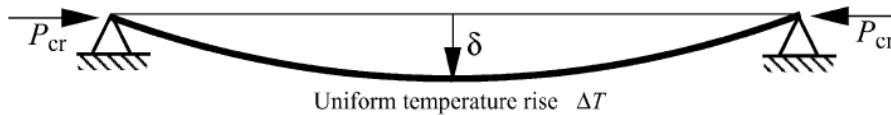


Figure 23: Buckling of an axially restrained beam subjected to uniform heating (Usmani et al., 2001).

From the above cases, it could be seen that the longer the beam is, the slender it becomes, the lower the critical buckling temperature.

$$\Delta T_b = \frac{\pi^2 I}{l^2 A \alpha}$$

In summary, yielding or buckling may occur, based upon the material properties, the degree of heating in temperatures and the slenderness of the beam itself. A combination of the yield and buckling makes simulating the response complex. Not taking account of the 3-dimensional geometry of the façade element.

Thermal expansion against finite lateral restraints

In the previous section, the axial restraints was assumed to be perfectly rigid. This is, just like the simple beam, one of the limits and practically impossible to achieve in real structures which offer only finite restraints. The figure below shows such a beam restrained axially by a translational

spring of stiffness k_t . The compressive axial stress developed by thermal expansion is given by the formula:

$$\sigma = \frac{E\alpha\Delta T}{1 + \frac{EA}{k_t L}}$$

and critical buckling temperature is now given by:

$$\Delta T_{cr} = \frac{\pi^2}{\alpha\lambda^2} \left(1 + \frac{EA}{k_t L}\right)$$

Buckling and post-buckling phenomena should be observable at high temperatures in structures with translational restraint stiffness, k_t , which are quite comparable with the axial stiffness of the member, EA/l , as shown in **Figure 24**.

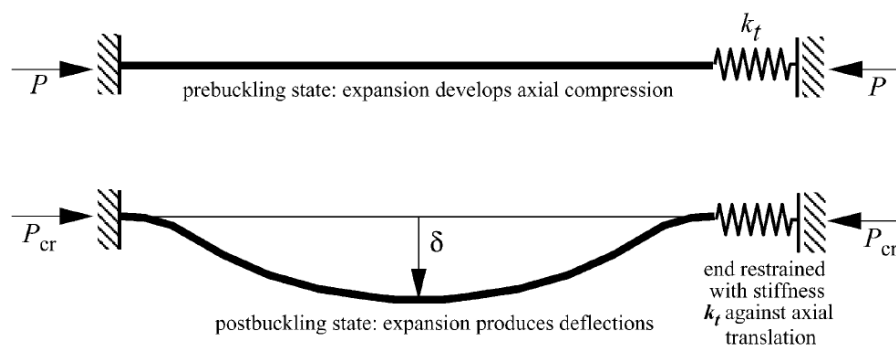


Figure 24: Buckling of an axially restrained beam subjected to uniform heating (Usmani et al., 2001).

Bearing in mind that the axial stiffness of the member EA/l is reduced by heating through the reduction in E .

3.6.2 Thermal bowing

Outdoor exposed thermoplastic objects can be subjected to very high-temperature gradients due to the high heat resistance of the thermoplastic polymer as found in the temperature development study in the previous section. Therefore, the surfaces exposed to heat (by the sun or fire) will be at a much higher temperature than the surfaces on the cooler side of the object. Hereby, to retain the simplicity a linear heat transient propagation is chosen within this thermal study. The non-uniform heating causes the inner surfaces to expand much more than the outer surfaces inducing bending in the member. This effect is called thermal bowing and is one of the main reasons for the deformations of other materials in building applications like concrete slabs and masonry walls during fires. Simply supported beam subjected to a uniform thermal gradient is seen in **Figure 25**.

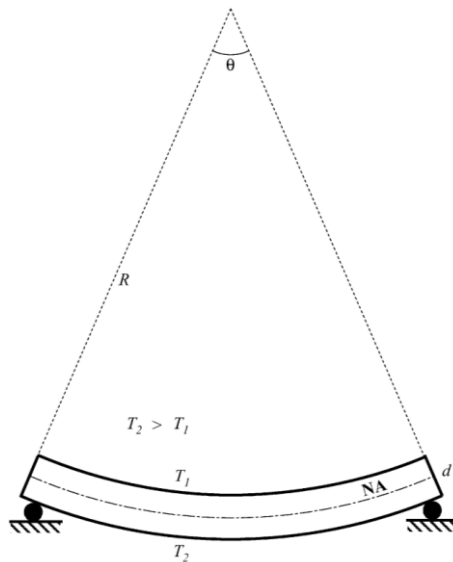


Figure 25: Simply supported beam subjected to non-uniform heating (Usmani et al., 2001).

Figure 25 shows a beam subjected to a uniform temperature gradient through its depth, d , along with its whole with its length, l . Assuming the beam is simply supported, we can derive the following relationships

1. The thermal gradient T_y over the depth is:

$$T_y = \frac{T_2 - T_1}{d}$$

2. A uniform curvature θ is induced along the length because of the thermal gradient.

$$\theta = \alpha T_y$$

3. Due to the curvature of the beam, the horizontal distance between the ends of the panel will decrease.
4. If this reduction is interpreted as a contraction inner strain ϵ_i , then the value of this strain can be calculated from analysing the figure. The outer strain, ϵ_o is the reverse strain of the inner-strain:

$$\epsilon_i = 1 - \frac{\sin\left(\frac{l\phi}{2}\right)}{\frac{l\phi}{2}}$$

With the following formulas known at which thermal gradient T_y , the outer strain, ϵ_o , will be that reduced that the strain will be irreversible:

$$\epsilon_i = 1 - \frac{\sin\left(\frac{l(T_2 - T_1)}{2d}\right)}{\frac{l(T_2 - T_1)}{2d}} < \epsilon_{irreversible}$$

Considering a the laterally restrained beam, of a uniform thermal gradient, T_y , is applied to this beam, then the result is a thermally induced tension in the façade panel and corresponding

reactions at the edges as shown in **Figure 26**. This is clearly caused by the restraint to end translation against the contraction strain, ϵ_f , induced by the thermal gradient.

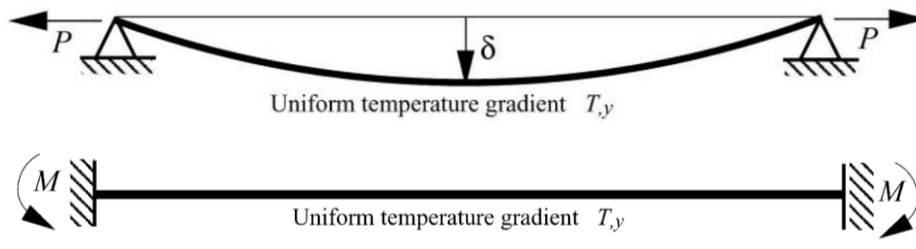


Figure 26: Laterally restrained beam subjected to non-uniform heating (Usmani ea., 2001).

A uniform curvature occurs in a simply supported beam with end rotational restrains, subjected to gradient uniformly T_y . The beam remains straight with a constant moment $M = EI\phi$ along its length. So, the maximum bending strength during a uniform temperature gradient is calculated by:

$$\sigma_{max} = \frac{Md}{2I} = \frac{E\phi d}{2} = \frac{E(T_2 - T_1)}{2}$$

$$T_2 - T_1 = \frac{2\sigma_{max}}{E}$$

From the above-mentioned formulas, when restraining the beam, thermal stresses could occur within the beam. As discussed earlier for lateral restraint beam, perfect rotational restraint is also not very easily achieved in real structures. **Figure 27** shows a beam restrained rotationally at the ends by rotational springs of stiffness k_r .

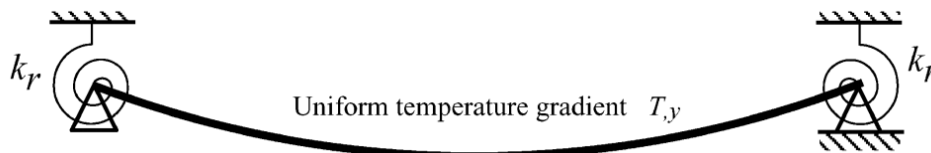


Figure 27: Beam with finite rotational restraint with non-uniform heating (Usmani ea., 2001).

In this case, the restraining moment in the springs because of a uniform thermal gradient T_y can be found to be:

$$M_k = \frac{EI\alpha T_y}{1 + \frac{2EI}{k_r l}}$$

This equation implies that if the rotational restraint stiffness is equal to the rotational stiffness of the beam EI/l , then the moment it attracts will be about a third of a fixed support moment:

$$\sigma_{max} = \frac{M_k d}{6I} \quad \text{and} \quad (T_2 - T_1) = \frac{\sigma_{max} \left(2 + \frac{4EI}{k_r l}\right)}{\alpha E}$$

3.7 Frost resistance

Due to the long stretchable molecule chains, thermoplastic polymers owe their strength and its ductility. The stretching molecules could absorb energy individually. Collectively, they spread the income stress from the point of impact and thereby preventing fracture or material failure. This “stretching” is only possible if the molecules could move past each other. If this motion is restricted, the absorbed energy concentration gets too great, cracks will occur and eventually break (Dunn 2009).

As mentioned, an important parameter in the molecules’ ability to spread is temperature. The “glass transition temperature” (T_g), is the point below which an amorphous solid goes from being ductile to brittle. Polypropylene has a T_g of between -20°C and 0°C , so it can easily lose break at low temperatures. When the façade panel is assembled outdoor, it will endure several weather conditions such as frost. It is well known that the thermoplastic polymer, polypropylene (PP), has a low impact strength at low temperatures (Jafari and Gupta 2000). Since the ambient air, of the Dutch climate, could decrease below the 0°C , this issue could be a potential risk during the winter.

A frost experiment has been conducted to observe the impact strength of the polypropylene-based material at negative temperatures with a hammering test. Parts of the façade panel were exposed to -20°C for 48 hours in a laboratory freezer at the faculty of Civil Engineering (TU Delft). After removal, both exposed and unexposed parts were smashed with a hammer to give an indication about material’s brittleness. After the test, it was found out that both sets of samples broke in a brittle manner. However, no extreme difference has been noticed since the material was already brittle.

The brittleness of the polypropylene-based test sample could have two causes. The first cause is the presence of talc and glass fibres, leading to a stiffer, but brittle material. The second cause is the manufacturing method. The fused deposition modelling-based technique, where the material is heated up and extruded at high levels could led to embrittlement of the extruded material (Wu ea., 2016).

Investigating the impact strength of the 3D printed material should be done in a more reproducible and repeatability manner to understand its vulnerability to frost. A standardized Charpy impact test setup within a controllable climate chamber is advised for further research. With this test, the impact strength of **the** Aectual façade could be determined under different temperatures.

3.8 Summary

A broadening research has been conducted on the potential environmental risks of the Aectual façade. Due to the limited time and the ongoing product development of this cladding, no clear answers or solution could be given for every potential risk. Future researchers, designers and engineers, who will work on this innovative product, could use the following information as a starting point for further product research and development:

The purpose of the wind load study in the broadening research is to have a better understanding what the influence of the geometrical characteristics of the façade panel is on its wind pressure coefficient when used in second skin application. The following aspects could be concluded based on the literature study:

- With increasing porosity of the cladding and increasing distance between the inner closed wall and the permeable second skin could be linked with a decrease of the wind pressure coefficient of the second skin panel.

- For the permeable second skin, the wind load pressure will be slightly higher towards the edges of the building.
- The geometry, including the overall thickness, of the second skin panel will have an influence on the friction drag coefficient of the whole panel.
- Using Computational Dynamic Fluid (CDF) Modelling to study the wind load coefficients of the façades could be an efficient way to compare different façade panels based on their geometrical characteristics. However, using CFD requires much time and skill of the user and the application must be verified with an actual in situ wind test or a wind tunnel test.
- Wind load assumptions were made based on literature study in Figure 113. To obtain the actual design wind pressure coefficients, a wind tunnel test is suggested to compare several façade designs.

The study on the fire resistance of the 3D printed thermoplastic polymer for the building façade consists of the following conclusions:

- The thermoplastic material of the 3D printed façade is polypropylene-based, which is known to be inherently flammable.
- An adjusted fire test is done on the Aectual façade panel and it is observed that the material burns immediately when it is in contact with a fire source. The fire spreads continued within the panel even when the fire source is removed. Flame droplets and dark smoke arise from the burning thermoplastic material.
- To record the fire resistance properties and define its fire safety class according to the building codes a Single burning item (SBI) test is suggested. The test provides fire safety properties to a building object like heat release, fire growth rate and smoke production.
- To increase the fire resistance properties of the façade panel, fire retardants could be added to the print compound. However, it should be noted that these additives may change the durability and mechanical properties of the 3D printed material. According to Aectual, fire retardants like chlorine and bromide should not be used since the materials could release dangerous chemicals during the printing.
- A fire-retardant coating could be applied to the façade panel to increase its fire resistance properties. However, polypropylene is known to have low adhesion properties. When the panel will be used outdoor, a weathering test should be done to test the quality of the adhesion between the coating and the thermoplastic. Sanding the printed material could increase the roughness of the printed material.

A study has been done of the temperature development and its effects on the mechanical properties of the façade panel when used as second skin application:

- According to the 2D heat transient analysis, it was hard to reach the maximum temperature and the maximum temperature difference between the outer and inner surface of the façade panel according to the international standards.
- The 2D heat transient analysis is based on the solid façade panel, while the Aectual façade consists of complex surfaces leading to more air contact. This suggests that more conventional heat transfer will occur and thereby a decrease in the material's heat build-up leading to a lower T_{\max} and ΔT .

- Thermal development of façade panel could lead to structural behaviour as in thermal expansion, thermal bowing or a combination. This behaviour depends on the geometrical, mechanical and thermal properties of the 3D printed material.

Since the material is more brittle than ductile, an experimental and adjusted study of the thermal shock resistance and impact test at low temperatures were done. For the first test, small parts of the actual façade were exposed to high temperatures below the melting point for a duration of time and were cooled rapidly afterwards. For the impact test, several façade parts were cooled below the -20°C for a chosen time duration and tested on their impact strength. Following observations and suggestions were recorded and suggestions:

- No cracks were observed within the material after the rapid cooling. Small delamination was observed within the first printing layers.
- The small test was inconsistent since the specimens were not of the same geometry and it is not recorded what the exact temperature of the material was.
- A thermal shock resistance test is suggested with more cycles, hereby focusing on the durability of the material.
- In combination with the thermal shock resistance test, a hygrothermal test is advised, which includes heating-cooling-wetting cycles and freezing-thawing cycle.
- For frost resistance test, a more standardized test, the Charpy impact test, is advised to determine the impact properties of the material in the combination of change in temperature, time or weathering factors.

PART II
In-Depth Research

Chapter 4

Ultraviolet Degradation

4.1 Introduction

The base material of the first 3D printed façade panel of Aectual is polypropylene (PP) and was chosen due to its availability as recycled material from industrial waste and its low cost. This semi-amorphous thermoplastic polymer is mostly used in industries as a material for packaging, food containers and water pipes. The reason that it is applied to this wide range of products is due to its strength and good thermal, electrical and chemical resistance and its low production costs (Azuma et al. 2009). However, thermoplastic polymers are also known to be vulnerable to outdoor weather conditions. It can be suggested that the sustainability and durability of polymers are depended on their weathering resistance. Weathering is the adverse response of a material or product to climate, causing premature product failure (Atlas, 2017). Therefore, it is important to understand the weather resistance of the 3D printed material during the product development of the Aectual façade.

Weathering whereby polymers degrade could be caused by the action and combination of several factors, including solar ultraviolet (UV) radiation, moisture, air pollutants, oxygen and temperature changes. However, when considering the influence of these factors, at any given temperature and moisture content, the rate of weathering increases with an increase in UV radiation (Oliani and Parra 2009). It could be seen that UV radiation is the main cause of degradation of polymers, which is the outcome of a large-scale of laboratory testing, using ultraviolet test chambers, to determine and compare the weather-resistance of different polymer compounds. Although the most damaging ultraviolet wavelengths are absorbed by the ozone layer, the minimal wavelengths of the income solar radiation are over the 290 nm. These wavelengths are enough to initiate degradation of polymers according to several studies.

As mentioned at the beginning, this thesis is based on the product development of 3D printed façade panel made of a recycled thermoplastic polymer. In the previous chapter, different environmental risks were discussed and should be considered when developing a new building product for outdoor applications. In this in-depth study, the risk of ultraviolet (UV) degradation on the polypropylene compound will be studied with the use of literature study and observations.

4.2 Ultraviolet degradation

When exposed to ultraviolet radiation (UV), thermoplastic polymers may undergo a series of chemical reactions that led to UV degradation. UV degradation is the combined effect of photolysis and photooxidation. Photolysis mostly happens in an inert atmosphere, while photo-oxidation often happens in the presence of air and for polypropylene (PP) the most dominating mechanism (Gijsman, Meijers, and Vitarelli 1999). Photo-oxidation, due to ultraviolet absorption by the polymer, is a sequence of chemical reactions such as crosslinking (Tong and White 1996). Crosslinking is the phenomenon when polymer chain links to another. Besides crosslinking, photo-oxidation led to the formation of radicals that induce oxidation of the material as can be seen in **Figure 28** (left). These reactions led to changes in molecular weight and the formation of chemical groups like carbonyl, carboxylic acids and hydroperoxides, which have consequences on the materials properties as loss of tensile strength (**Figure 28**, right), increased and discolouration and formation of surface cracks (Fechine and Demarquette 2008). These material changes could develop in a stage where a premature failure of the building product could occur.

In previous literature, degradation studies were carried out by accelerated weathering. After weathering, the mechanical properties are evaluated and it has been found that both phosphate glass fibre/PP composites degrade with increased ageing time (T. H. Shubhra et al. 2011) as can be seen in **Figure 28** (right).

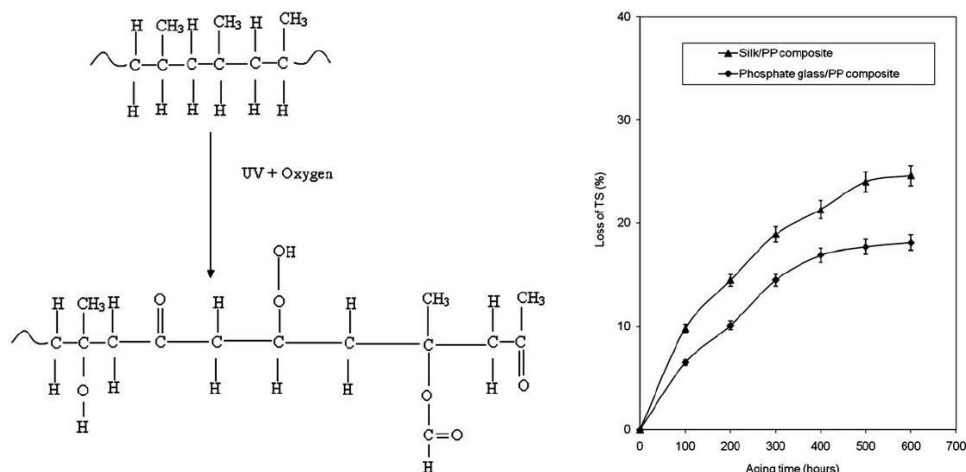


Figure 28: Degradation reaction of PP by UV radiation in presence of oxygen (left) Loss of tensile strength of both composites due to simulating weathering (right) (T. H. Shubhra et al. 2011).

4.3 The influence of additives

As described in the introduction, polypropylene (PP) is widely used due to its easy processability and low production cost. However, its application has been somewhat limited due to its relatively poor stiffness. Adding additives has been considered a useful way to improve the stiffness, colour and durability. However, these additives also will have an influence on the durability and sensibility of the material and have been studied by many researchers. Below, some additives, relating to the compound used for printing, are discussed based on their influence on the ultraviolet degradation of polypropylene.

Glass fibres, talc and carbon black are added to the recycled polypropylene by the plastic recycling company. The result is a bunch of black grains, ready to be used for 3D printing. Glass fibres in the compound will increase the stiffness of the compound, which also accounts for the higher tensile strength. While at the same a crystallization could be taken based resulting in an increase in brittleness with increase crystallinity (Tong and White 1996). Talc is added to the PP to improve its stiffness. Azuma et al. did a comparative study of the degradation behaviour of extruded polypropylene (PP) and PP/talc composites with the use of outdoor weathering and indoor accelerated weathering tests. It was found out that the materials which endured an outdoor exposure test had the highest degradation degree while being exposed to the lowest amount of UV exposure radiation. For both indoor and outdoor, the influence of talc in the composite had a negative effect on the PP's durability, resulting in a higher degradation rate. In this study, it is also concluded that the combination of UV exposure and acid rain have an influence on the accelerated UV degradation of PP (Azuma et al. 2009). Carbon Black (CB) is mainly given to a recycled plastic compound for a homogenous colour since the recycled polypropylene consists of several colours. CB is widely used for the improvement of the weather-resistance of thermoplastic polymers and rubbers. The UV stabilising activity and its UV absorption ability This additive is the reason that rubber tires are black and help PP pipes last longer (Horrocks et al. 1999).

4.4 Weathering test methods

Several weathering test methods have been developed to simulate natural weathering at an accelerated rate to investigate the durability of outdoor building applications. In this way, long-term weathering effects to the material can be observed in a relatively shorter testing time. The laboratory test is supposed to help researchers in their prediction of the service life of polymers under natural conditions. However there still are differences between natural and artificial weathering of materials, which not necessarily gives the same degradation result (Crewdson 2008).

During natural exposures, different factors play a role in the degradation of material such as exposure to sunlight, day and night temperature cycles, seasonal variations, humidity, or pollutants in the air (Wypych 1999). These factors are important but, impossible to control or even to record them. Besides a research in a natural environment may contain several years to obtain the result, which makes the progress time-consuming. On the other hand, when performing accelerated testing could be over-exaggerated which led to wrong failure type and could be misleading (Crewdson 2008).

Tidjani researched the UV degradation of high and low crystallinity PP samples under natural and laboratory weathering conditions. The samples in outdoor exposure were carried out during the summer in Tsukuba City (Japan), located at 140° E longitude and 36° N latitude. Laboratory test were performed in a Weather-O-meter with an incident light corresponding to an average of 161 KJ/m² per hour. It is observed that the crystallinity of PP under natural exposure have different outcomes. PP with high crystallinity was useless after a short exposure time and PP with low crystallinity retained its physical property for a longer period. During the laboratory weathering test, no difference in degradation of both PP's was observed (Tidjani 1998). This outcome also led to the conclusion that outdoor testing is essential for the validation of accelerated indoor testing.

It is concluded that laboratory weathering test should be verified by a natural outdoor test, to minimize the risk of wrong conclusions. However, since this graduation study possess a limited amount of time and a natural weathering test will be time-consuming, an accelerated weathering test will be advised based on its reproducibility and repeatability.

4.5 Natural weathering of the Aectual façade

In April 2018, a mock-up of the Aectual façade is installed in front of a machine building near train station Amsterdam Sloterdijk. The façade consists of eight panels and is installed to a steel frame, which is connected to the ground and the building behind which can be seen in **Figure 29**. The material compound consists of recycled thermoplastic polypropylene which is reinforced with glass fibres. Additives as talc and anti-oxidants are added to the compound for the colour and the printability of the compound. The façade is faced toward the south, which is fully exposed to solar radiation and other weathering conditions.

Three months later, the mock-up was disassembled from the machine building and transported to the building site and installed in front of the office of DUS Architects and Aectual. This time the façade panel was faced towards the south-west. The summer of 2018 was according to the KNMI the warmest summer since 1706. In De Bilt, the mean temperature was 18.9°C against a normal temperature of 17.0°C. The sun hours of this summer was an average over 765 hours of sunshine against 608 hours of normal (KNMI 2018).

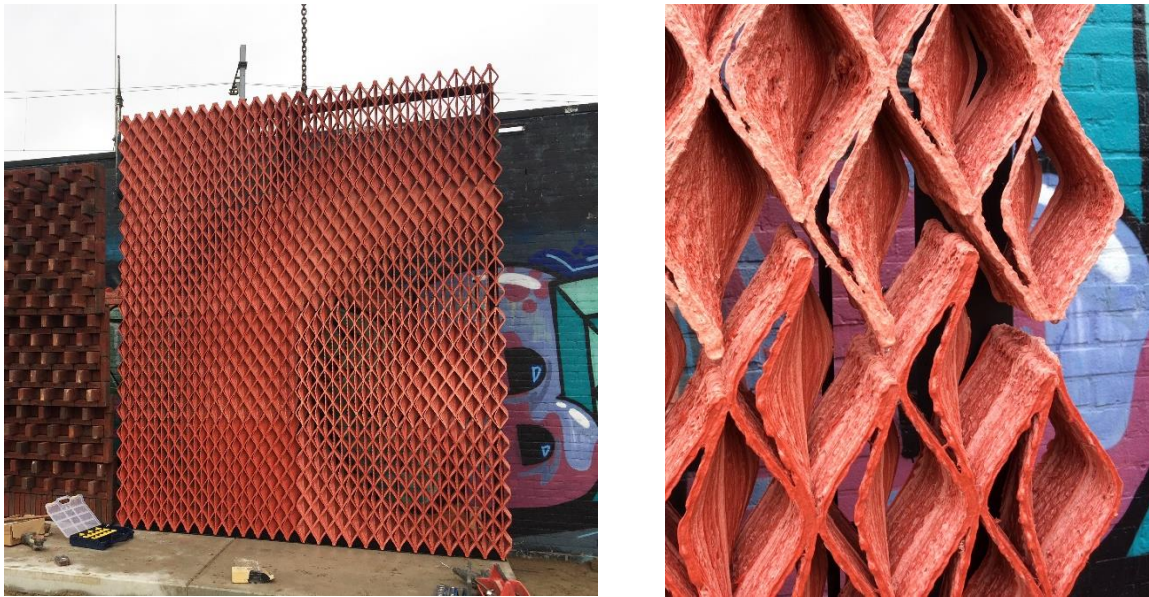


Figure 29: Installation of Aectual façade (Amsterdam Sloterdijk, April 2018).

In September 2018, the mock-up was observed after the intensive summer. The first remark was the discolouration of the façade panel as can be seen in **Figure 30**. It is clear to see that there have been some colour changes within the material. When focusing on the top a clear colour is observed: whitening. It is also noticeable that the material within the 'eyes' of the panel preserves more of the colour compared to the exterior surfaces. This could be the effect of that the fact that this area obtained less UV radiation or rain. No clear cracks or delamination was observed within the panel.

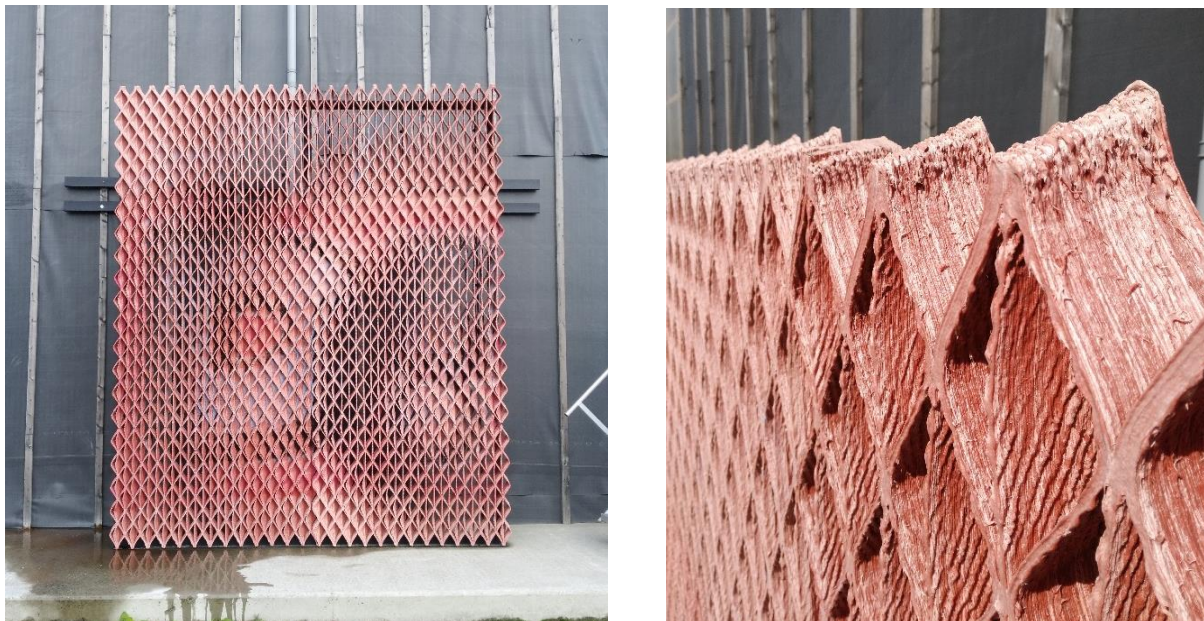


Figure 30: Aectual façade; after 3 months of natural weathering (DUS Architect, September 2018).

4.6 Summary

Weathering factors such as solar radiant, temperature cycles and moisture have an impact on thermoplastic polymers. The impact of each weathering factor depends on the physical properties of the material, the exposure duration and the location. Ultraviolet exposure is seen as the most damaging weathering factor for a polypropylene-based material. The effect of UV radiation on polymers could result in chalking, cracking, delamination, loss of physical properties and discolouring (Wypych 1999).

The first Aectual façade mock-up is installed in the Netherlands and is exposed to the Dutch climate. After one intensive summer polypropylene-based material of the façade clearly loses its colour after an intensive summer. White powdering on the top of the façade could be signs of chalking. Even though no mechanical testing has been done, the visual changes of the material imply that the Dutch weather conditions have an impact on the properties of the 3D printed thermoplastic. Preventing undesirable effects of UV radiation, like chalking, decolourisation or loss of mechanical properties of thermoplastics, could be done by adding additives to the pelletized polymer compound. Additives as carbon black or ultraviolet stabilisers could absorb ultraviolet radiation, lowering the initiation of UV degradation. However, the added additives will change the mechanical and thermal properties of the printed material.

The newly developed material should be tested on its strength and its weather-resistance. A natural weathering test is the most acute method since all involving factors are playing a role in the degradation of the material. The disadvantage of this method is the time-consuming and laborious procedure and the fact that weather conditions are uncontrollable and hard to record. Laboratory weathering testing allows for faster, more reproducible and systematic results. Unfortunately, there are no techniques that can take all the potential weathering factors. Most indoor weathering techniques hold a UV exposure room with temperature and water (spray, dew, relative humidity) cycles to simulate the weather conditions. To study the influence of ultraviolet exposure on the strength of 3D printed recycled thermoplastic, an experimental research has been done and will be discussed in the following chapters within this thesis.

PART III
Experimental

Chapter 5

Test Protocol

5.1 Introduction

The main goal of this experimental research is to have a better understanding of the durability of 3D printed recycled thermoplastic polymer when exposed to ultraviolet radiation. It is well-known that long-term ultraviolet exposure has its effect on the mechanical and aesthetical properties of polypropylene, resulting in discolouration and loss of mechanical integrity. Several choices have been made to develop a laboratory experiment and are summed up below:

Test materials

To investigate the effect of ultraviolet exposure on the 3D printed façade panel, DUS Architects and Aectual, choose the print material used for the Aectual façades: recycled polypropylene with 20% glass fibres and mineral infill. Material information can be found the **Figure 107**.



Figure 31: Raw material: PP-pellets (black) with 1% UV stabilisers (white).

The material is chosen due to its affordable price, its wide availability, its small CO₂ footprint and the potential for recycling after use. A practical reason was that the 'raw material' was already reinforced with additives, hereby it was instantly ready for printing. The plastic recycling company Ravago delivered the material to Aectual in the form of pallets as can be seen in **Figure 31**. Due to the recycling of different sorts of polypropylene from various industries the colour of the recycled plastic is non-consistent. When adding the colour pigment carbon black, the mixed compound changes into a consistent black coloured material. This carbon black could have a (positive) influence in the ultraviolet degradation of the thermoplastic (Horrocks et al. 1999). When exposing the material with ultraviolet radiation it is interesting to also test the same material with ultraviolet absorbers (1%) at the same time. The UV stabilisers were added to the mixture (the required dosage for the Western Europe environment is 1% with PPM UV: 2000 ppm inside the end-product). Product information could be found in Figure 108.

Accelerated laboratory weathering

Due to the limited time available for research, an accelerated laboratory weathering test was chosen instead of a natural weathering test. The disadvantage of an accelerated weathering test is that it could give a different outcome than a weathering test in situ since the device is not considered day and night cycles and wetness sprays. However, due to its controllability and

reproducibility, an accelerated weathering test could still provide useful information about the material behaviour. A UV test chamber is available at the faculty of Civil Engineering of the Delft University of Technology, which will be intensively used during this research.

Mechanical testing

Different mechanical testing could be done to determine the strength of the exposed print material. Testing the material in bending and tension, for example, could be done to show a clear transition from brittle to ductile. However, the purpose of this research is not to show every degradation of every property, but the effect of UV exposure. The most simple and universal test has been chosen: the tensile test. Also, the cost of preparing the small tensile specimen by 3D printing is substantially lower than the cost of preparation by machining the multipurpose test specimen. Since the space in the UV test chamber is limited. An adjusted and smaller geometry is considered for this test, based on the international standard norms. In this way, the number of samples could be increased per set (10 samples). The geometry of the tensile specimen is illustrated in **Figure 36**. In a later stage of this project, after the tensile test, a small Charpy impact test was performed within this study and will be discussed in the following sections.

Sample preparation

Since the Aectual façades are printed in the Z-direction, as shown in **Figure 9**, printing parallel to the plate would be no representative. A batch of 24 plates is geometrically designed with a plate dimension of 200 by 200m². These plates were separated with a hand saw and transported to a water jet cutter to cut the samples. Laser cutting was not used since high temperatures could influence the mechanical properties of the extruded thermoplastic polymer.

Unloaded exposure

When the façade element is installed on the load bearing structure, it will be affected by the mechanical load of its own weight and by external actions such as wind pressure and thermal load. This permanent load can cause creep in the material and contribute to the degradation of the print material in the long-term. It is determined that tensile stress accelerates molecular scission in injected moulded bars when exposed to ultraviolet radiation which led to a decreased in the tensile strength (O'Donnell and White 1994). Due to the limited space in the chamber, exposure of the loaded specimen was not possible. Still, it needs to be stated that accelerated weathering on itself cannot predict the total real-life degradation of the material since other factors are involved as well.

Exposure duration

The graduation project takes place in a period of 9 months, in which all the literature research, specimen preparation and experiments should be done. This limits the amount of time available for accelerated weathering. Therefore, a maximum of exposure time of 4 weeks is chosen per set and no conclusions can be drawn on the difference of the effect of natural and accelerated weathering on 3D printed recycled plastic.

Test directions

Due to the restricted space of the UV test chamber, a choice must be made in which direction the fibre should be oriented. In theory, the effective thickness will be much smaller in percentage in the transverse direction than the longitudinal. Cracks within in these thicknesses will occur faster in the transverse direction than in the longitudinal as illustrated in **Figure 32**. When the degradation of samples in the transverse direction is minimum, degradation in the longitudinal direction will be also safe. However, to test the transverse direction, it must be sure that the print quality is good enough. The risk exists that due to interlayer bonding issues between the layers the research could be spoiled. If so, after the transverse tensile test also a longitudinal test should be done to understand the influence of ultraviolet exposure on the tensile strength of the thermoplastic.

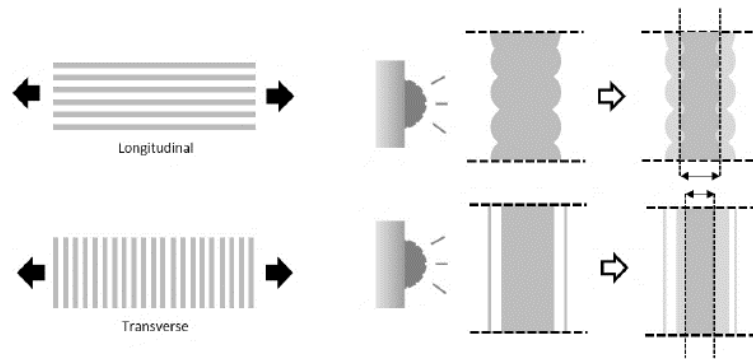


Figure 32: Print directions and their effect of UV degradation on the tensile specimen.

Sample distribution

When the plates have been printed and cut with the waterjet cutter, samples were divided into two groups as illustrated in **Figure 33**. The exposed (X) group will be exposed in the ultraviolet test chamber in an amount of time, while the reference group will be held in an unexposed space with controllable room conditions. In this way, the effect of ultraviolet exposure could be measured, when both groups undergo the same mechanical testing.

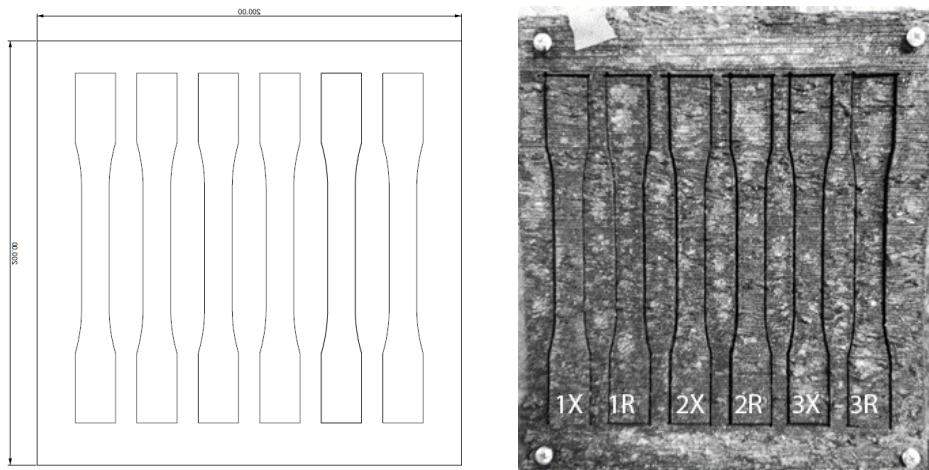


Figure 33: Sample division within a printed plate (exposed (X) and reference (R)).

Print quality classification

Due to the various print quality of the printed batch, a print quality classification system is conducted. After the sample division, each sample is labelled based on its visual quality, amount of aligned print layers and sample thickness. The print quality classification is shown in **Table 3**.

Print quality	Impurities	Material concentration	Aligned print layers	Sample thickness
High	None	None	All	Constant
Medium	Small	Few	More than $\frac{1}{2}$	Constant
Low	Large	Yes	Less than a $\frac{1}{4}$	Not constant

Table 3: Print quality classification system.

For both tensile tests in transverse and longitudinal direction, only medium and high-quality samples were used for the numerical outcome. Samples which have a low print quality mostly breaks at the clamping area or led to slippage, which results in unusable data. For the Charpy, impact test only high print quality samples were tested since the vulnerability of the small sample dimensions. The print quality classification system is conducted by a visual inspection **Figure 34**.

However, it is recommended for further studies that a more consistent print quality should be tested or a more extensive and better-structured investigation would be desirable to fully embrace this the various print quality issue.

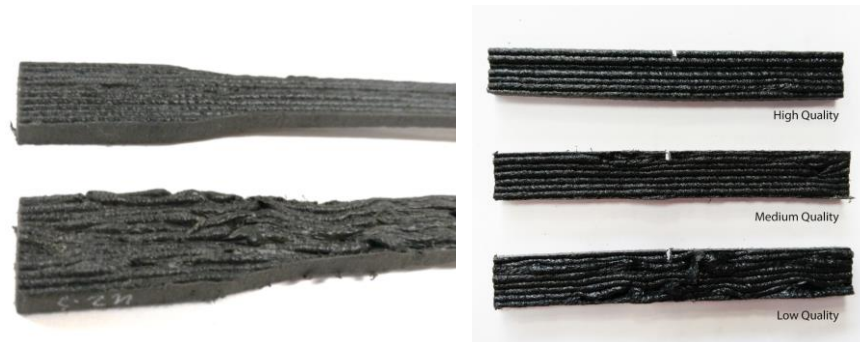


Figure 34: Difference in print qualities between samples (left; high quality, upper sample; low quality, lower sample), Charpy impact samples (right).

5.2 Test description

5.2.1 Test Materials

3D print-extruded thermoplastic polymer

Two print materials obtained from plastic and plastic recycle company Resinex and Ravago Group Headquarters were evaluated on their tensile strength and Young's modulus after sets of ultraviolet exposure in the UV test chamber. The printed materials are named in this research as PP and PPU:

Material PP: A commercial polypropylene-based material with 20% glass fibres and mineral filled. It is an industrial quality compound (trademarked as Mafill CR XTG 5344) with a melt flow rate of 9 g per 10 min (230°C, 2.16 kg). It has a density of 1.05 g/cm³ and is 100% industrial recycled waste. Although it wasn't mentioned in the material sheet in Figure 107, the material contains an unknown percentage of carbon black.

Material PPU: The same material compound as material A with added ultraviolet stabilisers (U) with the product name: VE82608. More information about the UV stabilisers could be found in Figure 108. The UV stabilisers are added to the mixture before printing. The required dosage for the Western Europe environment is 1% with PPM UV: 2000 ppm inside the end-product.

Flat-die-extruded thermoplastic polymer

To have a reference for the UV test with 3D printed PP, two sets of flat-die-extruded polypropylene are tested as well. In this way also, the influence of fabrication method of PP and UV testing itself could be researched. Surface-extruded or flat-die-extruded material is obtained from Ekon. Ekon is a leading manufacturer of polyethylene (PE) and polypropylene (PP) plastic sheets via surface extrusion. The PP's tested are named in this research as PPB and PPG.

Material PPB: Virgin black PP-based compound, delivered as a flat sheet with a thickness 1.2 mm. Additive: Masterbatch black PE8301F as can be seen in **Figure 110** and 1% of UV stabiliser as can be seen in **Figure 111**.

Material PPG: A recycled grey PP-based compound with a thickness of 3.0 mm, without ultraviolet absorbers. Additive: Talc. Ekon had no information about the material properties of the recycled compound.

5.2.2 Sample preparation

In general, the commercially available thermoplastic polymers come in the form of pellets. Glass fibres, minerals and the colour additive carbon black are already part of these pellets. To receive the tensile samples, a batch is printed Z-direction of the printing bed at the print company Aectual with the print settings shown in **Table 4**.

KamerMaker II	
Starting temperature [°C]	80,170,180,190,180
Temperature [°C]	80,150,160,178,172
Ambient temperature [°C]	25
Speed [%]	200
Flow [%]	160
Nozzle opening [mm]	2
Print height [mm]	180-200

Table 4: Printer settings of the KamerMaker.

There were multiple temperatures with the KamerMaker II because the extruder exhibits 4 chambers and a nozzle temperature. The material is heated up and flows from chamber to chamber, ending up out of the nozzle. A chance could be that due to low temperatures, the extruded material would not properly flow through the chambers or does not adhere in between layers. After the printing, the batches were conditioned in the ambient air temperature for 48 hours. A batch consists of 24 plates of 200 mm by 200 mm (as shown in **Figure 35**) which were separated with a hand saw. The plates were then attached to timber plates and transferred to the cutting company Schrijver B.V. The test samples were cut with a water jet cutter from the plates and were blown clean with an air blower.

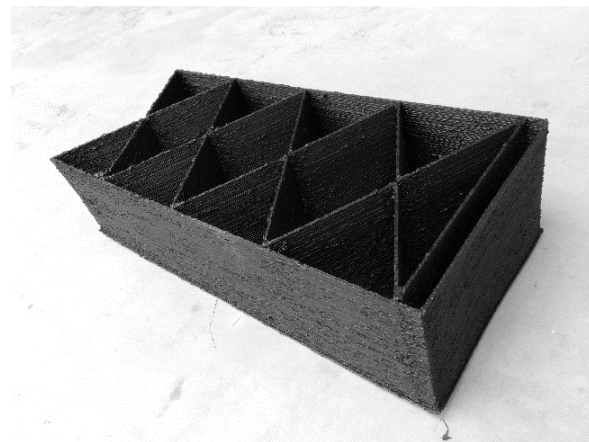
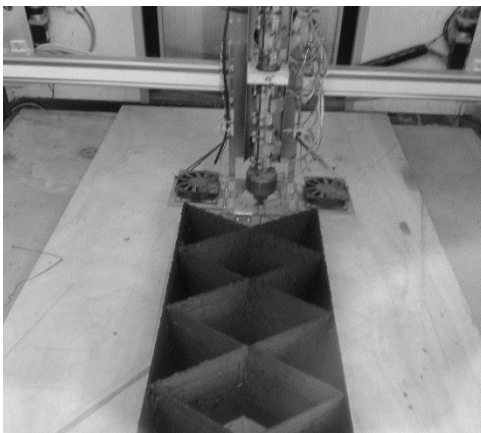


Figure 35: Printed batch with the material PP.

The dimensions of the tensile test specimen are based on the possible test area of the UV test chamber space and the tensile test ISO 527-4 standard. With a 150 mm in the length and a narrow part of 60 mm by 10 mm, it is the exact version of the specimen suggested in ISO 527-4 code for testing short fibre-reinforced thermoplastics.

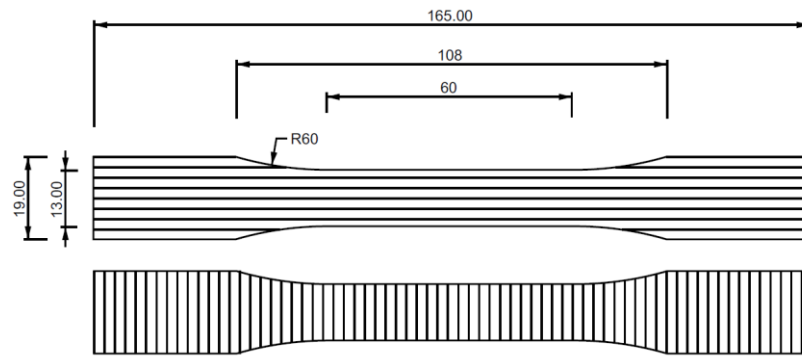


Figure 36: Specimen geometry for the tensile test.

5.3 Laboratory weathering testing

The main objectives for testing under simulated environmental conditions in laboratory instrumentation are to conduct the tests under more controlled and accelerated conditions as compared to exposure outdoor. For this research, a choice has been made between natural and artificial weathering for the degradation of the 3D printed material. Due to the combination of variable and uncontrollable weathering factors of the Dutch climate and the limited time duration for this research, applying a natural weathering experiment will be too time-consuming. An accelerated laboratory test is chosen based on its reproducibility and repeatability factors.

5.3.1 Ultraviolet Test Chamber

At the faculty of Civil Engineering and Geosciences of the Delft University of Technology, a UV test chamber was available for the weathering test. The LY-605A UV test chamber, as shown in **Figure 37**), is mostly used for yellowing thermoplastic polymers and rubbers by providing simulative heat of the sun and ultraviolet radiation. The specification of the UV test chamber could be found in **Table 17**.



Figure 37: Ultraviolet test chamber (right) and Ultra-Vitalux lamp (left).

5.3.2 Ultra-Vitalux lamp

In **Figure 38** the spectral radiation power (SRP) distribution of the OSRAM Ultra-Vitalux lamp, which is installed in the UV test chamber, is shown. The emitted light is visually and quite yellowish. Based on the specifications, the lamp emits 13.6 W of UV-A and 3.0 W of UV-B radiation. The remaining emission is 284 W of VIS, NIR and IR and generates heat to a chamber temperature

around 40°C. The temperature in the UV test chamber is kept stable at the room temperature of 50°C with an accuracy of $\pm 3^\circ\text{C}$.

When comparing the light exposure with the mean solar radiation in the Netherlands, a small comparison is made. For the annual UV irradiance in the Netherlands over 2012-2017, the UV interval is chosen between 340 - 350 nm. The associated irradiance is 21,75 MJ/m² (RIVM, 2018):

$$= 21.750.000 \text{ J/m}^2/\text{year}$$

Based on the information given by the UV test chamber supplier Liyi Tech: 250 W of the wavelength is 340 nm. (30 cm from the light source) at 50°C (Liyi Tech,2018):

$$= 90.000 \text{ J/m}^2/\text{hour}$$

A rough estimation is calculated when comparing the exposure within the UV test chamber and exposure in the outdoor Dutch climate: 241 hours and 40 minutes in the UV chamber equals 1 year of UV irradiance in the Netherlands.

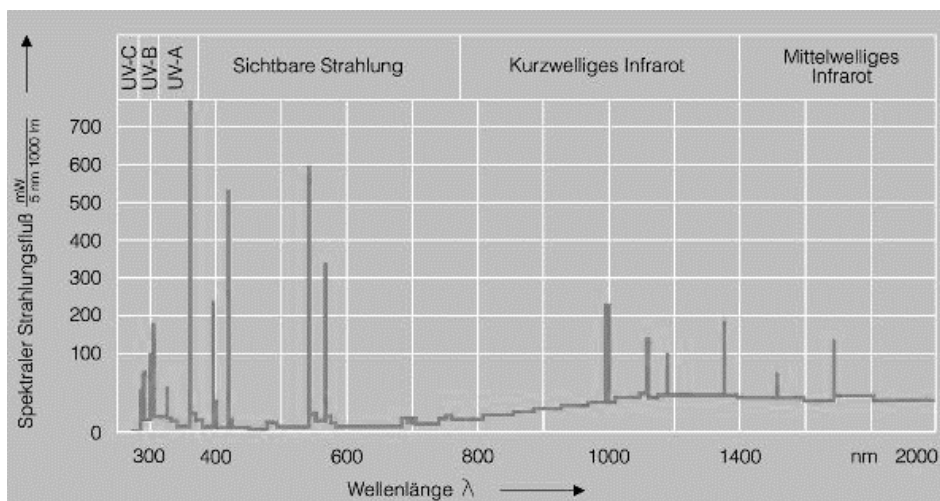


Figure 38: Spectral Radiation Power distribution of Ultra-Vitalux.

5.4 Mechanical testing

After the laboratory UV-exposure test, the exposed samples were tested on two mechanical properties by the tensile strength test and the Charpy impact test. These tests are briefly described below.

5.4.1 Tensile strength test

The exposed material will be analysed by a tensile test in its the longitudinal and transverse print direction. This simple tension test provides valuable information about stiffness, strength, toughness and ductility of a material (Eftekhari and Fatemi 2016). The tensile test will be carried out with the testing machine: Zwick Z100 (**Figure 39**). Standard tensile tests recording the deformation under increasing load in room temperature have been done repeatedly with the strain rate 5 mm/min for longitudinal direction and 2 mm/min for transverse direction. All measurements were carried out at room temperature (23°C). Extensometers have not been used due to the concerns regarding their reliability on uneven, layered surfaces.

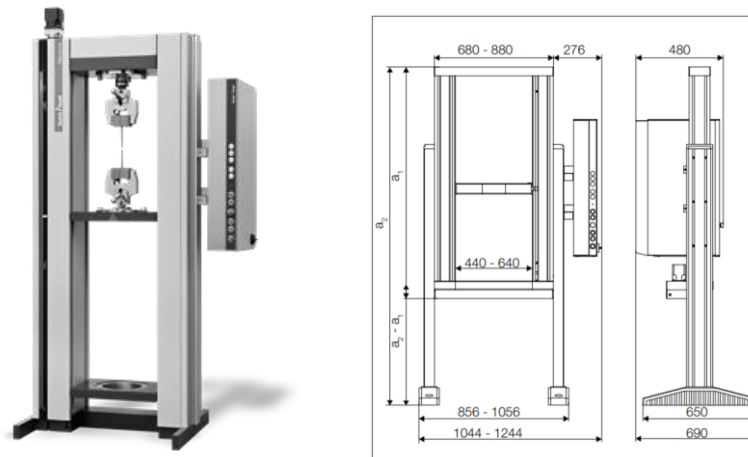


Figure 39: Test setup of the tensile strength test.

5.4.2 Charpy Impact test

The tensile test, where the samples suffer from bad interlayer bonding and voids, led to scattered data. A Charpy impact strength test is a good alternative and the test setup is illustrated in **Figure 40** (left). Smaller samples could be cut with an automated jigsaw by hand without using the water jet cutter. The test determines the amount of energy absorbed by a material during fracture. This absorbed energy is a measure of a given material's notch toughness. The main disadvantage is that the obtained results are only comparative (Sahin and Yayla 2005). In response to the impurities in the printed surface of the batches a print quality classification system is introduced, whereby only samples will be used with a high print quality as seen in **Figure 34**.

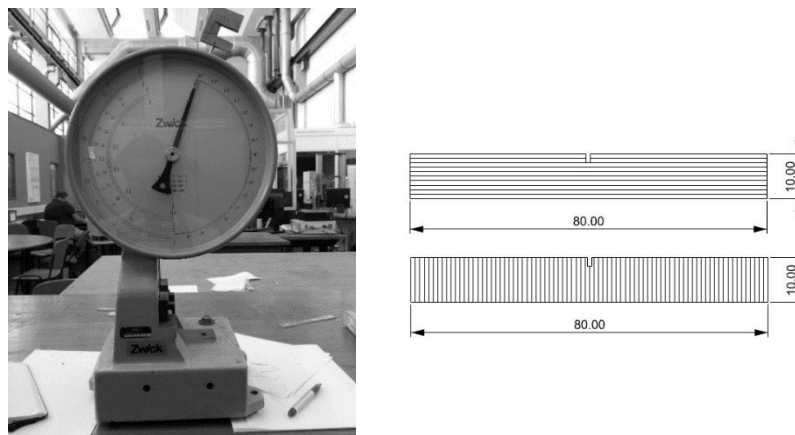


Figure 40: Test setup of the Charpy impact strength test: Device (left), sample dimensions (right).

During the sample preparation, it has been noted that the samples in transverse direction were too unstable to determine the impact strength. For this impact experiment, the samples in the longitudinal direction have been chosen due to its stability. The dimensions of the samples were 10 mm by 80 mm (**Figure 40**, right) with a thickness from about 5 mm.

5.5 Summary

To study the influence of ultraviolet exposure on the strength of 3D printed thermoplastic a material test is designed to simulate the UV degradation outdoor. Since the façade panel is printed in the Z-axis of the printer, this direction is used to print the batches. Compared to the previous graduation studies relating to this subject, the scope of the investigation had been limited due to the graduation duration and the test possibilities. The following properties have been measured:

1. **Tensile strength and stiffness** – most basic and reliable measure of material behaviour – done repetitively with different materials, ageing duration and ultraviolet exposure time.
2. **Charpy impact strength** – most basic measurement for façade material - done with only one material PP with different ageing durations and ultraviolet exposure time.

Since the printed product is highly orthotropic, strength and stiffness tests were executed for two directions – along (longitudinal) and across the print direction. Biaxial tests have not been done due to time and resource limitations. To compare the 3D print-extruded test specimen which will be used for the UV test, the flat-die-extruded polypropylene-based specimens obtained from the plastic company Ekon will be tested in the same manner as well.

Chapter 6

Test Results

This chapter contains the numerical outcome and its processing of all the test done during the experimental phase with different thermoplastic polymers. Factors which had an influence on the results will be described afterwards. In the end, quantitative conclusions are summed for each mechanical test. All materials tests were executed at the Material Science and Engineering Laboratory at the Faculty of Mechanical, Maritime and Materials Engineering (3ME) at the TU Delft under the supervision of Dr. Ir. F.A. Veer. All load experiments were conducted at a typical room atmosphere: ($20 \pm 2^\circ\text{C}$ and $50 \pm 10\%$ relative humidity).

6.1 Tensile strength

6.1.1 Tensile test properties

To obtain the tensile stiffness, yield strength and strain at yield, all specimen were tested with the same dimensional cut geometry as given in **Figure 36**. Since a measuring gage was not available a consistent effective length was calculated in Appendix B as:

$$l_{eff} = 97,83 \text{ mm}$$

Due to the print and the cut quality of the specimen, differences in thickness was measured and will be considered when determining the tensile properties. Each set of results, with an age or UV-exposure combination has been processed according to the following procedure:

1. Force-displacement data were cut at the lowest strain corresponding to the ultimate force. This is often noted as the strain and stress at yield.
2. The stiffness modulus, yield strength and elongation at yield/break was calculated according to D638 – 14: Standard Test Method for Tensile Properties of Thermoplastic polymers and is described below:

Yield strength

Strength at yield is the stress at which a material has a specified limiting deviation from the proportionality of stress to strain (ASTM International 2014). This stress will be the point as the yield point. When the strength at yield is expressed in relation to the tensile strength, this shall be designated either as tensile strength at yield or as tensile stress at yield as shown in **Figure 41**.

Elongation at yield

The percentage of elongation at break is calculated by dividing the extension (change in gage length) at the point of specimen's maximum stress (mm) by the effective length of the specimen (mm) and multiplied by 100 (%).

Modulus of elasticity

The modulus of elasticity, or Young's modulus, is determined by extending the initial linear portion of the load-extension curve and dividing the difference in stress corresponding to any segment of the section on this straight line by the corresponding difference in strain (ASTM International 2014). The result shall be expressed in N/mm^2 or MPA. The y-axis is the relevant cross-sectional property, and the x-axis is the relative displacement between clamps in the tensile test or the movement of the head in the bending test. Besides, the gradient of the curve can represent the stiffness of the

relevant property, where stiffness increases with increasing stiffens. Only the first linear part is used and compared since it covers the range relevant for practical design.

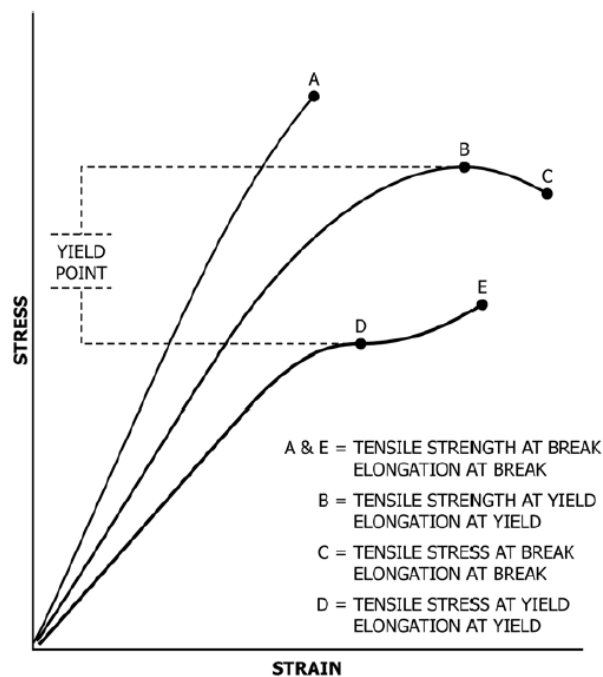


Figure 41: Tensile strength properties designations (ASTM International 2014).

6.2.2 Toe compensation

In many tensile test cases, the test result was affected by the machinery imperfection, such as the toe effect, a misleading representation of the tensile strength curve at the beginning of the test. This issue was modified by the toe compensation: extrapolating the first linear part of the output curve to obtain a more representable Young's modulus. There are two kinds of test result depending on the material (ASTM International 2014):

Material with a Hookean region

In the most tensile test with thermoplastic polymers, a typical stress-strain curve appeared called the toe region, which does not represent the actual tensile strength of the material. This could be caused by the take-up of slack and alignment or seating of the specimen. To obtain correct values of the parameters, e.g. modulus, strain, and offset yield point, this issue must be compensated to give the corrected zero point on the strain or extension axis (**Figure 42**, point B).

In the case of a material exhibiting a region of Hookean (linear) behaviour, a continuation of the linear (**Figure 42**, curve CD) region of the curve is made through the zero-stress axis. This intersection (**Figure 41**, point B), is the corrected zero strain point from which all extensions or strains must be measured, including the yield offset (**Figure 42**, curve BE), if applicable. The elastic modulus has been determined by dividing the stress at any point along the line CD by the strain at the same point.

Material with no Hookean region

In the case when the thermoplastic polymer results in a graph with no Hookean region, the toe correction could also be used. Where the zero-strain point can be made by constructing a tangent to the maximum slope at the point (**Figure 42**, point H'). This is extended to intersect the strain axis at Point B', the corrected zero-strain point. Using point B' as zero strain, the stress at any point (**Figure 42**, point G') on the curve can be divided by the strain at that point to obtain a secant modulus (slope of Line B' G') as seen in **Figure 42** (ASTM International 2014).

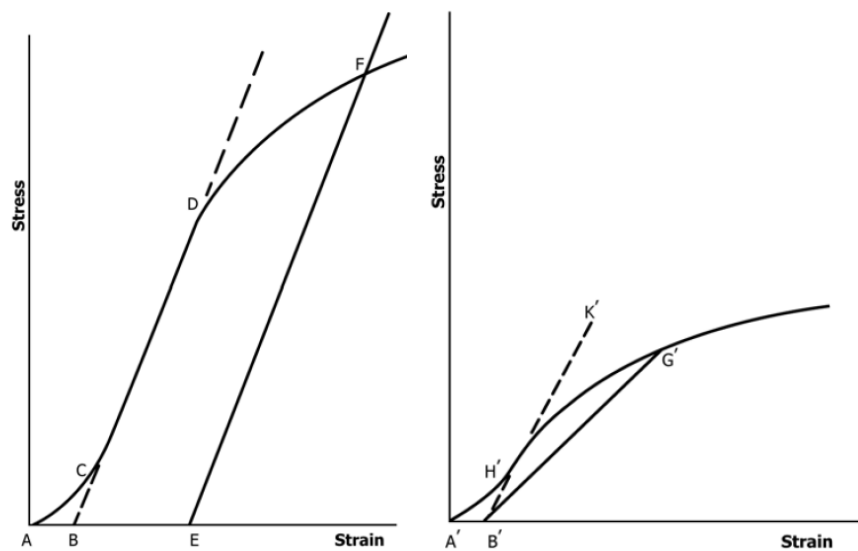


Figure 42: Material with a Hookean region (left) and no Hookean region (right) (ASTM International 2014).

6.1.2 Transverse tensile test results

Graphical results of the influence of ultraviolet exposure on the transverse tensile properties:

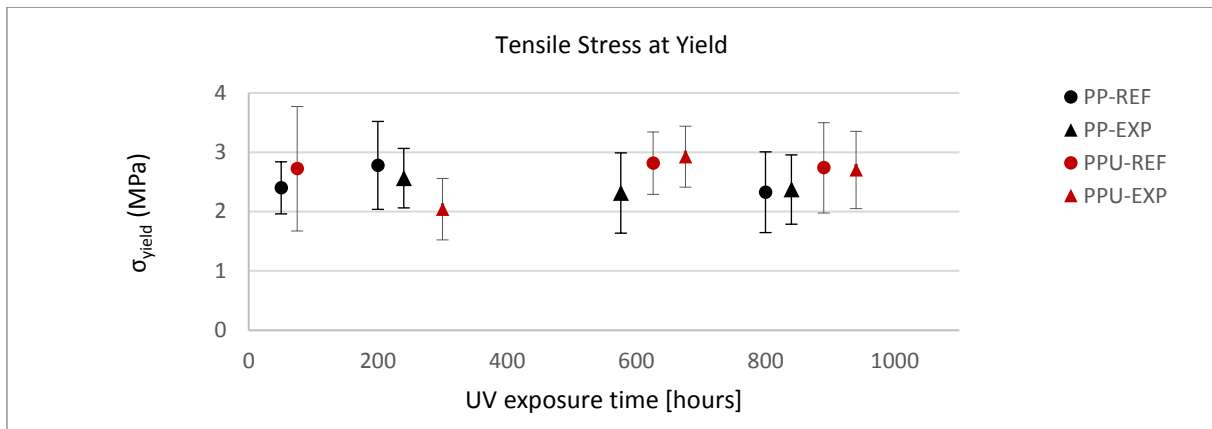


Figure 43: Results: influence of (un)exposure time on yield stress (transverse).

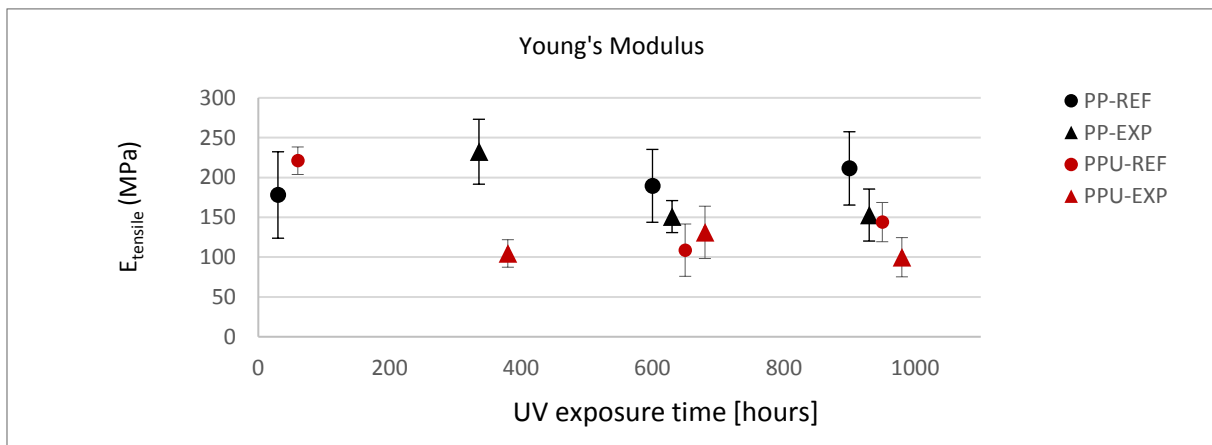


Figure 44: Results: influence of (un)exposure time on stiffness (transverse, Hookean region).

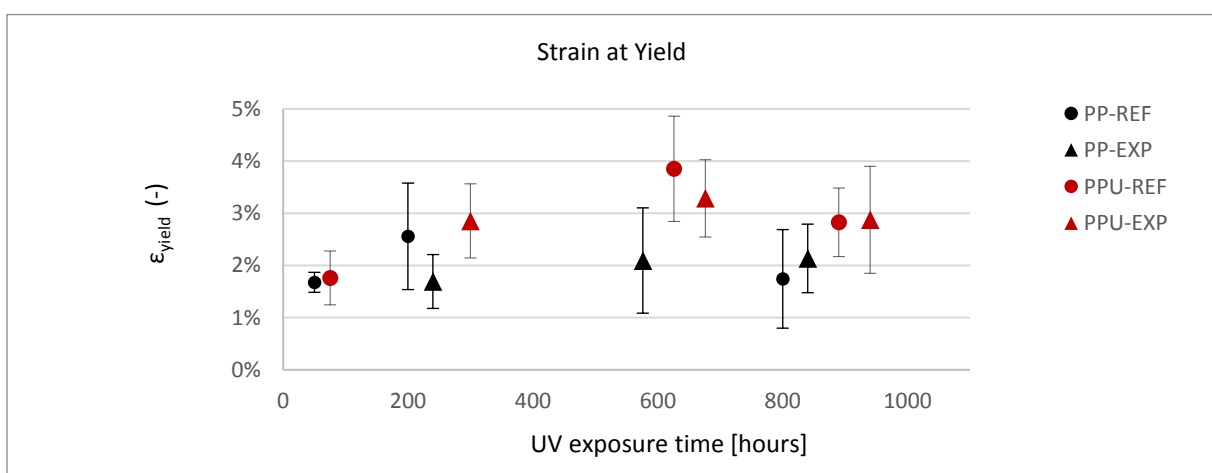


Figure 45: Results: influence of (un)exposure time on yield strain (transverse).

Graphical results of the influence of ageing time on the transverse tensile properties:

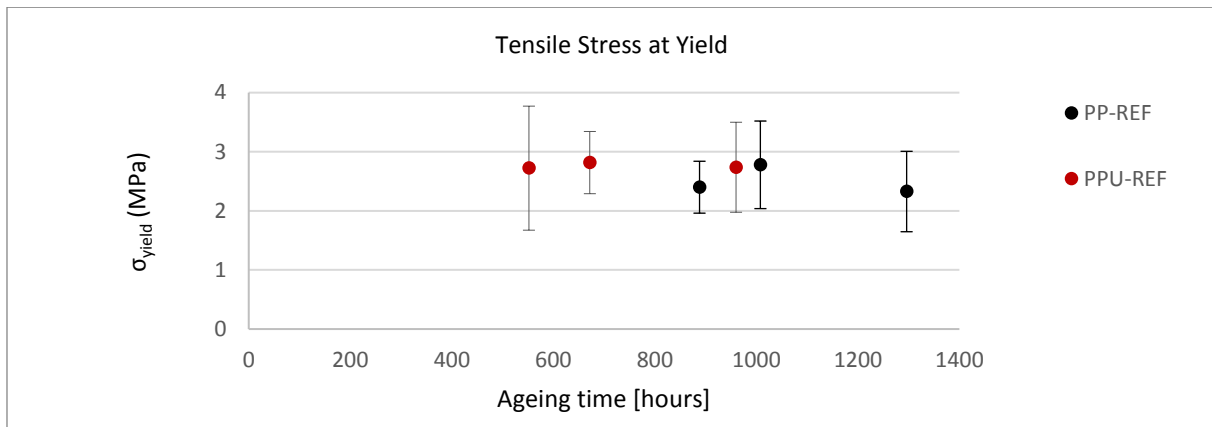


Figure 46: Results: influence of ageing time on yield stress (transverse).

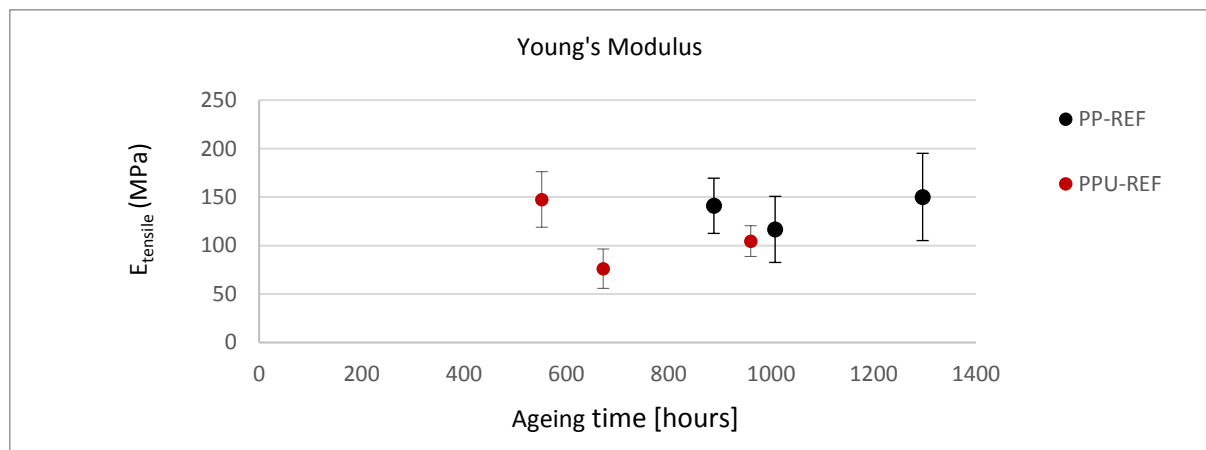


Figure 47: Results: influence of ageing time on stiffness (transverse, Hookean region).

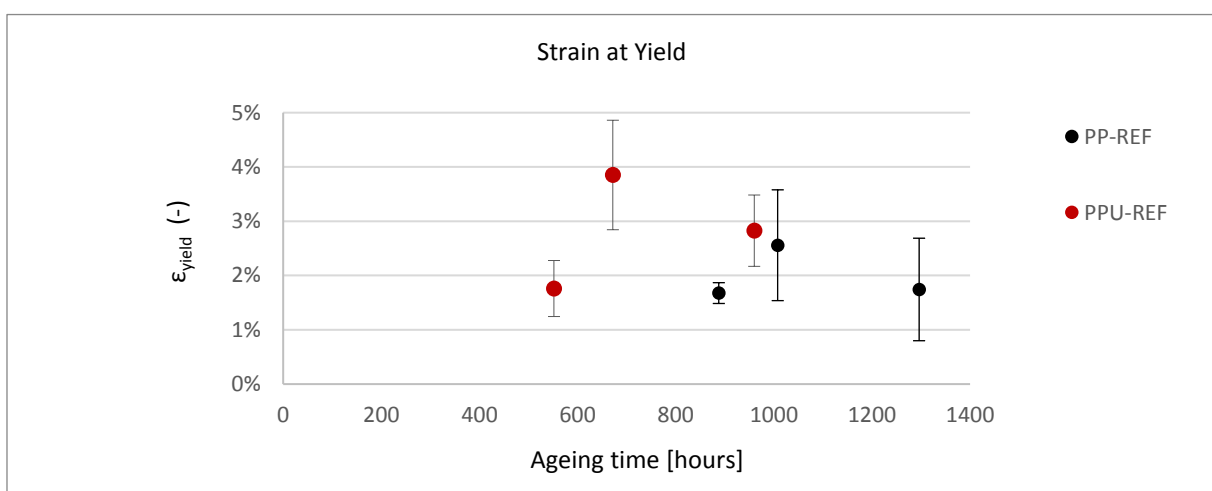


Figure 48: Results: influence of ageing time on yield strain (transverse).

Tabular results:

Material name	Count samples	Age Duration hours	UV Radiation hours	Yield Stress MPa	CV %	Tensile Modulus MPa	CV %	Yield Strain %	CV %
PP-REF	7	888	0	2.4	18	141	20	1.7	11
	6	1008	0	2.8	27	117	29	2.6	40
	8	1296	0	2.3	29	150	30	1.7	54
PP-EXP	6	1032	240	2.6	20	151	11	1.7	16
	8	1032	576	2.3	29	112	16	2.1	31
	7	1296	840	2.4	25	126	29	2.1	32
PPU-REF	7	552	0	2.7	39	148	19	1.8	29
	6	672	0	2.8	19	76	27	3.9	26
	7	960	0	2.7	28	105	15	2.8	23
PPU-EXP	7	667	240	2.0	25	74	12	2.9	25
	8	667	576	2.9	18	91	20	3.3	23
	7	960	840	2.7	24	87	12	2.9	36

Table 5: Summary of the transverse tensile test, 2 mm/min.

The previous graphics and tables represent the tensile test results for the material PP and PPU in the perpendicular direction of the print layer. Both materials were exposed and tested at the same time. However, it should be considered that both materials have different ageing durations. The following observations can be made based on the quantitative results of the tensile test in the transverse direction for the materials PP and PPU:

- The clamping during the tensile test wasn't sufficient due to the rugged and uneven surface of the samples. This led to much slippage, unusable data and therefore a lower sample count as can be seen in
- For both directions, the failure mode on the tensile strength showed brittle rupture as can be seen in **Figure 49**. Stress at yield lies closely at the ultimate breakpoint. No plasticization was observed.
- The various print qualities including different interlayer bonds, voids and thickness led to highly scattered data resulting in an unreliable building material property as can be observed in Appendix F (**Figure 119 - Figure 130**).
- No trend is recognized in the influence of ultraviolet exposure and ageing duration on the transverse tensile properties of PP and PPU as depicted in the **Figure 43 - Figure 48**.
- Unexposed PP had a 14 days more ageing time than unexposed PPU which may explain its relatively higher tensile modulus and lower yield strain as can be seen in **Figure 47** and **Figure 48**.
- Based on the high values of the coefficient of variance in **Table 5**, it could be implied that the tensile strength in the transverse direction of the 3D printed material is highly unreliable and unpredictable.
- No visual colour changes are observed comparing the exposed and unexposed samples after each set of ultraviolet exposure as can be seen in **Figure 50**.

Images of the transverse tensile test:

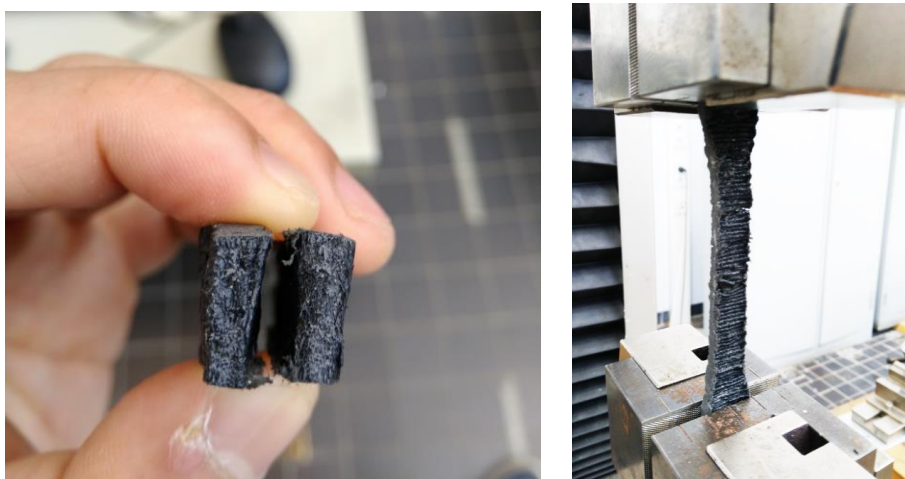


Figure 49: Result: a brittle break between the layers (left), transverse tensile test (right).



Figure 50: Degraded (upper) and unexposed (lower) tensile transverse sample (840 UV exposure hours).



Figure 51: Interior of the UV test chamber.

6.1.3 Longitudinal tensile test results for 3D printed material

Graphical results of the influence of ultraviolet exposure on the longitudinal tensile properties:

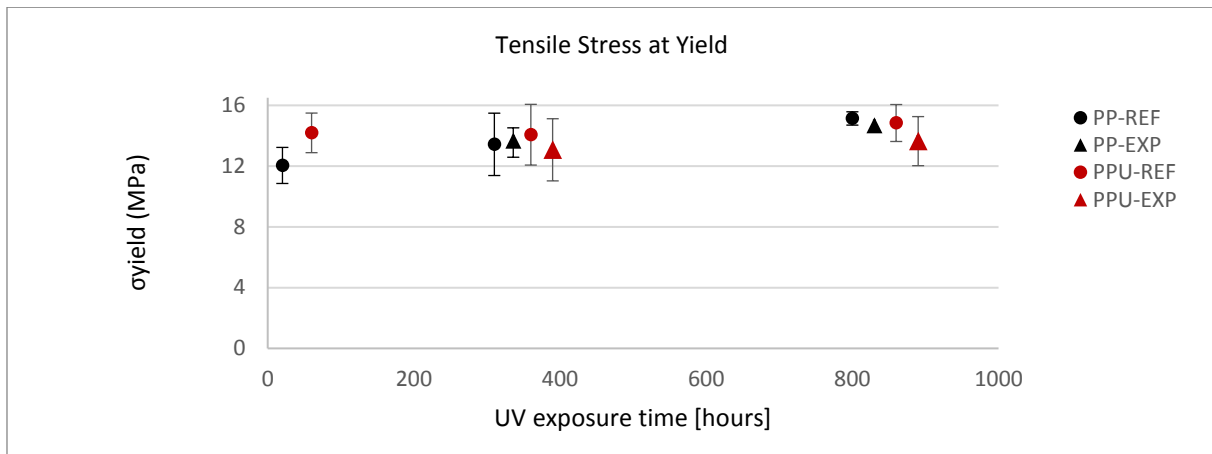


Figure 52: Results: influence of (un)exposure time on yield stress (longitudinal).

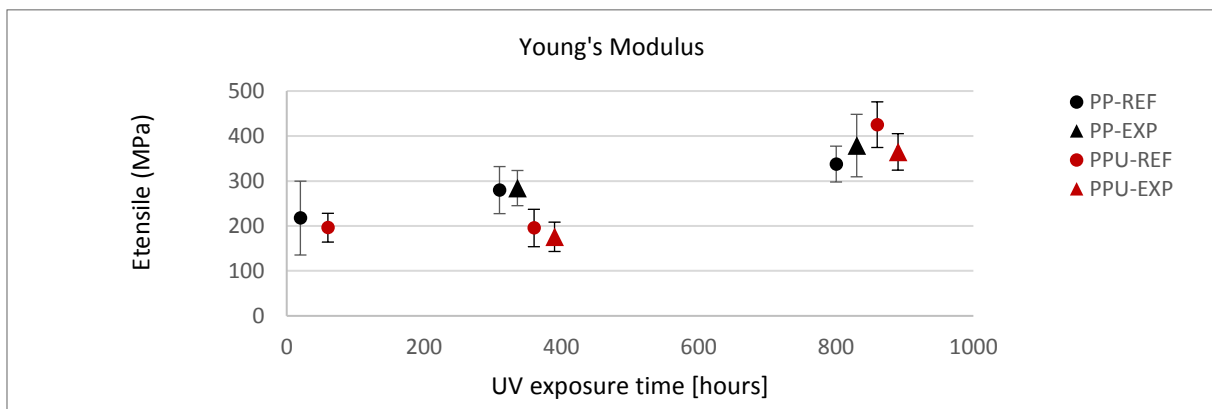


Figure 53: Results: influence of (un)exposure time on stiffness (longitudinal, Hookean region).

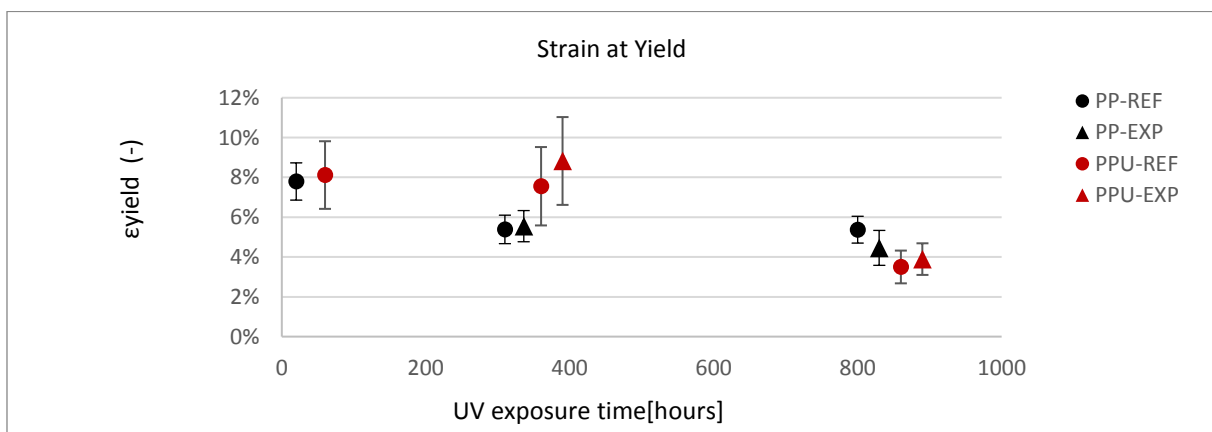


Figure 54: Results: influence of (un)exposure time on yield strain (longitudinal).

Graphical results of the influence of ageing time on the longitudinal tensile properties:

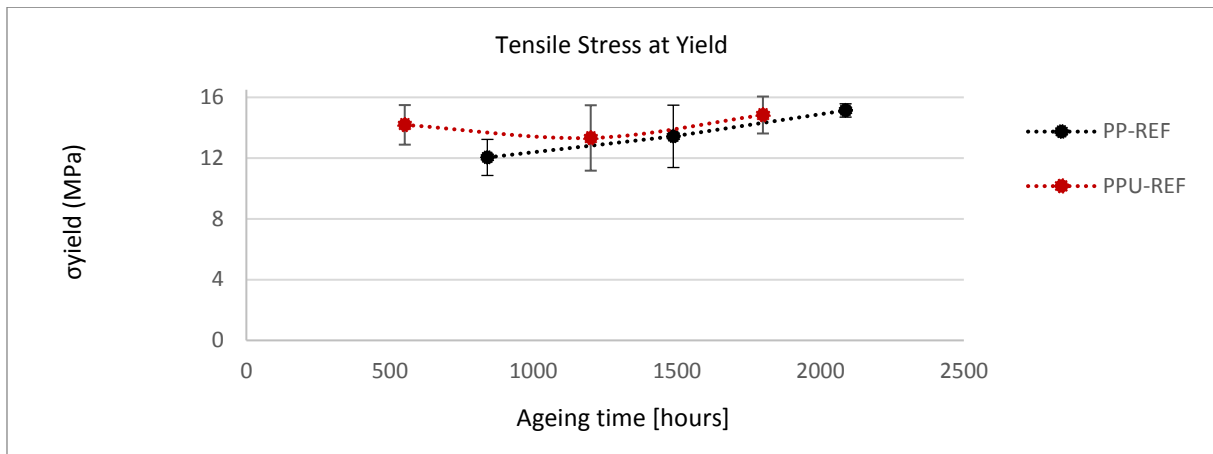


Figure 55: Results: influence of ageing time on yield stress (longitudinal).

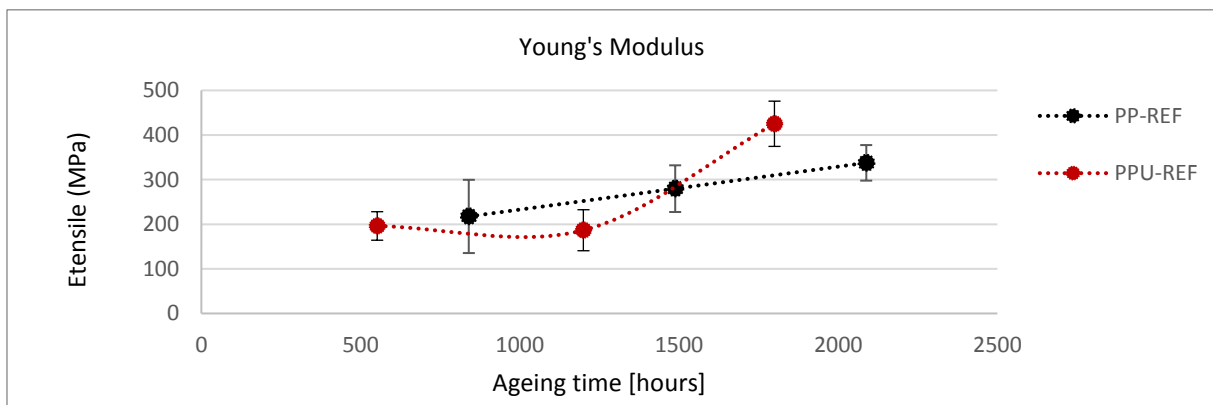


Figure 56: Results: influence of (un)exposure time on stiffness (longitudinal, Hookean region).

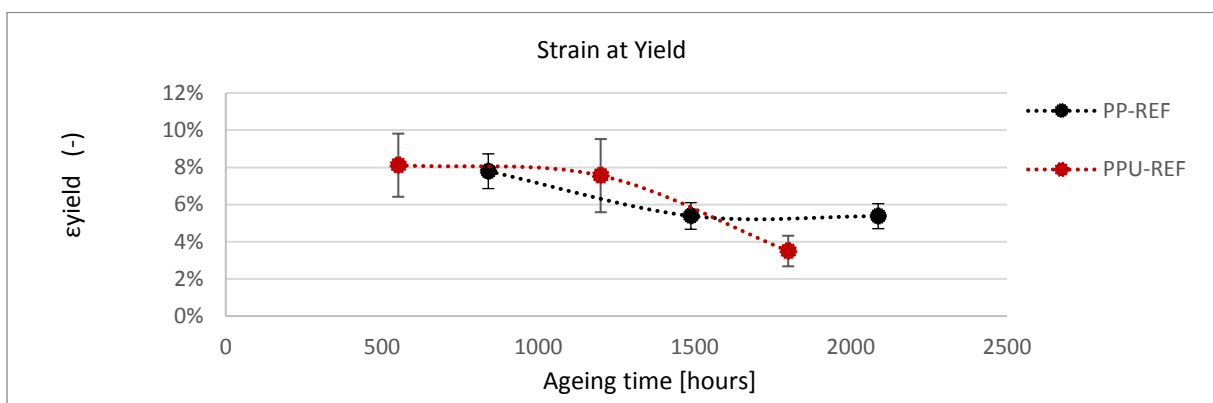


Figure 57: Results: influence of ageing time on yield strain (longitudinal).

Tabular results:

Material name	Count samples	Age Duration hours	UV Radiation hours	Yield Stress MPa	CV %	Tensile Modulus MPa	CV %	Yield Strain %	CV %
PP-REF	6	888	-	9.9	10	218	37.7	7.8	12
	11	1488	-	11.3	11	280	13.8	5.5	10
	10	2088	-	14.4	3	338	11.8	5.4	13
PP-EXP	10	1488	336	11.7	8	284	13.8	5.5	14
	10	2088	936	13.5	5	379	14.3	4.5	20
PPU-REF	7	552	-	11.9	9	196	16.3	5.1	21
	9	1200	-	9.3	17	187	24.6	4.8	22
	8	1800	-	12.7	8	425	11.9	2.1	24
PPU-EXP	7	1200	336	6.8	26	157	23.8	5.1	23
	9	1800	936	10.8	12	365	11.1	2.5	20

Table 6: Summary: longitudinal tensile strength properties, 5 mm/min.

Images of the longitudinal tensile test:

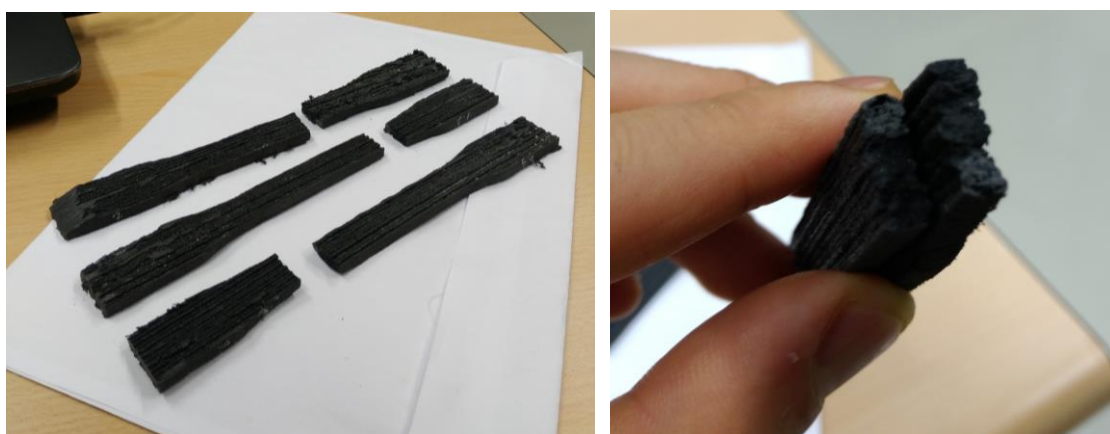


Figure 58: Picture of the tested sample of the material 3D printed PP.



Figure 59: Picture of the raw (left), injection-moulded (middle) and 3D printed PP-based composite.

The previous graphs and tables represent the tensile test results along the print direction for the material PP and PPU with respect to ultraviolet exposure time and ageing duration. Both materials were exposed and tested at the same time, but it should be considered that both materials consist of different curing time. From the test preparation, mechanical testing and the presented test results in this paragraph, several conclusions can be drawn:

- Tensile properties in the longitudinal direction for PP and PPU are time-dependent, both materials increased in yield strength, stiffness and decreased in yield strain over time. PPU tends to become stiffer than PP after 1500 hours of ageing as shown in **Figure 56**.
- The various print qualities including different interlayer bonds, voids and thickness still led to scattered data as can be observed in Appendix F (**Figure 131 - Figure 140**). It was experience that medium and high print quality samples led to more consistent results than samples of low print qualities.
- No trend is observed in the influence of ultraviolet exposure to the longitudinal tensile properties of PP and PPU as shown in **Figure 52 - Figure 54**.
- No visual colour changes are observed comparing the exposed and unexposed samples after each set of ultraviolet exposure.

Conclusions were made when comparing the tensile properties of the samples in the transverse and longitudinal print direction with the help of **Table 5 & Table 6**.

- Based on the coefficient of variance, it can be concluded that the tensile strength results in the longitudinal direction are more reliable and predictable than samples in the transverse print direction.
- The clamping complication was solved by sanding papering the rugged clamping area of the tensile sample. This led to less slippage and more usable data compared to the transverse tensile test.
- When comparing the results between the longitudinal and transverse test, both materials showed highly orthotropic behaviour. Much higher tensile strength and stiffness were found along the print direction (longitudinal>transverse).
- For both test directions, the failure mode on the tensile strength resulted in brittle rupture. Stress and strain at yield lied close to the breaking point. No plasticization was observed during the tensile tests.

6.1.4 Tensile test results of the flat-die-extruded polypropylene-based materials

Graphical results:

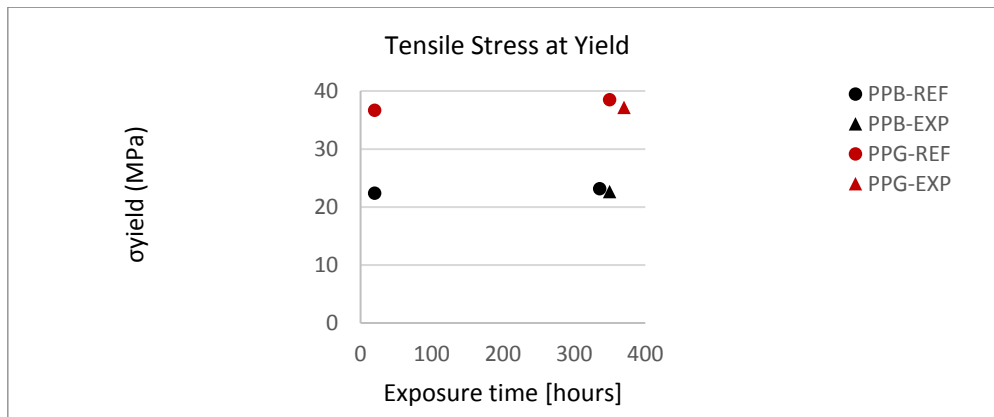


Figure 60: Results: influence of (un)exposure time on yield stress (longitudinal). *

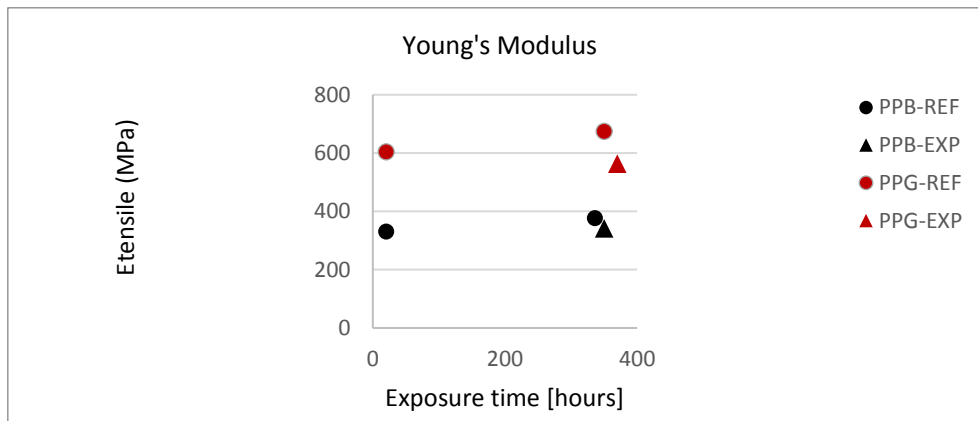


Figure 61: Results: influence of (un)exposure time on stiffness (longitudinal). *

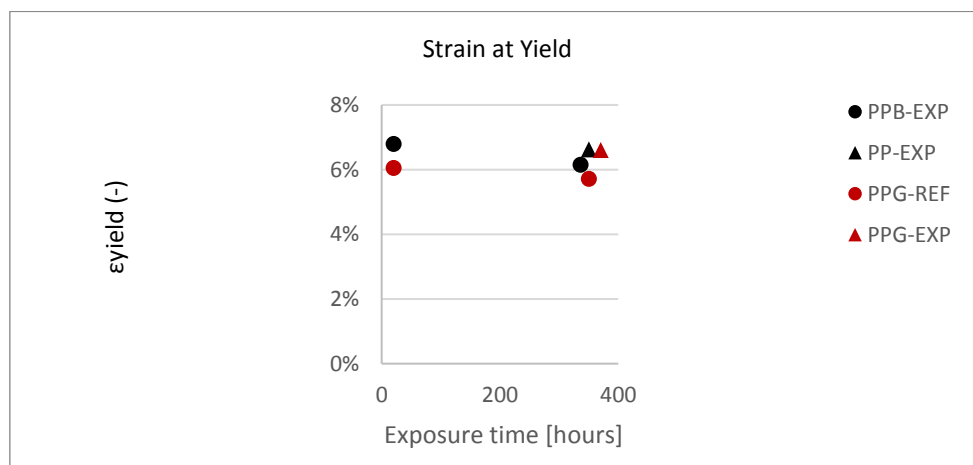


Figure 62: Results: influence of (un)exposure time on yield strain (longitudinal). *

*Since the standard deviation is reconsidered small, it couldn't be plotted within the graph.

Tabular results:

Material name	Count samples	UV Exposure hours	Yield Stress MPa	CV %	Tensile Modulus MPa	CV %	Yield Strain %	CV %
Virgin								
PPB-REF	7	0	22.4	0.8	331	5.7	6.8	5.8
	10	0	23.1	0.6	377	2.6	6.1	2.4
PPB-EXP	10	336	22.6	0.7	342	2.7	6.6	2.9
Recycled								
PPG-REF	9	0	36.6	1.4	604	2.3	6.0	2.4
	10	0	38.5	0.8	675	2.0	5.7	1.9
PPG-EXP	10	336	37.2	0.9	564	2.5	6.6	3.0

Table 7: Summary: tensile properties of flat-die-extruded PPB and PPG, 20 mm/min.



Figure 63: Picture of the tested sample of the material virgin black PPB.



Figure 64: Picture of the tested sample of the material recycled grey PPG.

The above graphical and tabular results represent the tensile test for the flat-die-extruded material PPB and PPG results in the extrusion direction. Both materials are exposed and tested at the same time. However, no information was required about the ageing age. From mechanical testing and the presented test results in this paragraph, several conclusions are drawn:

- The consistent surface of the flat-die-extruded polypropylene led to less clamping issues when compared to the 3D printed specimen tests, which resulted in more reliable and consistent test results as depicted in the (**Figure 141 - Figure 146**) of Appendix F.
- Both materials showed different failure modes. The grey recycled polypropylene (PPG, 3.0 mm) breaks in a brittle rupture as can be observed in **Figure 64**. The black virgin polypropylene (PPB, 1.2 mm), however, endures a plasticization with a high elongation as showed in **Figure 63**.
- Based on the coefficient of variance in **Table 7**, we found that the tensile strength results of the flat-die-extruded polypropylene are more reliable than the tensile properties of 3D print-extruded polypropylenes.
- Negligible changes in the tensile properties due to ageing or ultraviolet exposure were observed for the material PPG and PPB in the **Figure 60 - Figure 62**.
- No visual colour changes were observed by comparing the exposed and unexposed samples after each set of ultraviolet exposure for the material PPG. However, the material PPB, however, showed small loss of colour and warping during the ultraviolet exposure.

6.1.5 3D print-extruded versus flat-die-extruded

Graphical results of the relative change of (un)exposed polypropylene materials, with respect to the tensile properties of 0 hours exposure sets, after 336 hours of ultraviolet exposure:

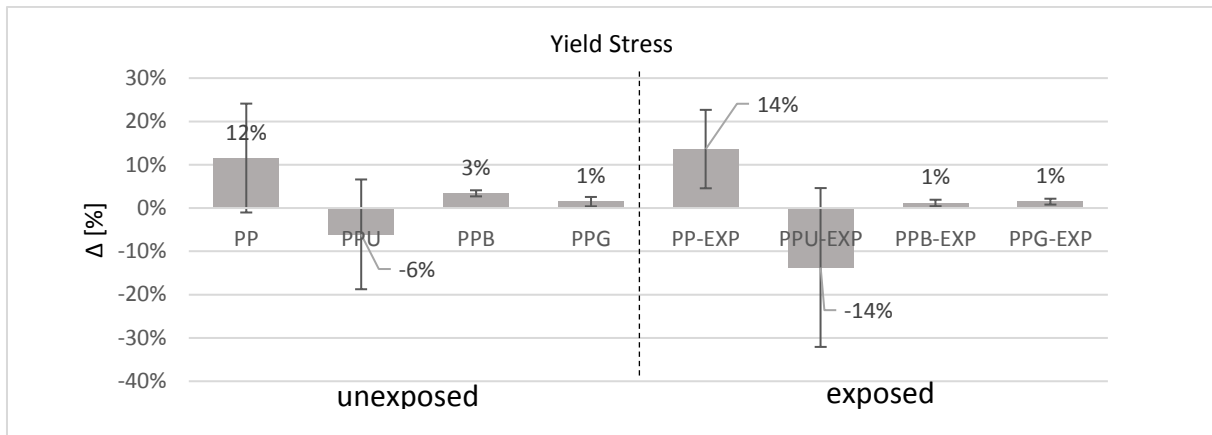


Figure 65: Results: influence of (un)exposure time on yield stress (longitudinal).

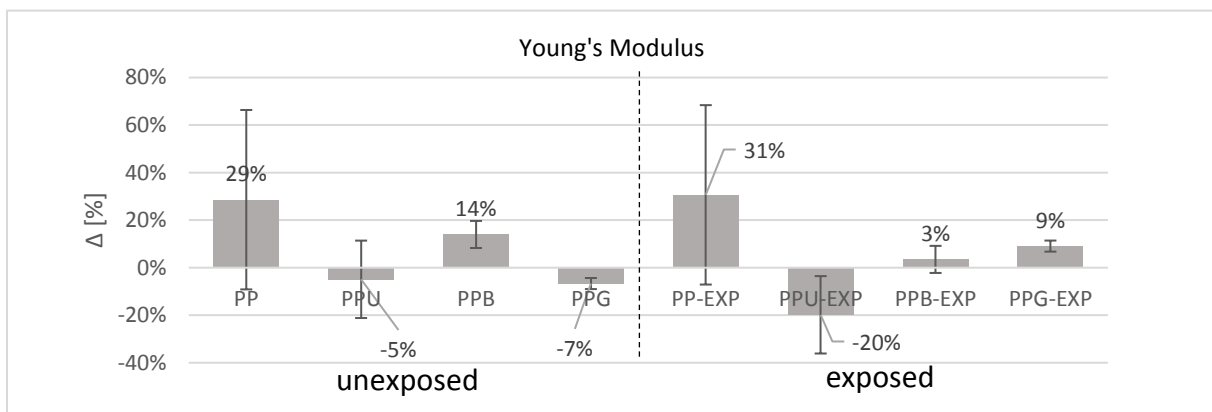


Figure 66: Results: influence of (un)exposure time on stiffness (longitudinal).

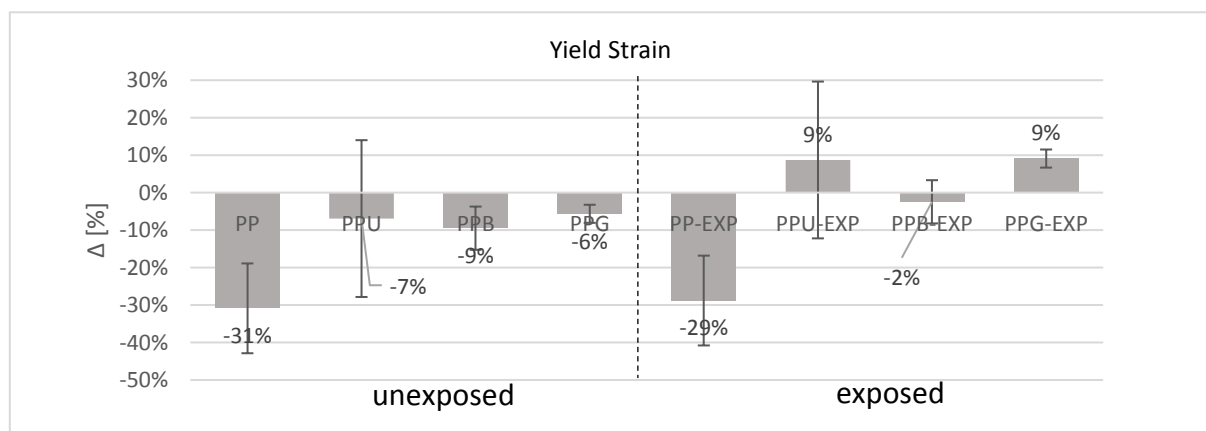


Figure 67: Results: influence of (un)exposure time on yield stress (longitudinal).

Graphical results of the relative difference of the tensile properties of exposed and unexposed polypropylene:

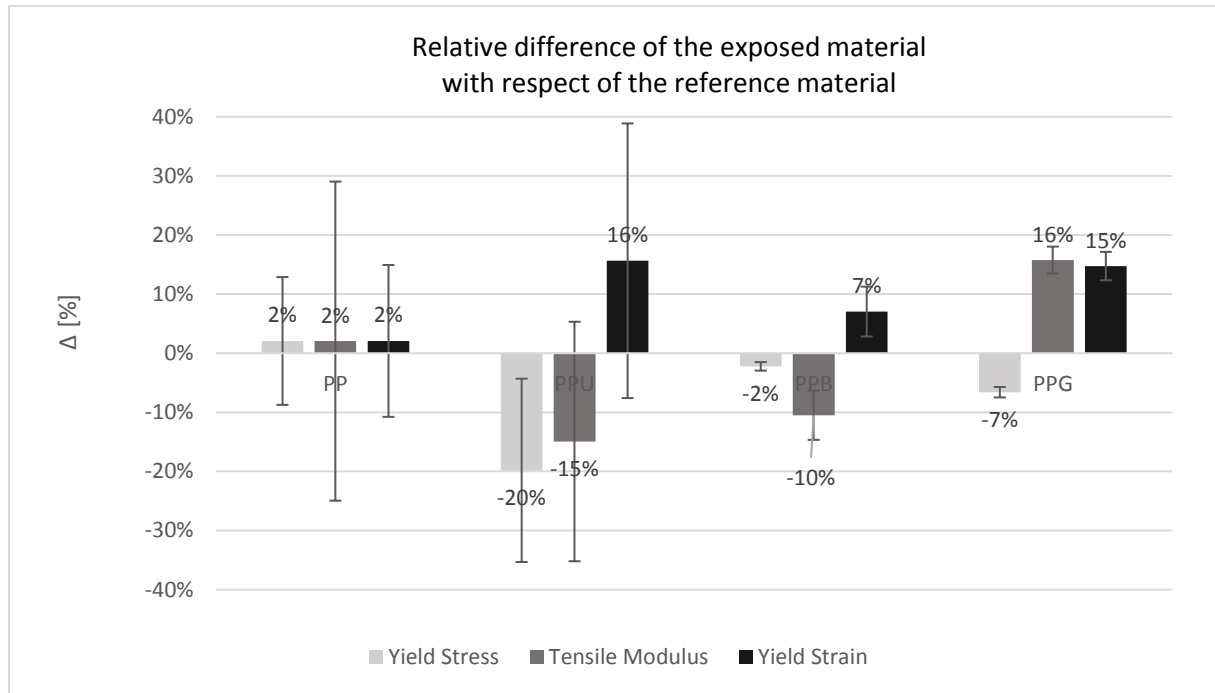


Figure 68: Results: change of tensile strength and stiffness of a 336h UV-exposed materials compared to its unexposed material.

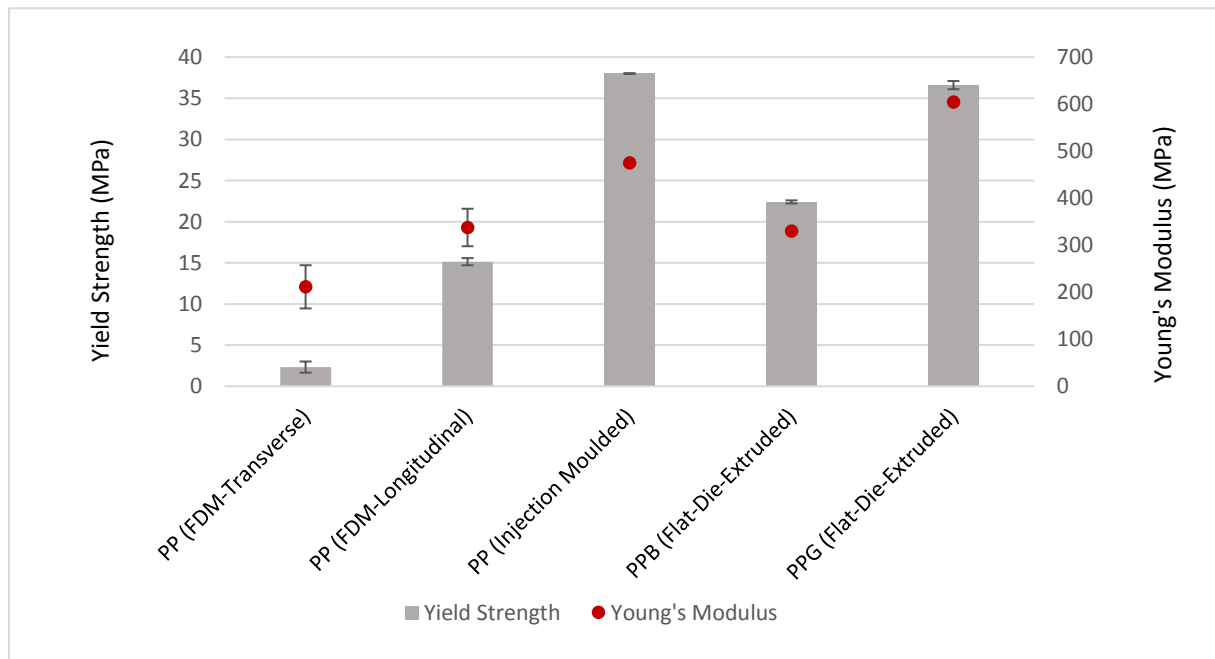


Figure 69: Tensile strength comparison between different PP-based materials. *

*Tensile properties of the inject-moulded material are subtracted from the mechanical sheet in Appendix A (Figure 107).

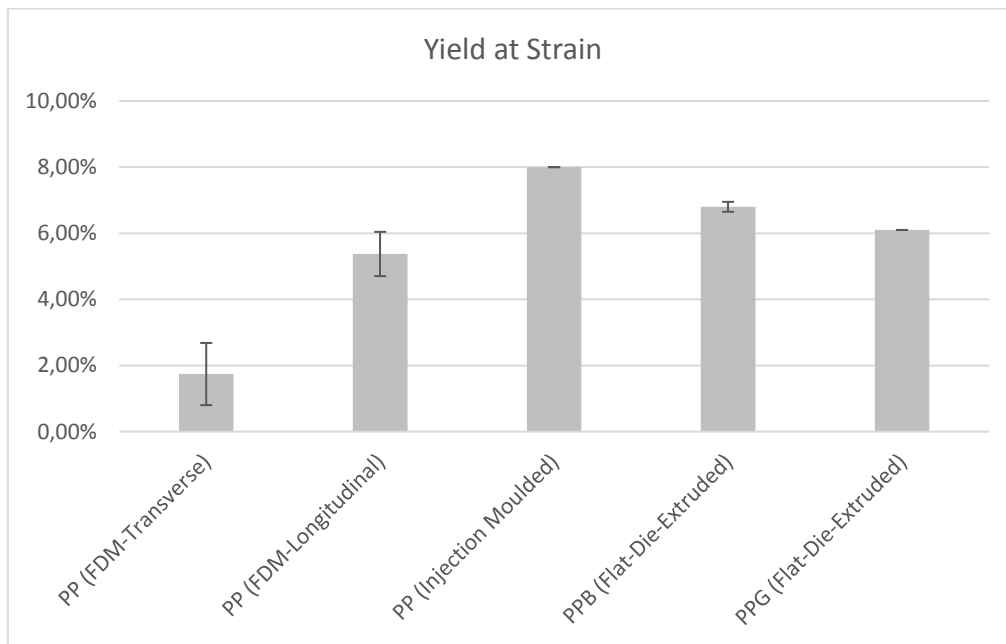


Figure 70: Comparison between different PP-based materials on their yield strain. *

*Tensile properties of the inject-moulded material are subtracted from the mechanical sheet in Appendix A (**Figure 107**).

The following observations can be made based on the comparative quantitative results of the tensile tests of the flat-die extruded polypropylene based materials PPG and PPB and 3D print-extruded PP & PPU.

- Comparison between the manufacturing methods is difficult, due to uncertainties of the scattered tensile test results of the 3D printed samples as depicted in the **Figure 65 - Figure 68**.
- Flat-die-extruded PP-based polymers tend to slightly increase in yield strength over time for both exposed and reference samples as can be seen in **Figure 65**. However tensile modulus tends to have different changes due to the influence of time and UV exposure (**Figure 66**).

In general, the 3D print-extruded PP-based composites, in transverse as in longitudinal direction, have the lowest tensile strength properties among the manufactured polypropylene-based materials as shown in **Figure 69 & Figure 70**.

6.2 Charpy impact strength

6.2.1 Charpy impact strength properties

The Charpy impact strength of the notched specimens, a_{cN} , expressed in kilojoules per square mini-metre using the following equation:

$$a_{cN} = \frac{E_c}{hb_N} 10^3$$

Where:

E_c is the corrected energy, in joules, absorbed by breaking the test specimen;

h is the thickness, in millimetres, of the test specimen;

b_N is the remaining width, in millimetres, of the test specimen;

6.2.2 Charpy Impact Strength Results

Graphical results:

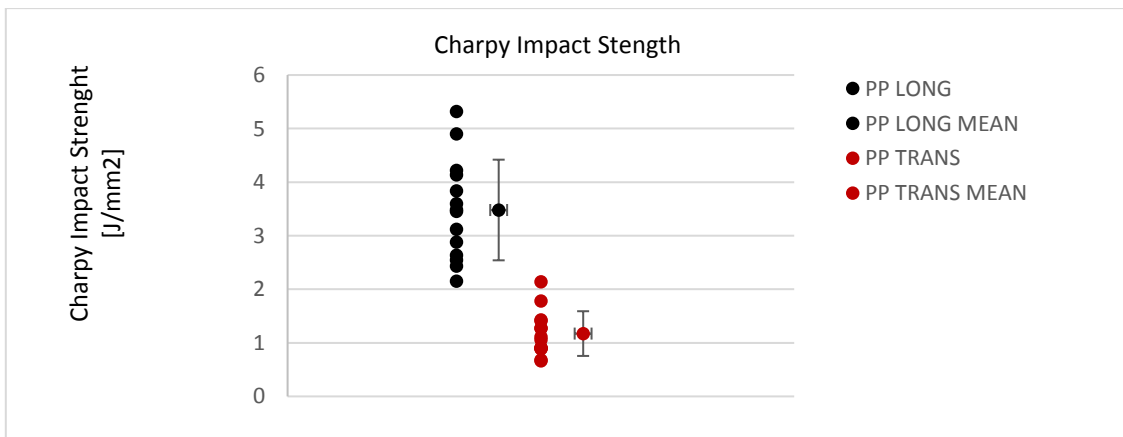


Figure 71: Results: influence of (un)exposure time on Charpy impact test in both directions.

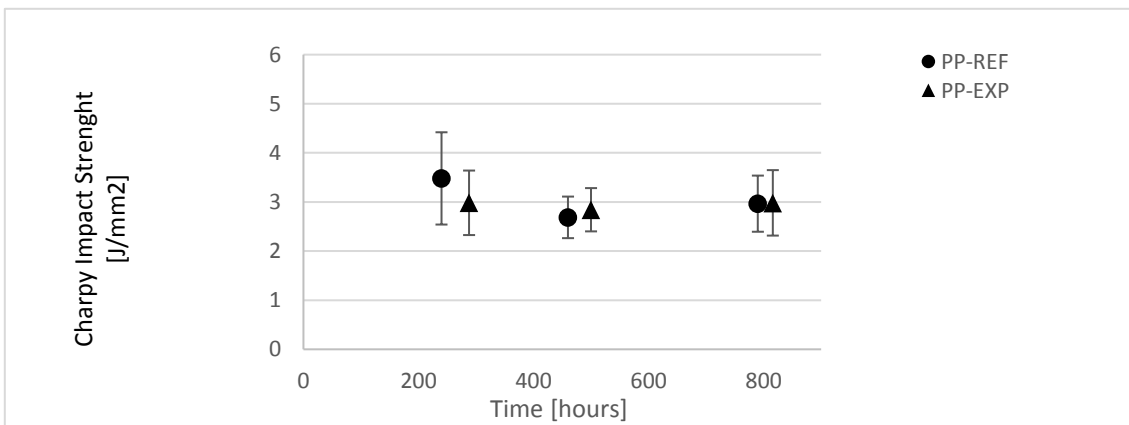


Figure 72: Results: influence of (un)exposure time on Charpy impact test (longitudinal).

Tabular results of the Charpy impact test:

Material name	Count samples	UV Exposure hours	Charpy Impact Strength J/mm^2	CV %
PP-REF (transverse)	14	-	1.17	35.6
PP-REF (longitudinal)	14	-	3.48	27.0
	15	-	2.89	15.7
	15	-	2.97	19.3
PP-EXP (longitudinal)	14	288	2.98	22.0
	15	480	2.84	15.5
	15	816	2.94	22.4

Table 8: Summary: Charpy impact test results.

The following observations can be made based on the comparative quantitative results of the Charpy impact test for print material PP:

- The test results of **Figure 71** showed that samples in the longitudinal direction exhibit a higher Charpy impact strength than test samples with the print layers in the transverse direction.
- The Charpy impact test results showed highly scattered data resulting in a high coefficient of variation as shown in **Table 8**.
- No trend is observed on the influence of ultraviolet degradation on the Charpy impact strength for the polypropylene-based material as can be seen in **Figure 72**.

6.3 Influencing factors

The outcomes in the previously described load tests were influenced by different factors. These factor, including the print/cut quality and the clamping issue, are discussed in this section.

6.3.1 Various print qualities

The print quality of the test specimen for the mechanical testing depends on the printing parameters such as nozzle height, printing speed, and printing temperature. Several studies have addressed this issue. Carneiro et al. found out that objects produced by extrusion-based additive manufacturing experience the disadvantage of consisting of many weld-lines, which consequently downgrade their mechanical properties due to their inconsistency (Carneiro, Silva, en Gomes 2015). Weak interlayer bonding and porosity could create a primary fracture path during the tensile test (W. Wu et al. 2015). Weak interlayer bonding could be the result of either residual stresses caused by shrinkage, or by the low molecular diffusion and low cross-linking between the printing layers after the extrusion. When material extrusion is unpredictable this could lead to printing layers that do not fully overlap with each other, which also weakens the interlayer bonding. The interlayer porosity reduces the load-bearing area across the layers and hence provided an easy fracture path (Spoerk et al. 2017).

When the extruded plate was visually checked, pores were mainly located between the printed layers and the overall interlayer bonding was highly inconsistent as can be seen in **Figure 73**. Especially for the transverse tensile samples, interlayer porosity had a big influence in decreasing the tensile strength and acts as stress concentration points. A variation in interlayer bonding and

porosity results in different print qualities and thickness. Subsequently, this resulted in scattered test data, making the material unpredictable and unreliable for building applications.

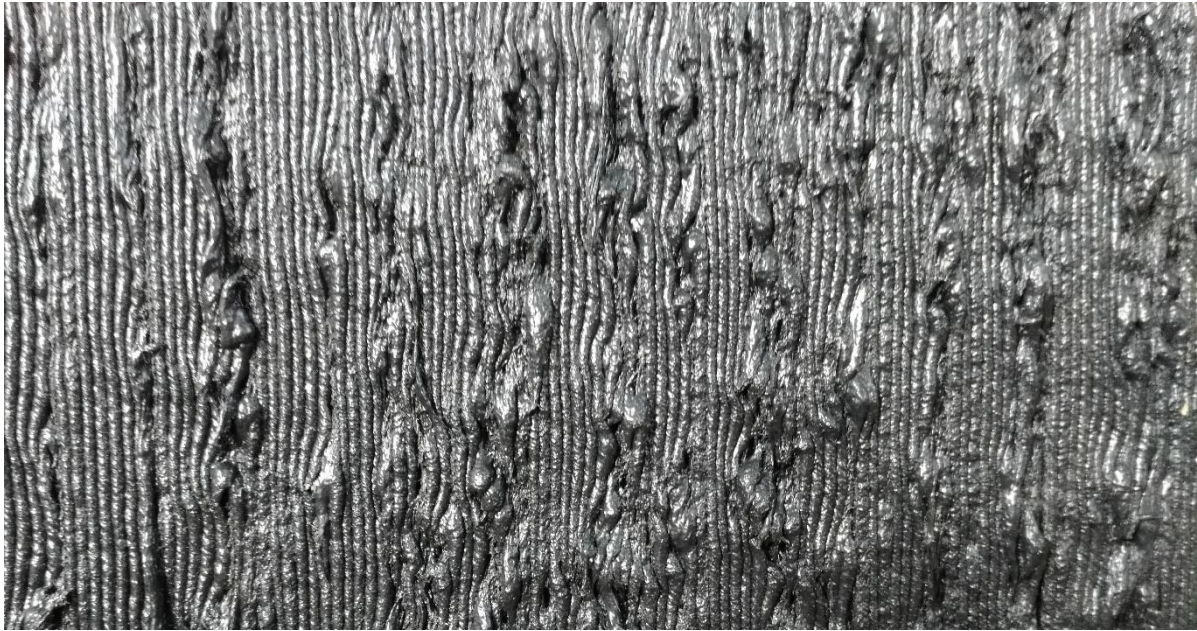


Figure 73: Various print quality of the material PP.

6.3.2 Cut quality

When the batches were cut in plates with a jigsaw, it could be observed that the plates were bent (see **Figure 74**). The bending is the result of warping during the printing process in the KamerMaker.



Figure 74: The bent extruded plate of the material PP.

The bent plates have a big influence on the cutting quality of the tensile samples. The water jet cutter with a cut diameter of 0.671 mm, must be as close to the plate as possible. The cut diameter will be more uncontrolled when its further away from the plates, despite its high speed. With a bent plate, it seems likely that due to the different cutting distance the end tensile samples will be slightly different. During and after cutting another aspect arises. The liquid in the water jet machine is filled with sand. Even after cleaning the material with an air blower, the sand particles could still be attached between the layers of the samples. This will certainly influence the ultraviolet absorption of the material.

6.3.3 Slippage

Two failure modes have been observed in the tensile strength test and are depicted in **Figure 75**. The first failure mode is depicted by the black line (10), an almost linear line from the start of the displacement and it results in a sudden brittle break without any plasticization. The yield point and the point of fracture lie close to each other.

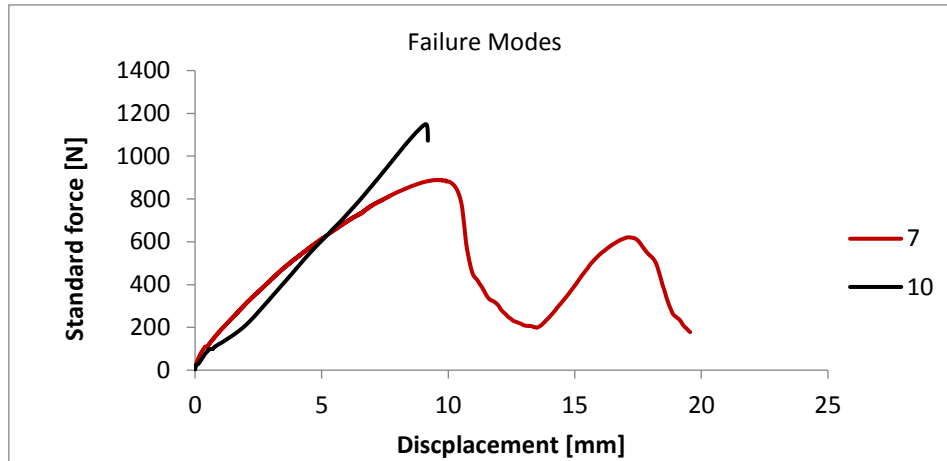


Figure 75: Different failure modes during the tensile tests.

The second failure mode is depicted by the red line (7) and won't break but ends in slippage of the sample between the grips. Due to the irregular surface of the test samples, it was difficult for the tensile machine to have a sufficient grip, as illustrated in **Figure 76**. This clamping issue often results in slippage and unrepresentative test results. At the tensile test in the transverse print direction, a too firm grip could damage the sample which led to lower sample counts and thereby a relatively higher coefficient of variance. The clamping issue is partly resolved for the tensile test with samples in the longitudinal print direction. The uneven clamping area of the tensile sample was sand scrubbed which led to more consistent sample thickness and more grip between the clamping and the test sample. The solution led to higher sample counts for the longitudinal tensile test than compared to the transverse tensile test as can be compared between **Table 5 & Table 6**.

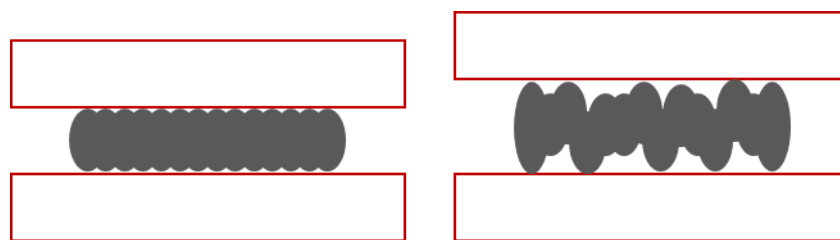


Figure 76: Sufficient clamping (left), insufficient clamping (right).

6.4 Characteristic value of the tensile properties

The numbers of specimen used were often 10 pieces per test, while the NEN-EN-ISO suggests a minimum of 5 pieces per set (Nederlands Normalisatie-Insituut 1997). This is chosen because of the recognizable variety of cross-sectional print qualities. A low sample amount could reduce the scientific value of the results. However, due to sample slippage, much of test results were unusable, which influences the characteristic values of the tensile strength properties. In this paragraph the characteristic values of the tensile strength properties were determined properties according to NEN-EN 1990 (Nederlands Normalisatie-Insituut 2011) with the following formula:

$$X_k = m_x(1 - k_n CV)$$

Where:

- m_x - mean value of a property
- k_N - value dependent on the sample length according to **Table 9**.
- CV - coefficient of variation

N	1	2	3	4	5	6	8	10	20	30	∞
k_n	2.31	2.01	1.89	1.83	1.80	1.77	1.74	1.72	1.68	1.67	1.64

Table 9: Values of k_n for the 5% characteristic value (Nederlands Normalisatie-Insituut 2011).

Table 10 - Table 12 show the characteristic values of the tensile properties of the PP-based composites. The percentage decrease (Δ), from the mean value to the chiastic value of the tensile property, is calculated with the following formula:

$$\Delta_i = (x_{m,i} - X_{k,i}) / (X_{k,i}) 100\%$$

Tabular results of the the characteristic transverse tensile properties of PP and PPU:

Material name	Count samples	Age		σ_{mean} MPa	σ_{yk} MPa	Δ_σ %	E_{mean} MPa	E_{yk} MPa	Δ_E %	ϵ_m %	ϵ_{yk} %	Δ_ϵ %
		Duration hours	UV Radiation hours									
PP-REF	8	888	0	2.4	1.6	32	141	91.1	35	1.7	1.34	20
	6	1008	0	2.8	1.5	47	117	56.4	52	2.5	0.75	71
	8	1296	0	2.3	1.1	51	150	71.9	52	1.7	0.10	94
PP-EXP	6	1032	240	2.6	1.7	35	151	123.0	19	1.7	1.22	28
	9	1032	576	2.3	1.2	50	112	81.9	27	2.0	0.96	53
	10	1296	840	2.4	1.4	42	126	63.1	50	2.0	0.75	56
PPU-REF	7	552	0	2.7	0.9	68	148	97.3	34	2.1	0.86	51
	6	672	0	2.8	1.9	33	76	40.2	47	3.5	2.07	46
	7	960	0	2.7	1.4	49	105	76.6	27	2.7	1.66	41
PPU-EXP	7	667	240	2.0	1.1	45	74	57.7	22	2.8	1.61	44
	8	667	576	2.9	2.0	31	91	60.4	34	3.3	2.00	39
	8	960	840	2.7	1.6	42	87	68.3	21	3.4	1.06	63

Table 10: Characteristic values of the transverse tensile test, 2 mm/min.

Tabular results of the the characteristic longitudinal tensile properties of PP and PPU:

Material name	Count samples	Age		σ_{mean} MPa	σ_{yk} MPa	Δ_{σ} %	E_{mean} MPa	E_{yk} MPa	Δ_E %	ϵ_m %	ϵ_{yk} %	Δ_{ϵ} %
		Duration hours	Radiation hours									
PP-REF	6	888	-	12.0	9.9	17	218	72	67	7.8	6.1	21
	11	1488	-	13.9	11.3	18	284	194	32	5.5	4.6	17
	10	2088	-	15.1	14.4	5	338	269	20	5.4	4.2	22
PP-EXP	10	1488	336	13.7	11.7	15	284	215	24	5.5	4.2	25
	10	2088	936	14.7	13.5	8	379	286	25	4.5	2.9	34
PPU-REF	7	552	-	14.2	11.9	16	196	140	29	8.1	5.1	37
	9	1200	-	13.3	9.3	30	187	98	48	8.2	4.8	41
	8	1800	-	14.8	12.7	14	425	337	21	3.5	2.1	41
PPU-EXP	7	1200	336	12.2	6.8	45	157	93	41	8.4	5.1	39
	9	1800	936	13.6	10.8	20	389	247	36	3.9	2.5	35
PP-INJECT	-	-	-	-	38.0	-	-	475	-	-	8.0	-

Table 11: Characteristic values of the tensile strength properties, 5 mm/min.

Tabular results of the the characteristic tensile properties of PPB and PPG:

Material name	Count samples	UV		σ_{mean} MPa	σ_{yk} MPa	Δ_{σ} %	E_{mean} MPa	E_{yk} MPa	Δ_E %	ϵ_m %	ϵ_{yk} %	Δ_{ϵ} %
		Exposure hours										
Virgin												
PPB-REF	7	0		22.4	22.0	1	331	298	10	6.8	6.1	10
	10	0		23.1	22.9	1	377	360	4	6.1	5.9	4
PPB-EXP	10	336		22.6	22.4	1	342	326	5	6.6	6.3	5
Recycled												
PPG-REF	9	0		36.6	35.8	2	604	580	4	6.0	5.8	4
	10	0		38.5	38.0	1	675	652	3	5.7	5.5	3
PPG-EXP	10	336		37.2	36.6	2	564	540	4	6.6	6.3	5

Table 12: Characteristic values of the tensile strength properties, 20 mm/min.

From **Table 10 - Table 12** we can see that the results the value of the coefficient of variation, CV , is higher for the 3D printed samples in both the transverse as the longitudinal print direction compared to the flat-die-extruded samples. Also, due to the specimen slippage, a part of the obtained results was unusable, which lowered the number of test samples. The scattered results and the low sample count decrease the characteristic value of the tensile properties of the 3D print-extruded material with a maximum percentage of 94% for the samples in the transverse direction and 67% for the samples in the longitudinal direction. While the flat-die-extruded tensile tests results show more consistency and less material slipping, they result in a higher characteristic value with a maximum percentage decrease of 10%. Although it is not discussed within this study, the unpredictability of the tensile properties of the 3D printed material will have a negatively impact of the safety factor using this material.

6.5 Summary

After the repetitive mechanical tests in combination with the ultraviolet radiation exposures, a relatively comprehensive overview was made of the materials mechanical properties and their dependence on ageing and the influence of ultraviolet exposure. The confidence in the mechanical results is lost due to the mentioned influencing factors. The first influencing factor was the different print qualities of the test specimen. This issue has been addressed by implementing the print quality classification system based on a visual inspection. However, it is recommended for further study that a more consistent print quality should be tested. Next to that, a more extensive and better-structured investigation would be desirable to get a better hold of this issue. The second influencing factor, the sample slippage, had a significant impact on the results. During the printing, extra residual material concentrates on the surface leading to an uneven the clamping area of the tensile samples. Which had immediate consequences on the outcome of the mechanical test and is mostly followed by slippage, which made the results unusable.

Nevertheless, collected information of all the tensile and impact tests was sufficient to draw a range of quantitative and qualitative conclusions, from which the most important are summed up below:

- Ageing of the extruded thermoplastic polymer changes in the mechanical properties with the general loss of ductility. The mechanical testing results showed an increase of the tensile modulus and a decrease in the yield strain of the polymers. No remarkably changes in the yield strength of the thermoplastic polymer was observed.
- Material behaviour of the 3D printed composite is highly orthotropic, with a strong influence of the visible print quality. Higher strength and stiffness were found in the longitudinal tensile test results.
- For the 3D print-extruded material PP and PPU, stress and strain at yield were close to the point of fracture; the general failure mode shows brittle rupture. No plasticization was observed during the tensile test.
- For longitudinal tensile tests, statistical dispersion of all results decreased as the time between printing and testing increases. This implies that the material becomes more stable over time.
- No significant difference is observed of the influence of ultraviolet exposure between the exposed and unexposed tensile specimens based on the results of the tensile strength test, Charpy impact test and visual (colour) quality comparison of the samples.

Conclusions from the comparison of the tensile test between 3D print-extruded and flat-die-extruded and injected moulded polypropylene:

- The consistent surface of the flat-die-extruded polypropylene led to less clamping issues when compared to the 3D printed specimen, which could be observed in consistent test results.
- Both materials showed different failure modes. The grey recycled polypropylene (PPG; 3.0 mm) breaks in a brittle rupture, the black virgin polypropylene (PPB; 1.2 mm), however, endures a plasticization with high elongation.
- Negligible changes in the tensile properties due to ageing or ultraviolet exposure were observed for the material PPG and PPB.
- In both direction, tensile strength and stiffness of 3D printed PP are relatively low compared to injection moulded PP.

- The loss of test samples due to slippage and the high variety of test results profoundly affects the predictability of the 3D printed material compared to the flat-die-extruded samples. This resulted in low characteristic values for the tensile test properties of the 3D-print extruded PP-based composite.

As seen in the results, the tensile properties of various PP-based materials prepared by flat-die-extrusion generally came superior in the tensile tests if compared to those of 3D printing. More material is needed for producing a façade element with the 3D print technique than the conventional flat-die-extruded technique to ensure equal structural safety. Based on the results, we conclude the use of the PP-based composite (Mafill) manufactured with the 3D Printer 'KamerMaker' is not sufficient enough for building applications ensuring predictable structural resistance. Improving the tensile properties of the samples could be found in the print parameters of the 3D printing technique itself such as the nozzle diameter and the printing temperatures. However, more research must be done on the effect of the processing technique on the mechanical properties of the 3D print extruded material.

PART IV
Further Analysis

Chapter 7

Thermal Analysis

The following chapters describes broadening material experiments performed to study the effect of 3D printing on polypropylene-based composites. Following experiments are performed and elaborated:

- Differential scanning calorimetry (DSC) Chapter 7
- Digital microscopy Chapter 8
- Scanning electron microscopy (SEM) Chapter 8
- Fourier-transform infrared spectroscopy (FTIR) Chapter 9

These results can bring new insights into the development of 3D printed material. However, obtained results need to be analysed with the utmost care as their reliability might be questionable due to low sample counts.

7.1 Thermal history of polymers

Thermal history of thermoplastic polymers includes the effect of previous heat treatments and storage conditions that have an influence on a polymer at the molecular level. It is important to understand the thermal history since 3D printed material undergoes several heating-cycles. These temperature changes, in combination with the effect of humidity and oxygen, can have a strong effect on the polymer chains. Overheating can decrease mechanical properties of a polymer (Zeus 2005), therefore it can be questioned what effect of the heat treatment has on the polymer chains. In the chapter the thermal history of the 3D printed and flat-die-extruded polypropylene-based polymers are discussed. Differential scanning calorimetry (DSC) measurements are used to increase knowledge regarding the influence of heat during 3D printing of the polypropylene-based composite.

7.1.1 Differential Scanning Calorimetry

Using DSC, researchers can determine to what extent a polymer is amorphous or crystalline. The technique analyses the response of materials when exposed to heat. Within a DSC test, the difference in the heat flow rates of the test samples as a function of time and temperature. Two pans are heated in the measurement device, one pan is empty (reference) and the other pan contains material to be investigated. The sensors in the device measure the rate at which the temperature changes in the pans. The output data will be shown on the screen. With the use of the DSC-analysis, properties of the sample could be determined such as the glass transition (T_g). The glass transition point is the temperature range during which a polymer changes from a hard, rigid or “glassy” state to a more pliable, compliant or “rubbery” state. In other words, the glass transition point is the temperature (range) at which the movements of chains in polymers can occur. A change of the T_g indicate a change in the polymer for example; the crystallinity, crosslinking, curing, polymerization, molar mass and chemical composition. Further properties obtained by the DSC are melting transition (T_m), crystallization transition (T_c) specific heat, the rate of curing, purity, the percentage of crystallinity (Schawe et al. 2000).

As mentioned, DSC measures differences in heat flow rate between a test sample and an inert reference as a function of time and temperature. Two heat flow curves can be distinguished. The endothermic curve represents the heat that will be absorbed by the material during heating (melting) and the exothermic curve represents the heat flow out of the sample during cooling

(crystallization). The enthalpy, ΔH_m or ΔH_c , is the heat energy required for melting or released upon crystallization and is calculated by integrating the area of the DSC peak on a time basis (J/g).

7.1.2 Thermal degradation of polymers

As mentioned earlier, temperature influences the mobility of molecular chains of polymers, which can influence the physical properties of the material. Overheating of polymers could result in thermal degradation of polymers and therefore the deterioration of polymer molecules. At high temperatures, the components of the long chain backbone of a polymer can begin to separate (chain-scission) and react with one another resulting a change in the properties of the polymer (Aboulkas, El harfi, and El Bouadili 2010).

Polypropylene is known to be susceptible to thermal degradation, even at chamber temperatures. Thermal degradation can cause chain-scissoring as illustrated in **Figure 77** (A); a phenomenon describing the breaking of polymer chains, reducing the chain length and molecular weight. This can considerably change mechanical properties and thus results in highly reduced ductility and increased embrittlement (Iring et al. 1978). Most types of degradation follow a similar basic pattern. A conventional model for thermal degradation is that of an autoxidation process which involves the major steps of initiation, propagation, branching, and termination (Zeus 2005).

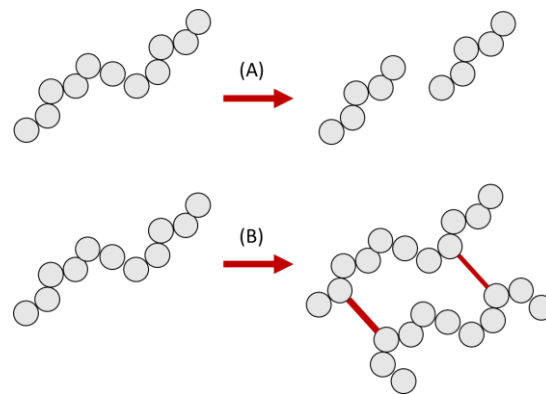


Figure 77: Chain-scission (A) and cross-linking (B) and of polymer chains.

Some polymers, are also susceptible to ‘branching’ of the polymer chains. This occurs when polymer chains become linked together, resulting in cross-linking. Crosslinking of chains form bonds that join two polymer chains together as illustrated in **Figure 77** (B). Mechanical properties of a polymer depend strongly on the cross-link density. Crosslinking, often is related to the ageing of a polymer and can results in a stiffer material (Kamrannejad et al. 2014).

7.2 Test procedure

The differential scanning calorimetry test was carried out on a Perkin–Elmer DSC 8000 instrument (**Figure 78**) at the Faculty of Aerospace Engineering of the Delft University of Technology under the supervision of Mr F.G.C. Oostrum and Dr. ir. M. Neijemeisland. Specimens from about 5 mg were removed from the material’s surfaces and placed in a test pan. Thermal scans were made at a heating/cooling rate of $10^{\circ}\text{C}/\text{min}$ over a temperature range between -50°C and 220°C . Cooling was achieved by using liquid nitrogen. Melting and crystallisation temperatures are defined as the peak temperature of the endothermic and exothermic curves. Afterwards, a DSC-software program is used to calculate the enthalpy from the melt peak areas (J/g).



Figure 78: Differential scanning calorimetry auto-sampler (left) and liquid nitrogen cooler (right).

To increase understanding of the difference in thermal history, a selection of the material has been made for the DSC-test and. Each material is divided into group and are summed up below:

- 3D printed PP (before printing (PP-RAW), after printing (PP-ZERO), aged 1000 hours (PP-REF) and ultraviolet exposed (PP-EXP).
- 3D printed PPU (PP with UV stabilisers): (after printing (PPU-ZERO), aged 1000 hours (PPU-REF) and ultraviolet exposed (PPU-EXP).
- Flat-die extruded black virgin PP (unexposed PPB-REF, ultraviolet exposed PPB-EXP).
- Injection-moulded PP (PP-INJ)

As mentioned, analysed material will be exposed to a temperature ranging from -50°C to 220°C under the following heat and cool-cycle:

1. Hold for 5.0 min at 25.00°C
2. Cool from 25.00°C to -50.00°C at $10.00^{\circ}\text{C}/\text{min}$
3. Hold for 5.0 min at -50.00°C
4. Heat from -50.00°C to 220.00°C at $10.00^{\circ}\text{C}/\text{min}$
5. Hold for 5.0 min at 220.00°C
6. Cool from 220.00°C to -50.00°C at $10.00^{\circ}\text{C}/\text{min}$
7. Hold for 5.0 min at -50.00°C
8. Heat from -50.00°C to 220.00°C at $10.00^{\circ}\text{C}/\text{min}$
9. Hold for 5.0 min at 220.00°C
10. Cool from 220.00°C to 25.00°C at $10.00^{\circ}\text{C}/\text{min}$
11. Hold for 5.0 min at 25.00°C

The test results only show the step 4, where the material is heated up from a material temperature of -50.00°C to 220.00°C with a heat rate of $10.00^{\circ}\text{C}/\text{min}$. In this step the glass transition temperature (T_g), melt peak temperature (T_m) and enthalpy (ΔH_m) were measured. The cycle was done to check if the first cycle was executed correctly.

7.3 Test results

Graphical results of the DSC-analysis:

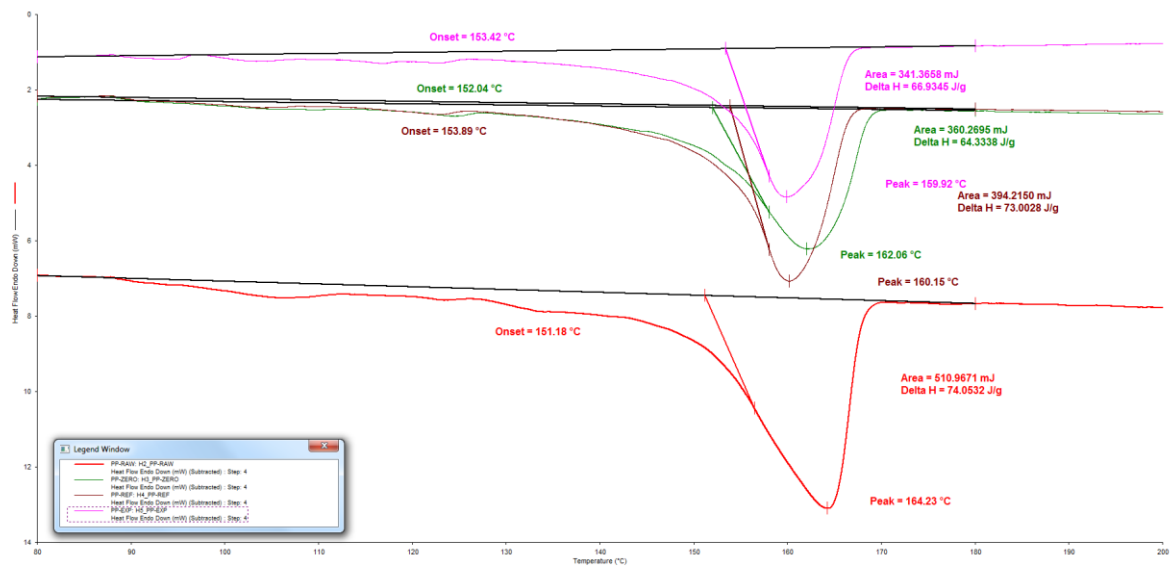


Figure 79: DSC-results: 3D printed PP: Raw material (red), just-printed (green), aged (brown) and exposed (purple).

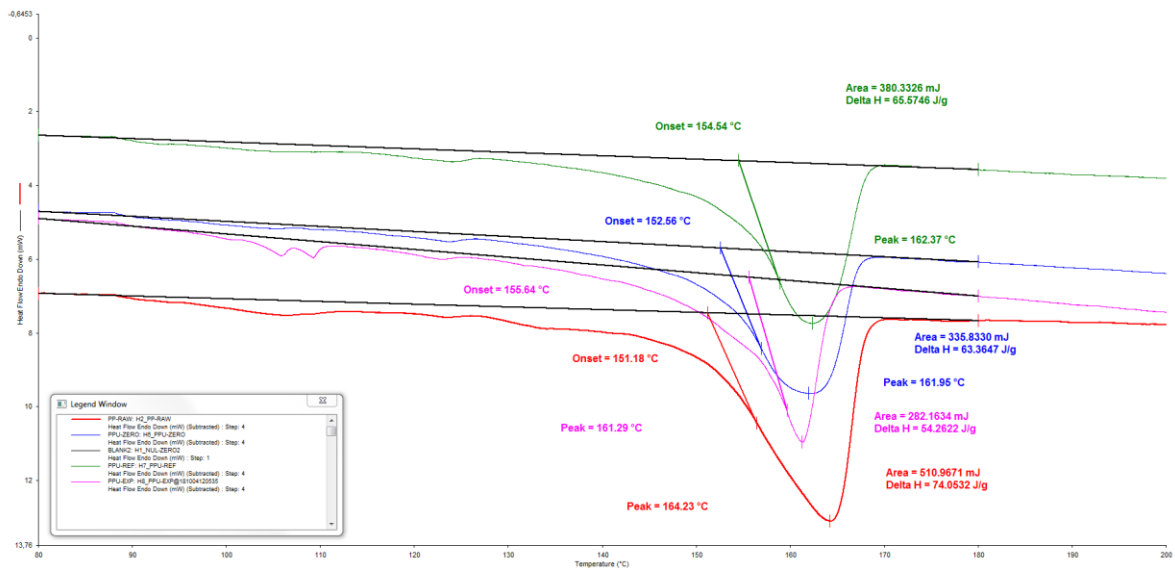


Figure 80: DSC-results: 3D printed PPU: Raw material (red), just-printed (blue), aged (green) and exposed (purple).

Graphical results of the DSC-analysis:

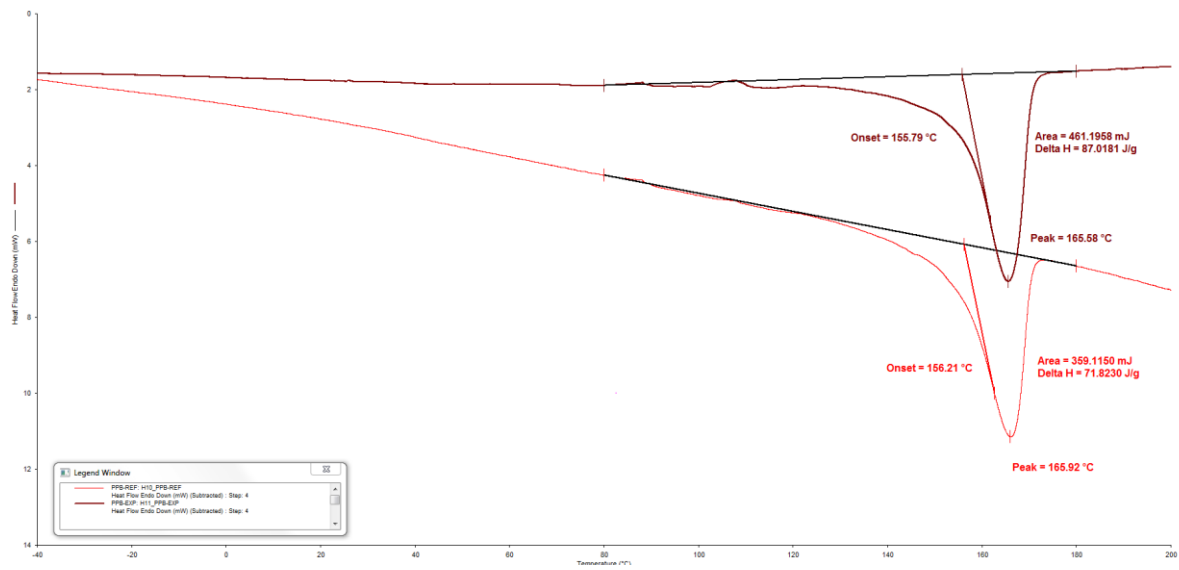


Figure 81: DSC-results: virgin PPB: reference (red) and exposed (brown), (thickness of 1.2 mm).

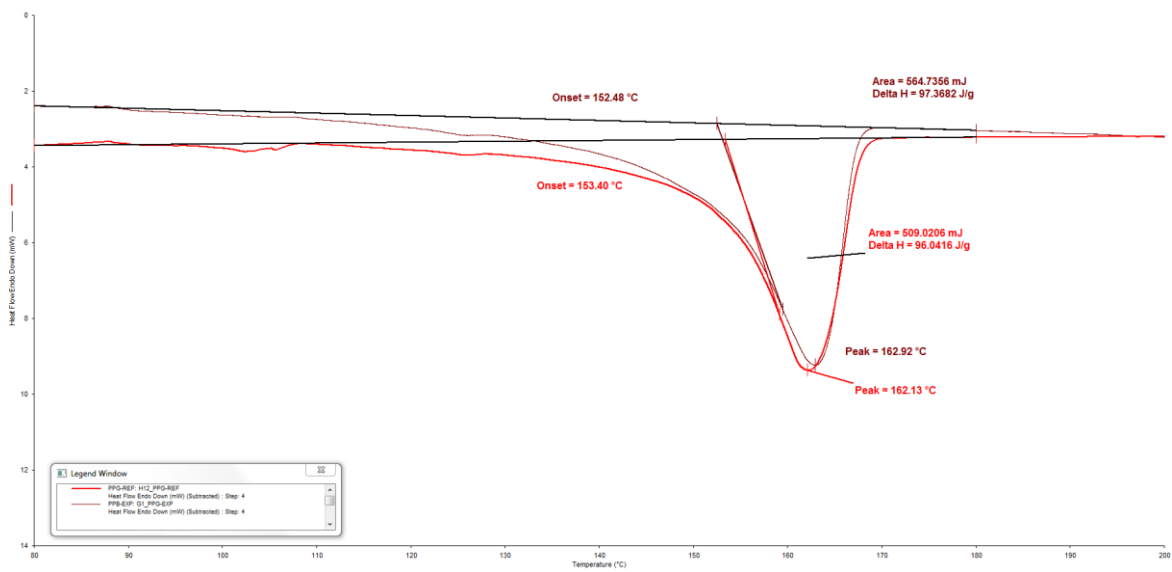


Figure 82: DSC-results: recycled PPG: reference (red) and exposed (brown).

Graphical results of the DSC-analysis:

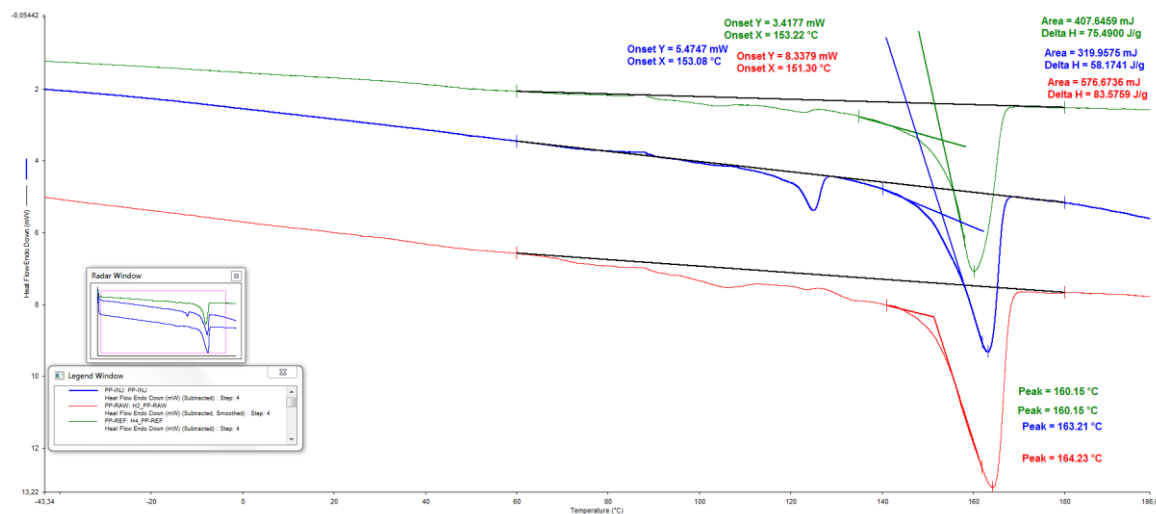


Figure 83: DSC-results: Raw (red), 3D printed (green), inject-moulded (blue) PP.

The degree of crystallinity of sample, X_c at the peak melting or crystallization temperature is calculated from the enthalpy of melting or crystallization, respectively (ΔH_m or ΔH_m (J/g)) obtained from the DSC measurements by comparison with literature data for 100% crystalline PP according to the following equation (Kong and Hay 2003):

$$X_c = \frac{\Delta H_m}{\Delta H^\circ}$$

Where ΔH° is the melting enthalpy of 100 % crystalline polymer ($\Delta H^\circ = 207 \frac{J}{g}$ for 100% crystallised PP).

Tabular results of the DSC-analysis:

Material [name]	Melt Peak Temperature °C	Melt Peak Onset °C	ΔH_m Enthalpy J/g	X_c Crystallinity %
Raw				
PP-RAW	163.4	151.2	74.1	35.8
3D printed				
PP-ZERO	162.2	152.0	64.3	31.1
PP-REF	160.2	153.9	73.0	35.3
PP-EXP	159.9	153.4	66.9	32.2
PPU-ZERO	162.0	152.6	63.4	30.6
PPU-REF	162.4	154.4	65.6	31.7
PPU-EXP	161.3	161.3	54.3	26.2
Injection-moulded				
PPJ-REF	163.2	153.1	58.2	28.1
Flat-die-extruded				
PPB-REF	165.9	156.2	71.8	34.7
PPB-EXP	165.6	155.8	87.0	42.0
PPG-REF	162.1	153.4	96.0	46.4
PPG-EXP	162.9	152.5	97.4	47.0

Table 13: Results of the first heating measurements of the DSC-analysis.

7.4 Observations and discussion

7.4.1 Observations based on the DSC results

Observations of the DSC-curves of the several 3D printed specimen are made:

- The raw polypropylene-based material before being printed (PP-RAW) has a higher degree of crystallinity than the fresh printed PP-based composites (PP-ZERO and PPU-ZERO) as can be seen in **Table 13**. This implies that the processing technique affects the physical structure of the material. Recrystallisation may have taken place.
- The ultraviolet exposed PP and PPU show lower degrees of crystallinity than unexposed PP and PPU (see **Table 13**). This implies photo-crosslinking of the polymer chains as literature confirms too (Kamrannejad et al. 2014).
- The melt peak temperature of raw PP is the highest amongst the PP-materials (printed, aged and UV exposed) which is depicted in **Figure 79 & Figure 80**. Melt peak temperatures of the 3D printed material are around the 160°C. Melt temperatures of the KamerMaker II are 30°C above this temperature with a maximum temperature of 190°C as can be seen in **Table 4**: Printer settings of the KamerMaker.
- The DSC-curves of **Figure 79 & Figure 80** show broad melting peaks for the 3D print materials which suggest a variety of size distributions of the crystallites (Schawe et al. 2000).

Observations of the DSC-curves of the several 3D printed specimen are made:

- Ultraviolet exposed PPB and PPG have a higher crystallinity degree than unexposed PPB and PPG. This suggests that ultraviolet exposure has an increasing effect on the crystallinity degree of the flat-die-extruded polymers as can be seen in **Table 13**.
- Ultraviolet radiation tends to have more impact on the crystallinity degree and DSC curve of virgin-black PPB than the recycled-grey PPG (**Table 13**). This may be explained by the difference in thickness of the PPB (1.2 mm) and the PPG (3.0 mm). The effect UV degradation on the material increases with decreasing sample thickness (Schoolenberg and Vink 1991).
- The DSC-curves show narrow melting peaks for virgin PPB than the recycled PPG, which suggest a lower variety of size distributions of the crystallites than the 3D printed materials (Schawe et al. 2000).

Observations for the injection-moulded material:

- Generally, the injection-moulded PP show a lower degree of crystallinity than the 3D printed material except for the UV degraded PPU (see **Table 13**).
- The DSC-curve of the flat-die-extruded print material, in **Figure 83**, show two narrow melting peaks which suggest a eutectic impurity (Schawe et al. 2000).

General observations of the DSC-analysis:

- Melt peaks of all the PP-based samples are between 161°C - 166°C, which corresponds with literature (Sahin and Yayla 2005).
- Glass transition temperatures were hard to determine for all the PP-based samples.
- Change in crystallinity due to the influence of ultraviolet radiation differs between 3D printed and the flat-die-extruded materials. Exposed flat-die-extruded tend to have a higher X_c than unexposed samples, while with 3D printed thermoplastic the effect is the other way around.
- Flat-die-extruded recycled PPG has the highest degree of crystallinity.
- The broadness of melt peak temperatures differs from the 3D printed and the conventional manufactured PP-based composites.

7.4.2 Discussion based on the DSC results

Untraceable glass transition temperature T_g

The DSC-results of the PP-based material has shown no clear glass transition temperature. There could be several reasons for the absence of this important material property. The first reason is the sensitivity of the differential scanning calorimeter, which is too low to measure the transition of the polymer's state. A second reason could be the high percentage of impurities within the material, which could obstruct the measurement of finding the T_g . Impurities include glass fibres, talc, ultraviolet stabilisers. Another reason, why the thermal history of the printed polypropylene showed no sign of a glass transition temperature, T_g , which could be explained by a high degree of crosslinked polymer chains. Some polymers which have a high cross-linked degree do not show a T_g . Those polymers melt without using the highly elastic state (Dechun 2013).

The relation between the X_c and the tensile properties

When observing the results of the DSC-analysis and the tensile test, a relation between the degree of crystallinity and mechanical properties can be observed. A high crystalline degree reduces the

freedom for the molecular chains to move. As a result, the polymer becomes stiffer and harder, increasing tensile strength. This seems to be in agreement with a previous study (van der A. J. Mulder. en J. Gaymans 1998). The longer the average molecular chain length, the harder it is to create such configurations. In such regions, it is more difficult for the chains to slide past one another due to higher friction forces. Hence, the greater strength levels as the degree of crystallinity increased. It could be that 3D printed polymers, based on the crystallinity degree, might have longer chain lengths before the extrusion. The thermal effect of the KameMaker II influence the molecular chain of the polymer resulting in smaller polymer chains and a lower tensile strength. For further research, a gel permeation chromatography (GEL) test can be performed to determine the molecular chains of a polymer before and after printing.

Sample [name]	Melt Peak	ΔH_m	Xc	Yield		Tensile		Yield	
	Temp °C	Enthalpy J/g	Crystallinity %	Stress MPa	CV %	Modulus MPa	CV %	Strain %	CV %
Raw Material									
PP-RAW	163.4	74.1	35.8	-	-	-	-	-	-
3D Printed									
PP-ZERO	162.2	64.3	31.1	-	-	-	-	-	-
PP-REF	160.2	73.0	35.3	15.1	2.9	337.6	11.8	5.4	12.5
PP-EXP	159.9	66.9	32.2	14.7	5.9	378.8	18.3	4.5	19.7
PPU-ZERO	162.0	63.4	30.6	-	-	-	-	-	-
PPU-REF	162.4	65.6	31.7	14.8	8.2	425.2	11.8	5.4	23.5
PPU-EXP	161.3	54.3	26.2	13.6	11.8	364.7	11.1	4.5	20.4
Extruded									
PPB-REF	165.9	71.8	34.7	23.1	0.8	376.8	2.6	6.1	2.4
PPB-EXP	165.6	87.0	42.0	22.6	0.6	342.1	2.7	6.6	2.9
PPG-REF	162.1	96.0	46.4	38.5	0.8	674.8	2.0	5.7	1.8
PPB-EXP	162.9	97.4	47.0	37.2	0.9	563.9	2.5	6.6	3.0

Table 14: Results: Thermal analysis and mechanical testing.

The tensile properties of PP prepared by injection-moulding and flat-die-extrusion generally are superior in all the conducted tests when compared those of 3D printed samples. This is related to the nature of the injection moulding process, in which molten material is introduced to a chilled cavity, allows the formation of consistent crystals. This can result in increased mechanical properties (Dawoud, Taha, and Ebeid 2016). These crystals can be found in the two narrow peaks of the inject-moulded material as can be seen in **Figure 83**. In contrast, in the 3D printing process, the molten pellets are deposited on a bed kept where it is then left to air cool. Which is a condition which favours the amorphous part of the polymer and thus less strong polymer structure and results in a distribution of smaller crystals in different sizes (Dawoud, Taha, and Ebeid 2016). The broad melt peak of the 3D printed material in **Figure 83** indicates the formation of a wide size distribution of crystals.

Reliability of the test results

One small specimen (5 mg) is removed from a randomly chosen tensile sample of the materials. The low sample count, indeed, reduces the scientific value of the results, but it is still enough to give a better understanding of the effect of 3D printing on the polymer. In general, however, obtained results need to be analysed with the utmost care as their reliability might be questionable due to low sample amount.

Chapter 8

Microscopy

8.1 Microscopy

Microscopy is the technical field of using microscopes to view (areas of) materials that cannot be seen with the naked eye. It can be helpful to analyse a material on small scale to develop an increased understanding of characteristics of the tested materials. In this graduation project, microscope tests have been conducted using of digital and a scanning electron microscope. The observations will be discussed at the end of this chapter.

8.2 Test procedure

Microscope images were made of the material's surfaces using the digital microscope 'Keyence' (**Figure 84**, left) under the supervision of Mr F.G.C. Oostrum at the Faculty of Aerospace Engineering of the Delft University of Technology. Samples of the tensile test were placed under the lens while a computer screen next to the microscope projected the digital representation of the material surface. Microscope images using a scanning electron microscope (SEM) (**Figure 84**, right), are obtained under supervision of Mr D. Bosma at the Faculty of Applied Science of the Delft University of Technology. The SEM (Jeol, JSM-6010-LA) is supported with an EDX X-ray detection and a backscatter detector through the images. Specimens were taken from the tensile test samples and placed under the lens with the cut section in the direction of the lens. In the SEM-images the white coloured objects represent the material with the highest density.

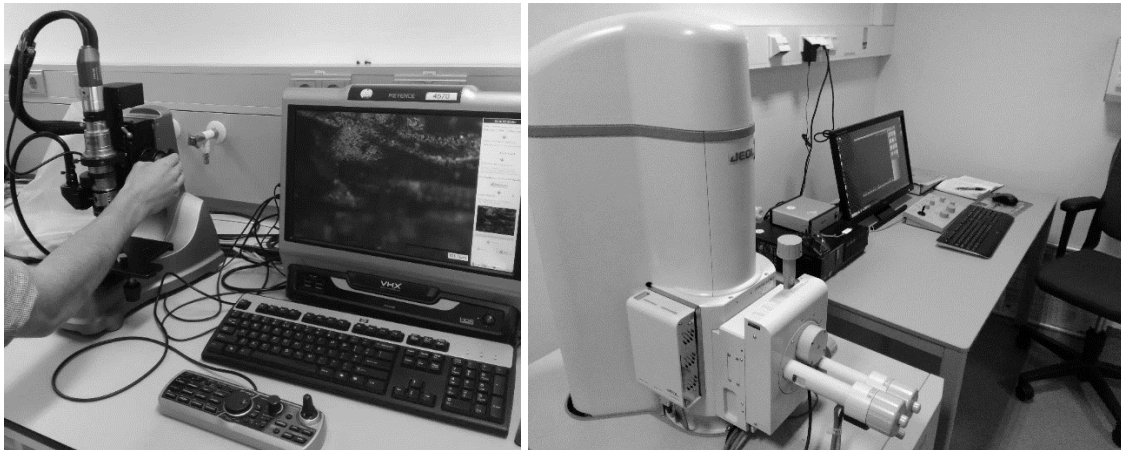


Figure 84: Digital microscope (left), Scanning electron microscope (right).

Since there was a limited budget for the research, a selection of the tested material has been made for the microscope test. For the digital microscope test, the following materials will be observed: 3D printed PP (undamaged and fracture surface), injection-moulded PP and both flat-die-extruded PPG and PPB. For the SEM, which were taken in the later stage of the project, only the raw, 3D printed and inject-moulded PP-materials (**Figure 59**) were analysed due to the limitations.

8.3 Test results

8.3.1 Digital microscopy results

Digital microscope representations of the surface of 3D printed material PP:

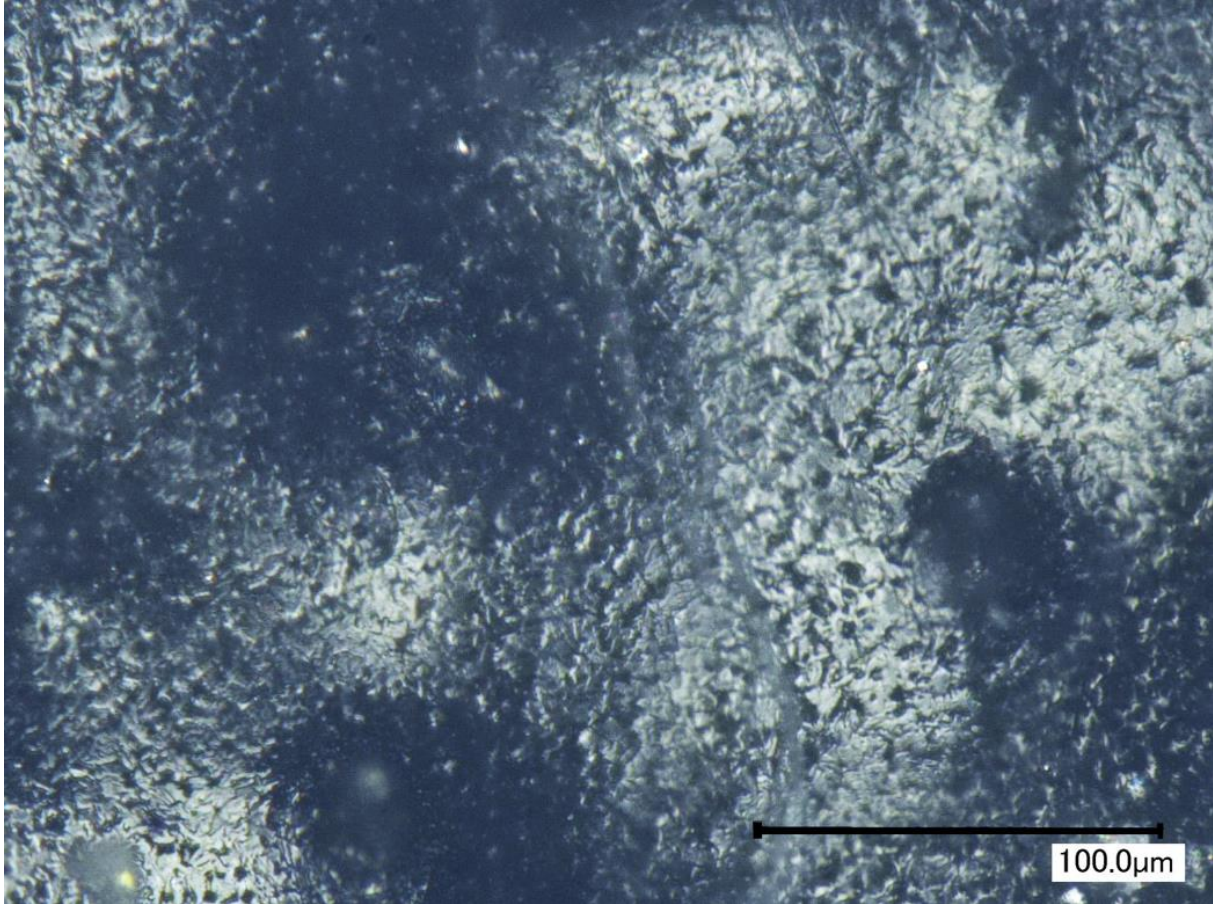


Figure 85: Microscope picture of the surface of 3D print-extruded PP.

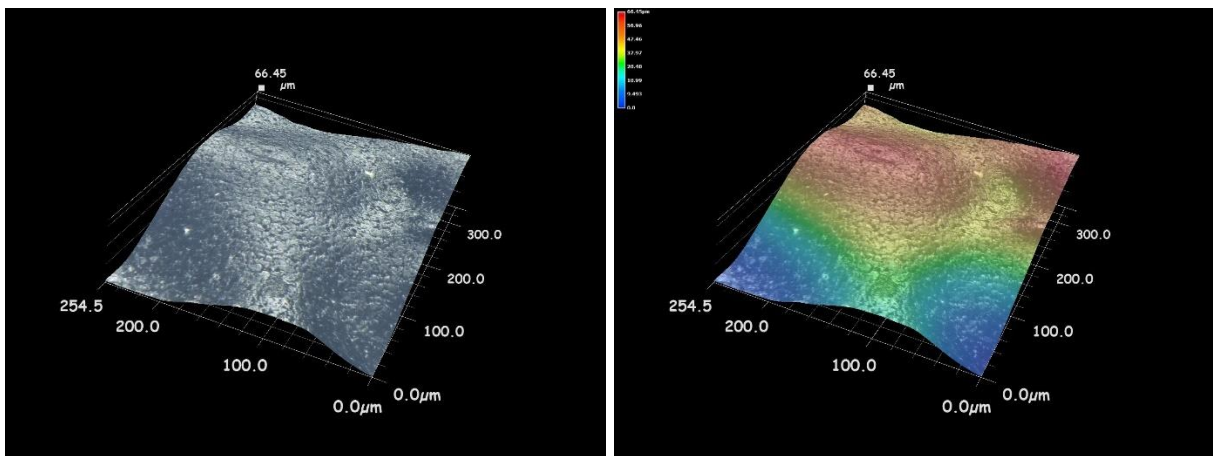


Figure 86: 3D representation: the surface of 3D print-extruded PP (thickness: 3.5 - 5.5 mm).

Digital microscope representations of the fracture surface of 3D printed material PP:

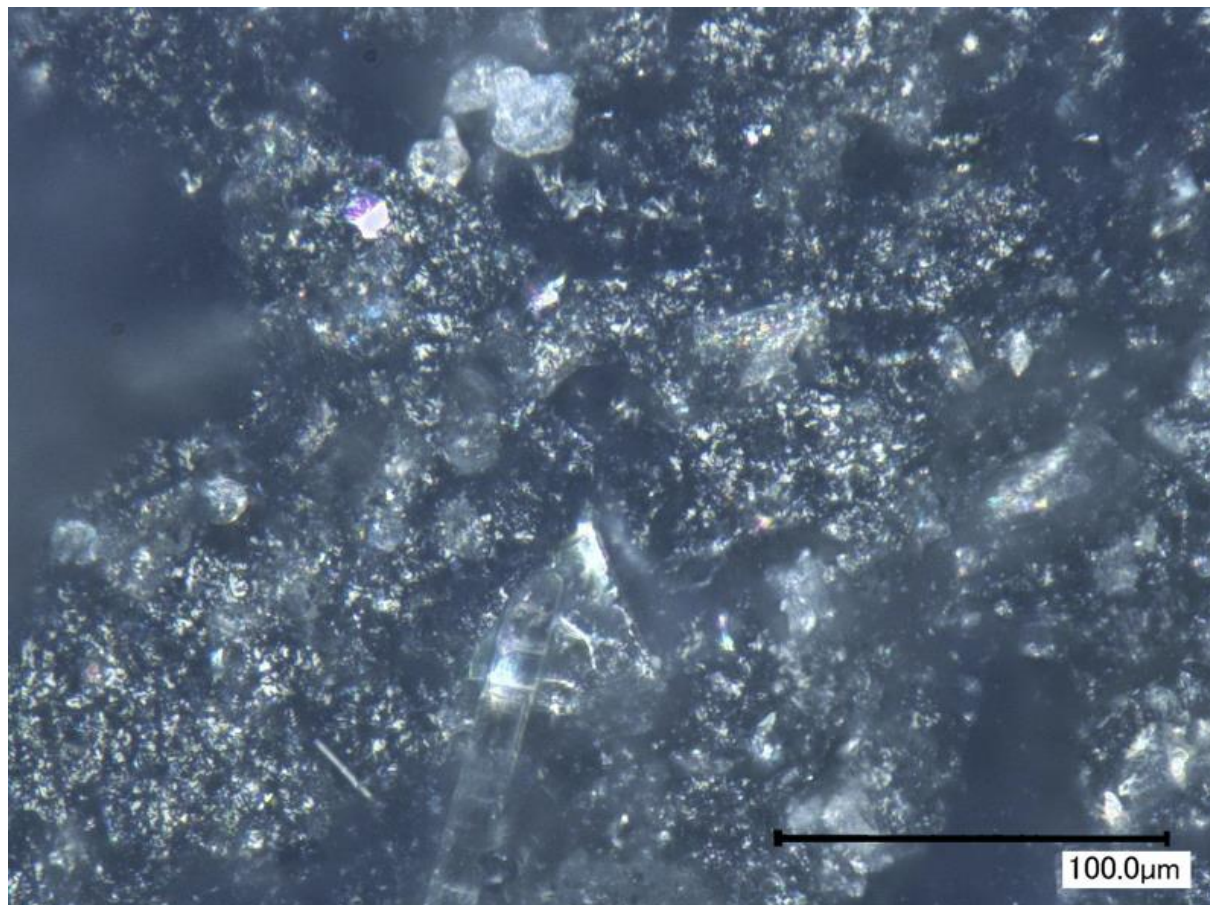


Figure 87: Microscope picture of the fracture surface of 3D print-extruded PP.

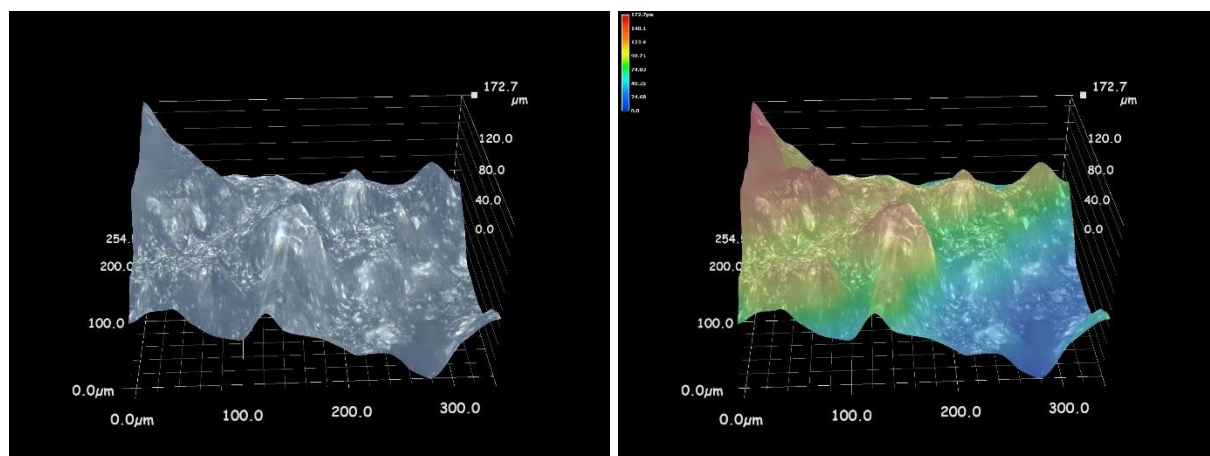


Figure 88: 3D representation: the fracture surface of 3D print-extruded PP.

Digital microscope representations of the inject-moulded PP:

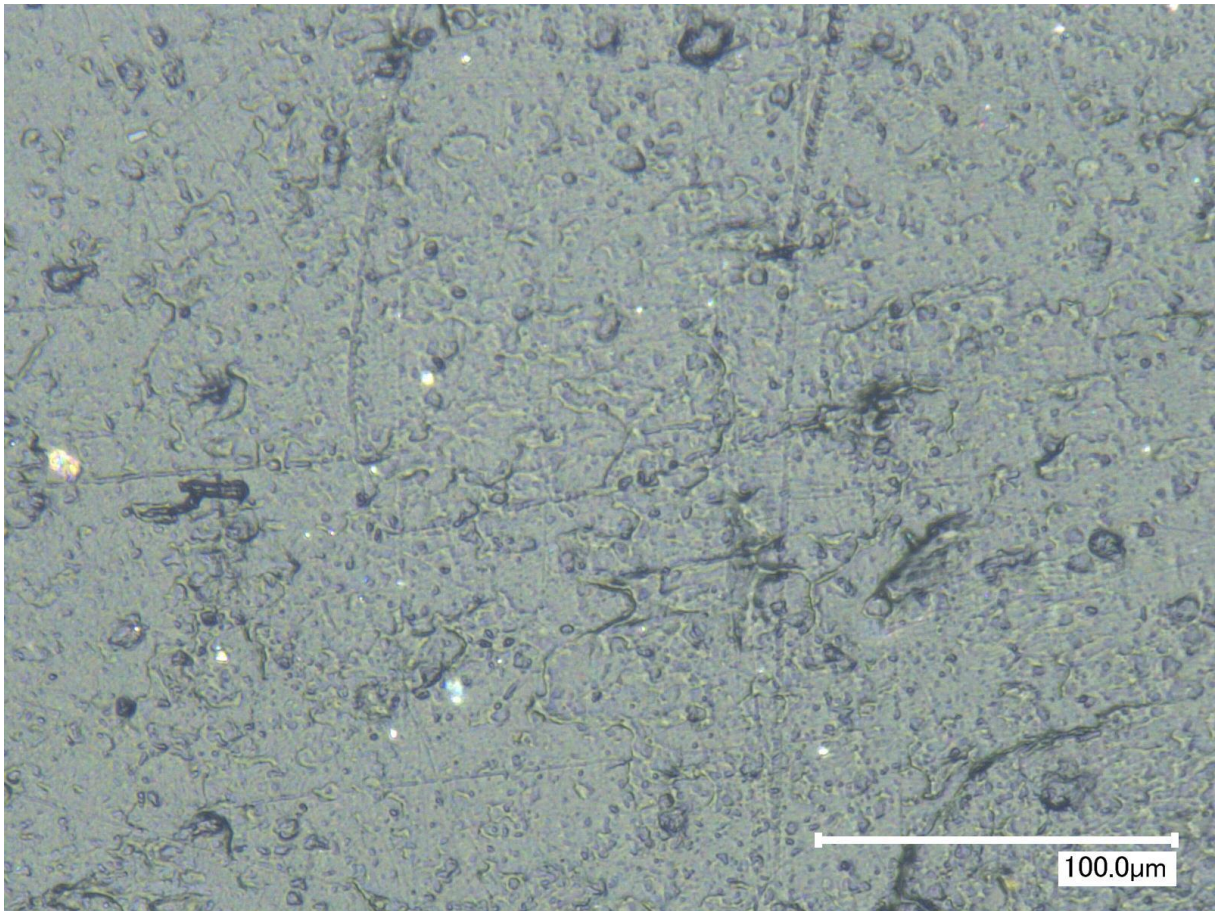


Figure 89: Microscope picture of the surface of inject-moulded PP.

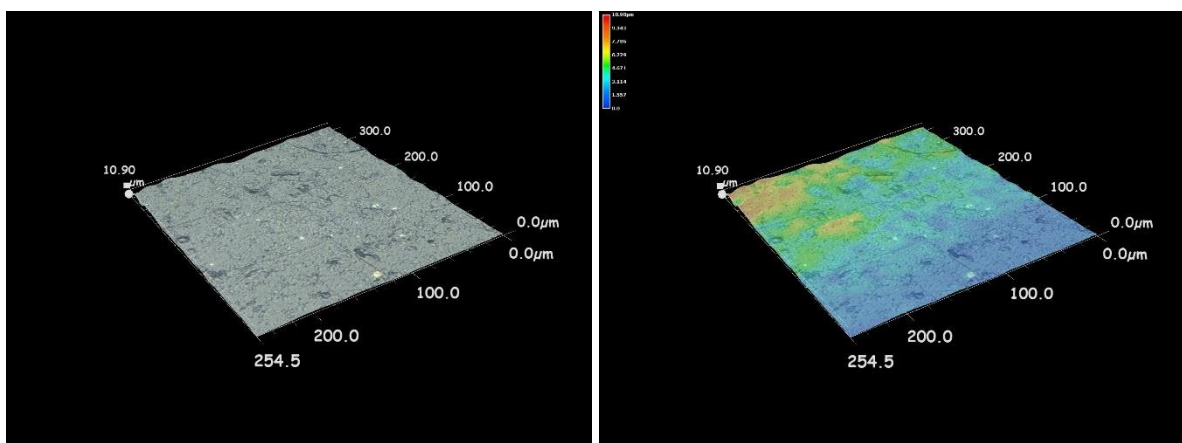


Figure 90: Microscope picture of the surface of inject-moulded PP (thickness: 3 mm).

Digital microscope representations of the flat-die-extruded PPB:

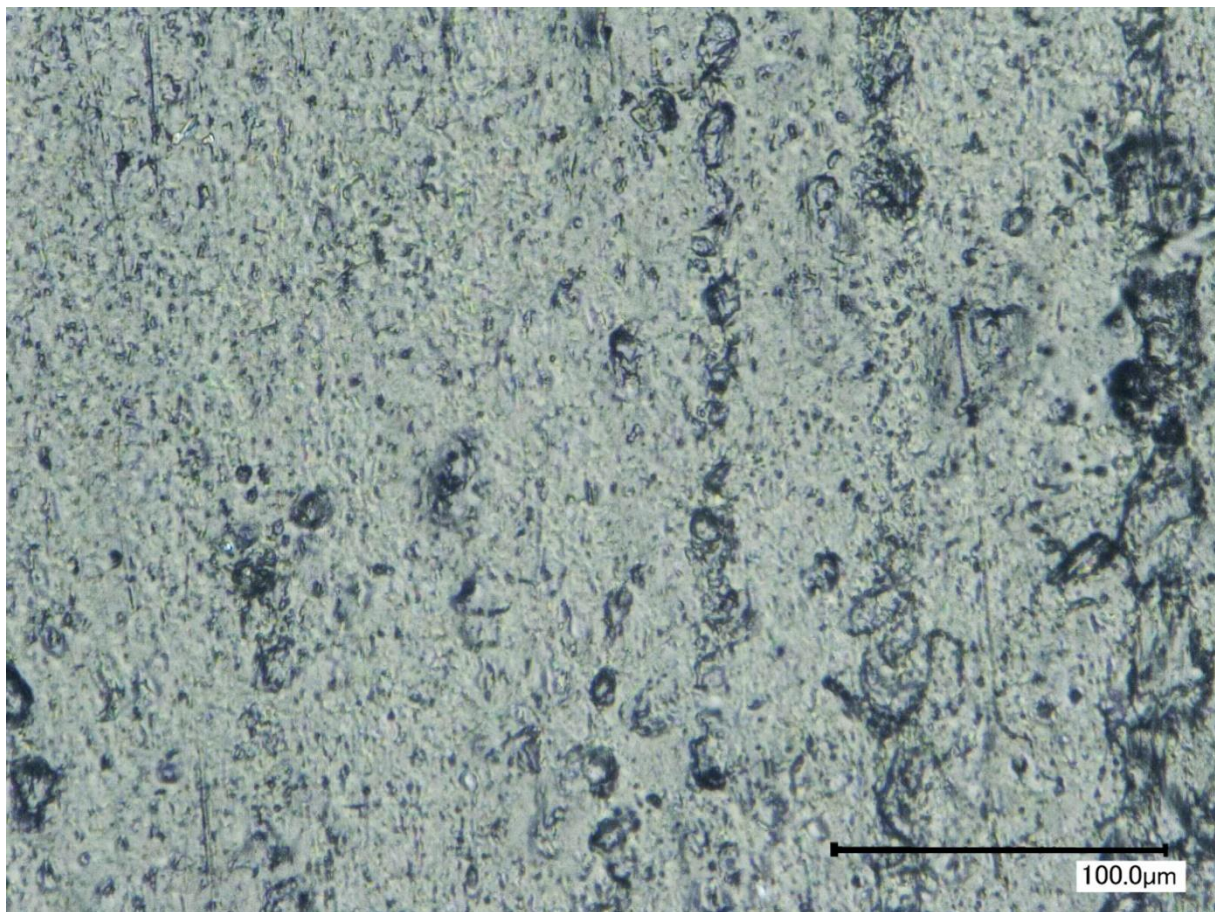


Figure 91: Microscope picture of the surface of flat-die-extruded PPB.

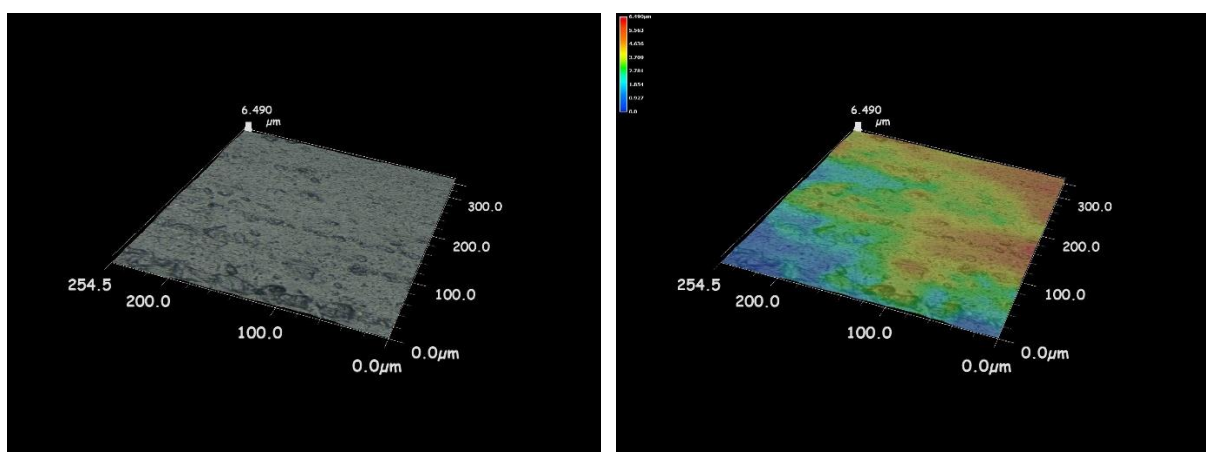


Figure 92: 3D representation: the surface of flat-die-extruded virgin PPB (thickness: 1.2 mm).

Digital microscope representations of the flat-die-extruded PPG:

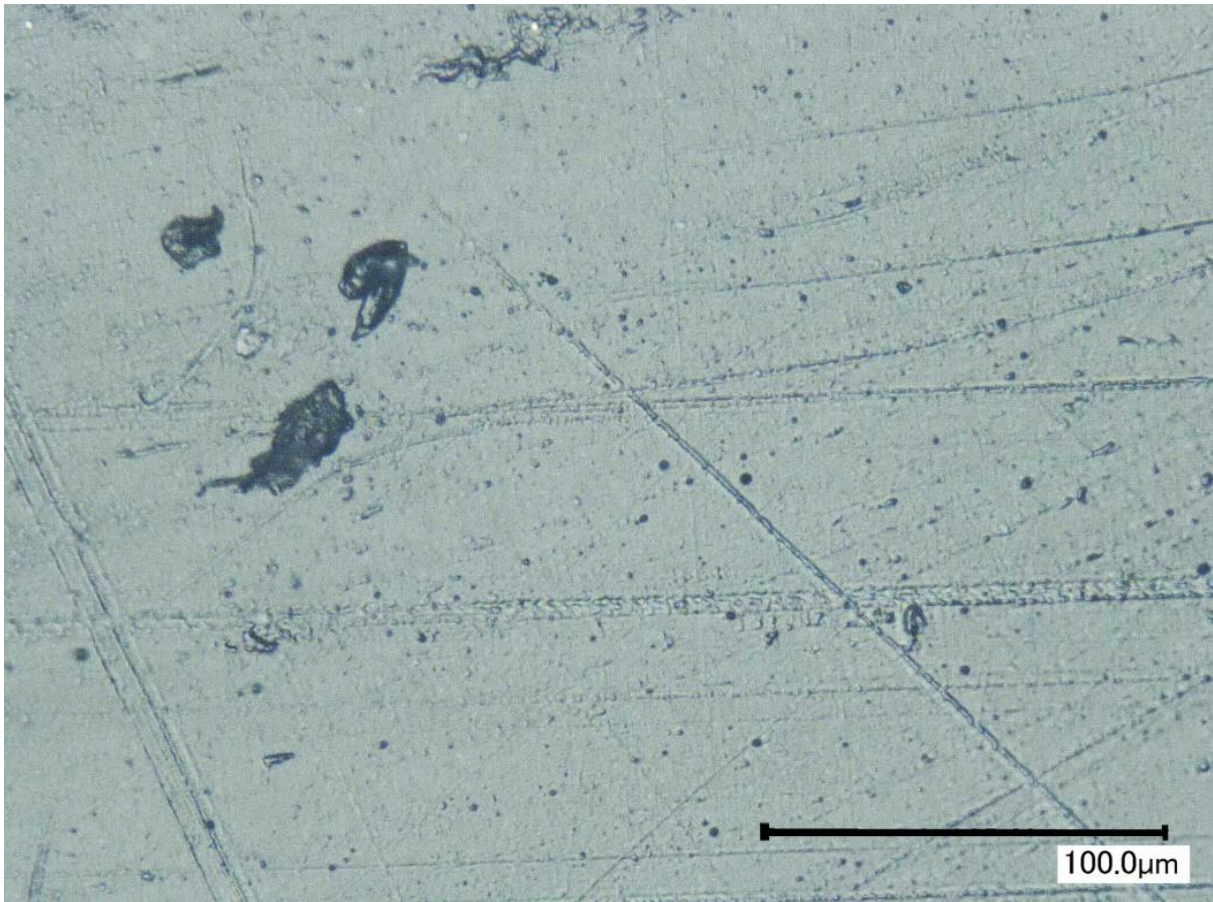


Figure 93: Microscope picture of the surface of flat-die-extruded PPG.

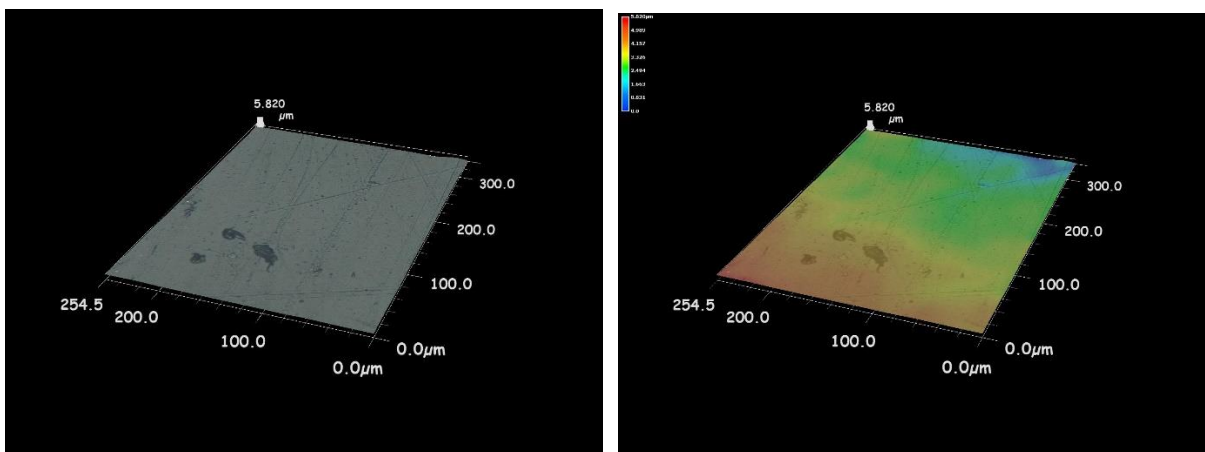


Figure 94: 3D representation: the surface of flat-die-extruded recycled PPG (thickness: 3.0 mm).

8.3.2 Scanning electron microscopy results

SEM-images of the cross-section of the polypropylene-based composites:

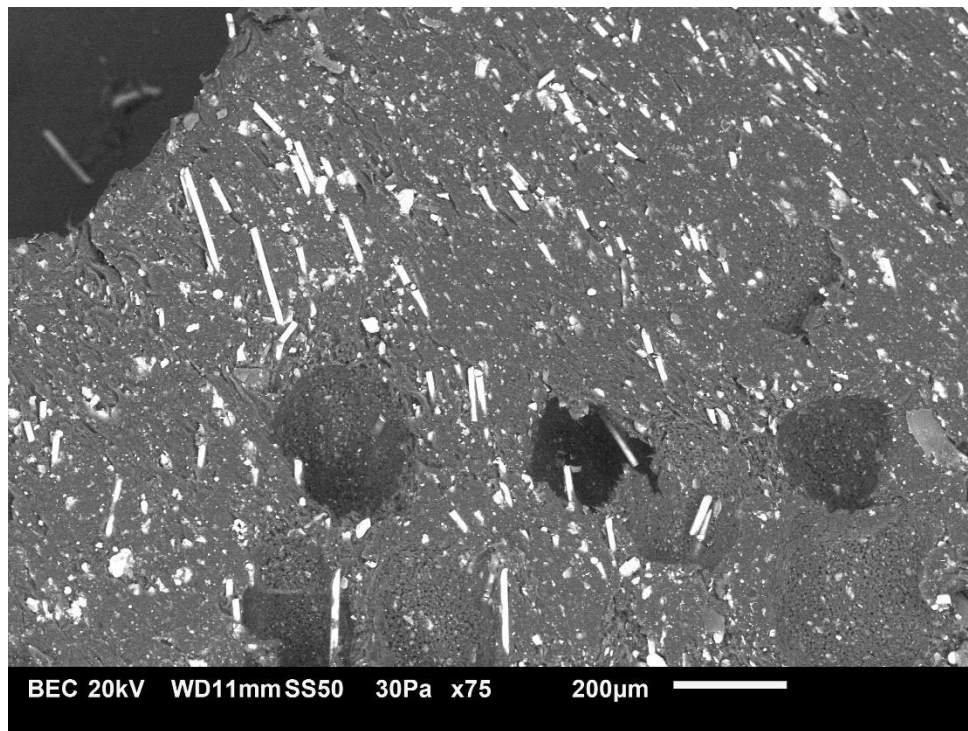


Figure 95: SEM-representation of the raw material PP.

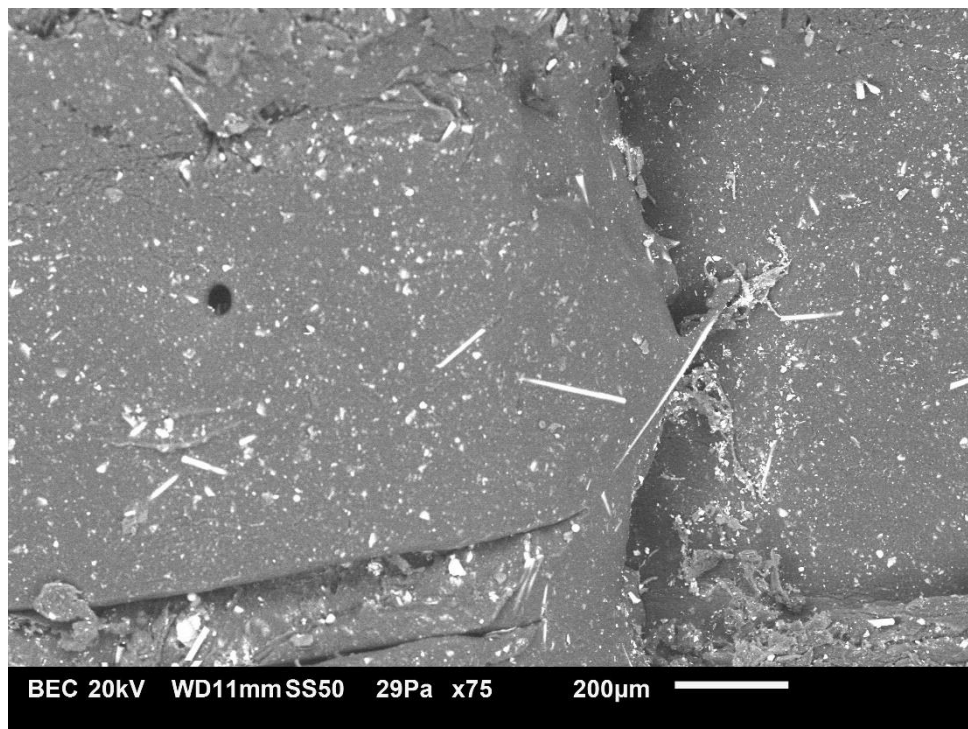


Figure 96: SEM-representation of the 3D printed PP.

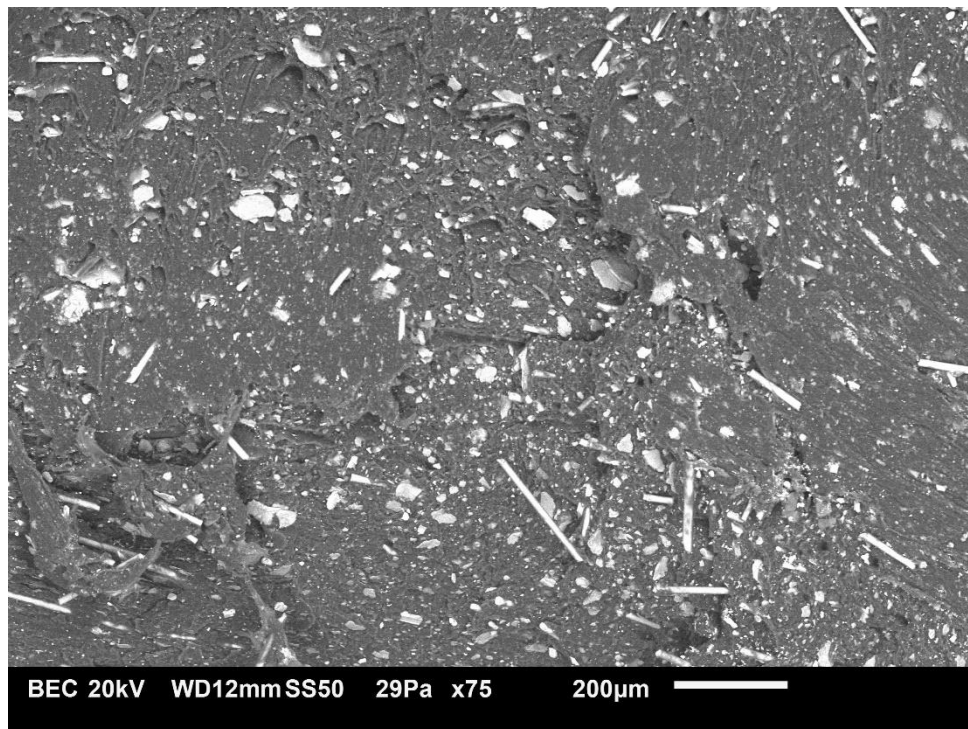


Figure 97: SEM-representation of the injection-moulded PP.

Tabular SEM data chemical composition of the investigated PP:

Atom	Raw		3D Printed		Injection-moulded	
	<i>wt</i> (%)	<i>at</i> (%)	<i>wt</i> (%)	<i>at</i> (%)	<i>wt</i> (%)	<i>at</i> (%)
C	87,8	91,6	90,1	93,7	80,2	85,9
O	9,1	7,1	6,2	4,9	14,4	11,6
Mg	0,8	0,4	0,7	0,3	1,5	0,8
Al	0,3	0,1	0,2	0,1	0,3	0,2
Si	1,4	0,6	1,4	0,6	2,5	1,2
Ca	0,7	0,2	1,0	0,3	1,0	0,3
Ti	0,0	0,0	0,4	0,1	0,0	0,0
Total	100	100	100	100	100	100

Table 15: Chemical composition of the PP-based polymers.

The chemical composition of the tested material is measured by the SEM, whereby the mass percent (*wt*) and the atomic percent (*at*) of each atom is given. The mass percent of an atom shows the amount each element in a molecule contributes to the total molecular mass. Each element's contribution is expressed as a percentage of the whole. The atomic percent gives the percentage of one kind of atom relative to the total number of atoms.

8.4 Observations and discussion

Digital microscopy

An analysis has been done by comparing the digital microscope images of the 3D printed and the conventionally fabricated thermoplastics as can be seen in **Figure 85** - **Figure 94**. The first observation is that the surface of the 3D printed PP-based material is highly pocked and uneven compared to the other conventional manufactured materials. The form of the surface could occur due to the extrusion technique of the 3D Printer 'KamerMaker'. The rough surface also may explain why there was a large amount of specimen slippage during mechanical testing occur for the 3D printed PP samples. An uneven surface results in less contact area between the clamping and the tensile specimen.

Furthermore, **Figure 87** shows signs of glass crystals sticking out of the 3D printed PP's fracture surface. However, images made with the SEM show clearer representations of the glass fibres. Finally, the extrusion directions of the flat-die-extruded polymers can be seen by the stripes of **Figure 91** & **Figure 93**. While for the 3D printed and injection-moulded materials this direction is less visible due to the different nature of the manufacturing process.

Scanning electron microscopy (SEM)

From the analysis of the obtained SEM-images, some useful observations could be mentioned. At first glance, the images of the raw (**Figure 95**) and injection-moulded PP (**Figure 97**) show more and scattered glass fibres than the image of the 3D printed polypropylene-based material (**Figure 96**). This difference could be explained by the fact that most of the glass fibres may be repositioned in the direction of the print layer after extrusion. The image of the 3D printed material is taken in the direction of the print layers, which explain the vast amounts of white dots, representing the cut glass fibres. To confirm this theory, another SEM-image should be taken in the perpendicular direction of the glass fibres.

Further observation of the SEM-image of the 3D printed material shows a clear separation of the polymer masses as can be observed in **Figure 96**. The boundary represents the contact area between two print layers, and it is clear to see that the glass fibres are not situated between the print layers. The oriented glass fibres and the interlayer separation could explain why the printed material is highly orthotropic, resulting in weaker tensile strength in the transverse direction of the print layers than in the longitudinal direction. This evidence correlates well with the results obtained from the tensile test.

Chemical composition

From **Table 15** the chemical composition of the PP-based polymers could be seen by their mass and atom percentages of the following observable atoms: carbon (C), oxygen (O), magnesium (Mg), aluminium (Al), silicon (Si), calcium (Ca) and titanium (Ti). Hydrogen (H) was not observable within the SEM results.

The composition of all three polymers consists of polypropylene (mostly consist of CH_3), carbon black (C), talc ($\text{H}_2\text{Mg}_3(\text{SiO}_3)_4$) and glass fibres (SiO_2). Based on the available atoms: silicon, aluminium, calcium and oxygen atoms, is suggested that the E-glass fibres were used in the polymers with the nominal composition: SiO_2 , Al_2O_3 , CaO and MgO (Azom 2001).

An important observation is that the mass percentage and the atom percentage of the atoms magnesium and silicon are measured higher in the injection-moulded material. Which suggests that the material composition of the injection-moulded material obtained from the plastic recycled company may be different comparing to the raw and 3D printed material.

If the polypropylene is oxidised by the to the printing process of the KamerMaker, it is expected that the atomic percentage of oxygen would increase, whereby oxygen particles bound with the polymer chains (Iring et al. 1978). When subtracting the oxygen atom percentages belonging to the glass fibre and talc molecules with the total oxygen atomic percentages, it is suggested that the

remaining oxygen atomic percentages belong to the polymer chains. As can be seen in **Table 16**, the 3D printed material has the lowest oxygen atomic percentage, which implies that the material is not oxidised. Still, this conclusion is questionable since insecurities lie in the atom proportion assumptions.

Atom	Raw <i>at (%)</i>	3D Printed <i>at (%)</i>	Injection <i>at (%)</i>
Oxygen	2,55	0,33	3,30

Table 16: Oxygen atomic percent of the chemical composition of the PP-based polymers.,

Reliability of the test results

Since that there is an unknown percentage (around 20%) of glass fibres (SiO_2) and talc ($H_2Mg_3(SiO_3)_4$) exists in the 3D printed compound, it could not be detected if the measured oxygen particles are from the degraded polypropylene or the high amount of glass fibres or talc. Moreover, the SEM-results are highly dependent on the location where the picture is taken. It is a snapshot. A location where, by chance, more or fewer glass fibres occur could end up in misleading results. It could be implied that the SEM-analysis is not necessarily a sufficiently useful tool to determine if the oxidation has taken place in the polymer. Furthermore, the made representations need to be analysed with the utmost care as their reliability might be questionable due to low sample amount.

Chapter 9

Fourier-Transform Infrared Spectroscopy

9.1 Infrared spectrum

Fourier-transform infrared spectroscopy (FTIR) is a laboratory technique for collecting the infrared spectrum of absorption or emission of a material. A Nicolet™ 6700 FTIR Spectrometer from Thermo Electron Corporation equipped with OMNIC Software) with wavenumber range from 4000-400 cm^{-1} with a 4 cm^{-1} resolution. This confers a significant advantage over a dispersive spectrometer, which measures intensity over a narrow range of wavelengths at a time (Griffiths and De Haseth 2007). Since there is a large amount of FTIR spectra of thermal degraded and oxidised polypropylene, it may worth a shot to measure the infrared spectra of the raw and 3D printed PP. Comparing these graphs could give an indication whether the polypropylene-based material is oxidised because of the 3D printing technique.

9.2 Test procedure

The FTIR analysis were made with a scanning FTIR spectrometer under the supervision of Miss M. van der Helm, at the Faculty of Applied Science of the Delft University of Technology.



Figure 98: Fourier-transform infrared spectroscopy test setup.

Due to the fact that there was a limited budget for the research, a selection is made of the materials for the FTIR measurements. The infrared spectrum of the following materials was observed: Raw, 3D printed and injection-moulded PP. The FTIR spectrometer simultaneously collects high-spectral-resolution data between the wavenumber 600-3500 cm^{-1} and measures 164 cycles per material. Specimen were taken from the materials (see **Figure 59**) with a sample thickness of 5 mm.

9.3 Test results

FTIR Spectra of the raw, 3D printed, injection-moulded PP-based material:

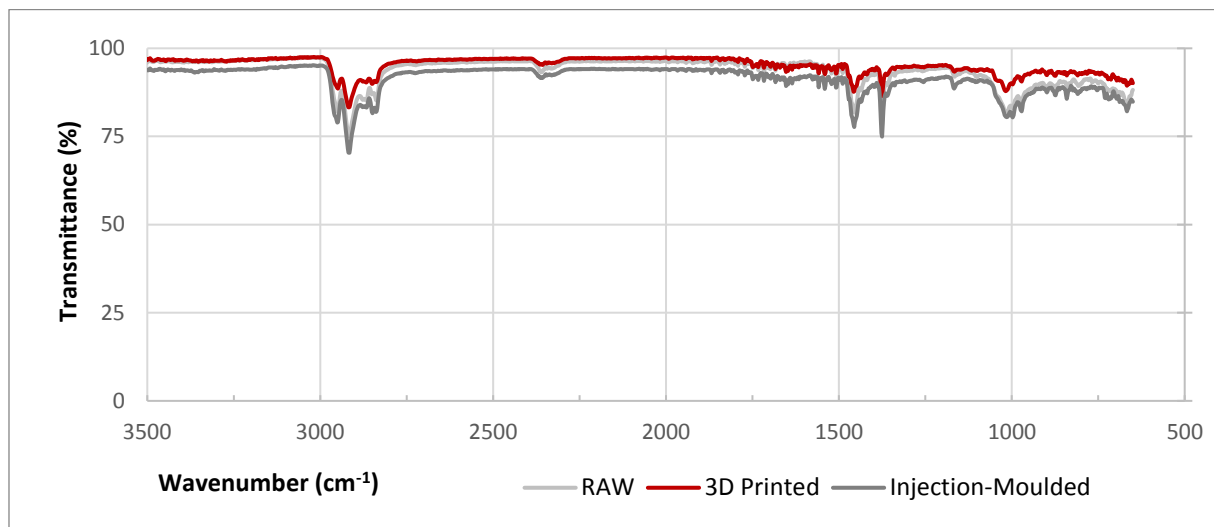


Figure 99: FTIR Spectra of the raw, 3D printed, injection-moulded PP.

The FTIR spectra of the raw, 3D printed and injection-moulded PP can be observed in **Figure 99**. High peaks in the FTIR spectra could be observed around the wavenumber $2970\text{--}2910\text{ cm}^{-1}$ (methyl group; $-\text{CH}_3$), $2870\text{--}2840\text{ cm}^{-1}$ (methylene group $-\text{CH}_2-$), 1460 cm^{-1} ($-\text{CH}_2-$) and 1370 cm^{-1} ($-\text{CH}_3$). These peaks indicate the methylene and methyl groups of the polypropylene and are in cohesion with previous FTIR experiments on a polypropylene-based material (Barbes, Radulescu, and Stihl 2014). However, a broad peak is shown around the 1000 cm^{-1} which indicates (C-O)-groups. The raw and injection-moulded spectra show stronger peaks than the 3D printed material. No strong peaks were observed around the $1700\text{--}1800\text{ cm}^{-1}$ region in the FTIR spectra, which indicates the presence of an oxidised group such as carbonyl groups (1715 cm^{-1}).

9.4 Observations and discussion

Comparing the FTIR spectra of the 3D printed material and of polypropylene found in literature could give an indication of whether the material is oxidised. During the oxidation process of polypropylene the category of polar groups such as ketones, carboxylic acids and ester groups are created on the polymer surface (Reisi Nafchi et al. 2015). This appeared in the peaks in the spectra at 1164 , $1700 - 1780$ and 3470 cm^{-1} . The absorbance peak in $1700\text{--}1780\text{ cm}^{-1}$ is related to the stretching mode of carbonyl group which exists in ketone, aldehyde and anhydride groups, the peak at 3470 cm^{-1} is attributed to the stretching mode of OH groups in alcohols and the peak at 1164 cm^{-1} is related to ester groups (C-O) (Gutiérrez and Palza 2015) as can be observed in **Figure 101** (right). Within the spectra of the 3D printed material, it could imply that the oxidation groups are not detected which implies that the 3D printed material is not oxidised.

Zoomed-in FTIR Spectra of the raw, 3D printed, injection-moulded PP-based material:

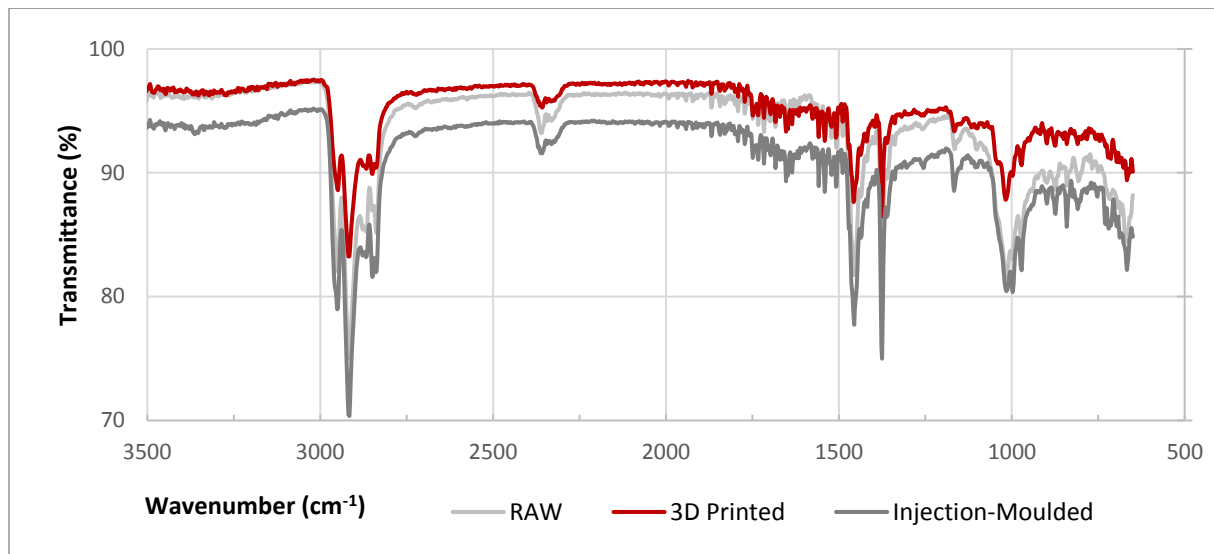


Figure 100: FTIR Spectra of the raw, 3D printed and injection-moulded PP (zoomed-in).

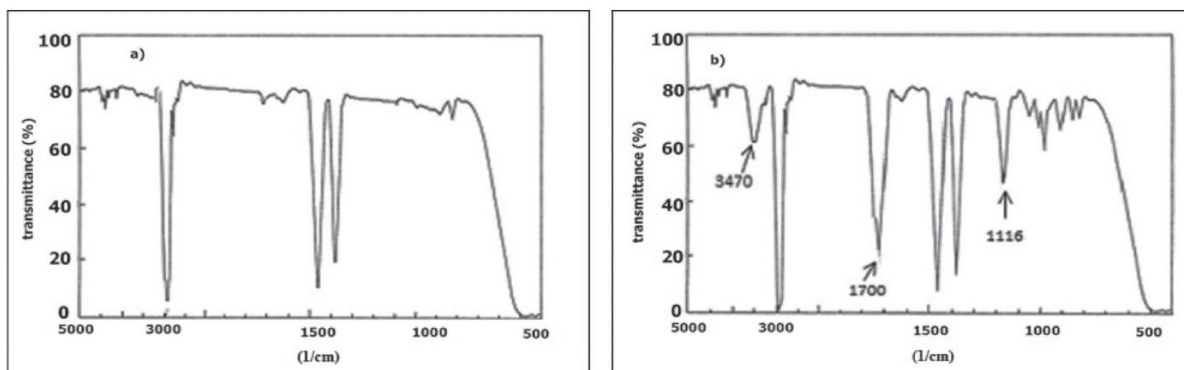


Figure 101: FTIR Spectra of raw (left) and oxidised polypropylene (right) (Gutiérrez and Palza 2015).

Reliability of the test results

The FTIR spectrometer has difficulties measuring the FTIR spectra of the raw, 3D printed and injection-moulded material. The main reason is that the infrared laser could not beam through the black and thick material. The consequence is that the obtained transmittance peaks won't reach the 0% transmittance. Instead of that, the maximum transmittance is around 70% for the measured samples, which means that 30% of the beam came through the material. Due to the insufficient measurements, not all the peaks are displayed which may result in an incorrect representation of the material. In addition to that, the sample amount for this test is low (1 specimen per test), which could question the reliability of the FTIR test results.

PART V

Evaluation

Chapter 10

Discussion

In this chapter, the content of this report is discussed and critically evaluated. The most important aspects of the in-depth research suggestions are summarized and recommendation are made on possible improvements of further research or improvement of the 3D print technology in Chapter 12. Section 10.1 focuses on the impact of ultraviolet radiation exposure and Section 10.2 covers the effects of the 3D printing on the polymer.

10.1 The influence of ultraviolet radiation

Results of the mechanical testing show no significant difference between the tensile properties of the ultraviolet (UV) exposed and unexposed 3D print-extruded samples. The results contradict literature (Tidjani 1998), which implies that exposed samples become more brittle over time. The embrittlement resulting from UV degradation is supposedly caused by photo-crosslinking of the polymers chains. Instead, experimental results showed an increase in brittleness over time for both sets of samples. In this paragraph several reasons are given to explain why no influence of UV on the tensile properties of the examined material were observed within the conducted experiments.

The thickness and permeability of the test samples affects the UV resistance of the 3D printed material. The limited light penetration of UV radiation explains why UV degradation only occurs on the surface of the material. In literature, experimental studies on UV degradation of polypropylene have been conducted on thin PP plates (1.0 – 2.0 mm), where the degraded layer reaches a maximum thickness of about 0.5 mm (Schoolenberg and Vink 1991; T. H. Shubhra et al. 2011). The thickness of the 3D printed sample is about 5.0 mm. The thickness of the 3D printed sample might be sufficient enough resulting in a negligible influence of UV radiation on the tensile strength. Printing samples with a smaller cross-sectional thickness may be more sensitive to the effect of UV degradation.

The material composition of the polymer composite, undoubtedly, plays a role in its UV sensibility. An unknown percentage of the colour additive, carbon black, is present within the 3D-printed polymer compound. Carbon black is known to have an increasing effect on the UV resistance of polymers (Horrocks et al. 1999). 3D printed thermoplastic composites with the exclusion of carbon black might have increased negative impact from the ultraviolet radiation. It is recommended to conduct the same accelerated ageing test using different polymer composites for building applications.

As mentioned in the conclusions of the tensile test results, much confidence has been lost within the data due to various print qualities and specimen slippage. These factors contributed to the broad range of test data and low sample counts per test. It is suggested that the influence of UV radiation exists within the results; however, the scattered data make it difficult to detect the difference between exposed and unexposed tensile test data. Testing samples of a more consistent cross-section in combination with less sample slippage would reveal the influence of UV degradation.

However, the tensile test results show that both exposed and unexposed samples of the printed material increase in brittleness over time. This led to the hypothesis that the embrittlement effect due to UV degradation is not the primary factor influencing the material. The 3D printing process has been examined to determine the cause of this additional embrittlement effect.

10.2 The effect of 3D printing

As mentioned, this research study started with the question of whether ultraviolet (UV) radiation influences the mechanical properties of 3D printed thermoplastic. However, tensile strength test results showed that the 3D printed material embrittles over time irrespective to the influence of UV radiation. In addition to that, the 3D printed material shows lower and more scattered tensile strength test results when compared to the flat-die-extruded material. In this section, the effect of the manufacturing technique, used by the 3D printer the 'KamerMaker', on the mechanical properties of the polymer composite is discussed.

10.2.1 Inconsistent print quality and sample slippage

Weak and inconsistent interlayer bonding and porosity of the print layers could influence the mechanical properties and indirectly affect the mechanical tests. The bonding strength between print layers is dependent on the print settings, such as printer temperature, ambient temperature, nozzle dimensions and cooling rate. The bonding can be weak when a new hot print layer is extruded above an under layer with a much lower temperature. Interlayer porosity, caused by the existence of voids between printed layers, creates faster fracture paths during the loading. The effect of weak interlayer bonding and porosity, due to insufficient and inconsistent printing, could result in lower and scattered strength data. This effect is more influential in the transverse tensile direction than along the print direction, according to the results extracted from the tensile test. Furthermore, insufficient clamping during the tensile test results in additional scattering of the data. Slippage between the clamps and the sample occurs, due to the inconsistent printed surface of the specimen, leading to more scattered or unreliable results.

10.2.2 Physical changes of the polymer

During the extrusion process, pellets of the raw material are heated up to their melting point, making it possible for the thermoplastic to flow through the nozzle and bond with the previous print layer. Differences, between the innovative 3D print and the conventional plastic technique, affect the physical structure of both polymers from the same raw material. Recognisable characteristics of the self-developed pellet-extrusion XL 3D print technique of the KamerMaker includes:

- A relatively small heating chambers, where the pellets are melted.
- Extruding and cooling of the composite in the open air.
- Different heating and cooling cycles of the 3D printed material due to the layer-on-layer composition.

These factors relating to the processing technique may contribute to the physical changes of the thermoplastic material. Two hypotheses were made to explain why the 3D printed material becomes brittle over time: thermal oxidation and the forming of spherulites.

Thermal oxidative reactions

The DSC results show, based on the change in the degrees of crystallinity, that physical changes within the polymer may take place due to the 3D print-extrusions process. The lower and scattered tensile test properties of the 3D printed material may be caused by the thermal oxidation reactions occurring when the composite is heated up in the presence of air. The mobility of the polymer chains increases at high temperatures resulting in the interaction with oxygen particles in the air. During this thermo-oxidative process, new molecules are formed resulting in the breaking of the polymer chains: chain-scissoring. Shorter polymer chains lead to lower tensile strength properties (Zeus 2005) and an increase in the degree of crystallinity (Kamrannejad et al. 2014). The lower tensile strength, as obtained from test results of both the 3D printed composite as well as the injection-material confirms this theory. However, the increase in the degree of crystallinity is in contradiction with the findings of the DSC. The DSC-results show that the 3D printed materials show lower degrees of crystallinity than the raw polypropylene-based composite.

As can be observed, the material becomes more brittle with a slight increase in yield strength, a vast increase in tensile modulus and a decrease in the yield strain. This toughening or hardening

of a polymer is due to cross-linking of polymer chains. The increase in brittleness of the polymer could be the consequence of oxidative reactions in the polymer which cause molecular recombination. This recombination of molecules could be initiated when the polymer is heated up in the presence of oxygen containing air. This thermal ageing led to the formation of free radicals and therefore to an increase in the degree of crystallinity within PP-material (Boubakri et al. 2011). However, the obtained chemical composition of the SEM shows that the 3D printed material has a lower oxygen atom percentage than the raw material. Also, the limited FTIR-test has shown no indication of peaks relating to oxidised polypropylene. These tests, which are still questionable due to the low sample count, have shown no sign of thermal oxidative reaction within the 3D print-extruded material.

Forming of spherulites

Polymer physics could explain the embrittlement of the 3D printed polypropylene-based material. Polypropylene is a semi-crystalline thermoplastic polymer and exhibits crystalline and amorphous regions. If a polymer is melted and then cooled, it can crystallise. During crystallisation, the formation of organised polymer units, called crystallite or lamellae, starts. A bunch of spherical semi-crystalline regions, consisting of amorphous polymer chains and crystalline lamella, is called a spherulite. A spherulite grows in time as can be seen in **Figure 102** (Gránásy, Pusztai, and Douglas 2013). The creation relates to the crystallisation of polymers, whereby the polymer structure and the cooling condition are important factors (Ehrenstein and Theriault 2001). Formation of spherulites embrittles the polymer material; the strain at failure of polymers decreases if the average size of the spherulites become larger over time, as can be seen in **Figure 103** (Gránásy, Pusztai, and Douglas 2013). The final spherulite size and the spherulite amount increases with decreasing cooling rate of the polymer resulting in a more brittle material over time (Sawyer, Grubb, and Meyers 2008).

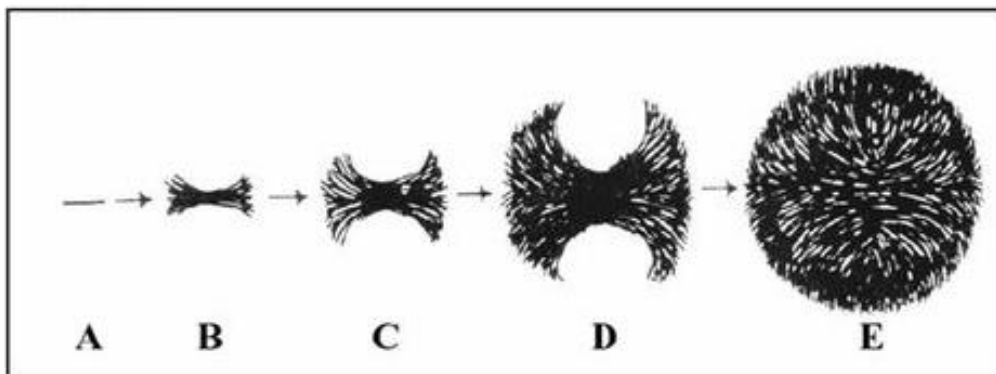


Figure 102: Concept for the formation of spherulite (Gránásy, Pusztai, and Douglas 2013).

The formation of spherulites could be the reason of the embrittlement of the 3D printed material as shown in the tensile test results. It can be assumed that the cooling rate of the 3D print-extrusion is lower than of injection-moulding since an extruded layer is slowly cooled down in the open air. Subsequently, this layer is reheated by the print layers above. The oxygen solubility in the spherulites is very low or zero (Shibryaeva 2012). While the obtained chemical composition results of the SEM test showed a lower oxygen atom percentage for the 3D printed material compared to the raw material as can be seen in **Table 16**. These finding might suggest that the cooling condition of the 3D printing technique might initiate the forming of spherulites in the polymer. An increase of the average spherulites size of a polymer affects its mechanical properties, resulting in an increase in tensile stiffness and a decrease of yield strain. However, more experimental research should be done to confirm this hypothesis. Solutions could be in quenching, subsequent annealing or suppressing crystallisation by rapid cooling of the 3D printed material after extrusion (Sawyer, Grubb, and Meyers 2008).

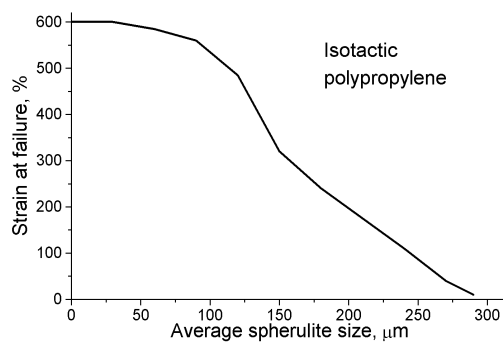


Figure 103: Strain at failure vs. spherulite size of isotactic polypropylene (Ehrenstein and Theriault 2001).

Chapter 11

Conclusions

Additive manufacturing of large-scale façade elements is a promising innovation for the building industry. The reported graduation project started based on the product development of the Aectual façade, which led to an in-depth study focussing on the effect of ultraviolet radiation on the strength of 3D printed thermoplastic. Due to the print quality difficulties, that arose during the experimental phase, the project has been slightly shifted to investigate the effect of 3D printing the strength of the extruded polypropylene-based material. In the following sections, an answer to each test is given in the form of a summary, which highlights the most important findings that have been discovered.

11.1 Mechanical testing

From the analysis of the experimental data obtained from mechanical testing, it can be concluded that:

- The investigated material exhibits highly orthotropic characteristics. Tensile strength properties are higher in the length of the print layers than perpendicular to the print layers.
- Mechanical properties of the extruded material are time-dependent with a slight increase in yield strength and tensile modulus and a decrease in yield strain over an increasing ageing time.
- No significant influence of ultraviolet exposure on the tensile strength properties and Charpy impact strength has been found for neither the extruded PP with and without UV stabiliser.
- The addition of UV stabilisers to the PP-based compound increases the tensile modulus and decreases the yield strain over an increasing ageing time. No significant change has been seen in the yield strength.
- Tensile test results of the flat-die-extruded PP-based thermoplastic are more consistent and show higher tensile properties.
- Influence of UV radiation has a higher and more various effect on the tensile properties of 3D print-extruded than those of flat-die-extruded PP-based material but cannot be stated due to the high variance.
- There is a lack of reliability due to the loss of sample count and the inconsistent print quality of the extruded material including various combinations of impurities, material concentrations on the sample's clamping area and the alignment of print layers. This has been resolved to certain extent by applying a print quality system and post-treatment of the samples.

In summary, the mechanical test results of the 3D print-extruded PP-based polymers show more unreliable and lower tensile strength properties than conventional flat-die extruded PP-based composites, reducing its characteristic values.

11.2 Thermal analysis

From the thermal analysis done with data from the differential scanning calorimeter test it can suggest that:

- Heat treatment during the 3D print-extrusion of the PP-based composite has a reducing effect on the degree of crystallinity.
- Glass transition temperatures, T_g , were hard to detect for all polymers.
- Melt peak temperatures, T_m , for all PP-based were in the range of 160°C to 166°C, which is relatively lower than the print temperatures of the KameMaker. The print maximum print temperature was 190°C.
- Flat-die-extruded PP-based thermoplastics show a relatively higher degree of crystallinity compared to when the polymer is 3D printed.
- The UV-exposed material has a lower crystallinity degree than the unexposed 3D printed samples, while for flat-die-extruded polymers, the crystallinity degree of the exposed samples is higher. Differences in the influence of ultraviolet radiation on the crystallinity degree of the polymers vary depending on the materials.
- The melt peaks of the 3D printed materials are broad, based on the melt peak onset, which suggest that the 3D printed material has a larger size distribution of crystallites.

The reliability of the described findings is uncertain because each test was done with one sample, which lowers the scientific value. However, due the limited time, the data received from the DSC-analysis could give a better understanding of the influence of 3D printing on the polymers.

11.3 Microscopy

From the microscope images, obtained from the digital microscope, one conclusion could be made about the tested thermoplastic composite:

- The digital images of the 3D printed PP-based material reveal a highly pocked and uneven surface compared to the conventional fabricated materials.

SEM-images were made of the section area of the raw, 3D printed and injection-moulded samples. The following conclusions were made:

- The images suggest that the composition and alignment of the glass fibres of the 3D printed PP are significantly different compared to the raw and injection-moulded composite.
- The image of the 3D print material shows clear gaps between the print layers. The orientation of the glass fibres may indicate that the fibres show no contribution to the bonding between the print layers.
- The mass and atom percentages of the atoms magnesium and silicon are higher in the injection-moulded material. Which suggests that the injection-moulded composite, obtained from the plastic recycled company, may be different from material composition when compared to the raw and 3D printed material.

- The mass and atom percentages of the oxygen particle are measured lowest in the 3D printed material among the other materials.

SEM is not necessarily a useful tool to measure the oxidation of the PP-based composite since the material contains an unknown percentage of glass fibres and talc which exhibit oxygen particles itself. Moreover, the SEM-results are highly dependent on the material area where the picture is taken. Forming conclusions on one area could lead to misleading interpretations of the material.

11.4 FTIR Spectroscopy

The Fourier-transform infrared (FTIR) spectra of the raw, 3D printed and injection-moulded PP-based composites has shown no difference in peaks. Strong peaks can be seen in the FTIR spectra around the wavenumber 2970-2910, 2870-2840, 11460 and 1370 cm^{-1} . These peaks indicate the methylene and methyl groups of the polypropylene and are in cohesion with previous FTIR experiments on polypropylene-based. In addition to that, broad peaks appear around the 1000 cm^{-1} which indicates (C-O)-groups. No strong peaks situate around the 1700-1800 cm^{-1} region in the FTIR spectra, which indicates the presence of an oxidation related chemical groups such as carbonyl groups (1715 cm^{-1}).

Although the peaks are evident within the zoomed in FTIR spectra, the conducted FTIR spectroscopy test did not measure the materials entirely. The infrared laser has difficulties beaming through the specimen since the sample thickness was around 5 mm and the colour of the composites is black. The maximum transmission reach of the peaks went no further than 30%, which may not be sufficient. Due to the low transmissions, it may be that some peaks could not be detected within the observed spectra. Forming conclusions on these limited spectra may lead to misleading interpretations of the material.

11.5 General conclusion

The graduation study started with the research question whether ultraviolet (UV) radiation influences the mechanical properties of a glass fibre reinforced polypropylene-based composite of a façade element. The mechanical test results have shown no significant difference between the tensile strength properties of exposed and unexposed PP-samples. Instead, the test data of both sets of tensile samples show an increase in stiffness and a decrease in yield strain over time. Moreover, the addition of UV stabilisers to the print compound tends to stimulate this embrittlement. The data of the mechanical testing suffers from sample slippage (which lowers the sample count) and scattered data due to the inconsistent print quality (which increase the coefficient of variance). These influencing factors led to remarkably low characteristic tensile strength properties for the 3D printed samples compared to the flat-die-extruded samples, reducing its application as building material e.g. façade elements. Further experiments show a difference in the degree of crystallinity, surface structure, chemical composition and orientation of the glass fibres exists between the raw and printed material. This led to the hypothesis that the embrittlement effect of the material may arise due to the 3D print process. The slow cooling of the 3D print technique may increase the amounts of spherulites in the material, which embrittles the polymer over time. In general, improvements could be found in the manufacturing process and the print material, to utilize the benefits of large-scale 3D printing of façade elements.

Chapter 12

Recommendations

The 3D printing technology creates new and challenging opportunities for manufacturing façade panels, even though not much research has been done into its effect on the material at this moment. It creates multiple opportunities and possibilities for further development, which cannot all be covered within a graduation project. Potential improvements could be found for both broadening as well as for in-depth research. These recommendations are summarised for researchers working on the product development of the Aectual façade or studying the effect of 3D printing on the strength of thermoplastic polymers.

12.1 Product development

The broadening research contributed to the product development of the Aectual façade. Different potential risks were studied. The fire resistance and the material ageing of the façade panel, are the potential risks which should be solved first. Fire safety tests should be done to determine the fire safety class of the façade element. Changes in the material, such as adding fire-retardant additives and applying fire-retardant coatings, should be tested in the same manner. Understanding the fire properties of the 3D printed polymer could provide more safety when applying the polymer to building applications.

The purpose of the in-depth study was to have a better understanding of what the effect of outdoor weather conditions has on the 3D printed material. Due to limitations of testing and exposure devices, only the impact of ultraviolet exposure is studied, since that is the most harmful factor contributing to the weathering of thermoplastic polymers. Nonetheless, to have a better simulation of the natural weathering effect, a test is advised including the combination of different factors as rain, day and night, frost and thaw and temperature cycles. Therefore, an accelerated ageing test with a Weather-O-meter device offers a better alternative.

The focus of this research was mainly on the strength properties of the extruded material itself, and less analysis has been done on the connections with the loadbearing structure. Experimental research should be done to investigate the strength of the 3D printed polymer and the design of its connections.

12.2 Mechanical testing

The various print qualities of the samples result in a random distribution of data, as seen in the tensile test results. This issue made it problematic to provide a sufficient analysis that enables to determine the effect of UV degradation. It is recommended that the clamping surface of the tensile specimen is as flat and consistent as possible. An uneven surface will increase the chance of slippage and lead to more unreliable data.

When there is no other way than using a print material of various print qualities, it is recommended to group the samples by print qualities, print figurations or print height within the printing object (temperature history). Changing the dimensions of the specimen could also help to reduce the impact of print impurities. However, it should be questioned whether the result will be representable considering the object's dimensions. Besides tensile testing, other strength properties tests should

be done to examine the change in strength due to UV radiation. However, as seen in the previous study on 3D printing, shear force and transverse bending could lead to unpredictable results (Wang 2018; Baran 2017). A longitudinal bending test could lead to more consistent results, however, it should specimen slippage should be considered.

12.3 The effect of 3D printing on the material

Further research should be done to understand the effect of 3D printing technique on the material. Since aspects of the 3D print-extrusion technique differs from the conventional injection-moulding or flat-die-extrusion technique such as:

- The printed object is manufactured by a layer-by-layer routine and cooled in open air. It is expected that every print layer will endure different heat and cool cycles, which will affect their mechanical properties.
- Thermal oxidation might occur within the material, due to the availability of oxygen around the screw and nozzle when the polymer is at melted and extruded.

These aspects could have (negatively) influence to the polymer chains, whereby chain-scission and recrystallisation could occur. Further research into the thermal effect of 3D printing on the thermoplastic polymer is of high importance. Techniques that can be recommended for the further study:

- A rheometer test can be conducted, to determine if crosslinking of the polymer chains of an aged material occurs. With a rheometer, the viscosity of a thermoplastic polymer sample could be measured. When a polymer has a higher viscosity than before, cross-linking has occurred.
- A gel permeation chromatography (GEL) is advised, to determine the average length of a molecular chain of the thermoplastic. The polypropylene-based material should be dissolved in an organic solvent and injected in the GEL-device. The device will supply the weight distribution of the polymer lengths. It must be noted that only the polymer should be dissolved since glass fibres or minerals could obstruct the test. It is known that polypropylene is chemical resistant against the chemical compound tetrahydrofuran (THF). In the case of a GEL-test, a more suitable solvent should be found.
- A transmission electron microscopy (TEM) Is recommended in a combination of film specimen of the 3D printed material, to confirm the formation of spherulites within the 3D printed composite.

12.4 Further development of the 3D printing technology

Improvements could be found in different aspects of the manufacturing process since it is proved that 3D print-extruded polymers show lower performance than when manufactured with conventional methods. Current capabilities of the KameMaker, do not provide adequate quality control, which results in a large variety of cross-sectional properties. Solving the problem will increase the predictability of the polymer's strength properties. In addition to that, for each print compound, a correct extruding temperature should be found to achieve the maximum polymer strength and a better print quality. The temperature should be high enough to melt the raw material, let it flow through the printer and adhere to the previous printed layer. However, the temperature should be low enough, before initiating thermal degradation of the material, lowering the strength of the polymers. Nonetheless, the printer itself should be reconsidered for a redesign. These

changes are based on the conventional plastic extrusion methods and will be discussed in this section.

12.4.1 Printing under the exclusion of oxygen

When it is proven that the availability of oxygen during the print process has a high effect on the strength of the printed material, printing in an atmosphere under the exclusion oxygen could be promising. A study has shown that an increase is found in the tensile properties of the polymer when printed in a nitrogen atmosphere (Lederle et al. 2016).

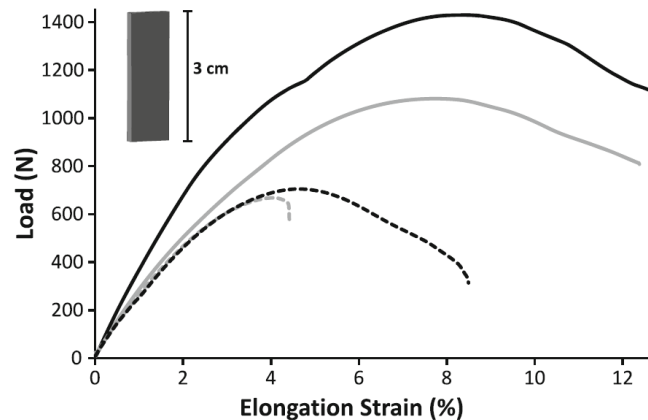


Figure 104: Averaged load-strain curves of plates made of ABS (dashed) and nylon copolymer (solid) printed at air (grey) and under a nitrogen atmosphere (black) (Lederle et al. 2016).

3D printing under the exclusion of oxygen may be realised by flooding the printing chamber with nitrogen to improve the mechanical properties of the printed objects. However, the experiment is conducted in a small and controllable chamber. Since the KameMaker is a chamber of larger dimensions than an original 3D printer box and the robot arm is used in open space, it seems unlikely to fill the volume with an inert gas because of safety and practical reasons. A solution to this issue could be found in the welding of metals. Inert gases are used during metal welding to protect the weld area from atmospheric gasses like oxygen, nitrogen, carbon dioxide and water vapour. These gasses influence on the weld quality. Improper choice of shielding gas may lead to a porous and weak weld, to excessive spatter, and reduced productivity. The six noble gases are helium, neon, argon, krypton, xenon, and radon. Of those gases, only helium and argon are cost-effective enough to be used in welding.

A redesign of the 3D printer could be made with the help of the welding process of metals and the injection-moulding fabrication. The goal is to exclude the availability of oxygen when the polymer is heated up. In the chamber of the screw, where the pellets are melted, and mixed, fresh air could still come in. It should be sure that no supply of fresh air could penetrate the chamber around the screw during the heating process. For the nozzle a new design could be made, based on the welding technique, to prevent oxygen between the print layers. A controlled and targeted supply of nitrogen, for example, could form a cloud around the nozzle, extruded material and the previous print layer. In this way, the effect of oxygen to the heated-up temperature could be minimised. The redesign is conceptually illustrated in **Figure 105**.

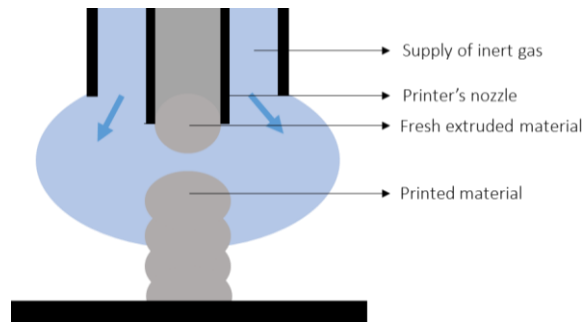


Figure 105: Redesign of the printer's nozzle including the supply of an inert gas.

12.4.2 Improvement of the interlayer bonding

Even though, this study is more focus on the degradation of the material itself than the interlayer bonding of the print layers. The weakness of 3D printing is that the freshly extruded material has a higher material temperature than the print layer under it, which is cooler depending on the print route. A longer print route means that the print can cool further in the ambient air than when the print route is short. This weak interlayer bonding can be seen in the in **Figure 96**. The image shows that there is still a clear separation between the print layers, resulting in a weaker strength in the transverse direction of the print layer as concluded from the mechanical testing.

Reheating the previous layer could be a solution. Strengthen the bonding between layers could be done by integrating an infrared laser and an infrared camera near the nozzle, which could be controlled with the 3D printing software by the user. The laser heat shortly the previous print layer, shortly, until it reaches the same temperature as the new extruded material. The infrared camera measures the temperatures during this process. In this way, the adhesion between print layers of different surface temperatures could be prevented, resulting in stronger adhesion strength of the polymer. The redesign is conceptually illustrated in **Figure 106**.

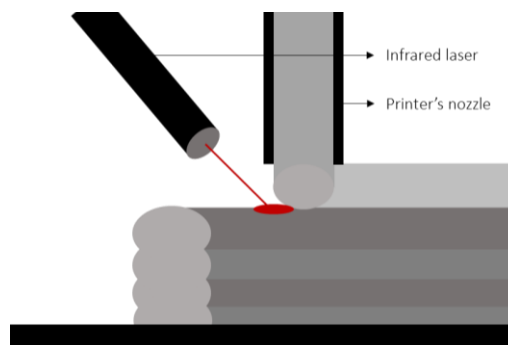


Figure 106: Redesign of the printer's nozzle including the infrared laser.

12.4.3 Health

When melting the thermoplastic polymer with the 3D printer, it should be taken into account that the extruded material could release toxic gasses (Wojtyła, Klama, and Baran 2017), which could be dangerous for the physical health of the people working around the 3D printer. After treatment, such as sanding plastics to make a smooth surface, should be done securely. As seen in the SEM-image of **Figure 96**. Small glass fibres are sticking out of the surface of the polymer. When these fibres, due to the sanding or another treatment, come in the air, this also could be dangerous for the health of the people working with these plastics.

Back Matter

Appendices

Appendix A

Material Information


 Mafill® CR XTG 5344 Polypropylene Industrial Quality Compound			
Description:			
PP 20% glass fiber and mineral filled industrial quality compound			
General			
MFI (230°/2,16kg)	ISO 1133	9	g/10min
Density	ISO 1183	1,05	g/cm ³
Linear mould shrinkage	ASTM D955	0,6-1,4	%
Thermal			
Vicat softening point (B50 (50N))	ISO 306	85	°C
Mechanical			
Tensile stress at yield	ISO 527	38	MPa
Tensile stress at break	ISO 527	34	MPa
Elongation at break	ISO 527	8	%
Flex modulus	ISO 178	2200	MPa
Izod impact (+23°C (notched))	ISO 180	5,5	kJ/m ²
Flammability			
Flammability (3,2mm)	UL94	HB	
Flammability (1,6mm)	UL94	HB	
Glow wire flammability index (2,0 mm)	IEC 60695-2-12	650	°C

Figure 107: Material Sheet PP: Mafill CR XTG 5344.


	PRODUCT INFORMATION	
	Version: 13,002 Last update: 16-10-2013 Print date: 16-10-2013	
<i>This update supersedes all previous updates.</i>		
Product:	Antistatic masterbatch with UV-stabilizers	
Catalog number:	VE82608	
Color:	Natural	
Application area		
VE82608 masterbatch is suited for usage in molded, blown and extruded articles made of various types of PE and PP.		
Carrier material		
The carrier resin is LLDPE. MFI = 20-25 g/10 min (ASTM D-1238; 190 °C/2.16 kg)		
Properties		
Max. processing temperature:	280 °C	
Light fastness (DIN 53387):	6	
Dosage recommendation:	Generally 0.5% but is application dependent	
Regulatory Affairs		
REACH: this product does not contain any substances on the candidate list of Substances of Very High Concern (Annex XIV, REACH legislation).		
Heavy metals: this product complies with EU Directive 2000/53/EC (and its amendments).		
Packaging and packaging waste: this product complies with EU Directive 94/62/EC.		
RoHS: this product complies with Directive 2011/65/EU.		
Food contact: this product complies with EU Regulation 1935/2004/EC and the relevant requirements of EU Regulation EU 10/2011 and its amendments (1282/2011; 1183/2012); the colorants in this product comply with EC Resolution AP (89) 1; this product contains UV-stabilizers (CAS # 71878-19-8 and CAS # 65447-77-0) that are subject to a SML (Annex I, table 1). This product contains no Dual Use Additives.		
Storage and shelf life		
This product has an expected shelf life of at least 2 years if properly stored in cool and dry conditions out of direct sunlight.		
Further remarks		
Compliance of this product with various food contact regulations (if applicable) does not relieve the manufacturer of finished articles intended for food contact from the final responsibility to ensure compliance of these finished articles with food contact regulations (such as migration tests).		

Figure 108: Material Sheet: UV stabilisers for PPU.

			PP-C
			PP-Copolymer Virgin
MECHANICAL PROPERTIES (at 23°C)			
E-modulus	ISO 527-2	N/mm ²	1300
Tensile strength	ISO 527-2	N/mm ²	28
Tensile strain at break	ISO 527-2	%	>600
Tensile stress at yield	ISO 527-2	N/mm ²	24
Tensile strain at yield	ISO 527-2	%	7
Impact strength, Charpy unnotched 23°C	ISO 179	kJ/m ²	no break
Impact strength, Charpy notched 23°C	ISO 179	kJ/m ²	30
Coefficient of friction vs. steel (dry)	-	-	0,2
Hardness	ISO 868	shore D	66
Density	ISO 1183	kg/m ³	920
THERMAL PROPERTIES			
Softening temperature, vicat A/50 (10N)	ISO 306/A	°C	147
Linear expansion	ISO 11359	mm/m/10°C	1,6
Coefficient of heat conductivity	ISO 22007	W/m.K	0,22
OTHER PROPERTIES			
Absorption of moisture	ISO 62	%	< 0,03
Fire test	DIN 4102	-	B2
Breakdown voltage	DIN 53481	kV/mm	> 60
Volume resistance	DIN 53482	Ohm	> 10 ¹³
Dielectric constant value	DIN 53483	-	2,25
CHEMICAL AND PHYSICAL RESISTANCE			

Figure 109: Material Sheet: Flat-die Extruded PPB.


Product information sheet		
Masterminds[®] PE black 8301F		
	Date	: October 30th 2013
	Version number	: 1.0
	Revision number	: 0
<u>General description:</u>		
<p>Masterminds[®] PE black 8301F is specially designed for high end applications that come into contact with food and/or where a higher UV protection of the end article is desired.</p> <p>Masterminds[®] PE black 8301F contains no filler and gives a high gloss coloration. It can be used in compounding, injection moulding, blow moulding and extrusion applications.</p>		
<u>Physical properties:</u>		
Property	Value	Test methods (*)
Carrier	Polyethylene	
Pigment	40 %Carbon Black – type P (<25nm)	
Density [20 °C]	approx. 1,2 g/ml	CTP-TP016
Bulk density	approx. 0,7 g/ml	CTP-TP004
MFI [190°/21.6 kg]	60 - 80 g/10 minutes	CTP-TP020
(*) Tests have been executed according to QolorTech's own internal testmethods which are related to international standard testmethods.		
<u>Packaging:</u>		
<p>Masterminds[®] PE black 8301F will be supplied as spherical granules in 25kg PE bags. On request, deliveries in big-bags or octabins is also possible.</p>		
Remark:		
<p>To be conform with the requirements of EU Regulation 10/2011 the plastic material in contact with food cannot contain more than 6,25% Masterminds[®] PE black 8301F. For more details regarding the food contact compliance in various European countries, please contact your QolorTech representative.</p>		

Figure 110: Material Sheet: Carbon black, a colour additive for PPB.


Product information sheet		
HiQontrol[®] PE UV Batch 1146		
	Date	: 28.07.2016
	Version number	: 1
	Revision number	: 1
<u>General description:</u>		
<p>HiQontrol[®] PE UV Batch 1146 is part of a range of polyolefin masterbatches, containing light stabilizer(s), which allow the customer to produce articles with optimized light stability properties for outdoor exposure in all regions of the world, for a wide variety of applications e.g. tapes and thick section, a.o.</p> <p>HiQontrol[®] PE UV Batch 1146 contains a combination of low and high molecular weight HALS, especially effective in PP based injection moulded articles.</p>		
<u>Physical properties:</u>		
Property	Value	Test methods (*)
Carrier	Polyethylene PE	
Active content	14-16%	
(*) Tests have been executed according to QolorTech's own internal test methods which are related to international standard test methods.		
<u>Guidelines for use:</u>		
<p>Addition levels of HiQontrol[®] PE UV Batch 1146 depend on various factors such as thickness of the final article, presence of other additives and fillers and commonly range from 0.5-6.0%. For particular demanding applications customer specific MB can be produced. Contact us for your specific application needs.</p>		
<u>Packaging:</u>		
<p>HiQontrol[®] PE UV Batch 1146 will be supplied as granules in 20kg PE bags. On request, deliveries in big-bags or octabins is possible.</p>		
<u>Remark:</u>		
<p>Storage conditions and shelf life It is recommended to avoid the exposure of HiQontrol[®] PE UV Batch 1146 to sunlight and high temperatures for longer times as this may impair the quality of the MB. Storage lifetime is 1 year.</p>		

Figure 111: Material Sheet: UV stabiliser for PPB.

Appendix B

Effective Length

Due to the limitation of the laboratory conditions, there was no gage used for measuring the strain of the samples. Therefore, the results derived from the tensile test need to use effective length for calculating the desired mechanical properties. The tensile specimen has the geometry that could be found in **Figure 112**.

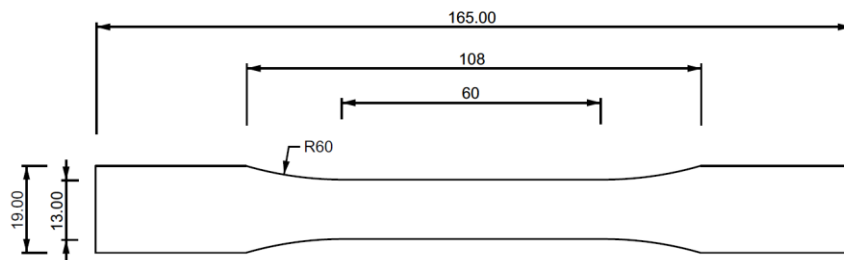


Figure 112: Specimen geometry for the tensile test.

The effective length L_{eff} can be determined by:

$$\frac{L_{eff}}{L_{actual}} = \frac{\delta_{eq}}{\delta_{actual}}$$

Considering a given coordinate system, the curvature of the rounded part of its perimeter can be expressed with a circle equation:

$$x^2 + (y - 60)^2 = 60^2$$

Which for the relevant section of the circle can be translated into:

$$y = 60 - \sqrt{3600 - x^2}$$

The narrowing part can be divided into three sections: a , b and c . the cross-sectional area of each section can be calculated:

$$A_a(x) \text{ } a: \quad t \left(165 - 2\sqrt{3600 - (24 - x)^2} \right) \quad \text{for} \quad 0 \leq x \leq 24$$

$$A_b(x) \text{ } b: \quad 10t \quad \text{for} \quad 24 \leq x \leq 84$$

$$A_c(x) \text{ } c: \quad t \left(165 - 2\sqrt{3600 - (x - 84)^2} \right) \quad \text{for} \quad 84 \leq x \leq 108$$

Hereby t is the nominal thickness.

Then the normal force/displacement relationship can be derived according to the linear theory:

$$\delta = \int_0^L \frac{N dx}{EA(x)}$$

Where N is the normal force, δ is the normal displacement, E is the Young's modulus and L is the length. Next, by combining the previous equations, the displacement with equivalent length can be derived as follow:

$$\delta_{equation} = \frac{N}{E} \left(\int_0^{24} \frac{dx}{A_a(x)} + \int_{24}^{84} \frac{dx}{A_b(x)} + \int_{84}^{108} \frac{dx}{A_c(x)} \right)$$

$$\delta_{equation} = \frac{N}{Et} (1.8917 + 6 + 1.8917) = \frac{N}{Et} (9.7834)$$

Finally, by comparing with the uniform cross-section with 108 mm long and 10t as area, the effective length can be derived:

$$\delta_{108} = \frac{N}{Et} \int_0^{108} \frac{dx}{108} = \frac{N}{Et} (10.8)$$

$$L_{eff} = \frac{\delta_{eq}}{\delta_{108}} \times 108 = \frac{9.7834}{10.8} \times 108 = 97.83 \text{ mm}$$

Appendix C

Coefficient of Variation

For most all experimental test that was described within this research report, it holds that from the obtained test results, the average value, the characteristic value and the standard deviation are determined according to NEN-EN 1990+A1+A/C2.

- X_d is the design value of the property and is determined by the following formula:

$$X_d = \eta_d \times \frac{X_{k(n)}}{\gamma_m} = \frac{\eta_d}{\gamma_m} \times m_x(1 - k_n V_x)$$

Consequently, the characteristic value formula can be derived:

$$X_k = m_x(1 - k_n V_x)$$

- V_x is the variation coefficient can is determined by the following formula:

$$V_x = \frac{s_x}{m_x}$$

- s_x is the standard deviation as within the following formula:

$$s_x = \sqrt{\frac{1}{n-1} \sum (x_i - m_x)^2}$$

- η_d is the design value of the conversion factor, this factor depends on the testing method and material type. .
- m_x is the average value of the series of measured values.

The coefficient of variation, represented in this report with CV is calculated from the following expression:

$$CV = \frac{s_x}{m_x}$$

Appendix D

UV Test Chamber

Specifications	LY-605A
Temperature range	Normal+5°C~200°C
Internal size W x H x D (cm)	50×60×50
External size W x H x D (cm)	70×122×65
Accuracy of temperature	± 0.3°C
Distribution of temperature	± 0.5°C
Temperature controller	Electronic LED digital display, automatic play several micro PID temperature controllers
Timer	0~999min
Test rack	The speed of 1~10rpm, adjustable, single-deck rotating stand
Internal material	SUS mirror finished stainless steel
External material	Special steel, galvanized antirust processing, the senior resin coating with the lacquer that bakes
Observation window	Whole sealing
Safety device	Over-temperature power-off protection, Over-temperature protection, Over-time protection
Standard accessories	2 groups of not adjustable stainless-steel layer
Power	1Φ, 220V, 50HZ

Table 17: Specification of the UV Test Chamber.

Appendix E

Wind Load Assumptions

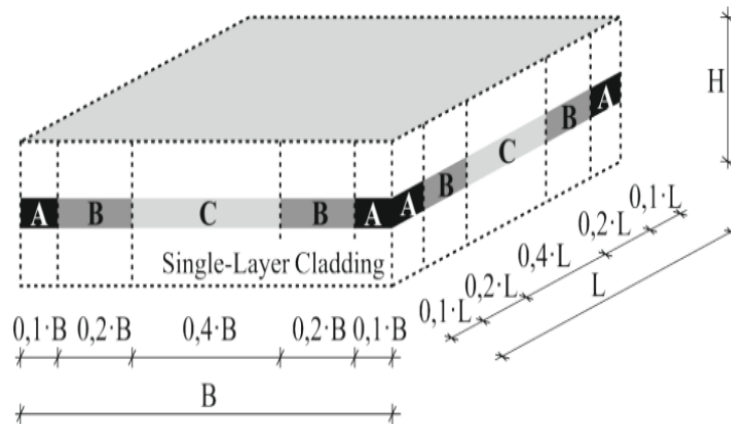


Figure 113: Situation A: Single layer (Kemper & Feldmann, 2012).

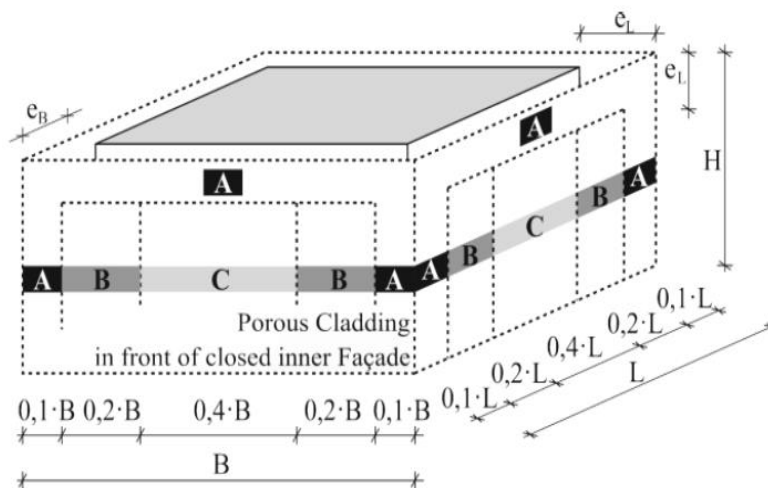


Figure 114: Situation B: Second skin layer (Kemper & Feldmann, 2012).

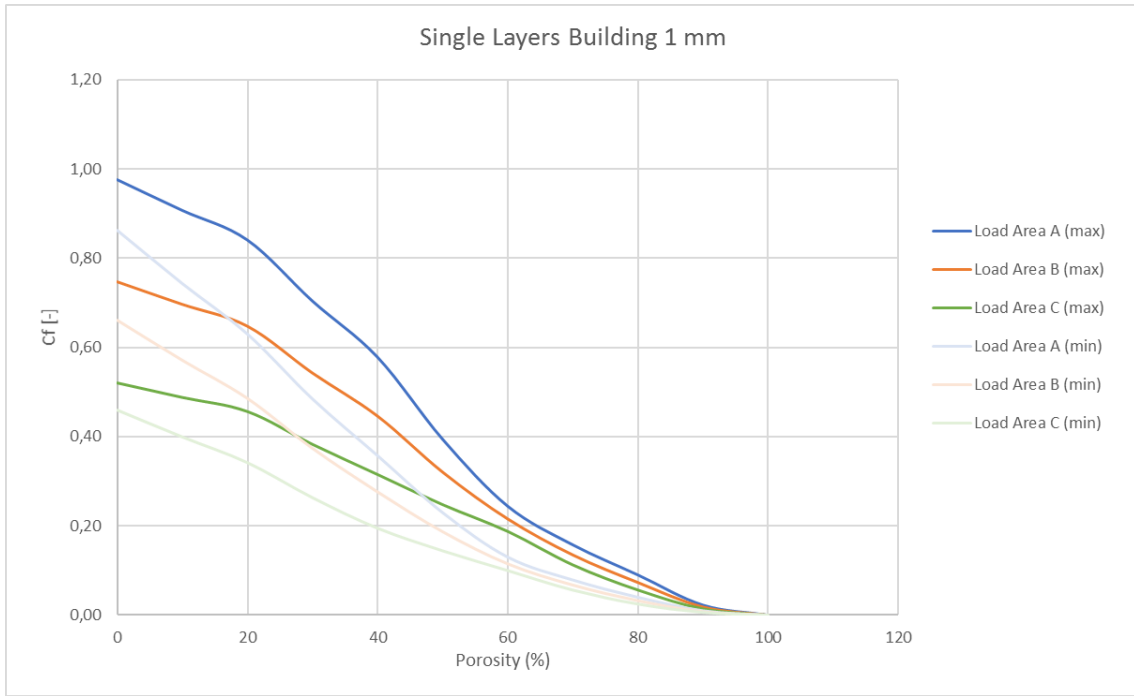


Figure 115: Wind load assumptions: Situation A, 1 mm.

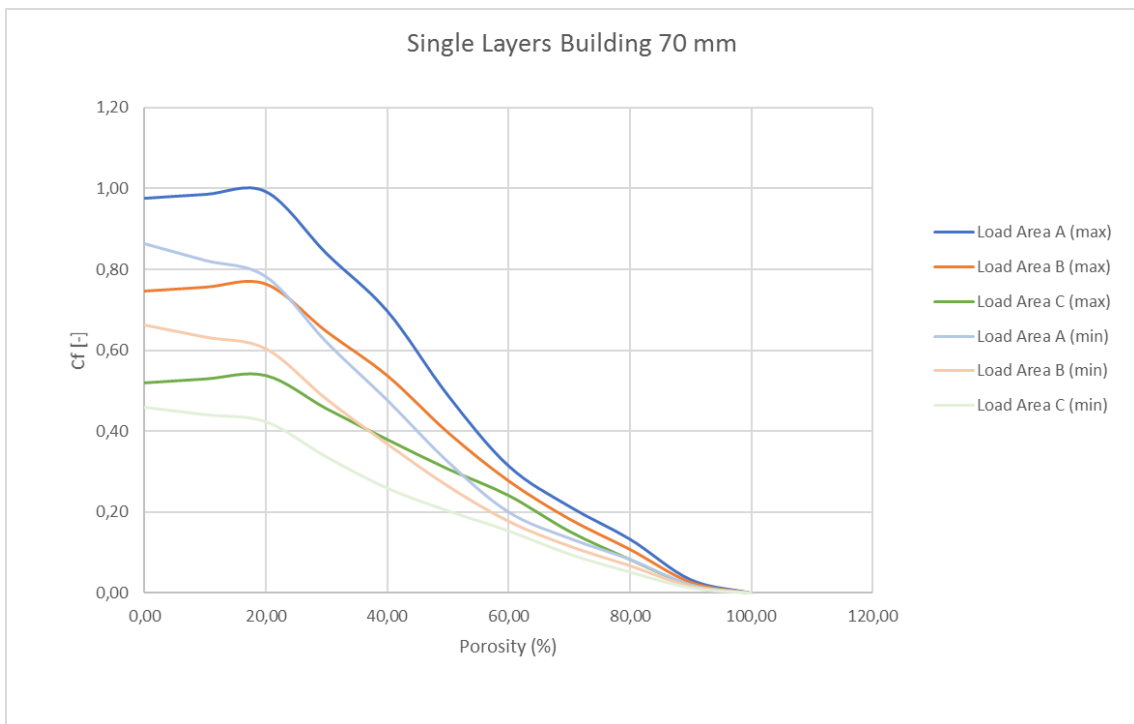


Figure 116: Wind load assumptions: Situation A, 70 mm.

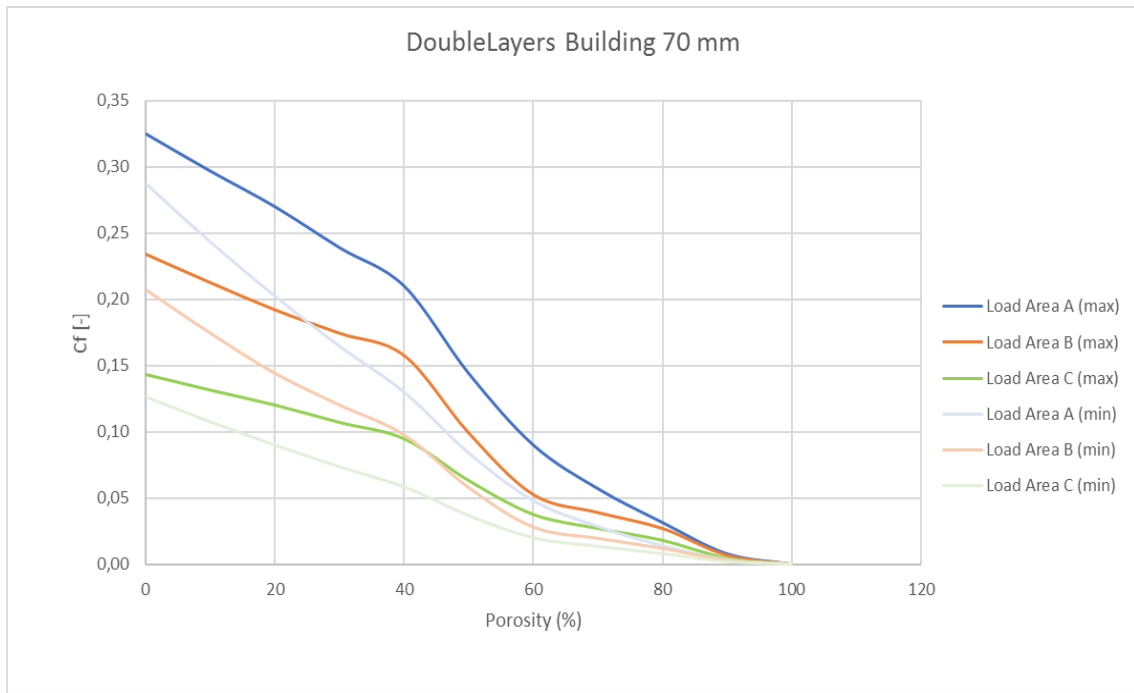


Figure 117: Wind load assumptions: Situation B, 70 mm.

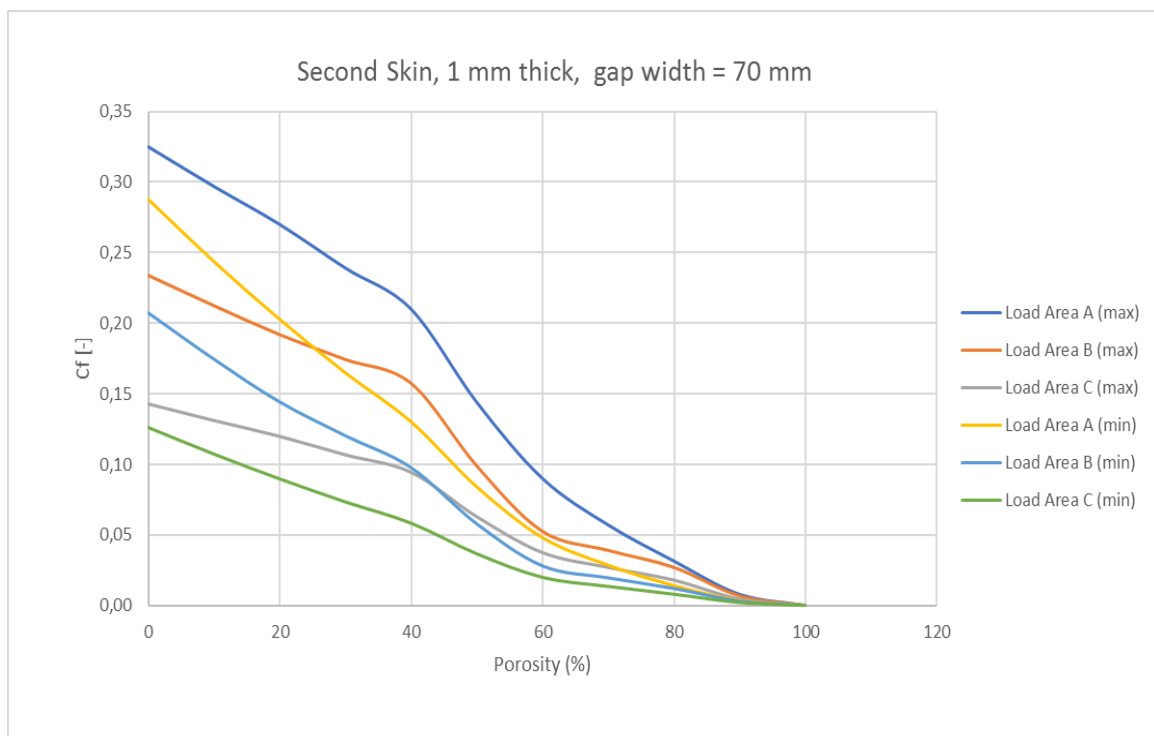


Figure 118: Wind load assumptions: Situation B, 70 mm..

Appendix F

Raw Test Results

Graphical results of the transverse tensile tests with the reference specimen:

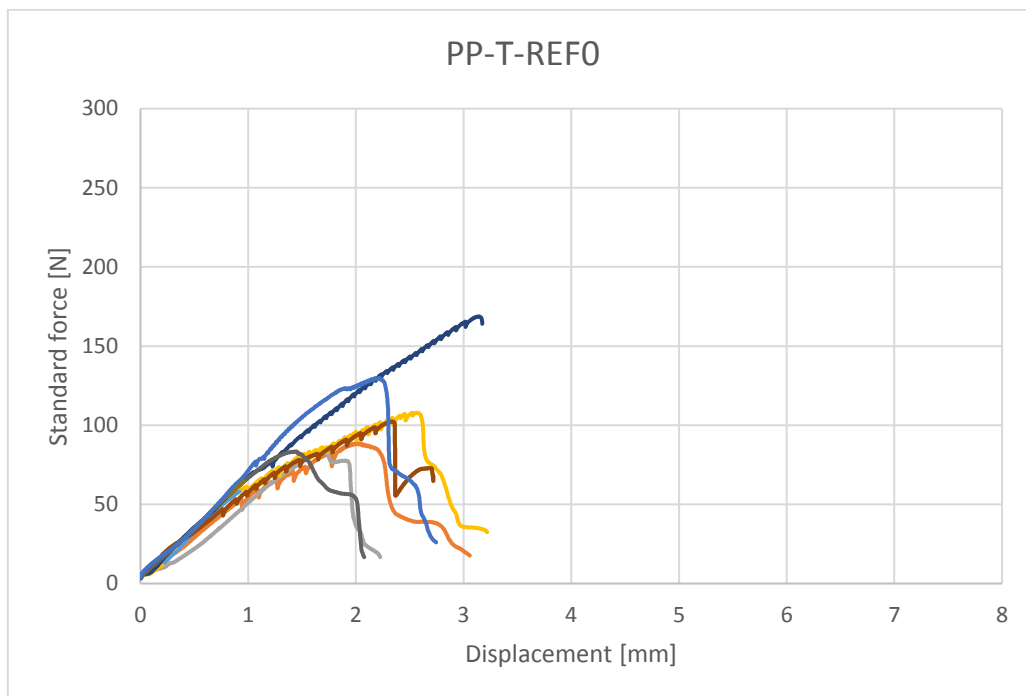


Figure 119: Raw result: PP, transverse tensile test, 888 hours aged.

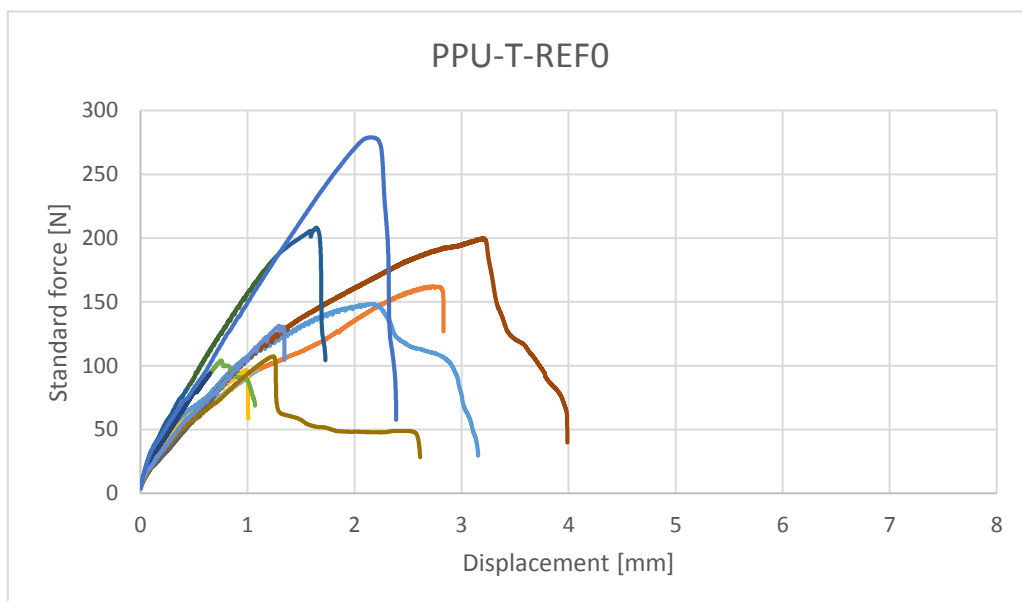


Figure 120: Raw result: PPU, transverse tensile test, 552 hours aged.

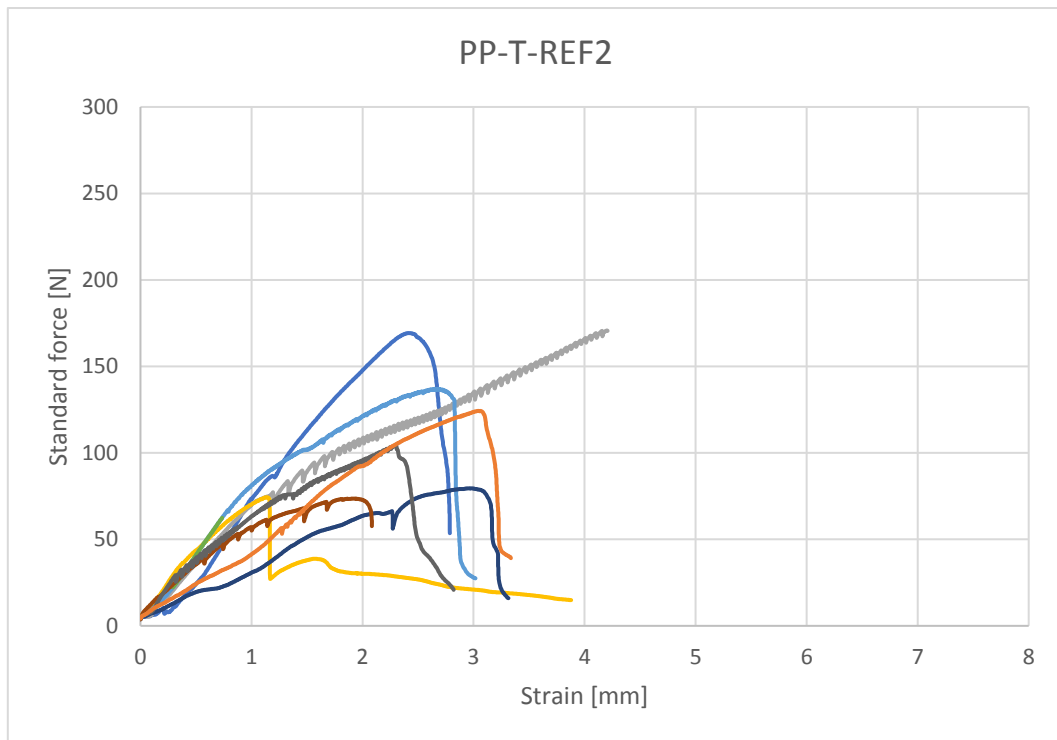


Figure 121: Raw result: PP, transverse tensile test, 1008 hours aged.

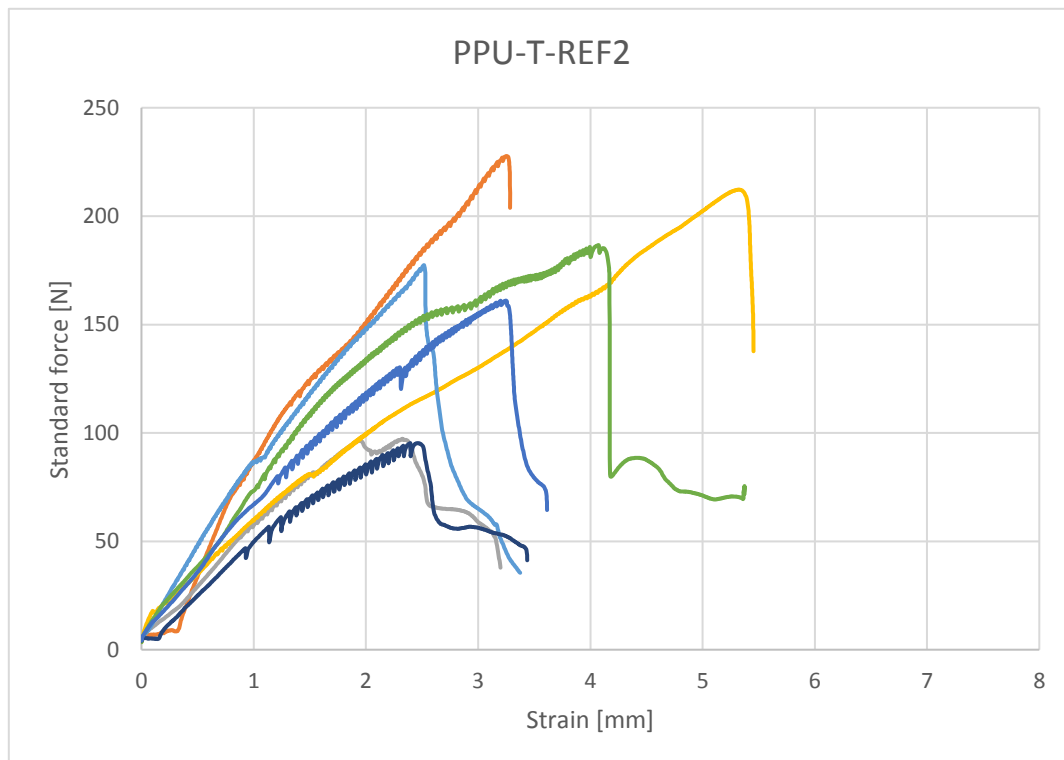


Figure 122: Raw result: PPU, transverse tensile test, 672 hours aged.

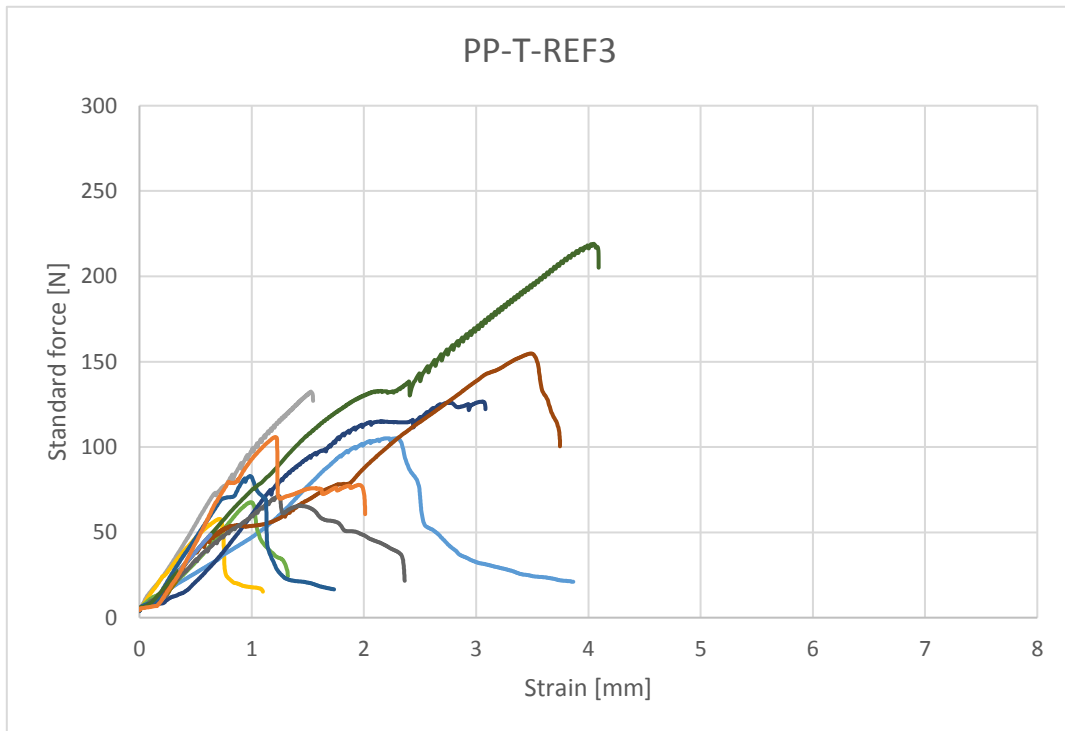


Figure 123: Raw result: PP, transverse tensile test, 1296 hours aged.

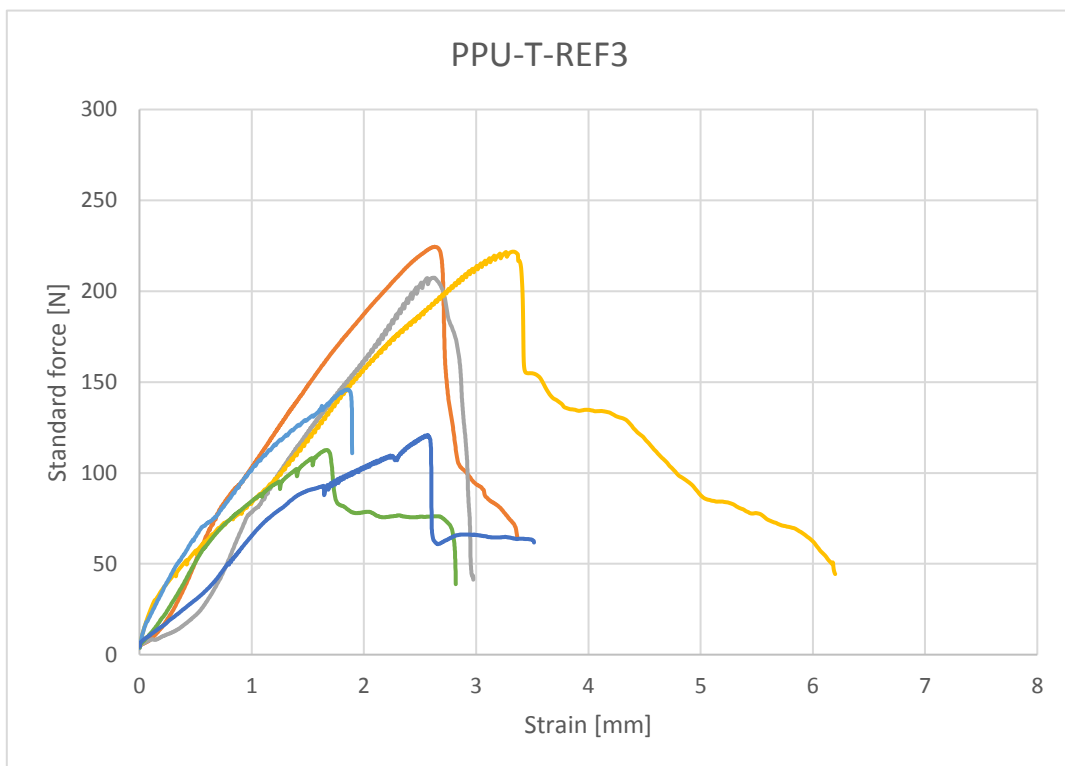


Figure 124: Raw result: PPU, transverse tensile test, 1296 hours aged.

Graphical results of the transverse tensile tests with the exposed specimens:

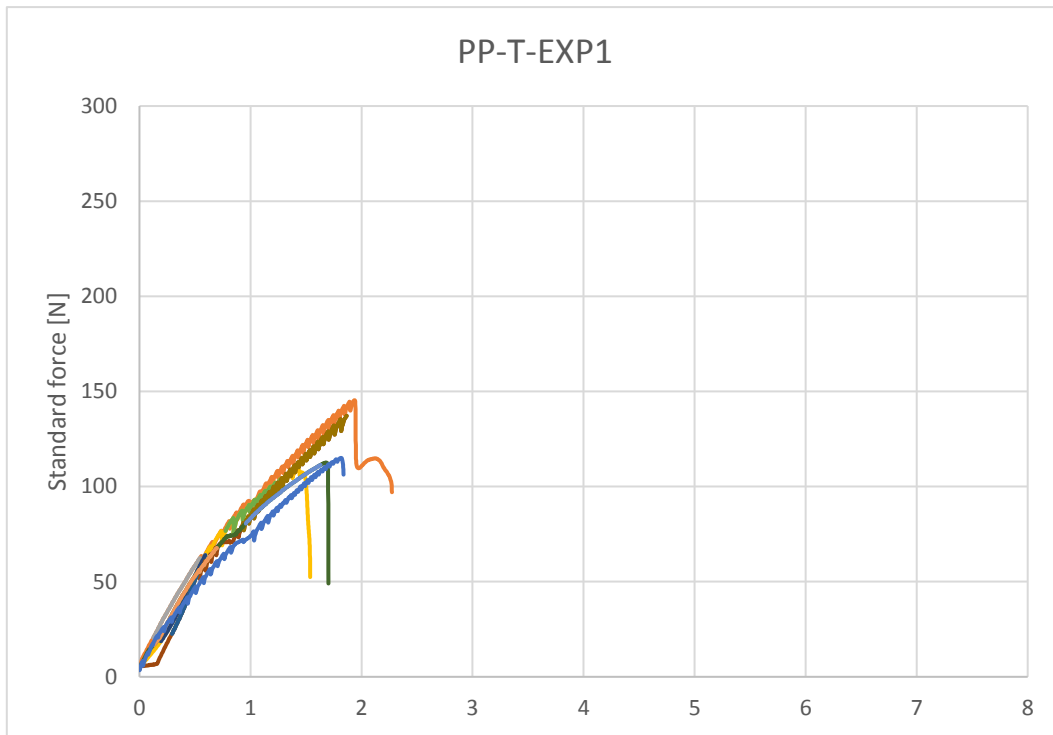


Figure 125: Raw result: PP, transverse tensile test, 240 hours exposed.

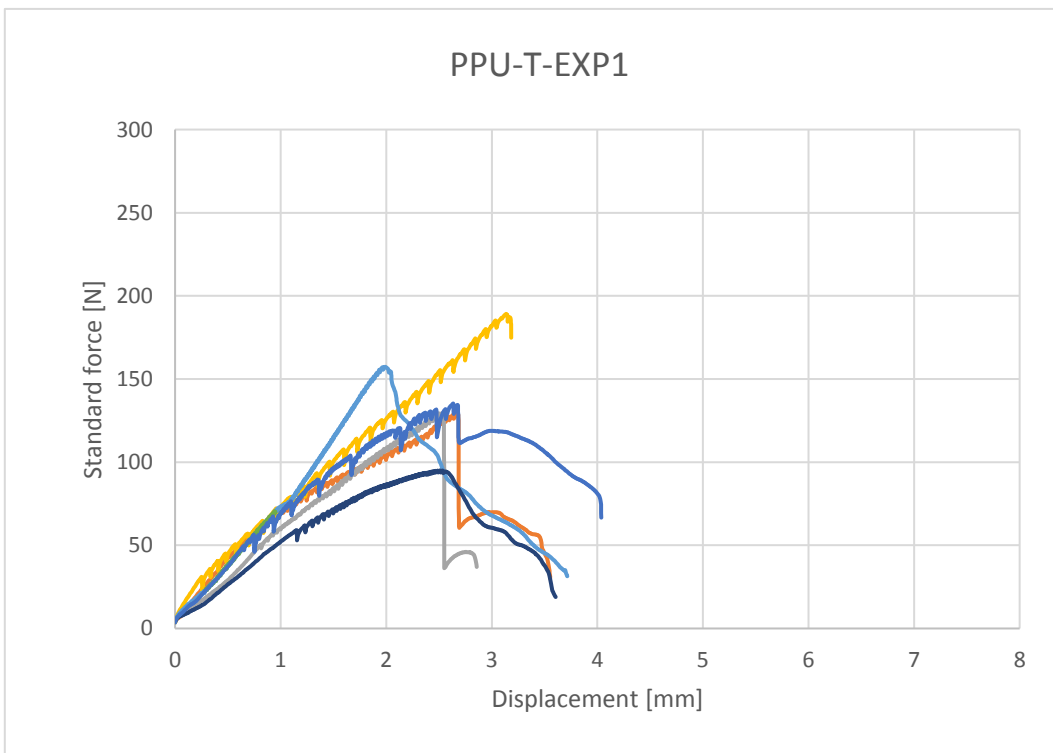


Figure 126: Raw result: PP, transverse tensile test, 240 hours exposed.

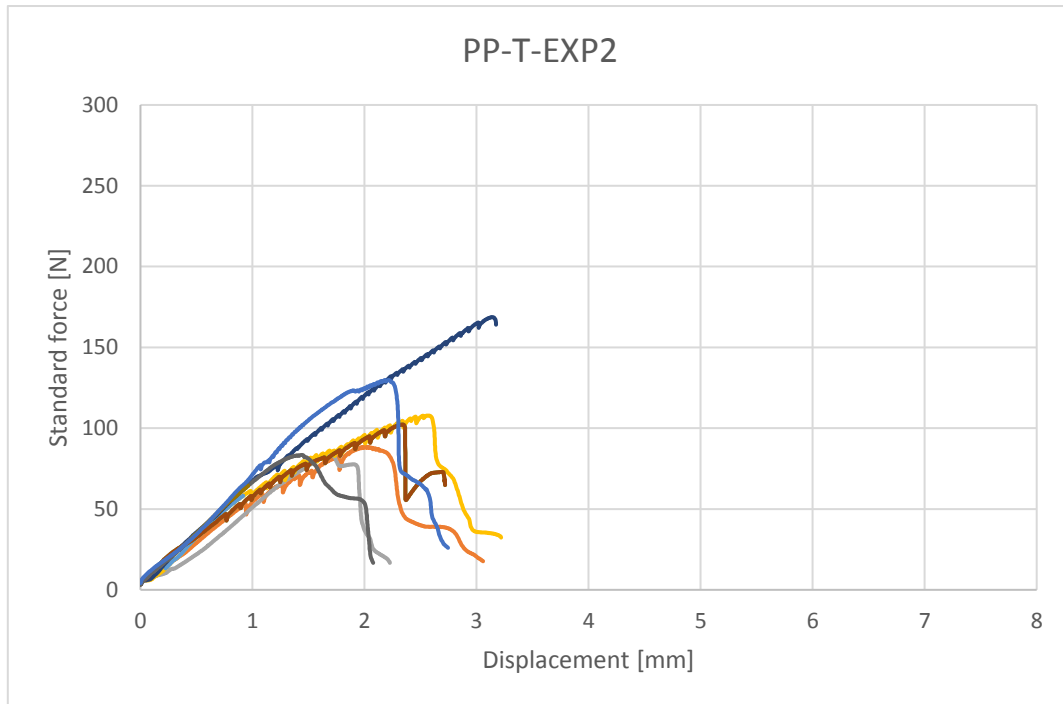


Figure 127: Raw result: PP, transverse tensile test, 576 hours exposed.

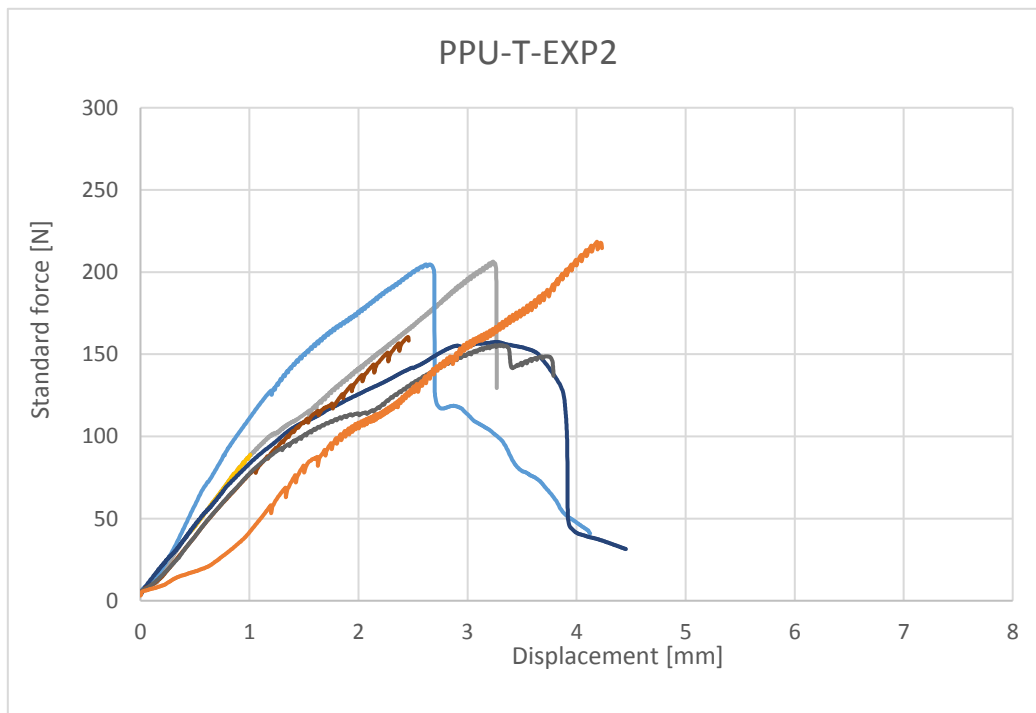


Figure 128: Raw result: PPU, transverse tensile test, 576 hours exposed.

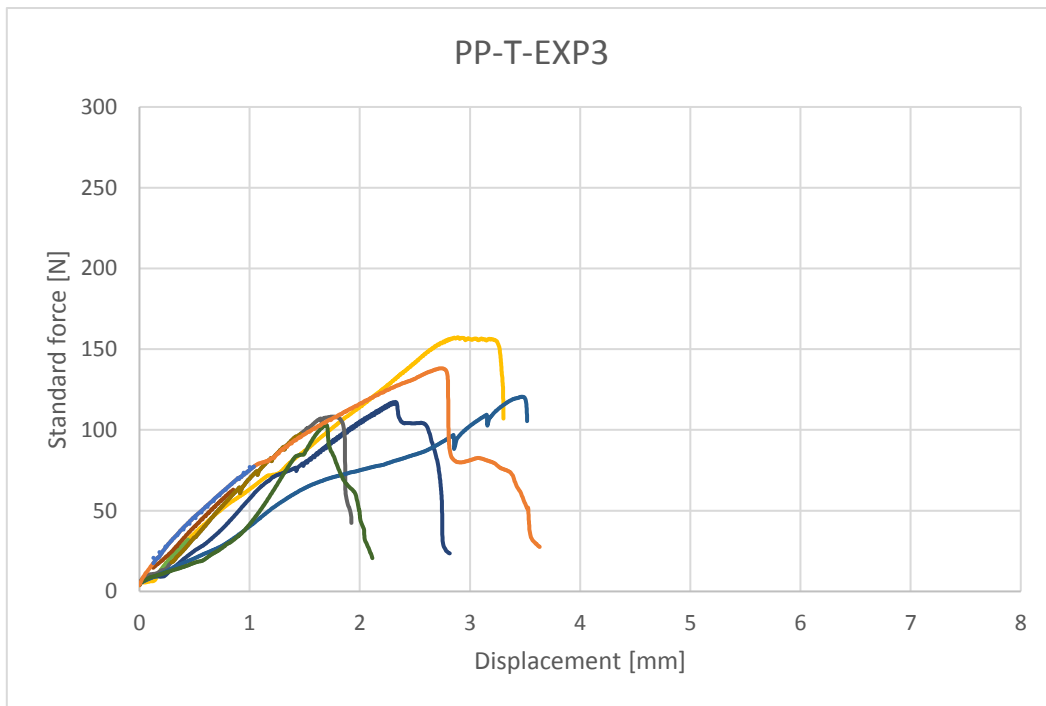


Figure 129: Raw result: PP, transverse tensile test, 840 hours exposed.

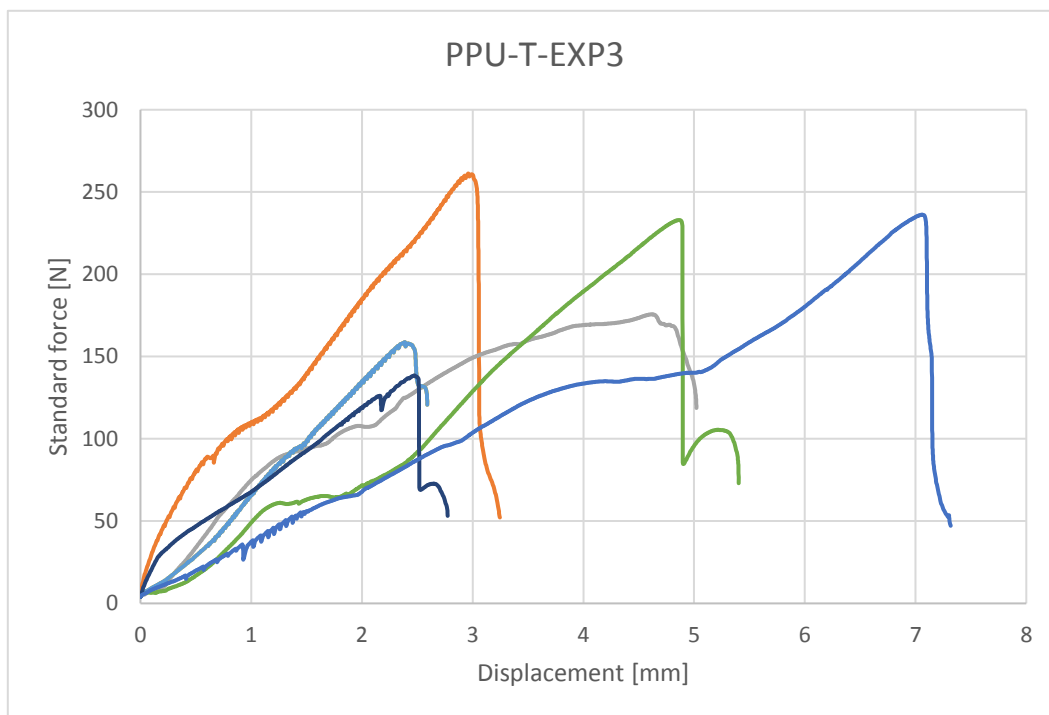


Figure 130: Raw result: PPU, transverse tensile test, 840 hours exposed.

Graphical results of the longitudinal tensile tests with the reference specimens:

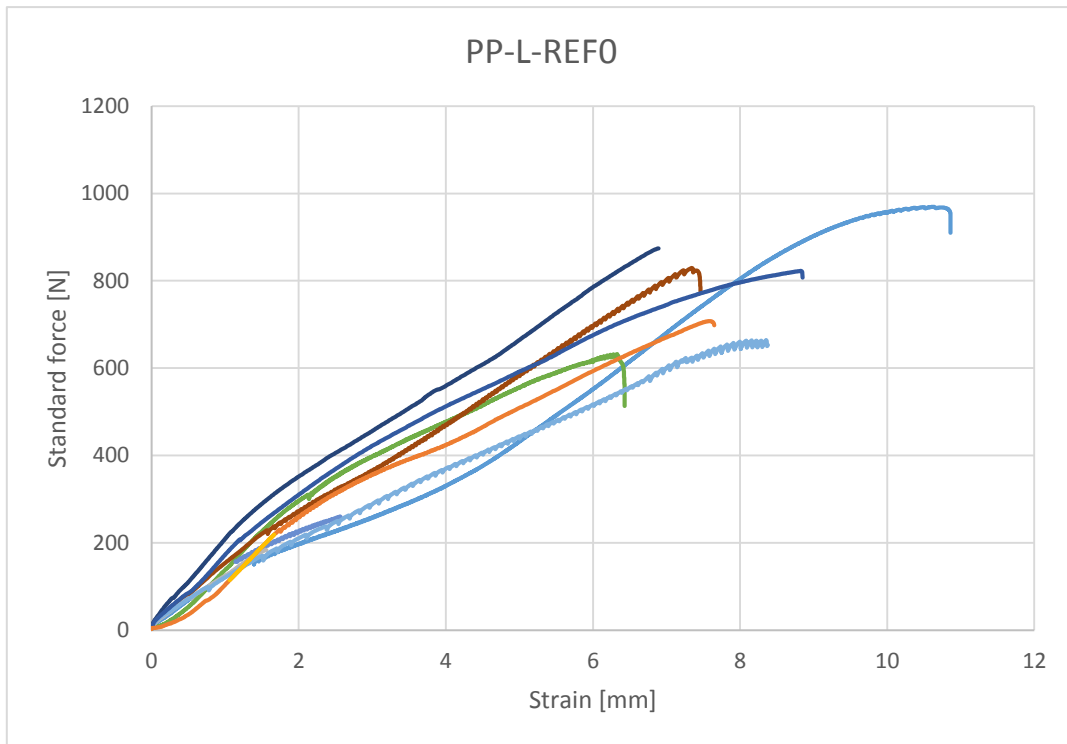


Figure 131: Raw result: PP, longitudinal tensile test, 888 hours aged.

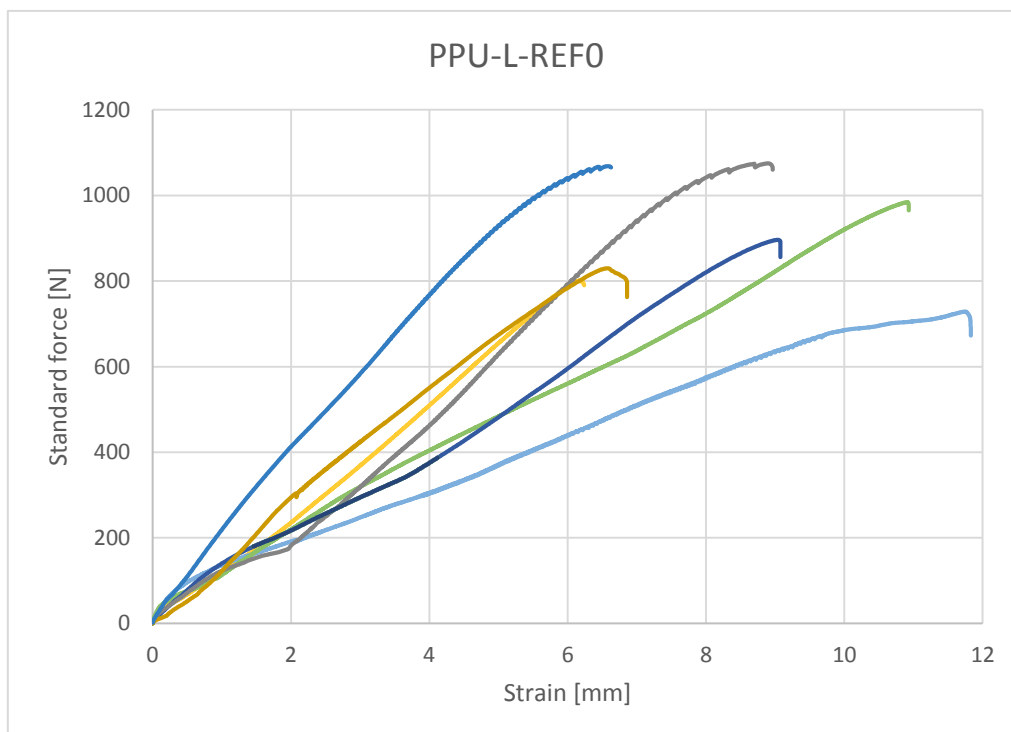


Figure 132: Raw result: PPU, longitudinal tensile test, 888 hours aged.

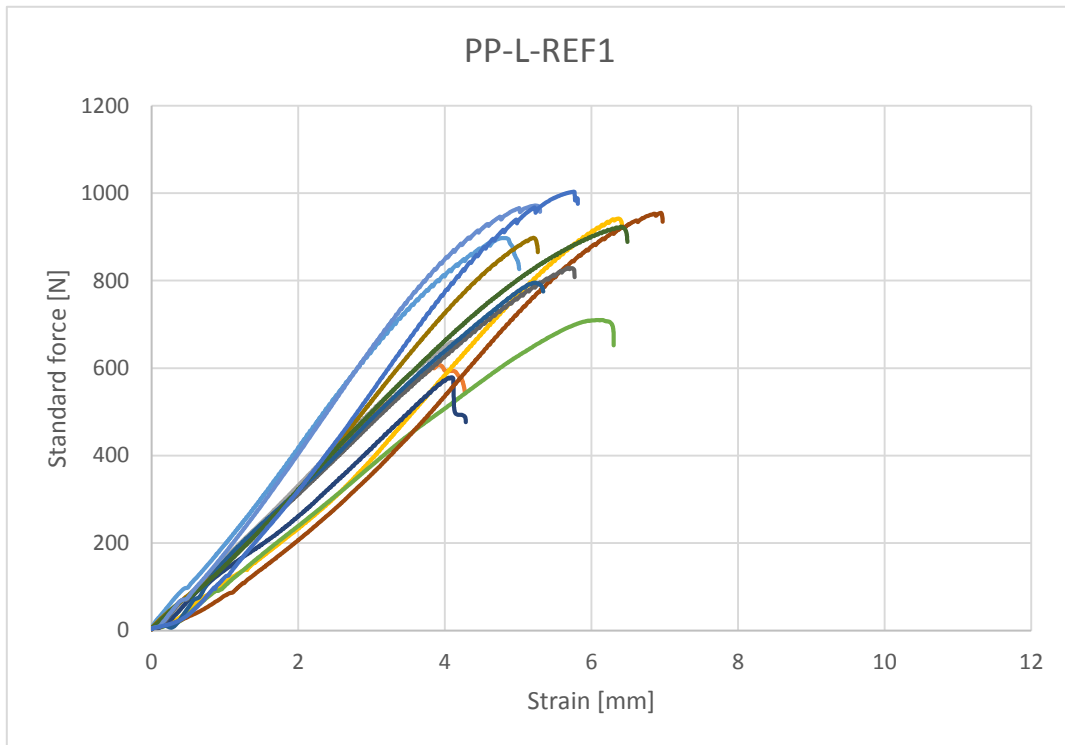


Figure 133: Raw result: PP, longitudinal tensile test, 1488 hours aged.

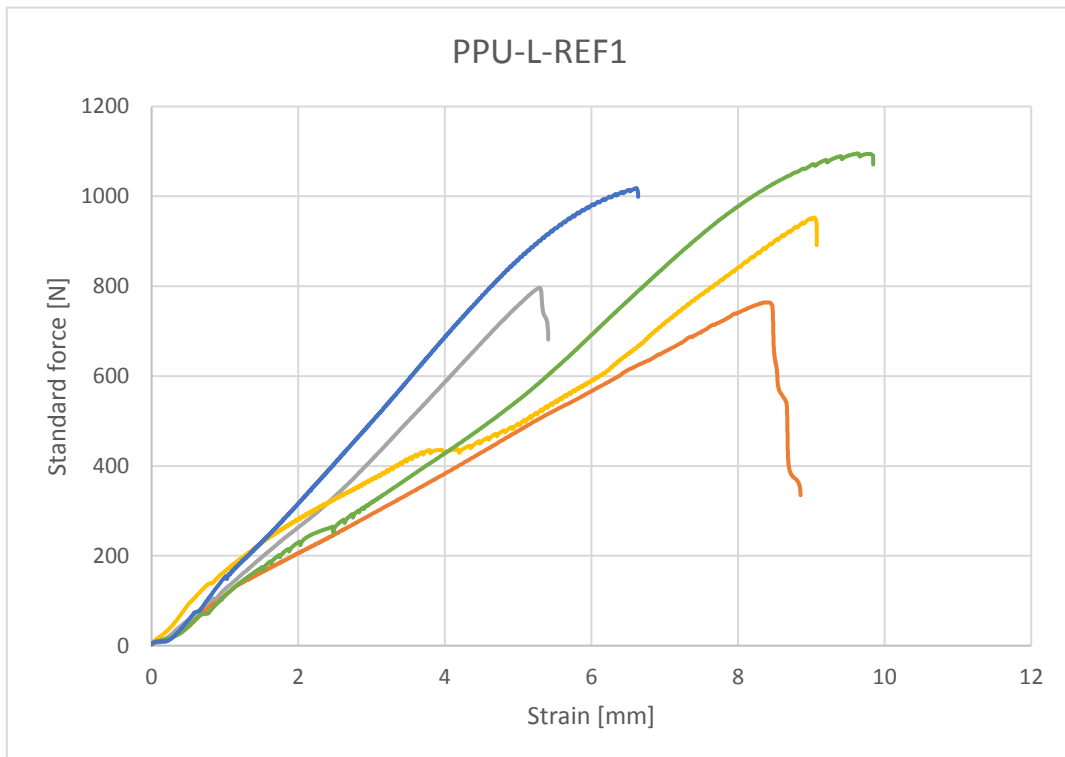


Figure 134: Raw result: PPU, longitudinal tensile test, 1488 hours aged.

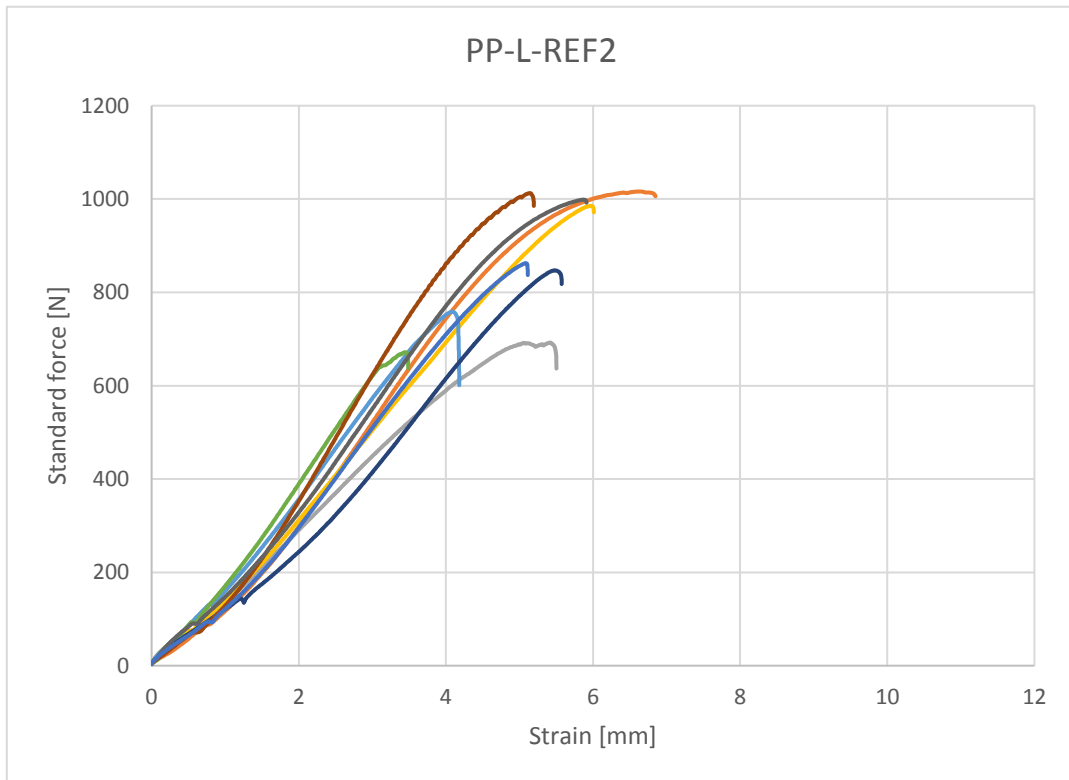


Figure 135: Raw result: PP, transverse tensile test, 2088 hours aged.

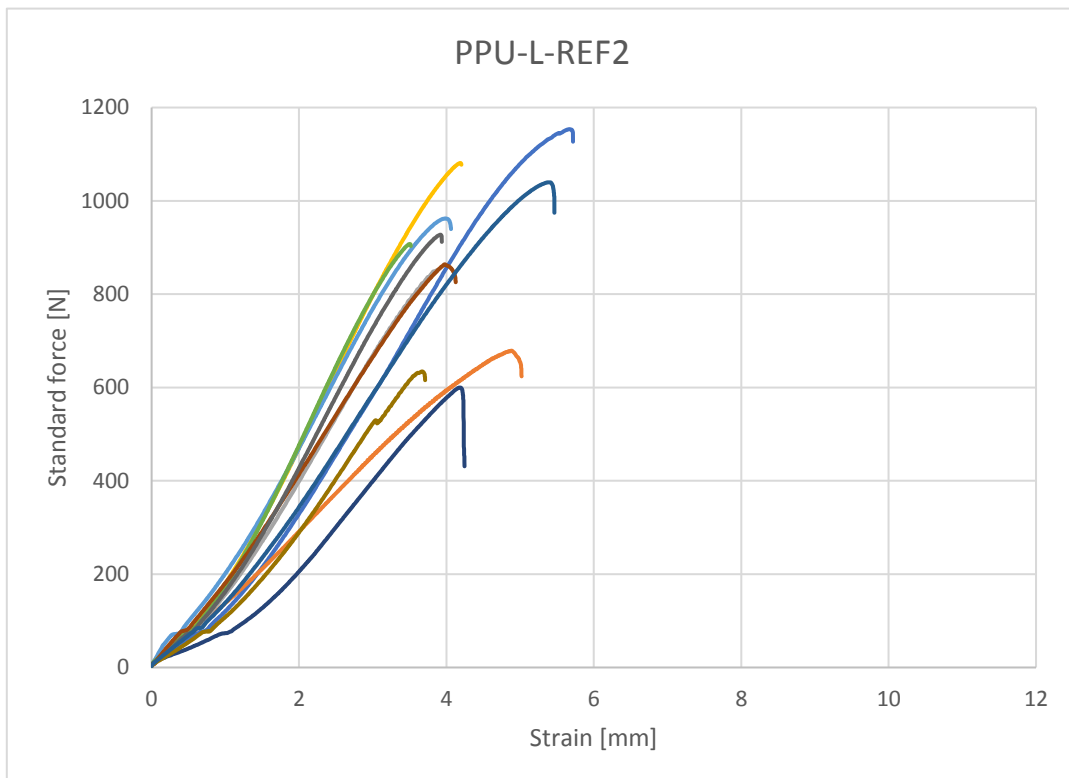


Figure 136: Raw result: PPU, longitudinal tensile test, 2088 hours aged.

Graphical results of the longitudinal tensile tests with the exposed specimens:

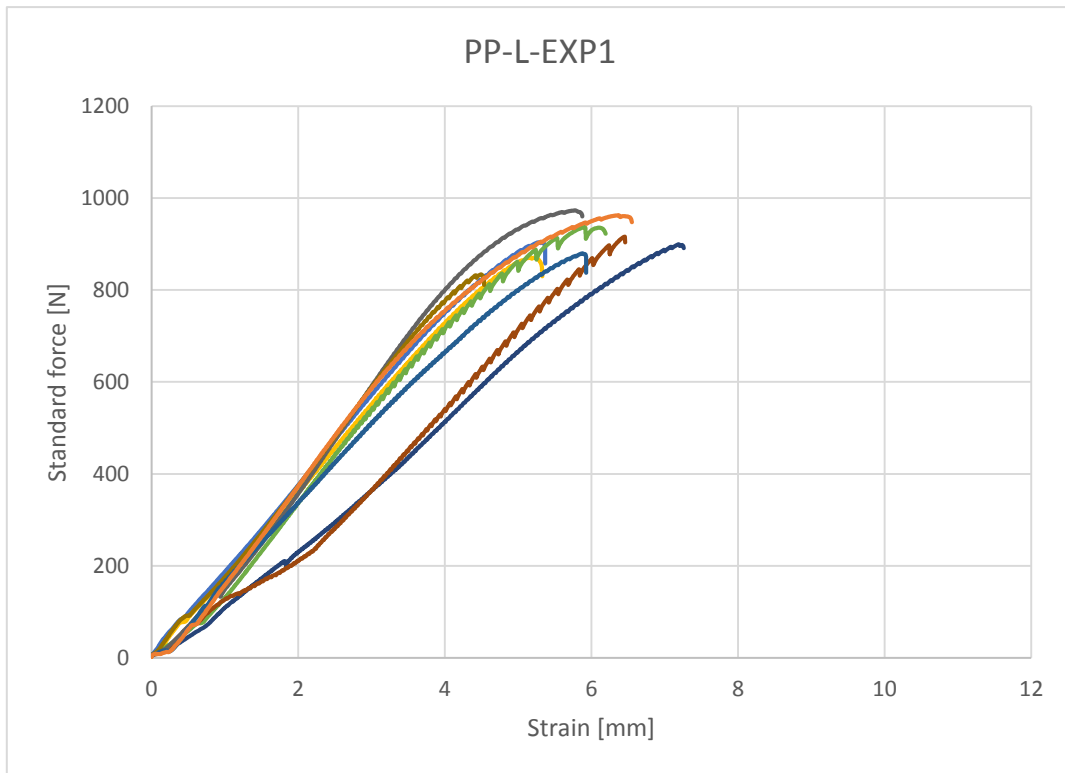


Figure 137: Raw result: PP, longitudinal tensile test, 336 hours aged.

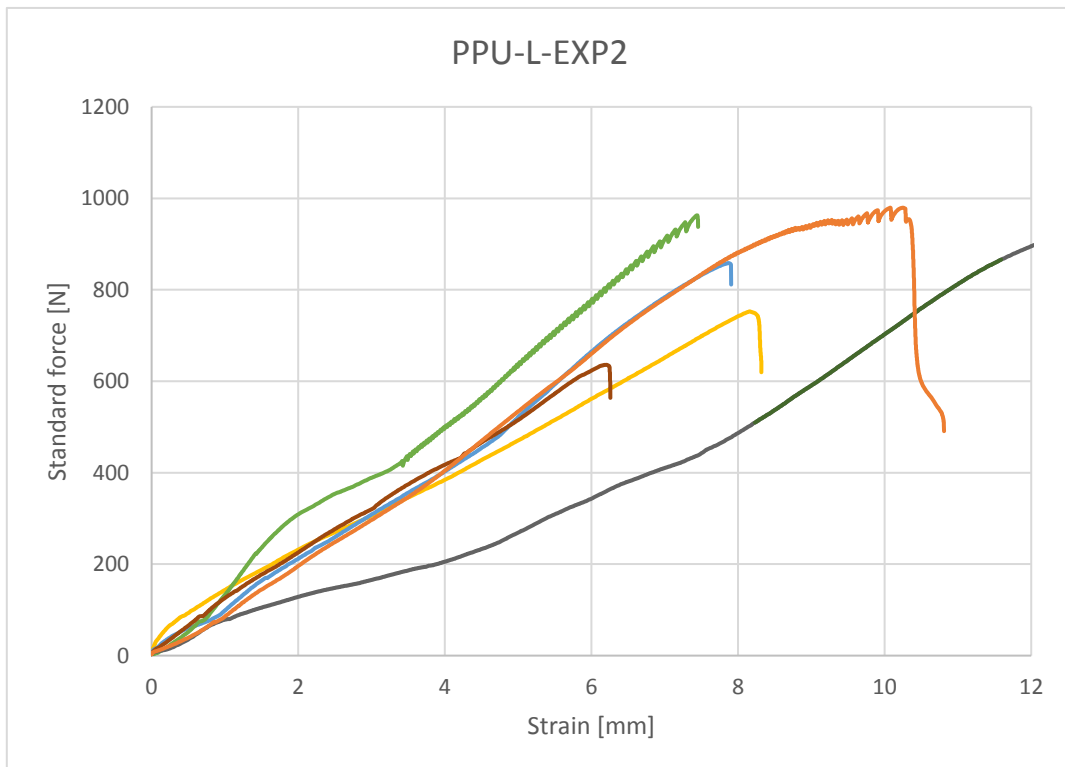


Figure 138: Raw result: PPU, longitudinal tensile test, 336 hours aged.

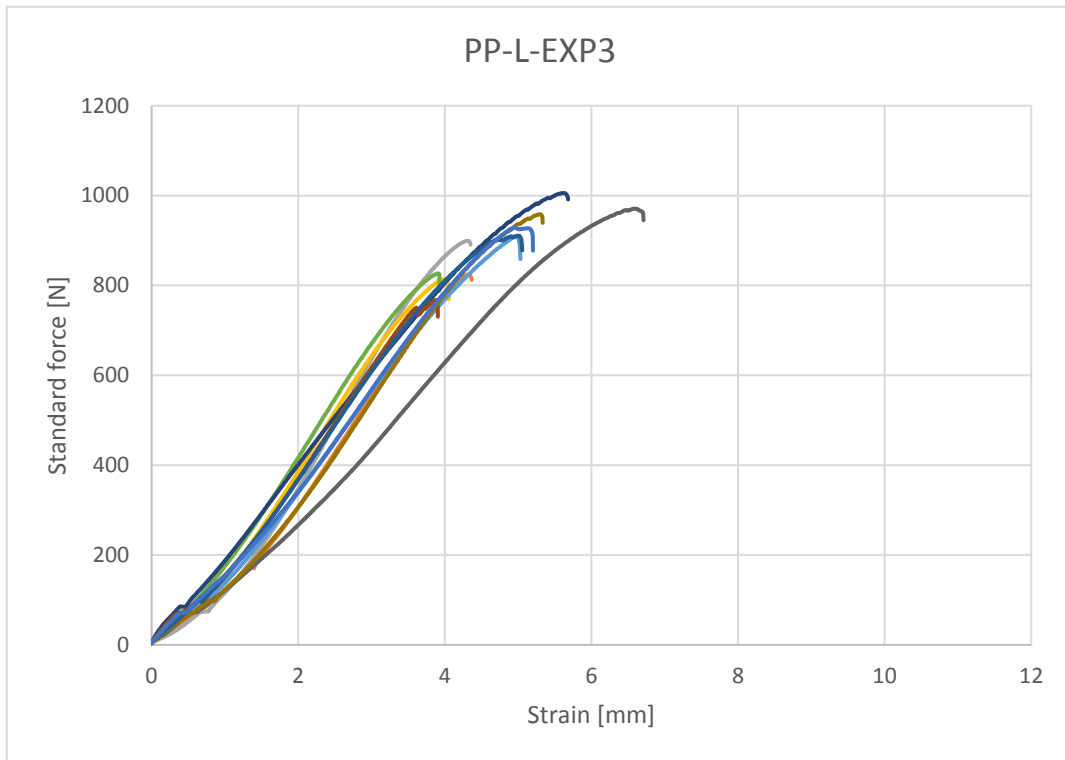


Figure 139: Raw result: PP, longitudinal tensile test, 936 hours aged.

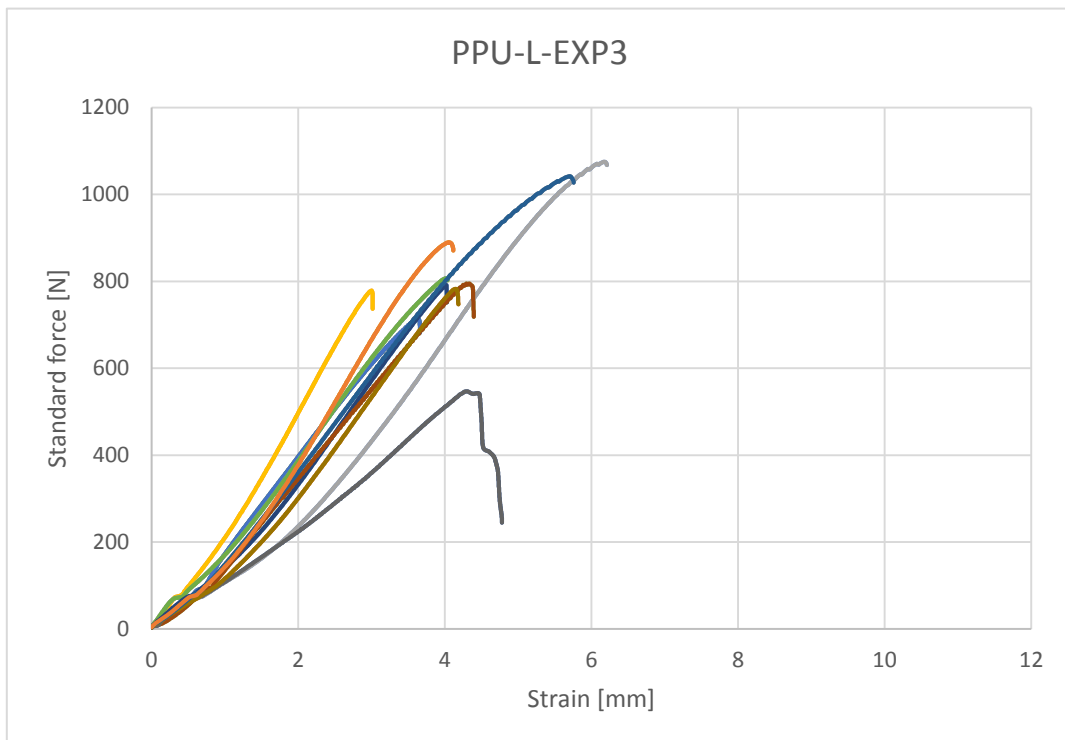


Figure 140: Raw result: PPU, longitudinal tensile test, 936 hours aged.

Graphical results of the tensile tests with the flat-die-extruded PP-based specimen:

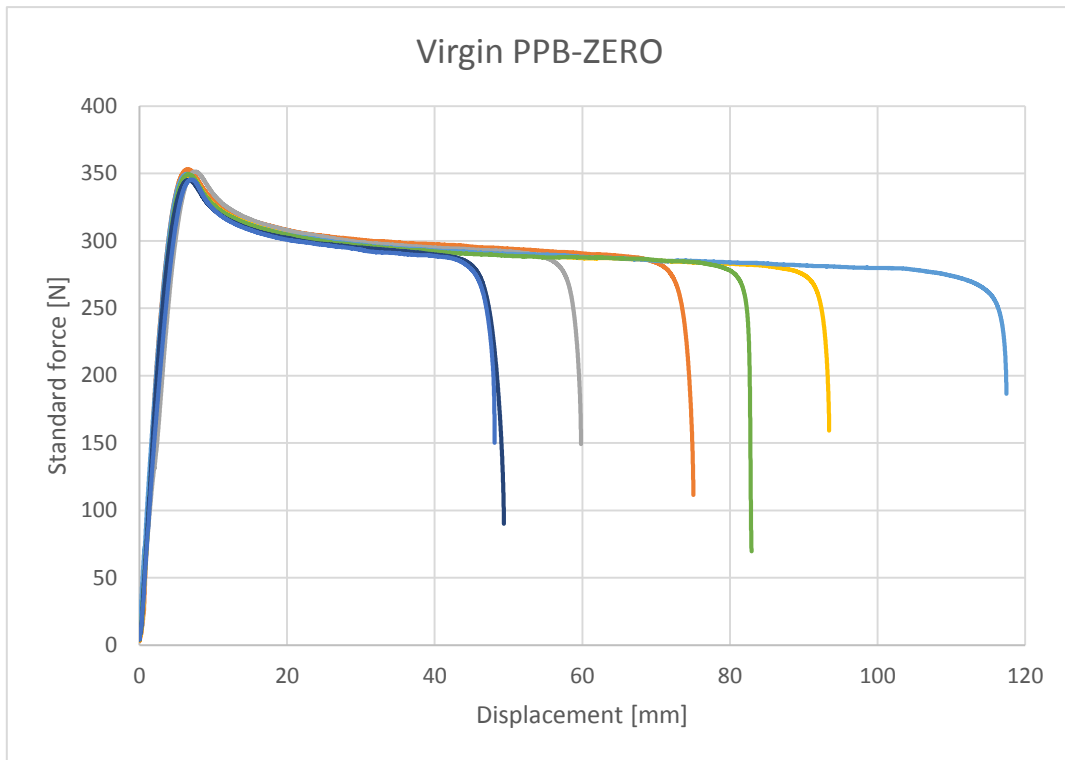


Figure 141: Raw result: PPB, tensile test, 0 hours aged.

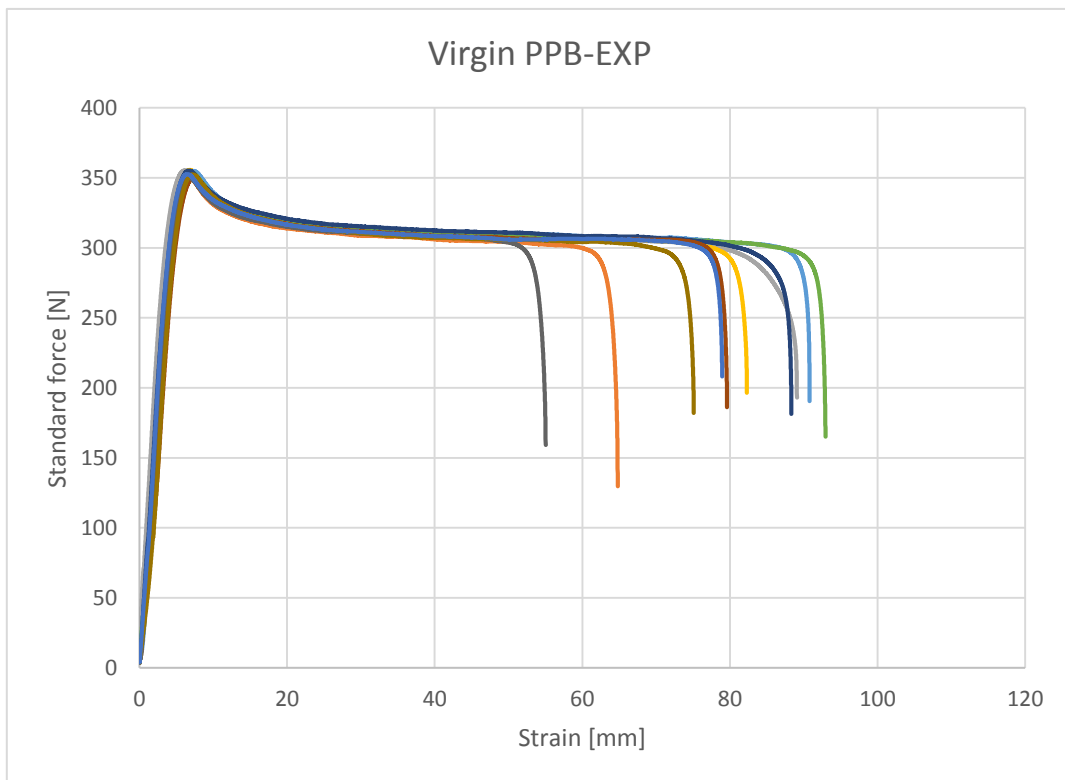


Figure 142: Raw result: PPB, tensile test, 336 hours exposed.

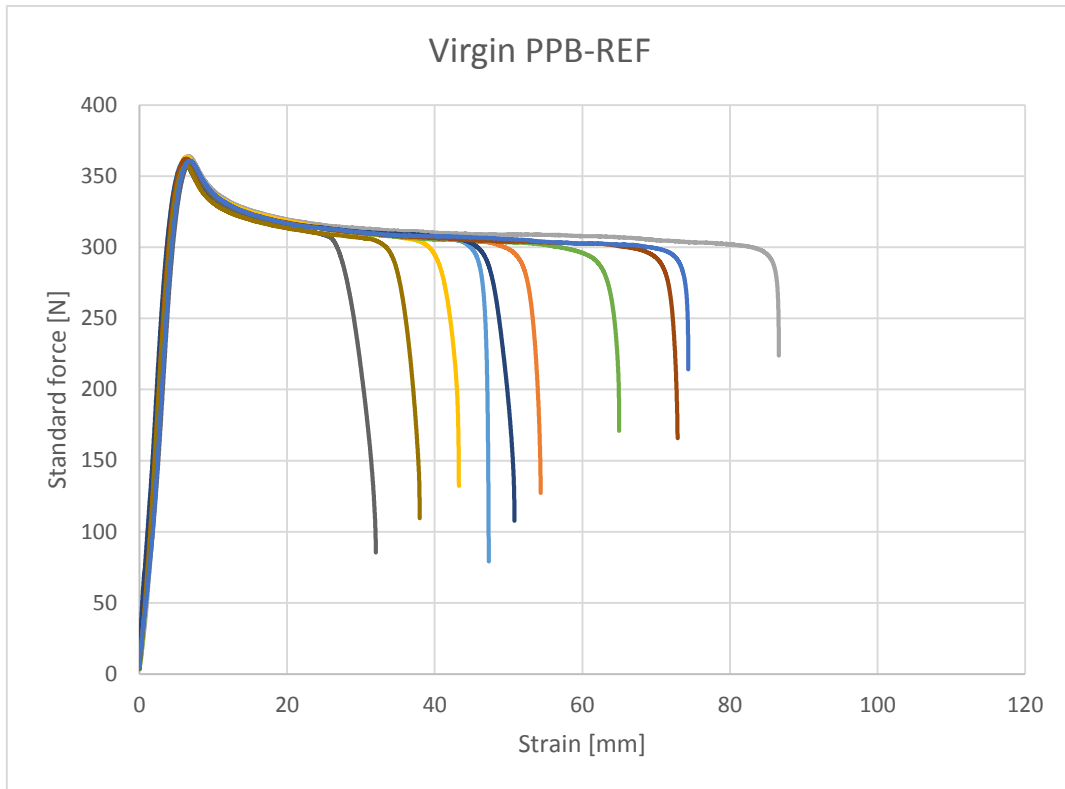


Figure 143: Raw result: PPB, tensile test, 336 hours aged.

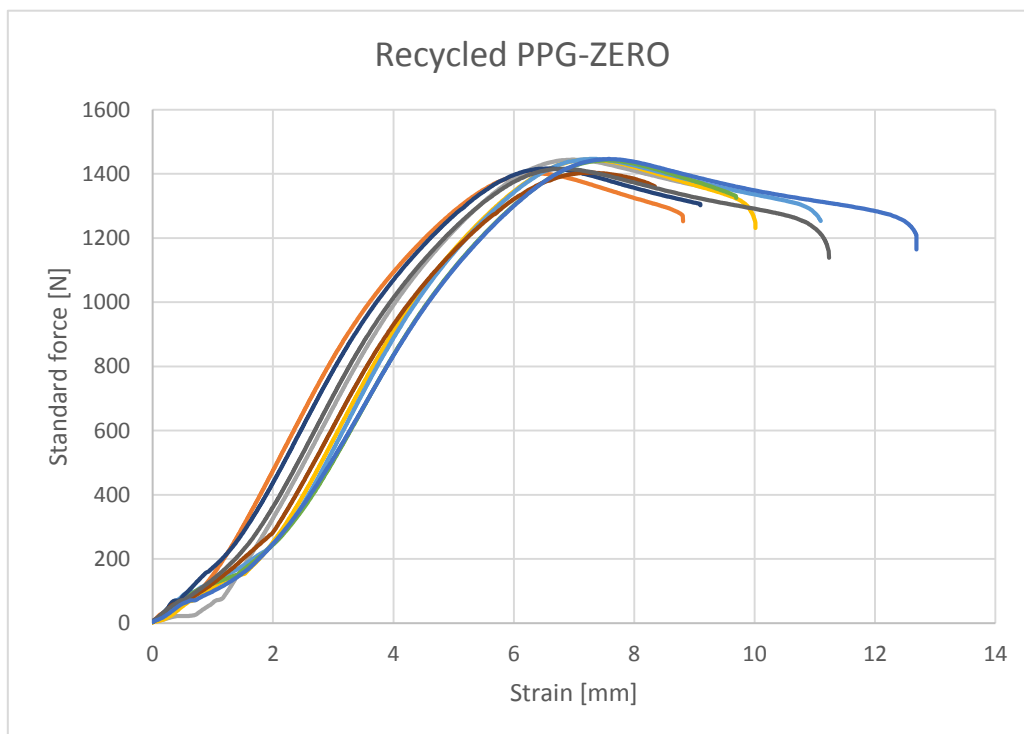


Figure 144: Raw result: PPG, tensile test, 0 hours aged.

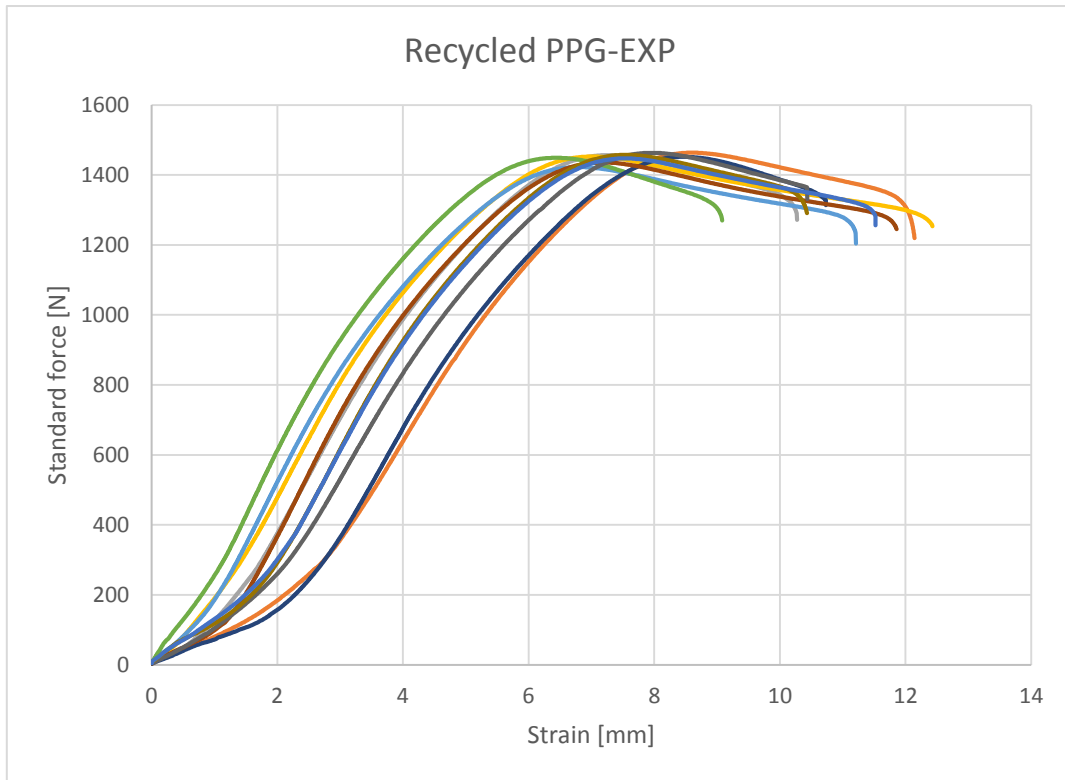


Figure 145: Raw result: PPG, tensile test, 336 hours exposed.

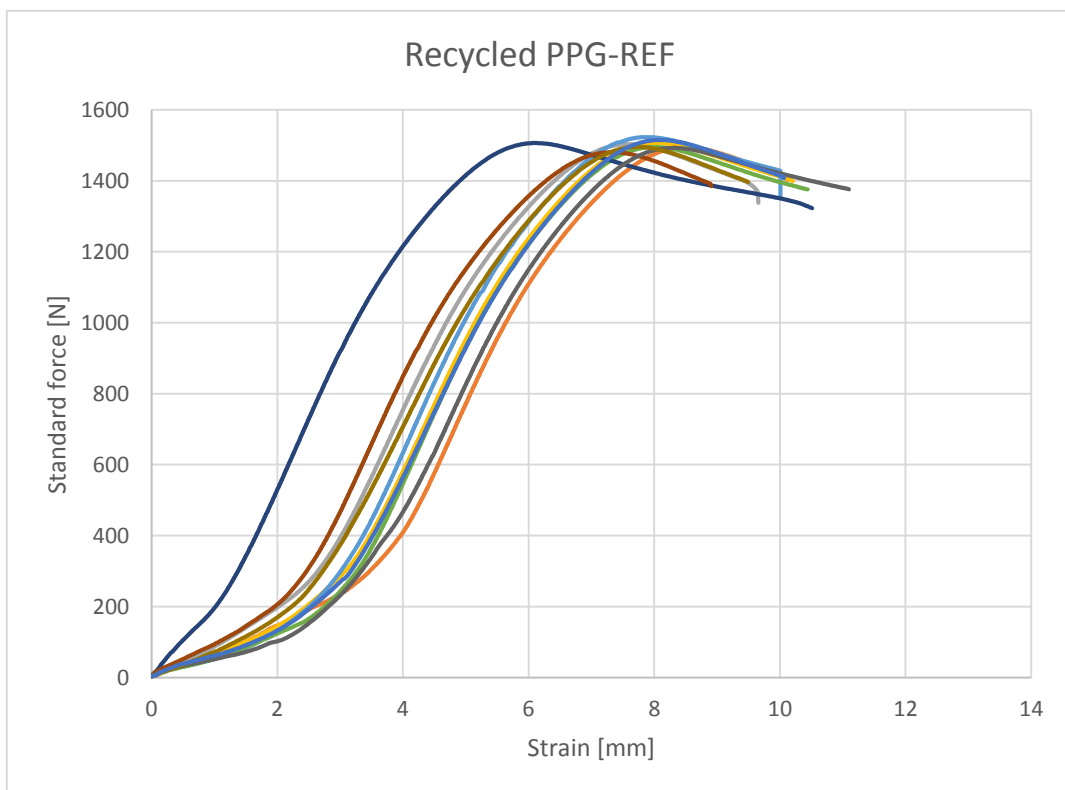


Figure 146: Raw result: PPG, tensile test, 336 hours aged.

Appendix G

Heat Transient Analysis

Tijd	TE	T0	T1	T2	T3	TI	VERSCHIL
05:00	16	13	8	6	3	16	10
05:30	16	12	9	6	3	16	8
06:00	14	12	9	6	3	14	9
06:30	14	12	9	6	3	14	9
07:00	15	13	9	6	3	15	10
07:30	15	13	10	6	3	15	10
08:00	17	16	9	6	4	17	13
08:30	17	15	11	6	4	17	11
09:00	19	24	11	7	5	19	20
09:30	19	21	15	8	5	19	16
10:00	21	30	14	9	6	21	25
10:30	21	27	18	10	6	21	21
11:00	22	35	19	12	7	22	28
11:30	22	32	22	13	7	22	25
12:00	23	38	22	14	8	23	30
12:30	23	36	25	15	8	23	28
13:00	24	39	25	16	9	24	30
13:30	24	38	27	17	9	24	29
14:00	24	38	28	18	10	24	28
14:30	24	38	28	19	10	24	28
15:00	24	34	28	19	10	24	24
15:30	24	35	27	19	10	24	25
16:00	22	28	27	19	10	22	18
16:30	22	31	24	19	10	22	21
17:00	21	21	25	17	9	21	12
17:30	21	25	21	17	9	21	16
18:00	20	19	21	15	9	20	10
18:30	20	21	18	15	9	20	12
19:00	20	18	18	14	8	20	9
19:30	20	19	16	13	8	20	11
20:00	20	17	16	12	8	20	9
20:30	20	17	15	12	8	20	10
21:00	19	15	15	12	8	19	8
21:30	19	16	14	11	7	19	9
22:00	18	14	14	11	7	18	7
22:30	18	15	13	11	7	18	8

Table 18: Summary: Point temperatures of the façade element over time, 1-June-2017, the Netherlands.

South		
Area	q_{sun}	Q_{Sun}
1	17	17
1	44	44
1	72	72
1	106	106
1	270	270
1	422	422
1	539	539
1	607	607
1	616	616
1	568	568
1	466	466
1	323	323
1	160	160
1	81	81
1	52	52
1	26	26

Table 19: Parameters: Solar radiation in the Netherlands, south direction.

Reference Bibliography

Reference

- A, Wal van der, J J. Mulder, and R J. Gaymans. 1998. *Fracture of Polypropylene: 2. The Effect of Crystallinity*. Vol. 39. [https://doi.org/10.1016/S0032-3861\(97\)10279-8](https://doi.org/10.1016/S0032-3861(97)10279-8).
- Aboulkas, A., K. El harfi, and A. El Bouadili. 2010. 'Thermal Degradation Behaviors of Polyethylene and Polypropylene. Part I: Pyrolysis Kinetics and Mechanisms'. *Energy Conversion and Management* 51 (7): 1363–69. <https://doi.org/10.1016/j.enconman.2009.12.017>.
- Agarwal, Sushant, and Rakesh K. Gupta. 2017. '29 - Plastics in Buildings and Construction'. In *Applied Plastics Engineering Handbook (Second Edition)*, edited by Myer Kutz, 635–49. William Andrew Publishing. <https://doi.org/10.1016/B978-0-323-39040-8.00030-4>.
- ASTM International. 2014. 'ASTM D638-14, Standard Test Method for Tensile Properties of Plastics'. West Conshohocken, PA.
- Azom. 2001. 'E-Glass Fibre'. AZoM.Com. 2001. <https://www.azom.com/article.aspx?ArticleID=764>.
- Azuma, Y., H. Takeda, S. Watanabe, and H. Nakatani. 2009. 'Outdoor and Accelerated Weathering Tests for Polypropylene and Polypropylene/Talc Composites: A Comparative Study of Their Weathering Behavior'. *Polymer Degradation and Stability* 94 (12): 2267–74. <https://doi.org/10.1016/j.polymdegradstab.2009.08.008>.
- Azwa, Z.N., B Yousif, Allan Manalo, and Warna Karunasena. 2013. *A Review on the Degradability of Polymeric Composites Base on Natural Fibres*. Vol. 47. <https://doi.org/10.1016/j.matdes.2012.11.025>.
- Baran, Pawel. 2017. 'Methodology and Tools for Testing, Numerical Analysis and Design of the 3D Printed Moulds'. Utrecht: Delft University of Technology.
- Barbes, Lucica, Cristiana Radulescu, and Claudia Stihl. 2014. *ATR - FTIR Spectrometry Characterisation of Polymeric Materials*. Vol. 66.
- Bogue, Robert. 2013. '3D Printing: The Dawn of a New Era in Manufacturing?' *Assembly Automation* 33 (4): 307–11. <https://doi.org/10.1108/AA-06-2013-055>.
- Boubakri, A., N. Haddar, K. Elleuch, and Y. Bienvenu. 2011. 'Influence of Thermal Aging on Tensile and Creep Behavior of Thermoplastic Polyurethane'. *Comptes Rendus Mécanique* 339 (10): 666–73. <https://doi.org/10.1016/j.crme.2011.07.003>.
- Brookes, Alan J., and Maarten. Meijs. 2008. *Cladding of Buildings*. 4th ed. 1 online resource (221 pages) vols. Hoboken: Taylor & Francis,. Ebook Library <http://public.eblib.com/choice/publicfullrecord.aspx?p=342946>.
- Bryce, Douglas M. 1996. *Plastic Injection Molding: Manufacturing Process Fundamentals*. Fundamentals of Injection Molding Series, v. 1. Dearborn, Mich: Society of Manufacturing Engineers.
- Carneiro, O.S., A.F. Silva, and R. Gomes. 2015. 'Fused Deposition Modeling with Polypropylene'. *Materials & Design* 83 (October): 768–76. <https://doi.org/10.1016/j.matdes.2015.06.053>.

Chew. 1998. *Building Facades: A Guide To Common Defects In Tropical Climates*. https://books.google.com/books/about/Building_Facades_A_Guide_To_Common_Defec.html?id=kZnVCgAAQBAJ.

Crewdson, Michael. 2008. *Outdoor Weathering Must Verify Accelerated Testing*. Vol. 91.

Dawoud, Michael, Iman Taha, and Samy J. Ebeid. 2016. 'Mechanical Behaviour of ABS: An Experimental Study Using FDM and Injection Moulding Techniques'. *Journal of Manufacturing Processes* 21 (January): 39–45. <https://doi.org/10.1016/j.jmapro.2015.11.002>.

Dechun, Z. 2013. '4 - Chemical and Photophysical Properties of Materials for OLEDs'. In *Organic Light-Emitting Diodes (OLEDs)*, edited by Alastair Buckley, 114–42. Woodhead Publishing. <https://doi.org/10.1533/9780857098948.1.114>.

Dunn, Peter. 2009. 'MIT School of Engineering | » Why Do Plastics Get Brittle When They Get Cold?' *Mit Engineering* (blog). 2009. <https://engineering.mit.edu/engage/ask-an-engineer/why-do-plastics-get-brittle-when-they-get-cold/>.

Eftekhari, Mohammadreza, and Ali Fatemi. 2016. *Tensile Behavior of Thermoplastic Composites Including Temperature, Moisture, and Hygrothermal Effects*. Vol. 51. <https://doi.org/10.1016/j.polymertesting.2016.03.011>.

Ehrenstein, Gottfried W., and R. P. Theriault. 2001. *Polymeric Materials: Structure, Properties, Applications*. Munich : Cincinnati, OH: Hanser ; Hanser Gardner Publications.

Fechine, G.J.M., and N.R. Demarquette. 2008. 'Cracking Formation on the Surface of Extruded Photodegraded Polypropylene Plates'. *Polymer Engineering & Science* 48 (2): 365–72. <https://doi.org/10.1002/pen.20958>.

Gerhardt, H.J., and F. Janser. 1994. 'Wind Loads on Wind Permeable Facades'. *Journal of Wind Engineering and Industrial Aerodynamics* 53 (1): 37–48. [https://doi.org/10.1016/0167-6105\(94\)90017-5](https://doi.org/10.1016/0167-6105(94)90017-5).

Geurts, C P W. 2004. 'Towards a Reliable Design of Facade and Roof Elements against Wind Loading', 17.

Giannoulis, Anastasios, Ted Stathopoulos, D Briassoulis, and Antonis Mistriotis. 2012. *Wind Loading on Vertical Panels with Different Permeabilities*. Vol. s 107–108. <https://doi.org/10.1016/j.jweia.2012.02.014>.

Gijsman, Pieter, Guido Meijers, and Giacomo Vitarelli. 1999. 'Comparison of the UV-Degradation Chemistry of Polypropylene, Polyethylene, Polyamide 6 and Polybutylene Terephthalate'. *Polymer Degradation and Stability* 65 (3): 433–41. [https://doi.org/10.1016/S0141-3910\(99\)00033-6](https://doi.org/10.1016/S0141-3910(99)00033-6).

Gránásy, László, Tamás Pusztai, and J Douglas. 2013. *Insights into Polymer Crystallization from Phase-Field Theory*. https://doi.org/10.1007/978-3-642-37179-0_30-1.

Griffiths, Peter R., and James A. De Haseth. 2007. *Fourier Transform Infrared Spectrometry*. 2nd ed. Chemical Analysis, v. 171. Hoboken, N.J: Wiley-Interscience.

Hager, Izabela, Anna Golonka, and Roman Putanowicz. 2016. '3D Printing of Buildings and Building Components as the Future of Sustainable Construction?' *Ecology and New Building Materials and Products* 2016 151 (January): 292–99. <https://doi.org/10.1016/j.proeng.2016.07.357>.

- Horrocks, A.R, J Mwila, M Mirafteb, M Liu, and S.S Chohan. 1999. 'The Influence of Carbon Black on Properties of Orientated Polypropylene 2. Thermal and Photodegradation'. *Polymer Degradation and Stability* 65 (1): 25–36. [https://doi.org/10.1016/S0141-3910\(98\)00213-4](https://doi.org/10.1016/S0141-3910(98)00213-4).
- Iring, M., S. László-Hedvig, K. Barabás, T. Kelen, and F. Tüdős. 1978. 'Study of the Thermal Oxidation of Polyolefines—IX: Some Differences in the Oxidation of Polyethylene and Polypropylene'. *European Polymer Journal* 14 (6): 439–42. [https://doi.org/10.1016/0014-3057\(78\)90065-4](https://doi.org/10.1016/0014-3057(78)90065-4).
- Jafari, S. H., and A. K. Gupta. 2000. 'Impact Strength and Dynamic Mechanical Properties Correlation in Elastomer-modified Polypropylene'. *Journal of Applied Polymer Science* 78 (5): 962–71. [https://doi.org/10.1002/1097-4628\(20001031\)78:5<962::AID-APP40>3.0.CO;2-5](https://doi.org/10.1002/1097-4628(20001031)78:5<962::AID-APP40>3.0.CO;2-5).
- Janevski, A., G. Bogoeva-Gaceva, and E. Mäder. 1999. 'DSC Analysis of Crystallization and Melting Behavior of Polypropylene in Model Composites with Glass and Poly(Ethylene Terephthalate) Fibers'. *Journal of Applied Polymer Science* 74 (2): 239–46. [https://doi.org/10.1002/\(SICI\)1097-4628\(19991010\)74:2<239::AID-APP1>3.0.CO;2-8](https://doi.org/10.1002/(SICI)1097-4628(19991010)74:2<239::AID-APP1>3.0.CO;2-8).
- Kamrannejad, Mohammad Mehdi, Amin Hasanzadeh, Nasim Nosoudi, Lee Mai, and Ali Akbar Babaluo. 2014. 'Photocatalytic Degradation of Polypropylene/TiO₂ Nano-Composites'. *Materials Research* 17 (4): 1039–46. <https://doi.org/10.1590/1516-1439.267214>.
- Kasperzyk, Cuong, Min-Koo Kim, and Ioannis Brilakis. 2017. 'Automated Re-Prefabrication System for Buildings Using Robotics'. *Automation in Construction* 83 (November): 184–95. <https://doi.org/10.1016/j.autcon.2017.08.002>.
- Kemper, Frank, and Markus Feldmann. 2012. 'Wind Loads for Permeable Cladding Elements with High Porosity', *Advances in Civil, Environmental, and Materials Research (ACEM' 12)*, , 12.
- KNMI. 2018. 'KNMI - Zomer 2018 (Juni, Juli, Augustus)'. [Www.knmi.nl](http://www.knmi.nl). 2018. <https://www.knmi.nl/nederland-nu/klimatologie/maand-en-seizoensoverzichten/2018/zomer>.
- Krassenstein, Eddie. 2015. 'Lab3d Prints The Side of a Prototype Building, Including Insulation, Piping, Window Frames & More'. *3DPrint.Com | The Voice of 3D Printing / Additive Manufacturing* (blog). 2 July 2015. <https://3dprint.com/78285/lab3d-parallel-printing/>.
- Lederle, Felix, Frederick Meyer, Gabriella-Paula Brunotte, Christian Kaldun, and Eike G. Hübner. 2016. 'Improved Mechanical Properties of 3D-Printed Parts by Fused Deposition Modeling Processed under the Exclusion of Oxygen'. *Progress in Additive Manufacturing* 1 (1): 3–7. <https://doi.org/10.1007/s40964-016-0010-y>.
- Lu, T.J., and N.A. Fleck. 1998. 'The Thermal Shock Resistance of Solids'. *Acta Materialia* 46 (13): 4755–68. [https://doi.org/10.1016/S1359-6454\(98\)00127-X](https://doi.org/10.1016/S1359-6454(98)00127-X).
- Nadal, Adolfo, Hugo Cifre, Juan Pavón, and Óscar Liébana. 2017. 'Material Use Optimization in 3D Printing through a Physical Simulation Algorithm'. *Automation in Construction* 78 (June): 24–33. <https://doi.org/10.1016/j.autcon.2017.01.017>.
- Nederlands Normalisatie-Insituut. 1997. NEN-EN-ISO 527-4:1997 (en). *Plastics - Determination of tensile properties - Part 4: Test conditions for isotropic and orthotropic fibrereinforced plastic composites*. Delft.
- Nederlands Normalisatie-insituut. 2011. 'Eurocode 1: Actions on Structures - Part 1-5: General Actions - Thermal Actions'. Delft.

Nederlands Normalisatie-Instituut. 2011. Eurocode 1: Belastingen op constructies - Deel 1-4: Algemene belastingen - Windbelasting. Delft.

O'Donnell, B., and J.R. White. 1994. 'Stress-Accelerated Photo-Oxidation of Polypropylene and Glass-Fibre-Reinforced Polypropylene'. *Polymer Degradation and Stability* 44 (2): 211–22. [https://doi.org/10.1016/0141-3910\(94\)90166-X](https://doi.org/10.1016/0141-3910(94)90166-X).

Oliani, Washington L, and Duclerc F Parra. 2009. 'Photooxidation Behaviour of HMS-PP', 10.

Petch, Michael. 2017. 'Aectual 3D Printing a Floor for Amsterdam's Schiphol Airport'. 3D Printing Industry. 2017. <https://3dprintingindustry.com/news/aectual-3d-printing-floor-amsterdams-schiphol-airport-123112/>.

Rabinovitch Elvira B., Quisenberry Joseph G., and Summers James W. 2004. 'Predicting Heat Buildup Due to the Sun's Energy'. *Journal of Vinyl Technology* 5 (3): 110–15. <https://doi.org/10.1002/vnl.730050308>.

Reisi Nafchi, Hajar, Majid Abdouss, Saeed Kazemi, Rahim Mohebbi Gargari, and Majid Mazhar. 2015. Effects of Nano-Clay Particles and Oxidized Polypropylene Polymers on Improvement of the Thermal Properties of Wood Plastic Composite. Vol. 17.

Sahin, Senol, and Pasa Yayla. 2005. 'Effects of Testing Parameters on the Mechanical Properties of Polypropylene Random Copolymer'. *Polymer Testing* 24 (5): 613–19. <https://doi.org/10.1016/j.polymertesting.2005.03.002>.

Sarakinioti, Maria Valentini, Michela Turrin, M Teeling, Paul de Ruiter, Mark van Erk, Martin Tenpierik, Thaleia Konstantinou, et al. 2017. 'Spong3d: 3D Printed Facade System Enabling Movable Fluid Heat Storage'. *SPOOL; Vol 4 No 2: Energy Innovation #4*. <https://doi.org/10.7480/spool.2017.2.1929>.

Sawyer, Linda C., David T. Grubb, and Gregory Frederick Meyers. 2008. *Polymer Microscopy*. 3rd ed. New York: Springer.

Schawe, J, R Riesen, J Widmann, M Schubnell, and U Jördimann. 2000. 'Interpreting DSC Curves Part 1: Dynamic Measurements'. http://www.masontechnology.ie/x/Usercom_11.pdf.

Schoolenberg, G.E., and P. Vink. 1991. 'Ultra-Violet Degradation of Polypropylene: 1. Degradation Profile and Thickness of the Embrittled Surface Layer'. *Polymer* 32 (3): 432–37. [https://doi.org/10.1016/0032-3861\(91\)90446-P](https://doi.org/10.1016/0032-3861(91)90446-P).

Scott, Clare. 2017. '3D Printed Translucent Building Façades Let the Light In'. *3DPrint.Com | The Voice of 3D Printing / Additive Manufacturing* (blog). 11 September 2017. <https://3dprint.com/187220/3d-printed-building-facades/>.

Shibryaeva, Lyudmila. 2012. 'Thermal Oxidation of Polypropylene and Modified Polypropylene – Structure Effects', 26.

Spoerk, Martin, Chethan Savandaiah, Florian Arbeiter, Stephan Schuschnigg, and Clemens Holzer. 2017. *Properties of Glass-Filled Polypropylene for Fused Filament Fabrication*.

T. H. Shubhra, Quazi, A K M M H Alam, Mubarak A Beg, Mubarak Khan, and Md Gafur. 2011. Reinforced Polypropylene Composites Mechanical and Degradation Characteristics of Natural Silk and Synthetic Phosphate Glass Fiber. Vol. 45. <https://doi.org/10.1177/0021998310380290>.

- Tidjani, Adams. 1998. 'Photooxidation of Polypropylene under Natural and Accelerated Weathering Conditions'. *Journal of Applied Polymer Science* 64 (13): 2497–2503. [https://doi.org/10.1002/\(SICI\)1097-4628\(19970627\)64:13<2497::AID-APP3>3.0.CO;2-8](https://doi.org/10.1002/(SICI)1097-4628(19970627)64:13<2497::AID-APP3>3.0.CO;2-8).
- Tong, Li, and J.R. White. 1996. 'Photo-Oxidation of Thermoplastics in Bending and in Uniaxial Compression'. *Polymer Degradation and Stability* 53 (3): 381–96. [https://doi.org/10.1016/0141-3910\(96\)00095-X](https://doi.org/10.1016/0141-3910(96)00095-X).
- Tumbuan, E.H., and J.J.M. Cauberg. 2005. *Zonbestraling En Atmosferische Bestraling*. Kennisbank Bouwfysica. Delft.
- Van der Veen, Arnaud. 2014. 'The Structural Feasibility of 3D-Printing Houses Using Printable Polymers'. Utrecht: Delft University of Technology.
- Van Leeuwen, Geert. 2018. 'Grenfell Tower: "How the (bleep) is this possible!?" (deel 1)'. Brandveilig. 25 July 2018. <https://www.brandveilig.com/nieuws/grenfell-tower-how-the-bleep-is-this-possible-deel-1-53866>.
- Wang, Jiayi. 2018. 'Optimisation Methodology of Large-Scale 3D Printing Using Recycled Plastics'. Utrecht: Delft University of Technology.
- Wojtyła, Szymon, Piotr Klama, and Tomasz Baran. 2017. 'Is 3D Printing Safe? Analysis of the Thermal Treatment of Thermoplastics: ABS, PLA, PET, and Nylon'. *Journal of Occupational and Environmental Hygiene* 14 (6): D80–85. <https://doi.org/10.1080/15459624.2017.1285489>.
- Wu, Peng, Jun Wang, and Xiangyu Wang. 2016. 'A Critical Review of the Use of 3-D Printing in the Construction Industry'. *Automation in Construction* 68 (August): 21–31. <https://doi.org/10.1016/j.autcon.2016.04.005>.
- Wu, Wenzheng, Peng Geng, Guiwei Li, Di Zhao, Haibo Zhang, and Ji Zhao. 2015. 'Influence of Layer Thickness and Raster Angle on the Mechanical Properties of 3D-Printed PEEK and a Comparative Mechanical Study between PEEK and ABS'. Edited by Reza Montazami. *Materials* 8 (9): 5834–46. <https://doi.org/10.3390/ma8095271>.
- Wypych, G. 1999. 'Basic Parameters in Weathering Studies'. In *Weathering of Plastics - Testing to Mirror Real Life Performance*. William Andrew Publishing/Plastics Design Library. <https://app.knovel.com/hotlink/pdf/id:kt0017ZWG1/weathering-plastics-testing/basic-parameters-in-weathering>.
- Zeus. 2005. 'Thermal Degradation of Plastics'. http://www.appstate.edu/~clementsjs/polymerproperties/zeus_thermal_degradation.pdf.
- Zhang, S., and R. Horrocks. 2003. 'Substantive Intumescent Flame Retardants for Functional Fibrous Polymers'. *Journal of Materials Science* 38 (10): 2195–98. <https://doi.org/10.1023/A:1023784232290>.

List of Figures

Figure 1: 3D printed house by DUS (left), the 'KamerMaker' (right) (Petch 2017).	16
Figure 2: Exposed 3D printed object by DUS Architects (left), close-up (right).	17
Figure 3: Research method.	20
Figure 4: Aectual façade: mock-up (left), close-up (right).	24
Figure 5: Aectual façade: the consistent and operational pattern.	24
Figure 6: Spon3D-project: mock-up (Sarakinoti et al., 2017).	25
Figure 7: Fluid Morphology project (Scott, 2017).	25
Figure 8: Lab3D: façade part (left), detail (right) (Krassenstein, 2015).	26
Figure 9: Printing coordinates of the KamerMaker II (Baran 2017).	27
Figure 10: Molecule structures of thermoplastics (Packham 1994).	28
Figure 11: The wind pressure coefficients w.r.t mesh's porosity (Giannoulis et al., 2012).	31
Figure 12: Assumption: The wind pressure w.r.t mesh's porosity, thickness: 1 mm.	32
Figure 13: Assumption: The wind pressure w.r.t mesh's porosity, thickness: 1 - 70 mm.	32
Figure 14: Representation: the Aectual façade with 600 mm gap distance.	33
Figure 15: Pressure equalization in the gap width (Gerhardt & Janser, 1994).	33
Figure 16: Sketch: Thermal expansion and bowing of the façade panels.	35
Figure 17: Temperature propagation of the Aectual façade: rain cladding.	38
Figure 18: Temperature propagation of the Aectual façade: second skin.	38
Figure 19: Thermal shock resistance test specimens.	39
Figure 20: Aectual façade panel during a fire resistance test.	40
Figure 21: Uniform heating of a simply supported beam (Usmani et al., 2001).	42
Figure 22: Axially restrained beam subjected to uniform heating (Usmani et al., 2001).	42
Figure 23: Buckling of an axially restrained beam subjected to uniform heating (Usmani et al., 2001).	43
Figure 24: Buckling of an axially restrained beam subjected to uniform heating (Usmani et al., 2001).	44
Figure 25: Simply supported beam subjected to non-uniform heating (Usmani et al., 2001).	45
Figure 26: Laterally restrained beam subjected to non-uniform heating (Usmani et al., 2001).	46
Figure 27: Beam with finite rotational restraint with non-uniform heating (Usmani et al., 2001).	46
Figure 28: Degradation reaction of PP by UV radiation in presence of oxygen (left) Loss of tensile strength of both composites due to simulating weathering (right) (T. H. Shubhra et al. 2011).	54
Figure 29: Installation of Aectual façade (Amsterdam Sloterdijk, April 2018).	56
Figure 30: Aectual façade; after 3 months of natural weathering (DUS Architect, September 2018).	56
Figure 31: Raw material: PP-pellets (black) with 1% UV stabilisers (white).	61
Figure 32: Print directions and their effect of UV degradation on the tensile specimen.	63
Figure 33: Sample division within a printed plate (exposed (X) and reference (R)).	63

Figure 34: Difference in print qualities between samples (left; high quality, upper sample; low quality, lower sample), Charpy impact samples (right).	64
Figure 35: Printed batch with the material PP.	65
Figure 36: Specimen geometry for the tensile test.	66
Figure 37: Ultraviolet test chamber (right) and Ultra-Vitalux lamp (left).	66
Figure 38: Spectral Radiation Power distribution of Ultra-Vitalux.	67
Figure 39: Test setup of the tensile strength test.	68
Figure 40: Test setup of the Charpy impact strength test: Device (left), sample dimensions (right).	68
Figure 41: Tensile strength properties designations (ASTM International 2014).	71
Figure 42: Material with a Hookean region (left) and no Hookean region (right) (ASTM International 2014).	72
Figure 43: Results: influence of (un)exposure time on yield stress (transverse).	73
Figure 44: Results: influence of (un)exposure time on stiffness (transverse, Hookean region).	73
Figure 45: Results: influence of (un)exposure time on yield strain (transverse).	73
Figure 46: Results: influence of ageing time on yield stress (transverse).	74
Figure 47: Results: influence of ageing time on stiffness (transverse, Hookean region).	74
Figure 48: Results: influence of ageing time on yield strain (transverse).	74
Figure 49: Result: a brittle break between the layers (left), transverse tensile test (right).	76
Figure 50: Degraded (upper) and unexposed (lower) tensile transverse sample (840 UV exposure hours).	76
Figure 51: Interior of the UV test chamber.	76
Figure 52: Results: influence of (un)exposure time on yield stress (longitudinal).	77
Figure 53: Results: influence of (un)exposure time on stiffness (longitudinal, Hookean region).	77
Figure 54: Results: influence of (un)exposure time on yield strain (longitudinal).	77
Figure 55: Results: influence of ageing time on yield stress (longitudinal).	78
Figure 56: Results: influence of (un)exposure time on stiffness (longitudinal, Hookean region).	78
Figure 57: Results: influence of ageing time on yield strain (longitudinal).	78
Figure 58: Picture of the tested sample of the material 3D printed PP.	79
Figure 59: Picture of the raw (left), injection-moulded (middle) and 3D printed PP-based composite.	79
Figure 60: Results: influence of (un)exposure time on yield stress (longitudinal). *	81
Figure 61: Results: influence of (un)exposure time on stiffness (longitudinal). *	81
Figure 62: Results: influence of (un)exposure time on yield strain (longitudinal). *	81
Figure 63: Picture of the tested sample of the material virgin black PPB.	82
Figure 64: Picture of the tested sample of the material recycled grey PPG.	82
Figure 65: Results: influence of (un)exposure time on yield stress (longitudinal).	84
Figure 66: Results: influence of (un)exposure time on stiffness (longitudinal).	84
Figure 67: Results: influence of (un)exposure time on yield stress (longitudinal).	84
Figure 68: Results: change of tensile strength and stiffness of a 336h UV-exposed materials compared to its unexposed material.	85
Figure 69: Tensile strength comparison between different PP-based materials. *	85
Figure 70: Comparison between different PP-based materials on their yield strain. *	86

Figure 71: Results: influence of (un)exposure time on Charpy impact test in both directions.	87
Figure 72: Results: influence of (un)exposure time on Charpy impact test (longitudinal).	87
Figure 73: Various print quality of the material PP.	89
Figure 74: The bent extruded plate of the material PP.	89
Figure 75: Different failure modes during the tensile tests.	90
Figure 76: Sufficient clamping (left), insufficient clamping (right).	90
Figure 77: Chain-scission (A) and cross-linking (B) and of polymer chains.	98
Figure 78: Differential scanning calorimetry auto-sampler (left) and liquid nitrogen cooler (right).	99
Figure 79: DSC-results: 3D printed PP: Raw material (red), just-printed (green), aged (brown) and exposed (purple).	100
Figure 80: DSC-results: 3D printed PPU: Raw material (red), just-printed (blue), aged (green) and exposed (purple).	100
Figure 81: DSC-results: virgin PPB: reference (red) and exposed (brown), (thickness of 1.2 mm).	101
Figure 82: DSC-results: recycled PPG: reference (red) and exposed (brown).	101
Figure 83: DSC-results: Raw (red), 3D printed (green), inject-moulded (blue) PP.	102
Figure 84: Digital microscope (left), Scanning electron microscope (right).	106
Figure 85: Microscope picture of the surface of 3D print-extruded PP.	107
Figure 86: 3D representation: the surface of 3D print-extruded PP (thickness: 3.5 - 5.5 mm).	107
Figure 87: Microscope picture of the fracture surface of 3D print-extruded PP.	108
Figure 88: 3D representation: the fracture surface of 3D print-extruded PP.	108
Figure 89: Microscope picture of the surface of inject-moulded PP.	109
Figure 90: Microscope picture of the surface of inject-moulded PP (thickness: 3 mm).	109
Figure 91: Microscope picture of the surface of flat-die-extruded PPB.	110
Figure 92: 3D representation: the surface of flat-die-extruded virgin PPB (thickness: 1.2 mm).	110
Figure 93: Microscope picture of the surface of flat-die-extruded PPG.	111
Figure 94: 3D representation: the surface of flat-die-extruded recycled PPG (thickness: 3.0 mm).	111
Figure 95: SEM-representation of the raw material PP.	112
Figure 96: SEM-representation of the 3D printed PP.	112
Figure 97: SEM-representation of the injection-moulded PP.	113
Figure 98: Fourier-transform infrared spectroscopy test setup.	116
Figure 99: FTIR Spectra of the raw, 3D printed, injection-moulded PP.	117
Figure 100: FTIR Spectra of the raw, 3D printed and injection-moulded PP (zoomed-in).	118
Figure 101: FTIR Spectra of raw (left) and oxidised polypropylene (right) (Gutiérrez and Palza 2015).	118
Figure 102: Concept for the formation of spherulite (Gránásy, Pusztai, and Douglas 2013).	123
Figure 103: Strain at failure vs. spherulite size of isotactic polypropylene (Ehrenstein and Theriault	124
Figure 104: Averaged load-strain curves of plates made of ABS (dashed) and nylon copolymer (solid) printer at air (grey) and under a nitrogen atmosphere (black) (Lederle et al. 2016).	130

Figure 105: Redesign of the printer's nozzle including the supply of an inert gas.	131
Figure 106: Redesign of the printer's nozzle including the infrared laser.	131
Figure 107: Material Sheet PP: Mafill CR XTG 5344.	135
Figure 108: Material Sheet: UV stabilisers for PPU.	136
Figure 109: Material Sheet: Flat-die Extruded PPB.	137
Figure 110: Material Sheet: Carbon black, a colour additive for PPB.	138
Figure 111: Material Sheet: UV stabiliser for PPB.	139
Figure 112: Specimen geometry for the tensile test.	140
Figure 113: Situation A: Single layer (Kemper & Feldmann, 2012).	144
Figure 114: Situation B: Second skin layer (Kemper & Feldmann, 2012).	144
Figure 115: Wind load assumptions: Situation A, 1 mm.	145
Figure 116: Wind load assumptions: Situation A, 70 mm.	145
Figure 117: Wind load assumptions: Situation B, 70 mm.	146
Figure 118: Wind load assumptions: Situation B, 70 mm..	146
Figure 119: Raw result: PP, transverse tensile test, 888 hours aged.	147
Figure 120: Raw result: PPU, transverse tensile test, 552 hours aged.	147
Figure 121: Raw result: PP, transverse tensile test, 1008 hours aged.	148
Figure 122: Raw result: PPU, transverse tensile test, 672 hours aged.	148
Figure 123: Raw result: PP, transverse tensile test, 1296 hours aged.	149
Figure 124: Raw result: PPU, transverse tensile test, 1296 hours aged.	149
Figure 125: Raw result: PP, transverse tensile test, 240 hours exposed.	150
Figure 126: Raw result: PP, transverse tensile test, 240 hours exposed.	150
Figure 127: Raw result: PP, transverse tensile test, 576 hours exposed.	151
Figure 128: Raw result: PPU, transverse tensile test, 576 hours exposed.	151
Figure 129: Raw result: PP, transverse tensile test, 840 hours exposed.	152
Figure 130: Raw result: PPU, transverse tensile test, 840 hours exposed.	152
Figure 131: Raw result: PP, longitudinal tensile test, 888 hours aged.	153
Figure 132: Raw result: PPU, longitudinal tensile test, 888 hours aged.	153
Figure 133: Raw result: PP, longitudinal tensile test, 1488 hours aged.	154
Figure 134: Raw result: PPU, longitudinal tensile test, 1488 hours aged.	154
Figure 135: Raw result: PP, transverse tensile test, 2088 hours aged.	155
Figure 136: Raw result: PPU, longitudinal tensile test, 2088 hours aged.	155
Figure 137: Raw result: PP, longitudinal tensile test, 336 hours aged.	156
Figure 138: Raw result: PPU, longitudinal tensile test, 336 hours aged.	156
Figure 139: Raw result: PP, longitudinal tensile test, 936 hours aged.	157
Figure 140: Raw result: PPU, longitudinal tensile test, 936 hours aged.	157
Figure 141: Raw result: PPB, tensile test, 0 hours aged.	158
Figure 142: Raw result: PPB, tensile test, 336 hours exposed.	158
Figure 143: Raw result: PPB, tensile test, 336 hours aged.	159
Figure 144: Raw result: PPG, tensile test, 0 hours aged.	159
Figure 145: Raw result: PPG, tensile test, 336 hours exposed.	160
Figure 146: Raw result: PPG, tensile test, 336 hours aged.	160

List of Tables

Table 1: Comparison of the several plastic extrusion methods.	28
Table 2: Input parameters for the heat transient analysis.	37
Table 3: Print quality classification system.	63
Table 4: Printer settings of the KameMaker.	65
Table 5: Summary of the transverse tensile test, 2 mm/min.	75
Table 6: Summary: longitudinal tensile strength properties, 5 mm/min.	79
Table 7: Summary: tensile properties of flat-die-extruded PPB and PPG, 20 mm/min.	82
Table 8: Summary: Charpy impact test results.	88
Table 9: Values of kn for the 5% characteristic value (Nederlands Normalisatie-Insituut 2011).	91
Table 10: Characteristic values of the transverse tensile test, 2 mm/min.	91
Table 11: Characteristic values of the tensile strength properties, 5 mm/min.	92
Table 12: Characteristic values of the tensile strength properties, 20 mm/min.	92
Table 13: Results of the first heating measurements of the DSC-analysis.	103
Table 14: Results: Thermal analysis and mechanical testing.	105
Table 15: Chemical composition of the PP-based polymers.	113
Table 16: Oxygen atomic percent of the chemical composition of the PP-based polymers.,	115
Table 17: Specification of the UV Test Chamber.	143
Table 18: Summary: Point temperatures of the façade element over time, 1-June-2017, the Netherlands.	161
Table 19: Parameters: Solar radiation in the Netherlands, south direction.	162